RCA REVIEW

a technical journal

Published quarterly by

RCA LABORATORIES

in cooperation with all subsidiaries and divisions of

RADIO CORPORATION OF AMERICA

VOLUME XXV SEPTEMBER 1964 NUMBER 3

CONTENTS

(Continued on next page)

CONTENTS—continued

RCA REVIEW is regularly abstracted and indexed by *Abstracts of Photographic Science and Engineering Literature. Applied Science and Technology Index, Bulletin Signalétique des Télécommunications, Chemical Abstracts, Electronic and Radio Engineer, Mathematical Reviews, and Science Abstracts* (I.E.E.-Brit.).

RCA REVIEW

SUPERCONDUCTING NIOBIUM STANNIDE—AN INTRODUCTION

IT IS AN interesting fact that much of our modern technology is based upon old principles that have been reinterpreted in the light of new theories, and that have been re-examined with new materials. A few solid-state examples are the electron–hole concepts in semiconductor devices; electron excitation→radiation in luminescent screens; and the direct conversion of heat into electrical energy by thermoelectric, thermionic, and photovoltaic techniques. The same is true of superconductivity and its applications. This branch of the physical sciences has a long tradition. It dates back to the liquefaction of helium in 1908 by the Dutch physicist Kammerlingh Onnes, and his discovery three years later that the electrical resistance of mercury abruptly vanished at temperatures a few degrees above absolute zero, in contradiction to the classical theories of electrical conduction in solids. Thus, a current induced in such a metal at these low temperatures would flow endlessly without further input of energy. This early pioneering work and the studies of Meissner in the 1930's formed the basis for characterizing superconductors, at least from a gross experimental standpoint. Below a critical temperature called the transition temperature these characteristics are (1) zero electrical resistance for direct-current flow, (2) almost (except for a very small but important penetration at the material surface) perfect diamagnetism with ability to exclude or confine a magnetic field, and (3) the ability to revert from the superconducting state of zero resistance to a normal resistive state in the presence of a sufficiently large magnetic field that can be applied externally or generated directly by current flow.

In spite of these fascinating properties, for nearly forty years the phenomenon of superconductivity remained largely a matter of academic interest. This seems particularly strange when one considers that during this period, from its discovery until 1950, such applications as superconducting magnets (Onnes, 1913) and superconducting switching elements (Casimer–Jonker and deHaas, 1935) had already been proposed. However, this picture changed dramatically in the past decade. Advances in more or less rapid succession in cryogenic refrigeration (Collins, 1949), materials exploration (Matthias, 1954), electronic engineering (Buck, 1956), microscopic theory (Bardeen, Cooper and Schrieffer, 1957), and high-field studies (Kunzler, 1961) have pro-

vided researchers with a better understanding of fundamental effects, a more intelligent basis in the search for new superconductors, and an increased awareness of the possibilities of exploiting the properties of superconductors. Whereas superconductivity was little more than a scientific oddity 20 years ago, today it is the subject of intensive investigation by scientists of all disciplines in solid-state research.

RCA Laboratories has been carrying out basic research in superconductivity since 1956. From the beginning the research was stimulated by the early work of Casimer–Jonker and deHaas on normal-to-superconducting switching phenomena, and later by the theoretical interpretation of superconductivity by Bardeen, Cooper, and Schrieffer (the BCS theory). Two features of the BCS theory offered challenges to the materials scientist: First, the explicit expression for the transition temperature suggested the possibility of finding materials with transition temperatures in the vicinity of their Debye temperatures. Materials parameters such as electron density of states at the Fermi level and phonon–electron interaction potentials could now be added to the empirical electron-to-atom ratio rules of Matthias in the search for new superconductors. Second, a superconducting energy gap was associated with the energy change of an electron in going from the normal to superconducting state. This concept suggested a normal-to-superconducting transition time in the range, 10^{-9} to 10^{-12} second, as well as phenomena such as tunneling (Giaver, 1960) and carrier injection across superconducting junctions analogous to that across p-n junctions in semiconductors. Thus, the materials research at RCA Laboratories became concerned with (1) the structure-sensitive factors influencing the kinetics of the superconducting transition, (2) exploring the area of intermetallic compounds and compound alloys for new superconductors, and (3) extension of these studies to include microwave and tunneling phenomena. In addition, theoretical considerations were carried out on the application of the BCS theory to existing phenomena, as well as modifications of existing theory towards predicting new phenomena.

At the start of our search for new superconductors in 1957, it seemed logical to investigate first the compound superconductor, niobium stannide (Nb_3Sn). This compound had the highest known transition temperature (18°K), and represented an excellent prototype of the then ill-defined hard (type-II) superconductors. As our research, as well as that in many other laboratories, progressed, it became even more apparent that a concentrated effort on the superconducting properties of this particular material could be more fruitful than undertaking a broad sweep of this multi-faceted area of research. These efforts have

been highlighted by (1) the development at RCA Laboratories of a vapor-phase transport technique for preparing Nb_3Sn (1960), and (2) the high-current-field studies of Kunzler at Bell Telephone Laboratories published in 1961, which clearly indicated the possibility of constructing high-field (at least up to 88 kilogauss) electromagnets with Nb_3Sn with virtually no power dissipation.

The RCA vapor-phase growth technique involved the reduction of the respective chlorides of the constituent elements, niobium and tin, with hydrogen on a properly heated substrate. This synthesis technique was the predominant factor in formulating our experimental research program. There were several reasons for this;

First, it was possible to prepare Nb_3Sn in single-phase, massive crystalline forms with theoretical density, high purity, and controlled chemical composition and grain structure; the technique also lent itself to the growth of single crystals such as "whiskers" of high structural perfection. These aspects of materials preparation were desirable prerequisites for a definitive examination of the role of lattice defects such as vacancies, dislocations, and structural order–disorder on superconducting properties, and in particular on the validity of the filamentary concept advanced to explain the high critical magnetic field properties of type-II superconductors (Abrikosov, 1957). This well-characterized material may be contrasted with the multiphase porous, polycrystalline, and brittle product obtained by metallurgical sintering techniques.

Second, single-phase Nb_3Sn could be deposited by the vapor-transport technique on both metallic and ceramic substrates in various configurations including planar and cylindrical geometries. This enabled us to carry out experiments on basic properties of Nb_3Sn, which were heretofore not possible or could not be done in a quantitative manner. On metallic substrates, it was possible to measure for the first time the London penetration depth ($\sim$3000 Å) of Nb_3Sn, and its flux-shielding and trapping characteristics when prepared in complex film patterns. This latter work led to the development of superconducting structures capable of trapping fields up to 60 kilogauss at 4.2°K, and eventually to the construction of permanent magnets with such field strengths. Deposition on insulating substrates is desirable for a number of reasons —the substrate does not interact with applied or induced currents and fields; diffusion of metallic impurities into the Nb_3Sn deposit is avoided, both during preparation and heat treatment; irradiated samples are not more active than the deposit itself; and unsupported Nb_3Sn films can be prepared by preferential chemical dissolution of the insulating substrate. Definitive studies made possible with Nb_3Sn films on such insulating substrates included the determination of the BCS energy

band gap by both tunneling and thermal conductivity measurements, tube magnetization experiments, dependence of normal resistance on temperature, determination of upper critical field by microwave surface impedance, neutron irradiation effects, and the angular dependence of current and field on the current-carrying properties of Nb_3Sn.

A *third* and most important feature of the RCA vapor transport technique was its adaptability to the continuous deposition of Nb_3Sn on a steel ribbon substrate with high mechanical strength. Ribbon lengths up to one kilometer could be readily produced with current densities in the superconductor as high as 2×10^5 amperes per square centimeter at a field strength of 120 kilogauss. Critical-current measurements on this material in coil form led to a gross characterization of anamolous current instabilities at low magnetic fields, a knowledge of which was vital to the design of high-field superconducting magnets. This applied research on Nb_3Sn ribbon culminated in April of 1964 with the construction of a 107 kilogauss solenoid magnet with a 1-inch bore and operating at 4.2°K.

The results of the Nb_3Sn-oriented research program, as outlined above, are presented in this special issue of *RCA Review* in the form of nineteen papers authored by Members of the Technical Staff of RCA Laboratories, and Members of the Engineering Staffs of the Electronic Components and Device and Defense Electronic Components Division of RCA. The first paper is concerned with early work on transition-temperature measurements of Nb_3Sn alloys prepared by metallurgical sintering techniques. It is included in this volume primarily to emphasize that such sintered products, though useful for measurements of gross properties of superconductors, are not suitable for more sophisticated studies such as magnetization. The next three papers deal with chemical and metallurgical aspects of Nb_3Sn. They include a detailed account of the vapor-phase transport technique for depositing Nb_3Sn on various substrates, phase-equilibria studies in the Nb-Sn system, and chemical analytical techniques. The bulk of this issue (paper 5 through 15) is devoted to physical measurements of the basic superconducting parameters of Nb_3Sn as well as its current–field characteristics; this is followed by three papers devoted to the utilization of synthesis techniques and phenomena in the construction of high-field magnets. The final paper is essentially an extension of the BCS theory.

This collection of papers, therefore, presents in logical fashion the synthesis, characterization, and application of Nb_3Sn; as such, it exemplifies the spectrum of materials research encountered in an electronics industry, particularly as it involves interdisciplinary activity. This volume also serves to underscore the importance of novel materials

synthesis techniques in the search for new knowledge, and in the practical utilization of this knowledge. Finally, it should be emphasized here that the research described in this volume is not to be regarded as a comprehensive critique, but instead represents only the first step in the early stages of a rapidly advancing science and technology of only one material in an important class of superconductors.

In conclusion, it is only proper to note the following acknowledgments: The experimental phase of the research, which includes synthesis and physical measurements, was supported in part by the Air Force Materials Laboratory, Wright-Patterson Air Force Base, Ohio, under Contract Nos. AF33(616)-6405 and AF33(657)-11208; the high-field solenoid work was supported by the National Aeronautics and Space Administration, Lewis Research Center, Ohio, under Contract Nos. NAS 3-2520 and NAS 3-5240; and finally, the high-field magnet facilities at Bell Telephone Laboratories, the NASA Lewis Center, and the Lawrence Radiation Laboratory were kindly made available during the course of the research.

F. D. Rosi
RCA Laboratories

Princeton, N. J.

SUPERCONDUCTING PROPERTIES OF THE $(Nb,Ta,V)_3Sn$ SYSTEM*

By

G. D. Cody, J. J. Hanak, G. T. McConville and F. D. Rosi

RCA Laboratories
Princeton, N. J.

Editor's Note: This paper represents one of the initial research efforts on Nb_3Sn using metallurgical sintering techniques to prepare the compound and its alloys. It is presented here to emphasize that such sintered products can indeed provide reliable data on gross measurements such as the transition temperature, but are inadequate for the more sophisticated magnetization studies.

ALTHOUGH THERE IS considerable information in the literature on compound superconductors,[1] little is known about solid-solution alloys of these compounds. In the present paper, data are presented on the superconducting properties of solid-solution alloys in the ternary system (Nb, Ta, V)$_3$Sn. This alloy system was selected since the compounds Nb_3Sn, Ta_3Sn, and V_3Sn have the same electron-to-atom ratio, and yet widely differing molecular weights and atomic volumes. Moreover, the published values of the transition temperatures cover the range 18° to 6°K.[2,3] Complete solid solubility was expected for these compounds since they have the same crystal structure (β-tungsten), and since the component elements are mutually soluble in the solid state.

The synthesis of these compound alloys was accomplished by powder metallurgical techniques. Powders of the component elements were thoroughly mixed and heated to ~650°C to effect a partial reaction. The mixtures were pulverized, pressed, and finally sintered at 1200°C in vacuum for times varying from two hours to two days.

X-ray analysis of the compounds prepared indicated predominant β-tungsten structure. For a few of the compounds, unidentified lines were present; for one, NbV_2Sn, an excess of one of the components (Sn) was noted. Table I gives the results of x-ray measurements. In this table, comparisons are made with literature values, and with lattice constants obtained by Vegard's law.

---

* Reprinted by permission from the *Proceedings of the VIIth International Conference on Low-Temperature Physics*, October 1960, Toronto, Canada, p. 382.

[1] B. Matthias in *Progress in Low Temperature Physics, II*, ed. C. J. Gorter, North Holland Publishing Company, Amsterdam, 1953.

[2] B. T. Matthias, T. H. Geballe, S. Geller, and E. Corenzwit, "Superconductivity of Nb_3Sn," *Phys. Rev.*, Vol. 95, p. 1453, 15 Sept. 1954.

[3] S. Geller, B. Matthias, and R. Goldstein, "Some New Intermetallic Compounds with the 'β-Wolfram' Structure," *Jour. Amer. Chem. Soc.*, Vol. 77, p. 1502, 20 March 1955.

Transition temperatures of the materials were measured by a mutual-inductance method. The transitions were determined in zero field, and the temperatures were measured by a carbon resistor calibrated with respect to helium vapor pressure. It is estimated that the maximum temperature uncertainty was about 1 per cent. For all samples except TaV_2Sn, only one transition was noted; for this alloy the transition corresponding to pure tantalum was also observed. Transition temperatures and transition widths are given in Table II. It should be noted that the widths of many of the alloys are characteristic of rather large compositional inhomogeneity.

Table I—Lattice Constants (Nb,Ta,V)$_3$Sn System (angstrom units)

	Literature	Observed	Vegard's Law
Nb_3Sn	5.289(3)	5.289 ± .001	——
Nb_2TaSn	——	5.287 ± .001	5.285
$NbTa_2Sn$	——	5.280 ± .001	5.282
Ta_3Sn	5.276(3)	5.278 ± .002	——
Ta_2VSn	——	5.174 ± .001	5.172
TaV_2Sn	——	5.041 ± .001	5.006
V_3Sn	4.94(3)	4.96 ± .02	——
V_2NbSn	——	5.115 ± .004	5.070
VNb_2Sn	——	5.171 ± .003	5.179
NbVTaSn	——	5.175 ± .001	5.176

A convenient way of plotting the data in Table II is shown by the ternary diagram of Figure 1. In this diagram the binary alloys are plotted along the sides of an equilateral triangle, and the lengths of the projection from any point to a side are a measure of the ternary components present. The transition temperature furnishes a third dimension. Table II thus represents a surface. A projection of this surface on the V–Ta plane is given in Figure 2. The nature of the surface is such that this projection can be used for interpolation of transition temperatures.

Using the diagram of Figure 1, it is possible to determine the variation of transition temperature along curves of constant atomic volume and constant mass. Analysis of the data in this manner leads to an empirical expression,

$$T_c(M,V) = T_0(M_0,V_0)\,(M_0/M)^3 \exp\{0.12\,(V - V_0)\}. \qquad (1)$$

Table II—Transition Temperatures for $(Nb,V,Ta)_3Sn$ System (°K)

Compound	T_c	ΔT_c	T_c (calculated)
Nb_3Sn	18.0	0.1	31
$Nb_{2.75}Ta_{.25}Sn$	17.8	0.5	—
$Nb_{2.5}Ta_{.5}Sn$	17.6	0.7	24.8
Nb_2TaSn	16.4	3.2	16.5
$NbTa_2Sn$	10.8	3.0	9.9
Ta_3Sn	6.4	0.2	6.2
Ta_2VSn	3.7	0.3	3.8
TaV_2Sn	2.8	0.3	3.2
V_3Sn	3.8	0.1	3.8
V_2NbSn	5.5	1.4	7.0
VNb_2Sn	9.8	1.0	14.3
$V_{.5}Nb_{2.5}Sn$	14.2	0.5	19.9
NbVTaSn	6.2	1.3	—
$Nb_2Ta_{.5}V_{.5}Sn$	12.2	0.6	14.5

Using for T_0 the transition temperature corresponding to NbTaVSn (6.2°K), one obtains

$$T_c(M,V) = (6.2)\,(453/M)^3 \exp\{0.12\,(V - 137.4)\}, \qquad (2)$$

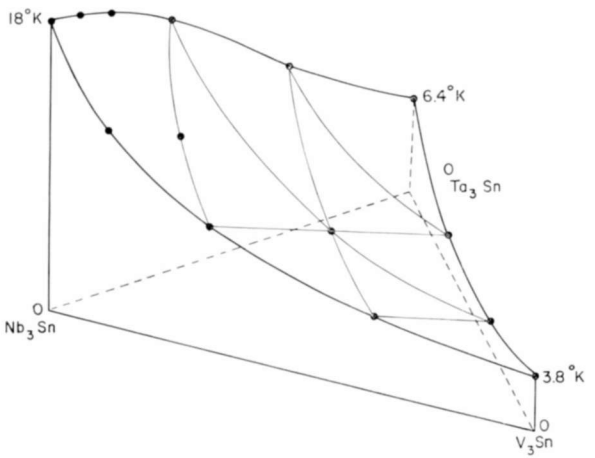

Fig. 1—Ternary representation of transition temperature versus composition.

where M is in grams and V is in cubic angstrom units.

The column T_c (calculated) in Table II gives transition temperatures obtained from Equation (2). Over this series of alloys the exponential varies from 0.13 to 3.4, the mass term from 0.32 to 4.6, and the transition temperature from 2.8° to 18°K. It is noteworthy that except for Nb_3Sn this expression gives the transition temperatures

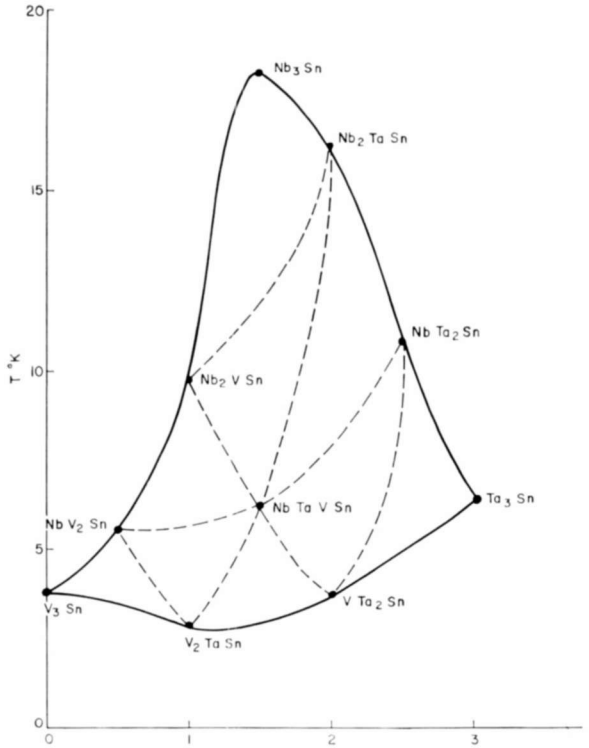

Fig. 2—Projection on V–Ta plane.

within 40 per cent. Moreover, if we exclude all compounds of the form $(Nb_x,V,Ta)Sn$, where $x > 2$, the agreement between calculated and experimental values is better than 10 per cent.

Some preliminary measurements have been made on the magnetization of these sintered compounds and alloys. These results have shown a large variation in the critical field and current of specimens with similar composition, which clearly reflects the manner of preparation. Thus, it would appear that in order to obtain significant magnetization data, it is necessary to make the measurements on single-crystal or polycrystalline specimens that consist of a single phase and are free of porosity and better defined structurally.

PREPARATION AND PROPERTIES OF VAPOR-DEPOSITED NIOBIUM STANNIDE*

By

J. J. Hanak,† K. Strater,‡ and G. W. Cullen†

Summary—*This paper gives an up-to-date review of work that has been carried out on the vapor deposition of Nb_3Sn. Techniques are described for depositing Nb_3Sn by simultaneous hydrogen reduction of gaseous niobium and tin halides on various substrates, including narrow and wide metallic ribbons and flat and cylindrical ceramics. These deposits are useful in the construction of high-field magnets and in research and applications where the presence of metallic substrates is undesirable. In the case of metallic substrates, platinum and other noble metals have been found to aid in the nucleation of Nb_3Sn, but deposits have been successfully prepared on various high-strength nickel-base alloys. For ceramics, adherent Nb_3Sn has been deposited on magnesium silicates. The chemistry of the vapor deposition process has been studied in some detail. Nb_3Sn can be formed at temperatures ranging from 675° to at least 1600°C. It has been found that the Nb_3Sn phase can be deposited over a composition range of 75.1 to 82.3 at.% Nb. The corresponding lattice constants and transition temperatures have been determined over this range of compositions. The effect of the concentration of the reacting gases and temperature on the composition of the deposit has been determined. The equilibrium constant for the deposition reaction has been found to increase with temperature and its value at 950°C is about 5×10^{-3}.*

Introduction

THE INTERMETALLIC compound Nb_3Sn was synthesized from the elements, using a sintering technique, by Matthias *et al.*[1] Subsequently, a vapor deposition technique was developed at RCA Laboratories by Hanak[2] in which the Nb_3Sn is prepared by the simultaneous hydrogen reduction of gaseous niobium and tin halides. The flexibility of this technique made it possible to prepare the material in various desired forms, such as dense crystallites and

*Research reported in this paper was sponsored by the Air Force Materials Laboratory, Research and Technology Division, Air Force Systems Command, Wright Patterson Air Force Base, Ohio, under contract AF 33(657)-11028; by RCA Electronic Components and Devices, Harrison and Princeton, N. J.; and by RCA Laboratories, Princeton, N. J.

† RCA Laboratories, Princeton, N. J.

‡ RCA Electronic Components and Devices, Princeton, N. J.

[1] B. T. Matthias, T. H. Geballe, S. Geller, and E. Corenzwit, "Superconductivity of Nb_3Sn," *Phys. Rev.*, Vol. 95, p. 1435, 15 Sept. 1954.

[2] J. J. Hanak, *Metallurgy of Electronic Materials*, G. E. Brock, ed., Interscience Publishers, New York, 1963, p. 161.

thin coatings deposited continuously on flexible metal wire or ribbon substrates. It was demonstrated that superconducting solenoids can be wound of the coated ribbon without damage to the inherently brittle Nb_3Sn deposit.

Following this initial development, a continued effort by one of the authors led to the refinement of the continuous ribbon deposition process to the point where material of the required quality and quantity could be reproducibly prepared. With this material, solenoids have been constructed that generated fields of 93 kilogauss,[3] and more recently in excess of 100 kilogauss.

The vapor-deposition process has been used by Cullen[4] to prepare Nb_3Sn deposits on ceramic substrates, thereby making it possible to fabricate well-defined material needed in research and applications where the presence of metallic substrates is undesirable. Another application of the technique has been the deposition of Nb_3Sn on wide metallic strips that can be fabricated, in a manner similar to that employed for printed circuitry, into magnetic devices such as flux shields and concentrators.[5]

During the development of these various applications, contributions have been made to the understanding of the chemistry of the vapor-deposition process, and correlations have been made between some of the low-temperature properties and crystallographic structure and chemical composition.[4,6]

The purpose of this paper is to give a review of the work that has been carried out on the vapor deposition of Nb_3Sn.

Vapor-Deposition Techniques

The synthesis of Nb_3Sn by a gas-phase reaction appeared to be feasible because both niobium and tin can be obtained by the hydrogen reduction of their gaseous chlorides at temperatures well below 1000°C.[7,8]

---

[3] E. R. Schrader, N. S. Freedman, and J. C. Fakan, "High-Field Nb_3Sn Superconducting Magnets by Magnetic-Field Stabilization," *App. Phys. Ltrs.*, Vol. 4, p. 105, 15 Mar. 1964.

[4] G. Cullen, "Preparation and Properties of Niobium Stannide on Insulating Substrates," *Trans. Metallurgical Soc.*, in press.

[5] J. J. Hanak, "Magnetization of Niobium-Stannide Films in Transverse Fields," *RCA Review*, Vol. XXV, p. 551, Sept. 1964 (this issue).

[6] J. J. Hanak, G. D. Cody, J. L. Cooper, and M. Rayl, "The Effect of Composition on the Superconducting Properties of Vapor-Deposited Niobium Stannide," *Proc. 8th International Conf. on Low Temperature Physics*, Butterworth Scientific Publications, Ltd., London, 1963, p. 353.

[7] C. F. Powell, I. E. Campbell, and B. W. Gonser, "The Deposition of Tantalum and Columbium from Their Volatilized Halides," *Jour. Electrochem. Soc.*, Vol. 93, p. 258, June 1948.

[8] B. W. Gonser and E. E. Slowter, Tech. Pub. of the International Tin Research and Development Council, Series A, Number 76, 1938.

A simultaneous reduction of a mixture of these chlorides yields crystalline Nb_3Sn without the intermediate formation of the free metals. The overall reaction for the production of deposits on ribbon used for superconducting solenoids is $3NbCl_4 + SnCl_2 + 7H_2 \rightarrow Nb_3Sn + 14HCl$.

Various sources of niobium and tin halide vapors have been used. Initially the mixed vapors were produced by direct chlorination of Nb and Sn powder sintered in the desired proportions, but this scheme was abandoned when it was found that the composition of the vapors changed with time as the more reactive Sn was depleted. A more satisfactory method is the separate chlorination of the metals, with control of the stoichiometry of the deposit by control of the chlorine gas flows. A sufficiently long metal bed is employed to prevent the flow-through of unreacted Cl_2. The lower gaseous halides of the metals, $NbCl_4$ and $SnCl_2$, are formed under the conditions used. Separate volatilization of pre-prepared $NbCl_5$ and $SnCl_4$ or $SnCl_2$ has also been employed as halide sources. For deposition on ceramic substrates, the vapor composition is controlled by simultaneous volatilization of $NbCl_5$ and $SnCl_2$ powders that have been mixed in the desired proportions.

The vapor-deposition reaction has been carried out at temperatures as low as 730°C and as high as 1600°C; however, the deposition is generally carried out between 900° and 1200°C. Depending on the reaction conditions, deposits range from smooth films to polycrystals in which the individual crystal faces are several mm in length (Figure 1). The original deposition apparatus was a simple quartz furnace tube with gas inlets and outlets. Modifications of varying complexity were designed into the apparatus for specific conditions of deposition on a variety of substrate geometries, as described in the following sections.

Vapor Deposition on Ceramic Substrates

There are basic studies and applications that are made possible or greatly facilitated by using Nb_3Sn supported by an insulator. Such studies include radiation damage, tunneling, thermal conductivity (material removed from ceramic), microwave surface impedance, tube magnetization, resistivity as a function of temperature, and dependence of current-carrying properties on field strength and orientation.

Insulating substrates are desirable for a number of reasons—the substrate does not interact with applied or induced currents and fields; diffusion of metallic species into the deposit is avoided, both during the preparation and during subsequent heat treatment; and irradiated samples do not become more active than the deposit itself. Unsupported

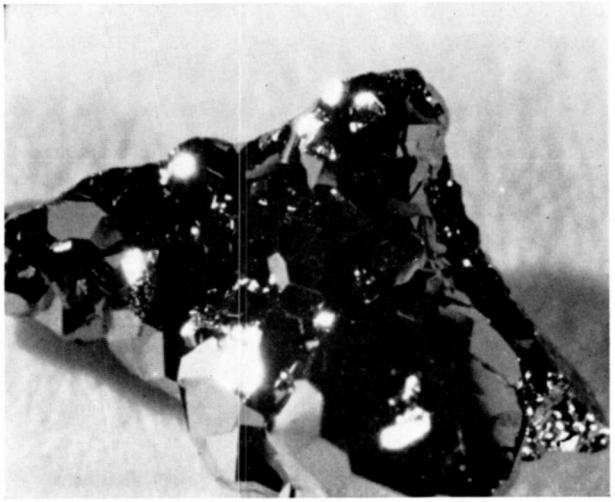

Fig. 1—Vapor-deposited Nb_3Sn polycrystal, 0.7 gram.

Nb_3Sn geometries may also be prepared by preferential chemical dissolution of the insulating substrate.

Preparation

Deposition apparatus has been designed to prepare 13 to 130μ deposits on ceramic flats and on cylindrical substrates up to 3.3 cm outside diameter. The apparatus shown in Figure 2a is used for the preparation of deposits on flat substrates; the apparatus in Figure 2b is used for deposition on cylindrical substrates. In both cases the entire

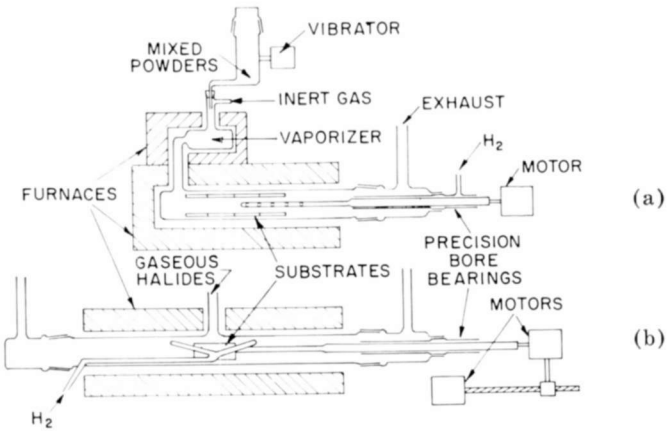

Fig. 2—(a) Apparatus for vapor deposition of Nb_3Sn on flat surfaces and (b) apparatus for vapor deposition of Nb_3Sn on cylinders.

reaction zone is heated to the deposition temperature. Various methods have been employed to heat the substrate alone, but such methods are restricted to simple geometries and have led to deposits of less uniform composition and thickness than when the entire zone is held at one temperature.

The mixed gaseous metal halides are introduced into one end of the tube from a vaporizing chamber (Figure 2a), and H_2 is introduced through evenly spaced outlets in a spinning quartz tube attached to a precision-bore glass fitting. The H_2 diffuses counter stream to the halides, and provides a deposition zone approximately 7.5 cm long. In the cylinder-coating apparatus (Figure 2b), the gas inlets are also arranged in such a manner that the hydrogen diffuses counter stream to the halides. This provides a deposition zone between the two inlets. In this case two exhausts and two H_2 inlets are used to provide symmetry. The cylindrical substrate, mounted on a quartz rod that is attached to a precision bore fitting, is rotated and drawn past the gas inlets. In this manner the cylinder is evenly coated over its entire length and circumference.

In both cases the metal halides are introduced by vibrating intimately mixed $NbCl_5$ and $SnCl_2$ powders into a vaporizer held at a temperature sufficient to volatilize both components completely. An inert gas is introduced into the vaporizer to dilute the halides and sweep them into the reaction zone. The hygroscopic solid halides must be manipulated in an efficient dry box.

A typical deposition is carried out at 900°C, with the halides introduced at a rate that provides a deposit growth rate of 15 microns/hr. The $NbCl_5$:$SnCl_2$ ratio is adjusted according to the composition of deposit desired and the operating temperature.

Substrates

Only a few of the ceramic materials evaluated as substrates meet the requirements of the proper coefficient of thermal expansion, high melting point, and chemical inertness. Of the ceramics tested, the magnesium silicates have proven to be the most satisfactory substrate material. The range of composition of various magnesium silicates provides a range of expansion coefficients from 7.9 to 11.2×10^{-6}/°C (25-700°C). This brackets the average coefficient of thermal expansion of stoichiometric Nb_3Sn, which J. White and R. Paff of these laboratories have found by x-ray diffraction to be 9.8×10^{-6}/°C (25-700°C). The composition of steatite ranges from $3MgO{\cdot}4SiO_2$ to $4MgO{\cdot}3SiO_2$ depending on the source of the starting materials of the various manufacturers. The composition of forsterite is nominally $2MgO{\cdot}SiO_2$. The

melting point of both ceramics is above 1400°C. The magnesium silicates are not corroded by the halides at 900°C, and no reaction products between the magnesium silicates and Nb_3Sn are revealed by microscopic examination of stained cross sections or x-ray diffraction of angle-lapped deposits. A preparation commonly used as a substrate material is Natite 150BM.* The Nb_3Sn deposits on this material have, with few exceptions, been adherent and crack free.

Since relatively thick deposits readily break away from sapphire, this material has been used to prepare unsupported disks of Nb_3Sn. For example, an 80-micron deposit on the polished end of a 1-cm-diameter sapphire rod falls away in one piece on cooling from the deposition temperature. Deposits will also often break cleanly away from quartz surfaces. In both cases the base material shows evidence of having been corroded. Nb_5Si_3 has been detected at quartz–Nb_3Sn interfaces.

Geometries of Nb_3Sn Films

The deposits on the ceramic flats can be polished to a mirror finish (Figure 3a). Various geometries may be sandblasted or etched into the deposit. Strips 1×0.02 cm are commonly cut in 15-micron-thick deposits for current-density measurements. This demonstrates the adherent and crack-free nature of the deposits. A convenient procedure for preparing reproducible or complex shapes is to perform recesses of the desired shape in the ceramic, deposit over the entire substrate, and grind off the unwanted material so that only the Nb_3Sn in the recesses remains (Figure 3b). Unsupported wafers of Nb_3Sn are available by dissolving the substrate in aqueous HF solutions.

Whiskers have also been produced in the halide-rich areas of the deposition zone near the halide inlet (Figure 4). The largest are 8 mm long and 0.2 mm in diameter. Both polycrystalline and single-crystal whiskers have been found. The axis of the single-crystal whiskers coincides with either the [110] or [111]. A mass of about 50 whiskers from one run exhibits a T_c of 17.7°K and ΔT_c of 0.8°K. An x-ray pattern on five powdered whiskers from the same run yields a lattice constant of 5.2866 ± 0.0005 Å.

Nb_3Sn on Wire and Metal Ribbon Substrates

The significance of producing Nb_3Sn in the form of wire or ribbon to be used as the windings in high-field magnets has previously been discussed. However the inherent brittleness of Nb_3Sn precluded the use of unsupported material for magnet windings. This problem was

* National Ceramic Co., Trenton, N. J.

overcome by the development of a continuous deposition process[2] in which a thin layer of Nb_3Sn is deposited on a flexible metal or alloy substrate.

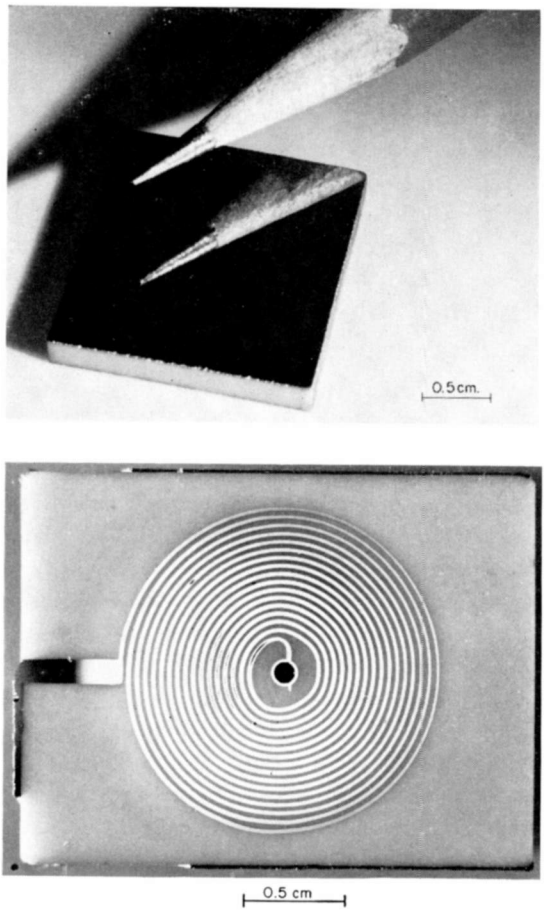

Fig. 3—(a) Polished Nb_3Sn on a flat ceramic substrate and (b) Nb_3Sn spiral on a ceramic substrate.

A schematic diagram of the apparatus used in this process is shown in Figure 5. It consists of two chlorinators and a deposition chamber enclosed within separate resistance furnaces. The chlorides are produced in the chlorinators by the reaction of chlorine directly with niobium and tin metals. Separate chlorination of the metals is used in the continuous process because of the ease of handling the starting materials. The gaseous metal chlorides, hydrogen, and hydrogen

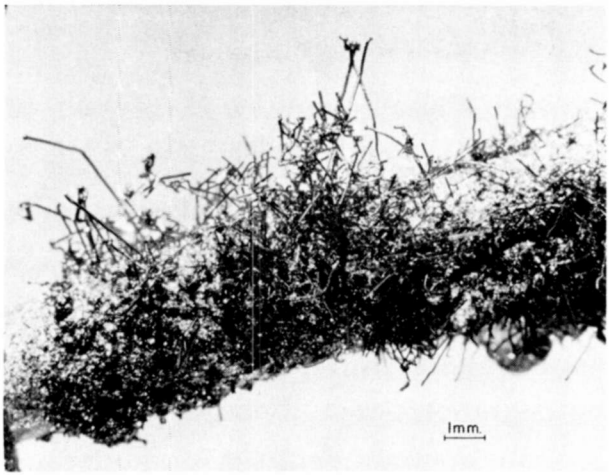

Fig. 4—Nb_3Sn whiskers.

chloride are introduced into the deposition chamber where reduction of the chlorides to Nb_3Sn occurs. The gaseous reaction product, hydrogen chloride, and the excess reactant gases are exhausted at the opposite end of the chamber.

The ends of the reaction chamber are fitted with slotted carbon electrodes through which the wire or ribbon is pulled as it is being coated with Nb_3Sn. Electrical contact is made to the electrodes so that

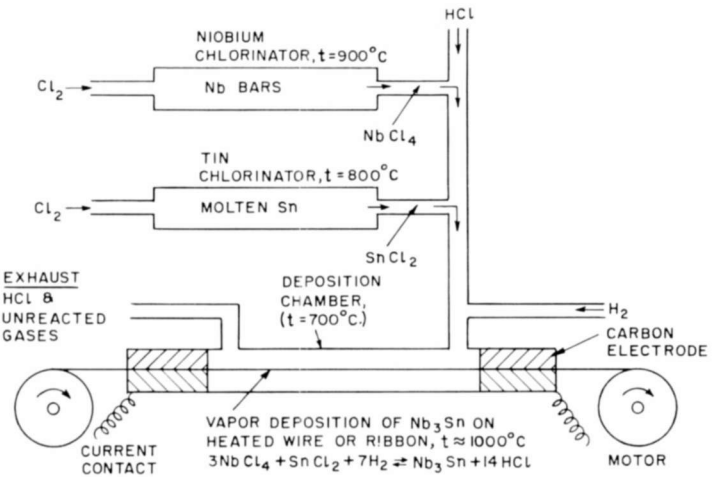

Fig. 5—Apparatus for continuous vapor deposition of Nb_3Sn on metallic ribbon and wire.

the moving substrate can be resistance heated to the temperature required for reduction of the chlorides.

Unless measures are taken to deposit Nb_3Sn exclusively on the ribbon substrate, the apparatus becomes clogged with accumulated deposits, and only short lengths of ribbon can be produced. These deposits may consist of Nb_3Sn, which forms at and above 700°C in amounts increasing with temperature, or of a lower chloride of niobium (presumably $NbCl_3$*) that forms at and below 700°C in amounts increasing with decreasing temperature. This overlapping formation of deposits on the quartz walls can be essentially eliminated by controlling the relative temperatures of the quartz and the ribbon substrate and by the addition of HCl gas into the reacting gases. This control over the solid deposits can be explained by considering the following deposition reactions:

$$3\,(NbCl_4 + 2H_2 \rightleftharpoons Nb + 4HCl) \quad (1)$$

$$SnCl_2 + H_2 \rightleftharpoons Sn + 2HCl \quad (2)$$

$$3Nb + Sn \rightleftharpoons Nb_3Sn \quad (3)$$

$$3NbCl_4 + SnCl_2 + 7H_2 \rightleftharpoons Nb_3Sn + 14HCl. \quad (4)$$

The expression for the equilibrium constant of the deposition reaction in Equation (4) is given by

$$K_p = \frac{(p_{HCl})^{14}}{(p_{NbCl_4})^3 (p_{SnCl_2})\,(p_{H_2})^7}. \quad (5)$$

The equilibrium constant increases with increasing temperature; therefore the substrate is maintained at a higher temperature than the quartz apparatus, and the HCl addition may be adjusted so that Nb_3Sn is deposited on the ribbon but not on the quartz. Therefore, the apparatus is kept at a temperature just high enough to maintain the incoming metal chlorides in a gaseous state (700°C), while the ribbon substrate is resistively heated to 1000°-1200°C. By a similar argument the addition of HCl also serves to suppress the accumulation of $NbCl_3$ in the apparatus:

$$H_2 + 2NbCl_4 \rightleftharpoons 2NbCl_3 + 2HCl. \quad (6)$$

This lower halide is a solid up to 900°C. Under the conditions described above, deposition runs have been sustained for as long as 90 hours, thus permitting the production of coated ribbon more than 1000 meters in length.

* $NbCl_3$ decomposes at 900°C.

Substrates

An important consideration in the development of the wire process was the selection of the substrate metal. Tungsten and tantalum proved to be unsuitable because free niobium deposited on them epitaxially prior to the nucleation of the Nb_3Sn phase. A cross section of such a deposit is shown in Figure 6a. Large cracks are seen in the Nb_3Sn phase in addition to a small number of nucleation points in the Nb_3Sn deposit. These results indicated that substrates with the β-tungsten structure were desirable to aid in the nucleation of Nb_3Sn. Such substrates are not commercially available. Hence, refractory metal sub-

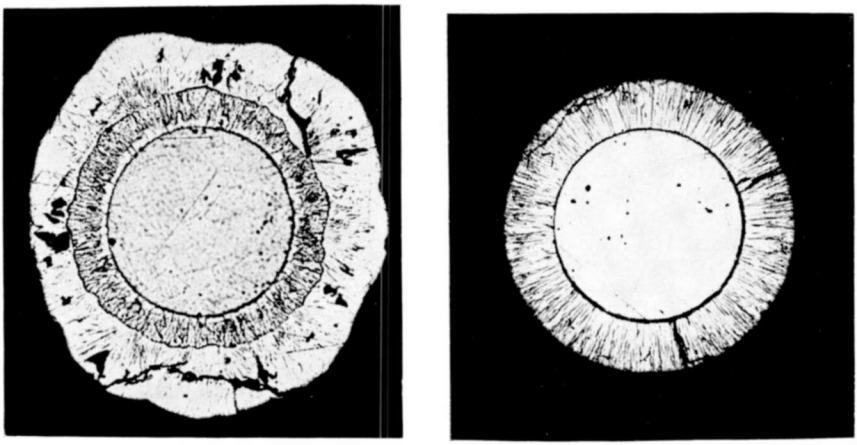

Fig. 6—Vapor-deposited niobium stannide (a) on tantalum wire and (b) on platinum wire. In (a), the inner deposit is free niobium and the outer deposit is niobium stannide. In both (a) and (b), the diameter of the wire substrate is 0.018 cm.

strates that react with niobium to form a β-tungsten compound were considered. Five metals belong to this category; they are rhodium, osmium, iridium, platinum, and gold.[9] When platinum wire was used as a substrate, a columnar single-phase deposit of Nb_3Sn was obtained, as shown in Figure 6b. The width of the columns determined by an electron microscope ranges between 750 and 1500 Å, indicating a high rate of nucleation (approximately 10^5 nuclei per cm of the surface).

Thermal coefficient of expansion is also an important consideration in the selection of a substrate material. On cooling the coated ribbon from the deposition temperature to ambient temperature, stress is induced within the deposit if the thermal expansion coefficients of the

[9] M. V. Nevitt, "Atomic Size Effects in Cr_3O-Type Structure," *Trans. AIME*, Vol. 212, p. 349, June 1958.

deposit and substrate are mismatched. Qualitative evidence of this was observed by the type of stress fracture seen when using different substrates. Nb_3Sn deposited on molybdenum and tungsten, which have thermal expansion coefficients less than Nb_3Sn, resulted in a residual tensile stress within the coating. The fracture pattern showed a series of radial cracks emanating from the interface, indicating a circumferential tensile stress greater than the tensile strength of the Nb_3Sn. Conversely, substrates having thermal expansions greater than Nb_3Sn, such as platinum, nickel, and nickel alloys, induced a compressive stress within the Nb_3Sn in cooling down to room temperature. In this case evidence of internal fracture was seen infrequently, and then only in heavy deposits. The pattern of such a fracture was circumferential, which is indicative of radial stresses. Thus, in order to minimize stress fracture of Nb_3Sn, substrates with expansion coefficients greater than Nb_3Sn are used.

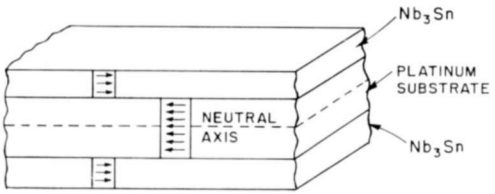

Fig. 7—Stress distribution within composite ribbon.

The magnitude of the residual stress produced by a substrate having a higher coefficient of expansion than Nb_3Sn was examined quantitatively. Based on a simplified concept of the stress pattern shown in Figure 7, and allowing for no plastic deformation during cooling, the residual stress of a thin Nb_3Sn deposit on a platinum substrate was estimated to be approximately 24,000 psi.

With this value for residual compressive stress a practical minimum solenoid diameter could be calculated such that bending would not cause cracks in the deposit. A wide safety factor was arbitrarily chosen to limit the tensile stress within the outer diameter of the Nb_3Sn coating to 1000 psi. The limiting minimum diameter, based on a platinum substrate and composite dimensions of 0.0013 cm deposit of Nb_3Sn on a 0.0081-cm-thick substrate, was 3 cm.

The tensile strength of the substrate metal is also an important factor. High-strength materials such as certain nickel-base alloys permit the use of considerably less magnet support structure to contain the stresses generated by the high field than do low-strength materials such as platinum. The room-temperature ultimate tensile strength of a com-

posite ribbon composed of a 0.00076-cm-thick Nb_3Sn deposit on a 0.0046-cm-thick nickel-base alloy substrate, Hastelloy,* is 95,000 psi. At liquid-helium temperature the tensile strength is about 150,000 psi. The same thickness of Nb_3Sn on a platinum ribbon of similar thickness has a room-temperature tensile strength no greater than 25,000 psi. A cross section of a typical Nb_3Sn ribbon is shown in Figure 8.

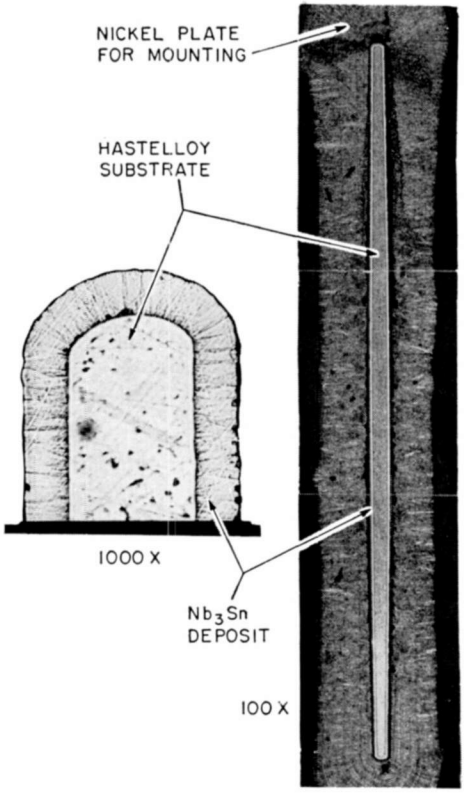

Fig. 8—Cross section of deposited Nb_3Sn composite ribbon.

Nb_3Sn on Wide Metallic Strip

The vapor-deposition process has been extended to the coating of Nb_3Sn onto a 2.54-cm-wide metallic ribbon substrate having a thickness of 0.0013 cm. Some characteristics of this material are given in Table I. This ribbon has been used in fabricating superconducting devices by printed-circuit techniques. One of these, a 60-kilogauss permanent magnet, is described by Hanak.[10]

[10] J. J. Hanak, "Magnetization of Niobium Stannide Films in Transverse Fields," *RCA Review*, Vol. XXV, p. 551, Sept. 1964 (this issue).

* Stellite Division, Union Carbide Corp., Kokomo, Indiana.

THE EFFECT OF PROCESS VARIABLES ON COMPOSITION OF DEPOSIT

Vapor-deposited specimens with the β-tungsten structure have shown a considerable solubility of niobium in Nb_3Sn and a corresponding degradation of superconducting properties. The magnitude of these effects varies with the design of the specific apparatus used. The composition of the deposit has been found to be a function of the operating conditions used during the growth of the deposit, as described below.

Table I—Characteristics of Nb_3Sn on 2.54-cm-Wide Tape

Thickness of Nb_3Sn deposit (on each side)	2.25×10^{-4} cm
Transition Temperature	14–16 °K
* α	1.73×10^7 kilogauss amp/cm^2
* B_0	10.3 kilogauss
Structure of deposit	β-tungsten

* The constants and B_0 define the critical current density J_c of a superconductor such as Nb_3Sn in transverse field H over the entire range of fields in which it is superconducting by the relation $J_c = \alpha/(H + B_0)$, described by Kim *et al.*[11] The average values of α and B_0 given above were obtained at 4.2°K.

Effect of Tin Halide to Niobium Halide Ratio

The ratio of the niobium chloride to tin chloride gases fed into the deposition zone strongly influences the composition of the deposits. The composition of deposits on the ribbon as a function of the input gas ratio is shown in Figure 9. Chemical compositions were determined by x-ray fluorescence as described by Bertin.[12] It should be noted that even though 40% more metal chlorides were used for one run, and the ratio of H_2 to total metallic halide was appreciably different, the data for two separate runs are nearly coincident. The break in the curve at approximately stoichiometric Nb_3Sn (75 at.% Nb) may be attributed to the fact that niobium is soluble in Nb_3Sn and tin is not. The deposit composition below 75% Nb is dependent on the feed ratio because of the appearance of free tin in the deposit. From these results it is evident that to obtain stoichiometric Nb_3Sn it is necessary to maintain an $SnCl_2$ to $NbCl_4$ ratio of approximately 4:1. These experiments were conducted with the deposition furnace temperature at 750°C, and a substrate temperature in the range of 900 to 1000°C.

[11] Y. B. Kim, C. F. Hempstead, and A. R. Strnad, "Magnetization and Critical Supercurrents," *Phys. Rev.*, Vol. 129, p. 528, 15 Jan. 1963.

[12] E. P. Bertin, "An Intensity Ratio Technique for X-ray Spectrometric Analysis of Binary Samples. Particular Application to Determination of Nb and Sn on Nb_3Sn-Coated Metal Ribbon," *Anal. Chem.*, Vol. 36, p. 826, April 1964.

In the static deposition in which different apparatus as well as different chlorides were used ($NbCl_5$ and $SnCl_2$) similar results were found. For deposition of stoichiometric material at 900°C, a 1:1 $SnCl_2$–$NbCl_5$ mixture is introduced into the reaction chamber. If a 4:6 $SnCl_2$–$NbCl_5$ mixture is employed at 900°C, the deposit is 2% rich in Nb. A 3:7 $SnCl_2$–$NbCl_5$ mixture yields a deposit 4% rich in Nb. A 7:3 $SnCl_2$–$NbCl_5$ feed mixture leads to the appearance of free Sn in the deposit. As with the wire process, the ratio must be adjusted for different deposition temperatures.

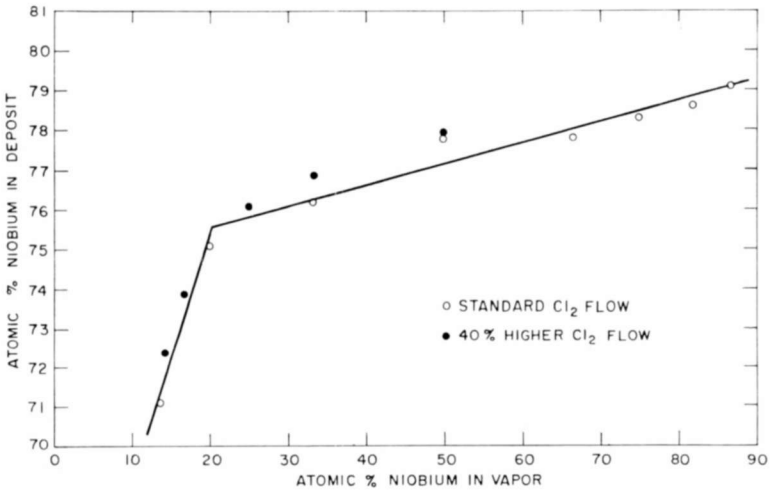

Fig. 9—Dependence of deposit composition on the relative composition of the metal chlorides in the vapor.

Effect of Hydrogen Chloride

The HCl introduced into the system to eliminate the formation of solid deposits in the continuous process apparatus also has an effect on the chemical composition of the deposit. From the data shown in Table II it can be seen that the niobium concentration in the deposit increases with increased HCl concentration. This compositional shift can be compensated for by increasing the Sn to Nb chloride ratio.

Effect of Substrate Temperature

As has been pointed out previously, in the continuous process the ribbon is resistively heated to a temperature higher than its surroundings. The data given in Table III show that the niobium content of the deposit increases with an increase in the substrate temperature. This observation is in accord with the known thermodynamics of the various halides, as discussed later.

Table II

% HCl Flow Relative to Standard Flow	$SnCl_2/NbCl_4$ Ratio	Deposit Composition (Atomic % Nb)
0	3/1	75.9
39	3/1	75.7
100	3/1	76.0
175	3/1	76.4
217	3/1	76.7
0	4.5/1	74.5
39	4.5/1	74.7
100	4.5/1	75.5
175	4.5/1	75.9

Thermodynamics of the Vapor-Deposition Process

It is possible to relate several of the deposition characteristics with the thermodynamics of the reactants. Therefore, data on the free energies of formation of the metal chlorides and hydrogen chlorides have been assembled in Figure 10. The temperature dependence of the free energy of formation for tin chlorides and for HCl was available in the literature.[13,14] For the niobium chlorides the free energies of formation have been calculated from room temperature enthalpy, absolute entropy, and heat capacity data obtained from the literature.[15]

The observation that the niobium concentration in the deposit

Table III—Ribbon Power Input Relative to Standard Conditions

%	Composition (Atom % Nb)
40	75.1
60	75.9
150	76.1

[13] A. Glassner, "Thermochemical Properties of the Oxides, Fluorides and Chlorides to 2500°K," Argonne National Laboratory Report No. 5750.
[14] O. Kubachewski and E. Evans, *Metallurgical Thermochemistry*, Pergamon Press, New York, 1958.
[15] H. Schäfer and F. Kahlenberg, "Die Thermochemie der Niobchloride," *Z. anorg. u. allgem. Chem.*, Vol. 305, p. 291, Aug. 1960.

increases with an increase in deposition temperature may be explained by the relative temperature dependence of the free energy of formation of the chlorides. From the data in Figure 10, it can be shown that above 900°C it is easier to reduce $NbCl_5$ or $NbCl_4$ to niobium than $SnCl_2$ to tin.

The equilibrium constant (Equation (5)) of the reduction reaction

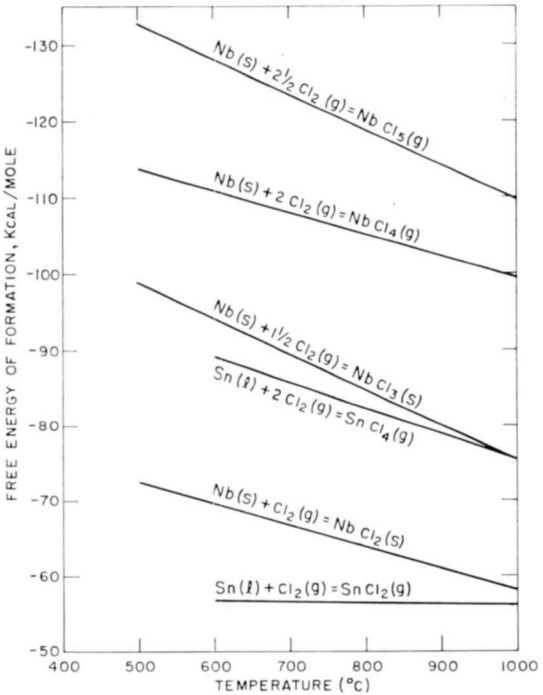

Fig. 10—Free energy of formation of niobium and tin chlorides.

(Equation (4)) is of considerable interest since it is helpful in establishing the operating conditions for deposition of Nb_3Sn. Theoretical values of K_p as a function of temperature could be obtained from data in Figure 10 if similar data for the free energy of formation of Nb_3Sn were available. Since this was not the case, an approximate experimental determination has been made. For this determination the gaseous reactants are assumed to be H_2, $NbCl_4$, and $SnCl_2$, with HCl as the gaseous product. The lower halides are used because, as has been previously stated, the higher metal halides formed are partially reduced in passing over the length of metal bed. This was determined by examining the color and physical state of condensed chlorination products.

The final product is assumed to be stoichiometric Nb_3Sn, so that its activity can be taken as unity.

In order to provide data for estimating the equilibrium constant of the reduction reaction, the normal operating flow rates of H_2, $NbCl_4$ and $SnCl_2$ were fixed, and the $NbCl_4$ to $SnCl_2$ ratio was held at 1:4. The flow rate of HCl gas was then varied for various set flow rates of H_2 until deposition on the ribbon disappeared. This point was assumed to be the point of equilibrium. Values of K_p for four different hydrogen flow rates were then calculated from the partial pressures of the reacting gases. The values of K_p at an estimated temperature of 950°C (Table IV) ranged from 2.2×10^{-3} to 9.4×10^{-3}, with an average of 5.2×10^{-3}.

Using the experimental equilibrium constant for the reduction reaction and the data in Figure 10, the free energy of formation of Nb_3Sn was found to be between −2.4 and −5.1 kilocalorie/mole. These values are probably not unrealistic since tin and niobium react easily at 950°C.

Table IV—Data on the Experimental Equilibrium Constant (K_p) at 950°C

% H_2 Flow Relative to Standard Flow	HCl/H_2	$K_p = \frac{(p_{HCl})^{14}}{(p_{NbCl_4})^3 (p_{SnCl_2}) (p_{H_2})^7}$
100	0.44	9.4×10^{-3}
117	0.40	5.0×10^{-3}
135	0.37	3.1×10^{-3}
154	0.34	2.2×10^{-3}

Properties of Vapor-Deposited Nb_3Sn

Vapor-deposited Nb_3Sn has been obtained under two appreciably different conditions—namely, the static deposition on ceramic substrates, which ordinarily requires several hours, and the continuous process on wires in which the deposit forms in about 2 minutes. The ratio of growth rates, approximately 1:10, is due to the different partial pressures of the reacting gases and temperatures of deposition employed in the two systems. Since the difference in growth rate has significant effects on the properties of the materials, both types of materials are considered in discussing the properties of the deposits.

Chemical Composition

Single-phase vapor-deposited niobium stannide can be formed over a range of compositions with both the static and the continuous processes.

Deposits grown on ceramics under conditions designed to yield stoichiometric material are typically 75.3 ± 0.3 atomic %Nb, as determined by gravimetric analyses of Nb and/or iodometric analyses of Sn. Details of the analytic procedures are described by Cheng and Bertin.[16] Optical microscopic examination of polished cross sections of this material, stained in the manner described by Picklesimer,[17] indicates the complete absence of a second phase (Figure 11). As previously mentioned, the deposits may be made Nb rich by adjustment of the $NbCl_5$ to $SnCl_2$ feed ratio.

Materials deposited on ribbon with little or no second phase present have been obtained with Nb concentrations ranging from 75.1 to 82.3 atomic %. The compositions obtained, and the conditions that influence the composition of the ribbon substrate, have been discussed in a previous section (see Figure 9).

The purity of vapor-deposited materials shows a strong dependence on the process used. Vapor-deposited materials are generally purer than the starting compounds with respect to all nongaseous impurities except for silicon, which is introduced from the quartz apparatus walls. Materials deposited by the slower static process and generally purer starting materials (powdered chlorides) tend to be considerably purer than the material deposited on ribbon by a process which uses less pure metal powders and commercial gaseous HCl and Cl_2. Mass-spectrographic results for the two types of Nb_3Sn deposits are given in Table V. Of the impurities listed only Si, F, Al and W are significantly higher in the statically deposited materials. The longer dwell time and higher temperature of the quartz apparatus is undoubtedly responsible for the Si. The difference in the F content may be attributed to the different etching treatments of the samples prior to analysis. The Al comes from the ceramic substrates, since Al_2O_3 is present in the steatite. Tungsten is one of the more abundant impurities in the $NbCl_5$ (500 ppm). An explanation for the comparatively high content of hydrogen in the ribbon deposits as compared to the static deposit is the fact that the ribbon is rapidly cooled as it leaves the deposition atmosphere, thereby quenching in dissolved hydrogen; in the case of the static deposit, hydrogen can diffuse out during slow cooling in an inert atmosphere.

Density

Materials grown statically under the conditions that yield nearly

[16] K. L. Cheng and E. P. Bertin, "Analytical Techniques for Determining the Composition Niobium Stannide," *RCA Review*, Vol. XXV, p. 379, Sept. 1964 (this issue).

[17] W. L. Picklesimer, Oak Ridge National Laboratory Report 2296, 1957.

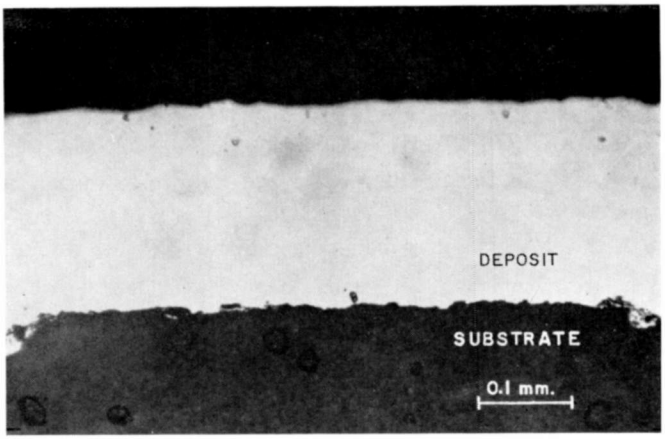

Fig. 11—Polished and anodized cross section of vapor-deposited Nb_3Sn.

Table V—Impurities Present in Typical Samples of Vapor-Deposited Nb_3Sn as Determined by Mass-Spectrographic Analysis (Impurities in ppm Atomic)

Element	Deposit on Ribbon	Deposit on Ceramic
O	1,000	1,000
Si	15	550
C	3,000	330
Cl	1,560	130
F	1	100
Al	36	100
H	9,000	100
Mg	9	33
S	15	25
Fe	45	20
Cu	130	15
W	<1	10
Ti	5	5
Na	120	4
Ta	3	3
Zr	2	2
B	12	<1
P	5	<1
Cr	55	<1
Zn	15	<1
As	3	<1
N	140	<1
All others*	<1	<1

* The ribbon deposits also showed the presence of noble metals.

stoichiometric Nb_3Sn exhibit densities between 8.82 and 8.92 gm/cc. This represents 98.8 to 100% theoretical density, assuming a lattice constant of 5.289 Å.[18]

Microstructure

Etched cross sections of the deposits on ceramics exhibit the distinctly columnar structure that is typical of many vapor-deposited metals.[19] No one crystallographic orientation predominates. If the material is grown rapidly in a halide-rich atmosphere, the columns grow perpendicular to the substrate surface with little contact between one another. It is this characteristic that limits the permissible growth rate for crack-free deposits.

Laminae in the plane of the substrate surface with linear densities as high as 5×10^3/cm are typically observed in etched, but not in anodized, cross sections. The source and nature of these laminae have not been established.

Lattice Constants

The lattice constants for vapor-deposited niobium stannide having the β-tungsten structure decrease with increasing Nb concentration, as shown in Figure 12. With sintered materials prepared at temperatures below 1200°C, there is no variation in the lattice constants with composition.[20] However, with sintering temperatures as high as 1800°C, a variation of lattice constants is observed[21] similar to that in vapor-deposited niobium stannide. Recent results on the Nb-Sn phase diagram indicate that there might not be a range of solubility of Nb in Nb_3Sn in materials sintered below 1200°C.[22] Hence, vapor-deposited niobium stannide with a range of solubility might be a metastable material that owes its existence to its rapid growth and to a slow rate of diffusion of niobium and tin atoms.

Transition Temperature and Lattice Disorder

The T_c of vapor-deposited niobium stannide was found to decrease

[18] S. Geller, B. T. Matthias, and R. Goldstein, "Some New Intermetallic Compounds with the 'β-Wolfram' Structure," *Jour. Amer. Chem. Soc.*, Vol. 77, p. 1502, 20 Mar. 1955.

[19] J. M. Blocher, Jr., "Chemical Vapor Deposition—A Rediscovered Tool for Molecular Engineering," *Battelle Technical Review*, Vol. 12, No. 3, p. 3, March 1963.

[20] H. G. Jansen and E. J. Saur, "Superconductivity in the System Niobium-Tin," *Proc. VII Intern. Conf. on Low Temp. Physics*, Toronto 1960, p. 380.

[21] T. D. Reed, H. C. Gatos, W. J. LaFleur, and J. T. Roddy, *Superconductors*, M. Tanenbaum and W. V. Wright, ed., Interscience Publishers, New York, 1962, p. 143.

[22] R. Enstrom, T. Courtney, G. Pearsall, and J. Wulff, *Metallurgy of Advanced Electronic Materials*, G. E. Brock, ed., Interscience Publishers, New York, 1963, p. 121.

with increasing niobium content for specimens deposited on wires[6] and on ceramics[4] as shown in Figure 13.*

Prior to the knowledge of the lack of solid solubility of Nb in Nb_3Sn in the sintered specimens,[22] a puzzling discrepancy existed between the composition dependence of T_c of the vapor deposited materials and of the sintered materials. According to Jansen and Saur,[20] for sintered materials with a nominal composition range between 75 and 80 atomic % niobium, T_c varied only about 0.3°K. The suspected cause of this discrepancy was thought to be lattice disorder of the type where some niobium atoms occupy normal tin sites and vice versa. Extensive lattice

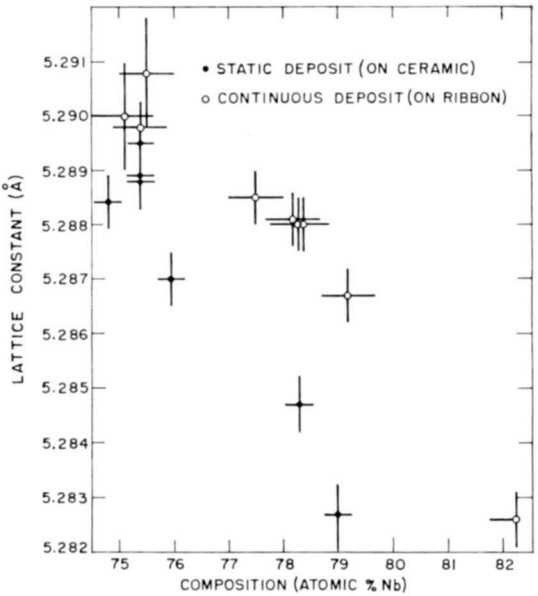

Fig. 12—Lattice constant versus composition of vapor-deposited niobium stannide.

disorder was indeed found in some specimens by measuring the intensity ratio of the (210) and (211) x-ray diffraction lines.[6] Data relating chemical composition, T_c and lattice disorder of several wire specimens are given in Table VI. It is interesting to note annealing the fifth specimen more than doubled the value of T_c. Subsequently,

* The relatively sharp transitions of the wire specimens is partly due to the geometry used. Since the coated wires are essentially continuous cylinders, the outer Nb_3Sn material shields the bulk of the sample. If the Nb_3Sn is removed from one side of the wire, transition widths are comparable to those seen on ceramics.

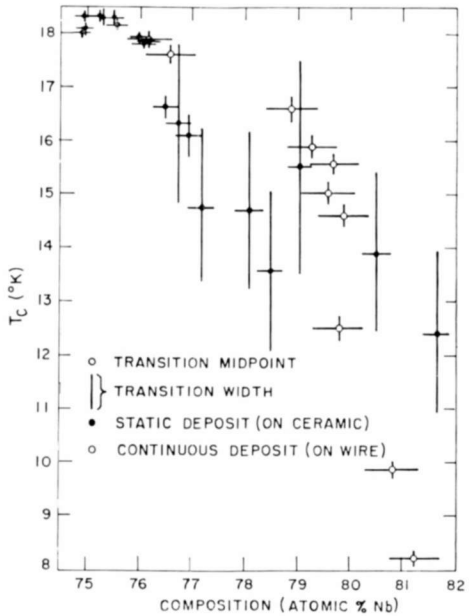

Fig. 13—Transition temperature versus composition of vapor-deposited Nb_3Sn.

all vapor-deposited materials with a low T_c have shown an increase in T_c upon annealing.

Since the evidence[22] indicates no solid solubility of Nb in sintered Nb_3Sn, there is some doubt concerning those conclusions drawn previously[6] about the effect of lattice disorder on T_c. The data in Table VI do not show a sufficient trend for deciding whether the lattice disorder

Table VI—Lattice Disorder in Vapor-Deposited Nb-Sn

Composition	T_c	Disorder
At. % Nb	°K	%
76.4	17.8	22
77.0	17.3	22
80.8	10.4	56
81.4	9.6	100
80.6	7.0	23
80.6*	16.0	2.6

* Specimen removed from the substrate and annealed for 37 hours at 1100°C.

or the chemical composition is primarily responsible for the changes in T_c.

Thermal Expansion

Thermal expansion of statically deposited Nb_3Sn has been measured by high-temperature x-ray crystallographic techniques.[23] The resulting lattice constants versus temperature are plotted in Figure 14. The average coefficient of expansion obtained from these data for the temperature range from 25° to 700°C is 9.8×10^{-6} per °C.

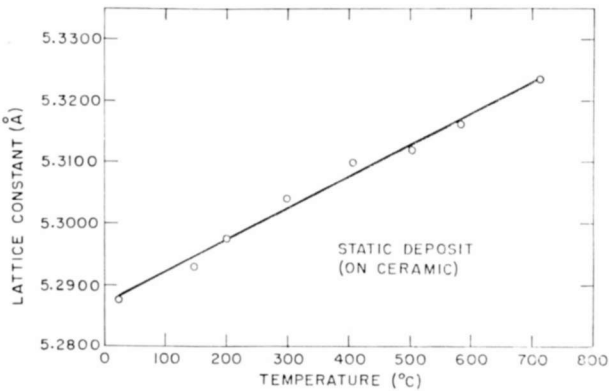

Fig. 14—Lattice constant of vapor-deposited Nb_3Sn versus temperature.

Conclusions

1. Techniques are described for depositing Nb_3Sn by simultaneous hydrogen reduction of gaseous niobium and tin halides on various substrates including narrow and wide metallic ribbon, and flat and cylindrical ceramics. These deposits have found use in research and in the construction of high-field magnets.

2. In the case of metallic substrates, platinum and other noble metals have been found to aid in the nucleation of Nb_3Sn, but deposits have also been successfully prepared on various high-strength nickel-base alloys. Adherent Nb_3Sn deposits have been achieved on magnesium silicate ceramics.

3. The formation of Nb_3Sn by this technique has been observed in the temperature range of 675°C to 1600°C. The equilibrium constant (K_p) for the reaction $3NbCl_4 + SnCl_2 + 7H_2 \rightleftharpoons Nb_3Sn + 14HCl$ at

[23] P. Chiotti, "Adaptation of a Geiger-Counter X-ray Diffractometer for High-Temperature Investigations," *Rev. Sci. Instr.*, Vol. 25, p. 683, July 1954.

950°C has an approximate value of 5×10^{-3} and it increases with temperature. The estimated value of the free energy of formation of Nb_3Sn at this temperature is between −2.4 and −5.1 kilocalories/mole.

4. Single-phase niobium stannide deposits having the β-tungsten structure have been prepared with a composition range of 75.1 to 82.3 atomic percent niobium when deposited in the range of 900° to 1200°C. The density of stoichiometric deposits is greater than 99% of the theoretical density.

5. The lattice constant decreases with increasing niobium concentration from 5.290 to 5.282 Å for compositions of 75.1 to 82.3 atomic % Nb.

6. The corresponding transition temperature range for the above composition range is 18.3° to 7°K. Materials with low T_c show substantial increases in T_c when annealed at 1100°C.

7. Extensive lattice disorder has been found in some niobium-rich deposits; however, its effect on transition temperature cannot be distinguished at this time from that of the composition variation.

8. The average linear thermal coefficient of expansion of Nb_3Sn determined by x-ray diffraction in the range of 20° to 700°C is 9.8×10^{-6} per °C.

ACKNOWLEDGMENTS

The authors are grateful to F. D. Rosi for his constant support and encouragement in this work, and to G. D. Cody for many constructive discussions. Acknowledgments are due to J. L. Cooper for making significant contributions to the development of the process, and to R. Berger and F. Dougherty for their efforts in the preparative phase of the study. The authors are also thankful to E. Bertin, B. Goydish, and R. Paff for the performance of chemical and x-ray analyses.

HIGH-TEMPERATURE PHASE EQUILIBRIUM AND SUPERCONDUCTIVITY IN THE SYSTEM NIOBIUM–TIN*

By

L. J. Vieland

RCA Laboratories
Princeton, N. J.

Summary—*Some high-temperature aspects of the phase diagram of the Nb-Sn system have been investigated. The solubility of Nb in Sn is low at moderate temperatures, reaching about 5 at. % at 1600°C. The β-tungsten phase becomes increasingly Nb rich at high temperatures, reaching a terminal composition of 81.5 at. % Nb, and melting peritectically at 2130°C. Diffusion in the β-tungsten phase appears to be very slow, and it is found that in compacts sintered much below 1800°C, equilibrium is not reached in short-term anneals. Instead, the composition of the β-tungsten phase is always close to Nb_3Sn, and any Nb present above 75% remains undissolved. In compacts sintered above 1800°C, equilibrium is reached in a reasonable time, and both the lattice constant and superconducting transition temperature are functions of composition. This is in contrast to most previous results on sintered material, but is in agreement with results for vapor-deposited materials. A sharp decrease in T_c is found near 80 at. % Nb, and no evidence of disorder was found in a sample with $T_c \simeq 5.6°K$.*

Introduction

Interest in Nb_3Sn as a high-field superconductor has prompted a number of studies on phase equilibria and metallurgical aspects of the Nb-Sn system and their possible relation to various physical properties associated with superconductivity. A number of phases intermediate between the β-tungsten (nominally Nb_3Sn) phase† and the terminal solutions have been discovered, and their structure and stability ranges have been worked out (e.g., Ref. (1)). Somewhat unexpected, however, is the fact that several important questions concerning behavior of the system above 950°C, where the β phase is the only stable intermetallic, and where most metallurgical operations (e.g., preparation and annealing) are carried out, have not yet been answered in a completely satisfactory manner. For example, in the case of phase equilibria, it is not certain whether the β phase melts congruently or peritectically, nor what the composition of the solid is

* This work was supported by the Air Force Materials Laboratory, Research and Technology Division, Air Force Systems Command, Wright-Patterson Air Force Base, Ohio, under Contract No. AF33(657)-11208.

† Hereinafter called the β phase. The α phase is the niobium-rich terminal solution.

near the melting point.[1-3] Even less is known about the tin-rich liquidus at high temperatures.

Of perhaps greater general interest is the problem of the possible homogeneity range of the β phase, and the relationship between composition and superconductivity. For the most part, metallurgical techniques have not proven satisfactory in attacking this problem, although the work of Reed *et al*[4] is a notable exception. One can suppose that real insight into this matter was recently provided by data obtained on vapor-grown materials,[5] but in any case, it is desirable to be able to correlate data for chemically and metallurgically prepared Nb_3Sn.

Finally, a matter of great interest in any materials investigation related to the superconducting properties of the β phase is the possibility of an order–disorder transformation. This possibility was first investigated for β-tungsten compounds by Geller *et al*,[6] who found an ordered structure for Nb_3Sn. Hanak *et al*[7] investigated the problem with Nb_3Sn-coated wires prepared by vapor deposition, and subsequent work on metallurgical specimens was done by Enstrom *et al*,[1] and Reed *et al*.[4] Again, critical evaluation of the data does not reveal a consistent picture, although an appreciable body of useful information has been accumulated.

EXPERIMENTAL

Sintered Compacts

Compacts were prepared by mixing −200 mesh niobium powder with Fisher "finest powder" tin and pressing in a single-action press to about 50 tons per square inch. The specimens were in the form of

---

[1] R. Enstrom, T. Courtney, G. Pearsall, and J. Wulff, *Metallurgy of Advanced Electronic Materials*, G. E. Brock, Ed., Interscience, New York, 1963.

[2] L. L. Wyman, J. R. Cuthill, G. A. Moore, J. J. Park, and H. Yakowitz, "Intermediate Phases in Superconducting Niobium-Tin Alloys," *Jour. Res. Nat'l. Bur. Std.*, Vol. 66A, p. 351, July-Aug. 1962.

[3] T. G. Ellis, *Niobium-Tin-Aluminum Alloy Studies*, Dissertation, Univ. of Iowa, 1962, Univ. Microfilms, Ann Arbor, Mich.

[4] T. B. Reed, H. C. Gatos, W. J. LaFleur, and J. T. Roddy, *Metallurgy of Advanced Electronic Materials*, G. E. Brock, Ed., Interscience, New York, 1963.

[5] G. W. Cullen, "Preparation and Properties of Niobium Stannide on Insulating Substrates," *Trans. Metallurgical Soc.*, in press; see also J. J. Hanak, K. Strater, and G. W. Cullen, "Preparation and Properties of Vapor-Deposited Niobium Stannide," *RCA Review*, Vol. XXV, p. 342, Sept. 1964 (this issue).

[6] J. Geller, B. T. Matthias, and R. Goldstein, "Some New Intermetallic Compounds with the 'β-Wolfram' Structure," *Jour. Amer. Chem. Soc.*, Vol. 77, p. 1502, March 20, 1959.

[7] J. J. Hanak, G. D. Cody, P. R. Aron, and H. C. Hitchcock, *High Magnetic Fields*, B. Lax and H. H. Kolm, Ed., J. Wiley and Sons, Inc., New York, 1962.

1/2-inch-diameter cylinders, 1/8 to 1/4 inch thick. For temperatures below 1250°C sintering was carried out in evacuated quartz ampoules. After sintering the ampoules were removed from the furnace and cooled in air. For higher-temperature work, induction heating in a helium atmosphere was used. The samples were contained in either a ceramic or niobium crucible resting inside a tantalum susceptor. In the very-high-temperature runs it was found necessary to remove the outer skin of the compacts, since its composition was different from that of the bulk. This could be seen either by x-ray analysis, which showed a change in lattice parameter near the surface, or in some cases visually, since the skin was Nb-rich (α) solid solution. The composition of the homogeneous core was checked by chemical analysis. Cooling was effected by shutting the power off abruptly, but without removing the sample from its nest inside the susceptor and radiation shields. A period of 5 to 15 minutes elapsed, therefore, before the sample cooled below red heat, depending on the initial temperature.

Castings

Melts were prepared in a 450-kc induction furnace by direct coupling into a charge of niobium and tin rods, again under helium to prevent excessive loss of tin by evaporation. The cleanest ingots were obtained in slip-cast thoria crucibles, although oxygen contamination could not be entirely eliminated. However, most of the runs were made in pressed calcia stabilized zirconia crucibles, because of its superior thermal shock resistance. In order to identify extraneous phases introduced by reaction with the crucible, a few runs were also made in niobium crucibles. All ingots were analyzed chemically for niobium content after melting.

Thermal Analysis

The liquidus was determined primarily from thermal arrests on cooling curves. The experimental arrangement was similar to that described by Hume-Rothery *et al.*[8] Temperatures were measured by sighting an optical pyrometer into a slip cast zirconia sight tube with a 3/16-inch bore. Immersion of the sight tube in the melt to a depth of about five times its bore was found to be sufficient to ensure black-body conditions. Losses in the reflecting prism were taken into account by measuring the loss at 1300°C with the aid of a black-body furnace and applying the appropriate temperature dependence correction. Excellent agreement (±10°C) was obtained between the measured platinum point and the scale provided with the instrument. The thermal-

[8] W. Hume-Rothery, J. W. Christian, and W. B. Pearson, *Metallurgical Equilibrium Diagrams*, Rheinhold Pub. Co., New York, p. 144, 1953.

arrest method was satisfactory for concentrations greater than 10 at.% Nb. Below this region the arrests were very weak, and weight-loss methods were used.

Melting-point determinations were also made on a number of cast and sintered ingots containing 75 to 85% Nb. The principal difficulty in making such measurements is in ensuring true black-body conditions in the furnace and still being able to observe the sample. This difficulty was circumvented by using a rectangular sample that fitted loosely into a black-body hole drilled in a niobium rod. The rod served as the crucible, and rested inside a tantalum susceptor. Before melting, the bar extended to near the top of the hole, so that the top surface appeared darker than the space between the sample and the wall. By sighting the tip of the (curved) filament into this space with the sample in the field of vision, melting was readily observed under true black-body conditions. In many cases macroscopic melting was not observed at temperatures above the melting point, particularly for the very Nb-rich ingots. However, a change in microstructure was always found, although the external structure of the sample remained intact.

Microstructure

The anodization technique of Picklesimer[9] was found to be indispensible in revealing a multitude of extraneous phases which would be very difficult to see under ordinary microscopic examination. No attempt was made to standardize the anodizing procedure, except for the use of a 22.5-volt battery, it being sufficient to develop some color in the specimen to differentiate the phases. One phase present in varying amounts in all the specimens was the same as that observed by Enstrom *et al*[1] and identified by them as NbO. This phase anodizes light blue, and in castings showing an inordinate amount of this phase the diffraction pattern of NbO was observed.

Measurements

Lattice parameters were obtained by averaging the results for the three high-intensity back-reflection peaks using Cu$K\alpha$ radiation and a $36/\pi$ cm camera. Unless otherwise noted, the lines were sufficiently sharp to give lattice constants to $\pm.001$ Å or better.

Order–disorder measurements were made with a Siemens diffractometer using an oscillating sample and scanning at 1/8 degree per minute. Net integrated intensities were usually measured for several

[9] W. L. Picklesimer, Oak Ridge National Laboratory Report 2296, 1957.

peaks to provide an internal check on any pair. The precision is believed to be between 5 and 10%.

Transition temperatures were measured by an a-c inductance method described by Cooper.[10] Chemical analysis was used to check the composition of all ingots where processing was felt to have resulted in a loss of tin. The methods of analysis are described by Cheng and Bertin.[11]

Results

The results of typical sintering and casting experiments are shown in Table I. Phase identification was made by microscopic examination of anodized specimens. Approximate percentages are given where relevant. In the case of sample A-O, area counting was employed to get an accurate volume concentration of the α phase. The value found corresponds closely to that expected for a mixture of Nb_3Sn and Nb of overall composition 79%. The presence of tin in samples A-1-1 and HS-2 is an indication of incipient melting. Sample α-1 is close to the terminal solubility of tin in the α phase, which must lie between 10 and 12.5% (α-2). The Nb present as a second phase in predominantly β-phase materials has a diffuse diffraction pattern that makes an accurate determination of the lattice parameter virtually impossible. This is also the case in specimen α-1, which was single phase and of uniform microhardness (~550 kilogram/mm^2 Vickers).

Good diffraction patterns were obtained on melted material, although the variation of lattice constant with melt composition and the fairly rapid cooling rates employed would indicate a solid of variable composition. Microstructures of three ingots are shown in Figures 1-3. In specimen 11-11 the matrix is β and the bright regions are tin. The crystalline material dispersed along grain boundaries is most likely NbO. Low-temperature intermetallic phases can be seen outlining the tin areas. An equivalent melt made in an Nb crucible shows essentially no NbO. The structure of specimen C-14, which is typical of ingots near 80% Nb, is somewhat obscure. In this case the oxygen appears to be trapped primarily in the core of the grains, while the grain boundaries are relatively oxygen free. Although the boundary between the core (speckled region) and periphery of a grain is often very sharp, no change in microhardness is observed across the boundary. The

---

[10] J. L. Cooper, "Transition Temperature of Niobium Stannide," *RCA Review*, Vol. XXV, p. 405, Sept. 1964 (this issue).

[11] K. L. Cheng and E. P. Bertin, "Analytical Chemical Techniques for Niobium Stannide," *RCA Review*, Vol. XXV, p. 379, Sept. 1964 (this issue).

Table I—Preparation and Properties of Sintered and Cast β-Tungsten Niobium Stannide

Sample Type	Sample #	Composition (At. % Nb)	Temperature (°C)	Time (Hours)	Lattice Constant (Å)	Major Transitions (°K)	Phases other than β-tungsten
Sintered	A-0	79	950	16			Nb, 22%
	A-1-1	76	1975	3	5.2866	17.6	Sn
	A-1-2	79	1975	3	5.2839	15	none
	A-1-3	82	1975	3	5.2814	<7	Nb, <5%
	P-2-3	86	950	274	5.291 ± .002		Nb
	MS-1	85	1500	4.5	5.285 ± .002	7.5, 8-16	Nb
	MS-2	80	1500	4.5	5.2880	13, 14-17.3	Nb
	MS-3	75	1190	120	5.2903		Nb, 5%
	MS-4	87.5	1190	120	5.285 ± .002	6-12, 13-18.1	Nb
	HS-1	75	1750	2			Nb, <5%
	HS-2	75	1800	2		17.6	Sn
	α-1	90	2150	.1	3.30 — 3.33		Nb only
	α-2	87.5	2150	.1			Nb + β
Cast	11-11	60			5.2869	5-16, 17	Sn, NbO, Nb_xSn_y
	C-14	80			5.2834		Sn, NbO
	12-17	85.5			5.2803		Nb, trace NbO

Fig. 1—Microstructure of 11-11, 60% casting (×150).

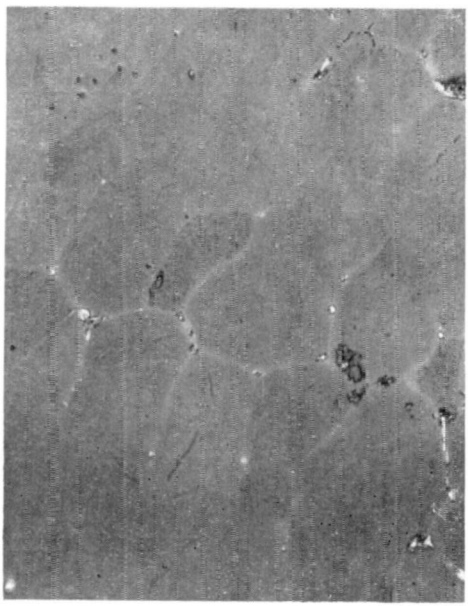

Fig. 2—Microstructure of C-14, 80% casting (×150).

Fig. 3—Microstructure of 12-17, 85.5% casting (×150).

diffraction pattern shows single-phase material, and the back reflection peaks show only a single maximum. Again, a small amount of tin can be found in the grain boundaries. Figure 3 shows an Nb-rich melt obtained from an Nb crucible. The dendritic α phase is embedded in a matrix of β, with a small amount of NbO at the interface.

Results of order–disorder measurements are shown in Table II. The actual compositions of the β phase of samples A-1-3 and MS-4 differ from the nominal composition, but all are close enough to 80% Nb so

Table II—Observed versus Theoretical X-ray Intensity Ratios

$I_{hkl}/I_{h'k'l'}$	A-1-2	A-1-2*	A-1-3	A-1-3*	MS-4	Order	Disorder
210/211		1.03	1.09	1.19	1.13	1.115	1.355
222/320	.280	.29	.318		.32	.298	.392
222/321	.135		.149		.11	.139	.215
320/321	.483		.468	.469	.36	.460	.563
420/421				.698		.646	.521
421/332				1.71		1.70	2.07

* Annealed for 60 hrs. at 950°C.

that negligible errors are introduced by comparing the ratios to those calculated for the 80% case. The theoretical values are taken from the compilation of Enstrom *et al.*[1] No sensible change in lattice constant or order–disorder ratios was observed after annealing. All samples must be considered ordered within experimental error.

The phase diagram of the Nb-Sn system above 1200°C is shown in Figure 4. The tin-rich liquidus is drawn through the thermal-arrest points only. The curve as drawn between 60 and 90% tin is roughly the lower envelope of results obtained by weight loss, which show considerable scatter. In most cases melting points were determined by

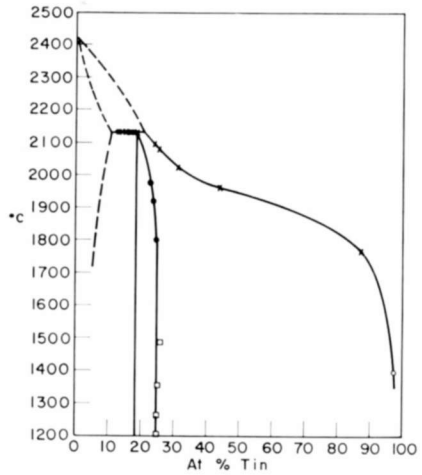

Fig. 4—Phase diagram of the Nb-Sn system above 1200°C.
x—thermal arrests
•—melting points
□—single crystals
o—weight loss

observing the microstructure of specimens heated to known temperatures, although materials close to 80% Nb showed complete melting at the peritectic temperature. The peritectic temperature, as determined from both melting point and thermal arrest methods, is 2130 ± 15°C. Ellis[3] obtained 2130 ± 20°C, but the agreement is somewhat fortuitous, since he melted 75% Nb compacts. Reliable thermal arrests were not obtained for precipitation of the α phase, although a rounding from the peritectic point extending up to 2180°C was observed for an 86% melt. The composition of the β phase at the peritectic was determined from the lattice constant of Nb-rich ingots (e.g., sample 12-17). The solubility of Nb in the β phase at lower temperatures may be somewhat smaller (see below), but the solidus has been taken as being tempera-

ture insensitive within experimental error. The tin-rich side below 1500°C was determined by analysis of crystals grown from tin solutions by a thermal gradient technique. The departure from stoichiometry above ~1300°C may be attributed to a superficial layer of phases of higher tin concentration formed as the furnace cools. This is supported by the appearance of very weak extra diffraction lines for these crystals. Recent work by Maier and Wilhelm[12] on similar material, from which the surface layers were etched off, indicates that the limiting composition is less than 75% (72.8 at. % Nb at 1400°C). However, comparison of their data with that of the present work and Refs. (5) and (7) suggests a systematic discrepancy in analysis. Hence, for the present the solubility limit is taken to be 75% Nb.

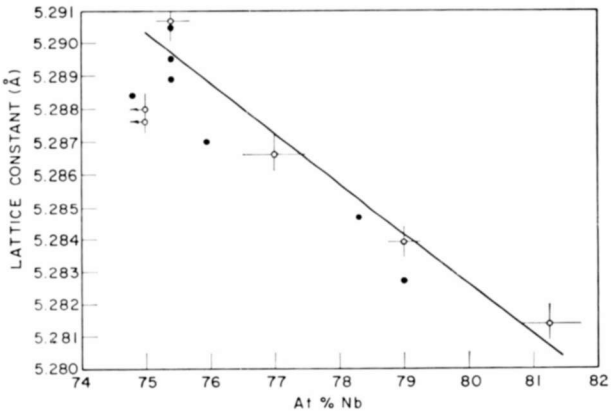

Fig. 5—Lattice parameter versus composition of the β-tungsten phase. Open circles, this work; solid circles, Ref. (5).

Lattice constants as a function of composition are shown in Figure 5. Reasonable agreement among vapor-grown, solution-grown, and sintered material is observed. The two samples that analyzed less than 75% Nb are shown as being stoichiometric. A possible maximum in lattice constant is seen near 75% Nb.

Discussion

Solid–Liquid Equilibrium

The very low solubility of Nb in Sn at relatively high temperatures is no doubt a reflection of the large difference in cohesive energies of the two elements. The inflection in the liquidus and the rapid decrease

[12] R. G. Maier and G. Wilhelm, "Neuere Ergebnisse an Nb_3Sn," *Z. Naturforschg.*, Vol. 19a, p. 399, March 1964.

of solubility below 1950°C are indeed indications of near immiscibility. The exact position of the liquidus at the peritectic is subject to some uncertainty, about 2%.

The β-Tungsten Phase

An important feature of the lattice-parameter data is that the variation of lattice constant with composition for compacts sintered at high temperatures, e.g., 1975°C, agrees closely with that obtained for chemically deposited films grown at low temperatures (~1000°C). On the other hand, lattice constants of compacts sintered at temperatures near 1000°C are essentially independent of composition, and characteristic of the tin-rich solubility limit (Nb_3Sn).

At first glance, the metallurgical evidence favors the interpretation of a lack of solid solubility (of Nb in Nb_3Sn) at low temperatures. Enstrom *et al*[1] found that the lattice constant, as measured by peak height position for high-order reflections, shifted to lower values with increasing Nb content for compacts sintered above 1300°C, while similar data at 1200°C showed no shift. Significantly, the downward trend in lattice constant starts at concentrations of more than 85% Nb, although the 80% compacts still contained excess Nb. This suggests that the problem is one of kinetics rather than solubility; that is, the peak shift is not observed unless the ratio of Nb to β-phase is increased to the point where the diffusion layers surrounding the Nb particles occupy sufficient volume to be visible to x-rays. If this assumption is valid, then the equilibrium lattice constant must be equal to, or less than, the observed peak height value. The value reported for 1300°C and 1400°C, 5.283 Å, is comparable to the lattice constants obtained for Nb-rich vapor-grown material. The shift in peak height should, therefore, be associated with a broadening of the diffraction lines. This was observed in samples MS-1 and MS-2. As indicated in Table I, the diffraction pattern for the former was diffuse, showing very weak lines in the back-reflection region and a great deal of incoherent scattering. Further evidence of sluggishness of the diffusion process can be seen in sample HS-1, where excess Nb was found in a 75% compact sintered at 1750°C.* The difficulty in extending the solubility measurements to lower temperatures can be seen by assuming some reasonably high activation energy for the diffusion process. A value of 4.6 eV, for example, would necessitate an order-of-magnitude increase in time to extend results obtained at 1300°C down to 1200°C. Sample MS-4 shows the expected behavior, with a broad diffusion pattern. The {611} peak,

* Excess tin is present in such materials, but it is difficult to perceive.

for example, occurs at $2\theta = 127.95°$ (5.284 Å) and broadens towards higher angles, completely obscuring the $K\alpha_2$ peak.

If solid-state diffusion is indeed a very slow process with negligible effect in the sintering process, then it must be inferred that the formation of the β-phase takes place from the liquid phase. Hence, the solid is always formed by precipitation from a tin-rich melt, and shows the lattice constant appropriate to the tin-rich solubility limit. When there is no further contact between Nb particles and the liquid phase, the reaction effectively ceases.

Order–Disorder

It is clear from the preceding discussion that the superconductive properties of sintered material must be correlated with the lattice parameter of the β phase, and not the nominal composition of the compact. However, there is still the question of whether any such correlation is a function of composition only, or reflects a change in the ordering of the Nb_3Sn superlattice.*

This possibility was first investigated by Hanak *et al*[7] on vapor-deposited material. These authors found a dependence of T_c on composition that has been verified semiquantitatively by more recent work.[5] However, the conclusion that disorder is responsible for low T_c is not warranted by the data. Enstrom *et al*[1] made extensive order–disorder measurements on sintered specimens; in the light of the preceding discussion, their results may be taken as evidence that disorder is not observed in furnace-cooled specimens sintered at temperatures up to 1400°C, nor in stoichiometric material quenched from 1100°C. The most satisfactory results were obtained by Reed *et al*,[4] who also investigated specimens sintered at higher temperatures. Two separate experiments must be distinguished. In the first, which involved a 1500°C anneal of an 80% compact, the specimen exhibited a low T_c (7.2°K). On subsequent annealing at 1200°C, T_c was restored to 18.0°K. Order–disorder measurements were not reported for this sample, and the lattice constant (5.287 Å) does not correspond to the equilibrium value for 80%. In addition, the high T_c observed after annealing is characteristic of material close to stoichiometry (see Reference (5)), although no evidence of disorder was found by these authors in 76% compacts quenched from 1800°C. In the second experi-

* Obviously, any increase in Nb concentration over 75% involves a decrease in order, unless more extended superlattices are formed. However, we refer here only to disorder in the Nb sublattice, which is related to the simple nonstoichiometric ordered lattice through a first-order phase change; see F. C. Nix and W. Shockley, "Order–Disorder Transformations in Alloys," *Rev. Mod. Phys.*, Vol. 10, p. 1, Jan. 1938.

ment of interest, an 80% Nb sample, sintered at 1800°C and with a lattice constant of 5.282 Å, appeared completely disordered by x-ray analysis and had a transition temperature of 5.6°K. It was not reported that T_c could be increased by annealing. It is therefore seen that while x-ray evidence of disorder has been obtained, interpretation of the transition-temperature data in terms of disorder is not straightforward.

That the present work does not reveal any evidence of disorder may be attributable to a lower quench rate than that employed by Reed *et al*, and does not necessarily contradict the earlier work. However, the important result would appear to be the decrease of transition temperature with increasing Nb content for fully ordered compacts with a homogeneous β phase (A series). This variation is in semiquantitative agreement with results obtained on vapor-deposited materials.[5] The rapid decrease in T_c above 79 at. % Nb implies that significant changes in the electronic structure occur over a very narrow composition range near the phase boundary, in the absence of any lattice rearrangement.

Acknowledgments

The author is indebted to H. Gossenberger and A. Wicklund for assistance in carrying out this work, to J. L. Cooper for transition-temperature measurements, and to R. Paff for x-ray analysis.

ANALYTICAL TECHNIQUES FOR DETERMINING THE COMPOSITION OF NIOBIUM STANNIDE

By

K. L. Cheng* and Eugene P. Bertin†

Summary—*Chemical and x-ray spectrometric methods have been developed for analyzing Nb_3Sn. In the chemical methods, niobium is determined as niobium pentoxide, Nb_2O_5, after volatilizing the tin as its bromide, or it may be determined as peroxyniobate complex with hydrogen peroxide; tin is determined iodometrically. The x-ray spectrometric method employs a ratio method in which the net intensities of x-ray spectral lines of niobium and tin are measured and their ratio calculated. The x-ray method is particularly useful in analyzing Nb_3Sn-coated metal ribbon and ceramic plates.*

Introduction

THE BINARY niobium–tin alloy Nb_3Sn is superconducting below 18°K. Since small variations in its composition affect its superconducting properties, accurate analytical methods are needed for the control of its preparation. No analytical methods for the analysis of such alloys are reported in the literature. This paper reports both chemical and x-ray spectrometric methods.

Chemical Methods

In the chemical methods, niobium is determined gravimetrically as niobium pentoxide after volatilization of the tin as its bromide; niobium may also be determined photometrically as the peroxyniobate complex with hydrogen peroxide in concentrated sulfuric acid. Although pure tin can be titrated with ethylenediaminetetraacetic acid (EDTA), as has been noted by various workers, or by N-hydroxyethylenediaminetriacetic acid (HEEDTA) at *p*H 2-5.5, niobium has now been found to interfere. Good results were obtained with an iodometric procedure after reduction of tin(IV) by iron and antimony without separation of niobium, which is kept in solution with fluoboric acid.

Gravimetric Procedure for Niobium

Using a semimicrobalance, an Nb_3Sn sample (50-200 mg niobium) is weighed into a 50-milliliter platinum crucible (with its cover). Five

* RCA Laboratories, Princeton, N. J.

† RCA Commercial Receiving Tube and Semiconductor Division, Harrison, N. J.

milliliters of 8*M* HNO_3 followed by 5-6 drops 48% HF is then added, and the crucible is covered and gently heated. After dissolution, about 2 milliliters concentrated H_2SO_4 is carefully added. With the crucible 1/3 uncovered, the mixture is evaporated to strong fumes. After cooling, about 4 milliliters 48% HBr is added, and the mixture is evaporated on a hot plate to dryness, and then the crucible is ignited (covered) over a Meker burner. The crucible, contents, and cover are weighed. The relevant gravimetric factor $2Nb/Nb_2O_5$ has the value 0.69904.

Photometric Procedure for Niobium with Hydrogen Peroxide

Using a semimicrobalance, an Nb_3Sn sample (6-8 mg niobium) is weighed into a 100-milliliter volumetric flask. About 20 milliliters concentrated H_2SO_4 is added and the mixture is evaporated on a hot plate to strong fumes until dissolution is complete. It is then cooled, 0.5 milliliter 30% H_2O_2 is added, it is cooled again under tap water, and diluted to mark with concentrated H_2SO_4. The absorbance at 365 mμ is measured against a reagent blank. A calibration curve is prepared with known amounts of niobium metal in a similar manner.

Iodometric Procedure for Tin

A weighed Nb_3Sn sample (5-30 mg tin) is dissolved with gentle heating in a platinum dish with 5 milliliters 8*M* HNO_3 and 4-5 drops 48% HF, and the dish is covered. After dissolution is complete, the cover is rinsed with minimum amounts of water, 6 milliliters concentrated H_2SO_4 is carefully added, and the mixture is evaporated to strong fumes. After cooling, the mixture is transferred to a 500-milliliter conical flask, rinsed with 40 milliliters concentrated HCl and 50 milliliters water, and 100 milliliters more of water and 5 milliliters 48-50% HBF_4 are added. Eight grams of reduced iron (powder) and 0.5 gram antimony metal (granular) are added. The flask is closed with a 2-hole stopper, one hole being fitted with a 1/4-inch glass tube connected to a CO_2 source via rubber tubing, and the other open as a gas outlet and for the subsequent insertion of a buret tip. The mixture is gently boiled for 40-45 minutes while passing in CO_2 slowly. On completion of the boiling step, the CO_2 flow is increased and the flask is cooled in water and ice to 10-15°.

Five milliliters 10% KI solution and 5 milliliters 1% starch solution are added to the cooled solution through the stopper hole, using a pipet. The rubber tubing from the CO_2 source is disconnected and immersed in a beaker containing $NaHCO_3$ solution. With the tip of the buret in the stopper-hole, titration with 0.01*N* iodate-iodide solution is imme-

diately carried out to an end point color change of light green to dark purple. The iodate-iodide solution is standardized against pure tin under the conditions of this procedure.

Discussion and Results

It is known that microgram amounts of tin can be separated quantitatively from most metals, but poor results were obtained even in the milligram range in its separation from niobium. In contrast, tin can be completely removed by volatilization as its bromide without loss of niobium. No accurate, reliable titrimetric method is known for niobium. The gravimetric method, here described, is simple and highly

Table I—Gravimetric Determination of Nb in Synthetic Nb-Sn Mixtures

Niobium Concentration (%)		
Present	Found	Difference
19.88	20.09	+0.21
30.46	30.30	−0.16
47.64	47.68	+0.04
58.86	58.64	−0.22
66.91	66.74	−0.17
77.91	77.39	−0.52
90.40	90.22	−0.18
99.70	99.46	−0.24
none*	none	0.00

* 100% tin

accurate, and requires about 2 hours. Some representative results are given in Table I. The amount of hydrobromic acid added should be sufficient to volatilize all tin present.

The simple hydrogen peroxide photometric method for niobium also gives good results if carried out carefully using a calibration curve prepared at the same time. The amount of tin present in Nb_3Sn does not interfere, although hydrogen peroxide forms a colorless complex with tin. Representative results are given in Table II. The principal objection to this method is the use of concentrated sulfuric acid.

The Nb_3Sn alloys in the 10-milligram range are easily dissolved with concentrated sulfuric acid on fuming. For larger quantities, difficulties were encountered with the formation of bluish niobium(III) sulfate; this is slightly soluble in concentrated sulfuric acid, with part of this acid being decomposed into sulfur dioxide and elemental sulfur. Niobium–tin alloys can be rapidly decomposed with nitric-acid–

hydrofluoric-acid mixture, but the use of such a mixture in photometric procedures often caused the peroxyniobate complex to be unstable, forming gas bubbles on the walls of the cell.

In the photometric procedure, care should be taken to destroy any organic matter that might be present as a contaminant in the volumetric flask used, since charring with sulfuric acid colors the solution. For best results the flask, after cleaning and drying, should either be ignited to remove any organic matter or be pretreated by heating with sulfuric acid to strong fumes.

Table II—Comparison of Gravimetric and Photometric Methods for Determining Nb in Nb-Sn Alloys

Niobium Concentration (%)		
Gravimetric	Photometric	Difference
69.90	70.16	+0.26
70.81	71.96	+1.15
71.10	71.85	+0.75
71.22	71.34	+0.12
71.29	71.88	+0.59
71.44	70.62	−0.82
71.54	70.76	+0.78
71.77	70.96	−0.81
72.18	71.63	−0.55

The differential spectrophotometric peroxy method for niobium is stated[1] to have an accuracy within ±0.1%. Application of this method to the analysis of Nb_3Sn was unsuccessful because it requires a large amount of sample. Also, the method requires sample decomposition with nitric acid and hydrofluoric acid followed by color development with sulfuric acid and phosphoric acid. The presence of these acids, except sulfuric, tends to decrease the stability of the peroxyniobate complex. It was found that niobium forms an intensely yellow color with ascorbic acid in a weakly acidic medium in the presence of HEEDTA, which forms a water-soluble colorless complex with tin and with many polyvalent metals in both acidic and alkaline media. Study of this reaction for the determination of niobium in the presence of tin is in progress.

Niobium is not easily reduced by iron or antimony; therefore, its presence does not interfere in the iodometric determination of tin,

[1] H. O. Backer, V. R. Wielerkehr, and G. W. Goward, *U.S.A.E.C. Rept. WAPD-204*, Sept. 1958.

provided that it is kept in solution. The results presented in Table III confirm this statement. Niobium in large amounts is easily hydrolyzed if insufficient sulfuric acid is present. Such hydrolysis causes low recovery of tin because of its coprecipitation. Addition of fluoboric acid or tartaric acid prevents this hydrolysis and does not interfere in the iodometric finish.

In the present work, reduced iron powder with a small amount of antimony is used for the reduction of tin(IV). Most procedures recommend standardization of the iodate or iodine solution against pure tin under the experimental conditions. When this is done in the present case, the results for tin were excellent, as shown in Table III, and reproducible. If the iodate-iodide solution was standardized against a thiosulfate solution, the results for tin were about 1.5% low.

Table III—Iodometric Determination of Sn in Presence of Nb

Millequivalents Tin		Error	Nb Present
Taken	Found	(%)	(Millimoles)
0.1322	0.1321	−0.07	0.5
0.2613	0.2616	+0.11	0.5
0.3257	0.3250	−0.21	0.6
0.4457	0.4453	−0.09	0.6
0.4806	0.4806	0.00	0.6

Since Nb_3Sn is a binary alloy containing only small amounts of impurities (to the total extent of 0.2%), for some control purposes it suffices to determine either niobium or tin and obtain the other by difference. However, it is sometimes desirable to determine both elements. The iodometric method for tin is accurate to within ±0.1%, the gravimetric method for niobium to within ±0.2%, and, as might be expected, the photometric method for niobium only to within ±0.7%.

Nondestructive X-Ray Spectrometric Method

In addition to chemical methods, there was also a need for a rapid, convenient, and reasonably precise and accurate method capable of: (1) analysis of large lots of samples (as many as 150) for evaluating the many operating parameters in the coating apparatus; (2) immediate analysis of samples for process control; and (3) nondestructive analysis of samples required for future cryogenic testing. Such a method must be applicable to: (1) various forms of substrate, including various sizes of wire, ribbon, disks, plates, and cylinders; (2) various substrate compositions, including platinum, platinum-plated

nickel-base alloy, and ceramic; (3) a range of Nb-Sn coating thickness; (4) a range of Nb-Sn composition; and (5) small and/or irregularly shaped samples. Finally, the method must be insensitive to reasonable variations in sample position and orientation arising from the difficulty of reproducibly positioning small samples, particularly irregularly shaped ones. X-ray secondary emission (fluorescence) spectrometry[2] held promise of filling most of these requirements.

X-ray spectrometric methods for conventional samples,[2] for multiple platings,[3,4] and for plated wires[5] are all unsuitable for the analysis of Nb_3Sn because of the nature of the samples. The problem was resolved by a ratio method, described in detail elsewhere,[6] in which the net intensities of spectral lines of niobium and tin are measured and their ratio calculated and plotted as a function of concentration ratio according to the following relationship:

$$\log_{10}\left(\frac{I_{Nb}}{I_{Sn}}\right) \sim \log_{10} K + n\log_{10}\left(\frac{C_{Nb}}{C_{Sn}}\right),$$

where I and C are net intensity and concentration respectively, and K and n are constants. Thus a log-log plot of I_{Nb}/I_{Sn} as a function of C_{Nb}/C_{Sn} should be linear. The calibration curve is established from measurements on standards having known concentrations.

Equipment

The work was done on a General Electric model XRD-3 x-ray secondary emission (fluorescence) spectrometer having flat-crystal optics and conventional (that is, not inverted) geometry, and fitted with the following components: Machlett type AEG-50S x-ray tube with tungsten target, lithium fluoride crystal, $1\frac{5}{8} \times 0.070$-inch soller source collimator, $3\frac{1}{2} \times 0.005$-inch soller detector collimator, and G.E. type

---

[2] H. A. Liebhafsky, H. G. Pfeiffer, E. H. Winslow, and P. D. Zemany, *X-ray Absorption and Emission in Analytical Chemistry*, John Wiley and Sons, Inc., New York, 1960.

[3] W. C. Keesaer, "Establishment of a Q Rating Factor for Decorative Chromium Plate by X-ray Fluorescence," *Advan. X-ray Anal.*, Vol. 3, p. 77, 1960.

[4] L. S. Birks, E. J. Brooks, and H. Friedman, "Fluorescent X-ray Spectroscopy," *Anal. Chem.*, Vol. 25, p. 692, May 1953.

[5] E. P. Bertin and R. J. Longobucco, "X-ray Spectrometric Determination of Plate Metals on Plated Wires," *Anal. Chem.*, Vol. 34, p. 804, June 1962.

[6] E. P. Bertin, "An Intensity Ratio Technique for X-ray Spectrometric Analysis of Binary Samples; Particular Application to Determination of Niobium and Tin on Nb_3Sn-coated Metal Ribbon," *Anal. Chem.*, Vol. 36, p. 826, April 1964.

SPG-2 sealed krypton-filled proportional counter. Rectangular sample mask windows having dimensions $\frac{3}{4} \times \frac{1}{2}$ inch and 8×8 mm were used for wire or ribbon and ceramic plate samples, respectively.

Preparation of Standards

Niobium powder (> 99.9%, 325 mesh) was purchased from Kawecki Chemical Co., Boyertown, Pa. Tin powder ("finest powder, ~200 mesh") was purchased from Fisher Scientific Co., Pittsburgh, Pa. The powders were mixed in various proportions, pressed into bars at 10,000 lb./inch^2, sintered in a sealed evacuated quartz tube at 1050°C for 16 hours, and reduced to powder having particle size <5 μ. A slurry was prepared from each powder.[7-9] It was necessary to sinter the mixtures to enable fine pulverization; the softness of the free tin precludes grinding the unsintered mixtures. It was necessary to reduce the particle size to <5 μ so that the slurries would not settle too rapidly.

Calibration standards for Nb_3Sn-coated wires and ribbons were prepared by dip-coating clean substrate in the slurries. Standards for Nb_3Sn-coated ceramic plates were obtained by chemical analysis of a portion of the coating on each of several selected samples.

Preparation of Standard and Sample Specimens

Coated ceramic plate samples required no preparation. 1¼-inch lengths of wire and ribbon were mounted mutually parallel on 1¼-inch squares of stiff cardboard and secured at both ends with masking tape. Seven, five, and two lengths were mounted for, respectively, wire, ribbon 0.020 inch wide, and ribbon 0.090 inch wide. Uncoated wires and ribbons were also mounted in the same way for use in measuring background intensities. When required by scarcity of sample, measurements were made on single lengths of sample. However, higher intensities, shorter counting times, and improved statistical precision were realized with the numbers of lengths given above.

X-ray Measurements

The Nb$K\alpha$ and Sn$K\alpha$ peak intensities were measured on all standard and sample cards and ceramic plates at 21.41 and 14.04 deg 2θ, respec-

---

[7] J. J. Finnegan, "Thin-film X-ray Spectroscopy," *Advan. X-ray Anal.*, Vol. 5, p. 500, 1962.

[8] V. Raag, E. P. Bertin, and R. J. Longobucco, "Distribution of Cathode Sublimation Deposits in a Receiving Tube as Determined by X-ray Spectrometric Scanning," *Advan. Electron Tube Techniques*, Vol. 2, p. 249, 1963.

[9] E. P. Bertin and R. J. Longobucco, "X-ray Spectrometric Determination of Composition and Distribution of Sublimates in Receiving-type Electron Tubes," *Advan. X-ray Anal.*, Vol. 7, p. 566, 1964.

tively. Background intensities for card specimens were measured on the cards having uncoated substrates at the same 2θ settings as the lines. Background intensities for coated ceramic specimens were measured at 26.00 and 16.00 deg 2θ for Nb$K\alpha$ and Sn$K\alpha$, respectively. It was necessary to measure these backgrounds on only one specimen because the backgrounds were constant within a few counts per second over the entire concentration range. The x-ray tube potential was 50 kv for all measurements. The x-ray tube current for the Sn$K\alpha$ line and background intensities was 45 ma; the current for Nb$K\alpha$ line and background intensities was 15 ma for card specimens, 10 ma for ceramic plate specimens. The intensity measurements were made by scaling preselected counts of 102,400, 51,200, 1024, and 2048 for Nb$K\alpha$ and Sn$K\alpha$ lines and Nb and Sn backgrounds, respectively. Each preselected count was scaled two or three times, the counting times were averaged, and the intensity was calculated from the average time.

Calibration curves of Nb$K\alpha$/Sn$K\alpha$ net intensity ratio versus Nb/Sn concentration ratio were established from the data for the standards. The Nb/Sn concentration ratios for samples were derived by applying their Nb$K\alpha$/Sn$K\alpha$ intensity ratios to the appropriate calibration curve. The Nb and Sn concentrations were calculated from these concentration ratios. Typical calibration curves are shown in Figure 1.

Results and Discussion

Precision

The precision was established in three ways as follows. A series of 10 consecutive measurements of the Nb$K\alpha$/Sn$K\alpha$ intensity ratio was made on the same sample of coated ribbon without disturbing the sample. A second series of 10 measurements was made with the sample reloaded after each measurement of the two lines. The long-term reproducibility was established by analyzing a control standard each time a series of samples was analyzed. Twenty such determinations were made by two operators over a period of a year. Each time, the calibration standards were measured and a calibration curve was plotted from which the niobium concentrations of the control standard and samples were derived. The results of all these evaluations are summarized in Table IV, which gives the average, highest, and lowest values, the difference Δ between the highest and lowest values, and the standard deviation σ. The analytical precision of the x-ray method is $\pm 0.4\%$ absolute for 1σ.

Instrumental Variables and Sample Orientation and Position

The instrumental variables include x-ray tube potential and current

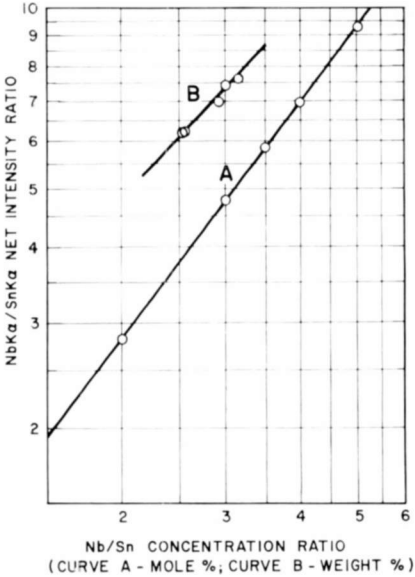

Fig. 1—Typical x-ray spectrometric calibration curves: (A) Nb-Sn-coated 0.020-inch Pt ribbon, 5 lengths per card; (B) Nb-Sn-coated ceramic plates. The Nb/Sn concentration ratio is in mole % for curve A, weight % for curve B.

and x-ray spectrometer setting (2θ). The variables related to sample position and form include orientation of the sample ribbons with respect to the sides of the mask window, position of the ribbons in the window, spacing between the ribbons, and number of lengths of ribbon. Variables related to the nature of the sample include the substrate composition, coating thickness, and alloying and diffusion effects at the interface between coating and substrate.

Test card samples were prepared from a 2-meter length of Nb_3Sn-coated 0.090 × 0.002-inch platinum-plated nickel-base alloy ribbon having particularly uniform coating composition as ascertained by x-ray spectrometric analysis of samples taken at 0.5-meter intervals. The

Table IV—Evaluation of Precision for the Determination of Niobium in Nb_3Sn-Coated Metal Ribbon by the Ratio Method

Experiment	No. of Detns.	Nb Concentration (mole %)				
		Av.	High	Low	Δ	σ
Sample undisturbed	10	78.8	79.0	78.6	0.4	±0.10
Sample reloaded	10	78.9	79.5	78.3	1.2	±0.40
Long-term reproducibility	20	78.7	79.4	77.6	1.8	±0.45

same card sample was used for all evaluations of variations in potential, current, 2θ, orientation, and position, and for all evaluations at normal conditions. Other cards were prepared with various spacings, numbers of ribbons, and forms. An identical set of cards was prepared with uncoated ribbon for making background measurements.

Table V summarizes the results of all the experiments for evaluation of effect of variables. The first column lists the variable evaluated by each group of data. X-ray tube current was evaluated in two ways—with the tube current for Nb$K\alpha$ and Sn$K\alpha$ always in ratio 1 to 3, and without regard to this ratio. *Orientation* signifies the angle between the ribbons and the sides of the window in the sample mask. *Position* signifies placement of the ribbons in the window at the right edge (R), center (C), or left edge (L), or, for 90-degree orientations, at the top edge (T), center (C), or bottom edge (B). For the miscellaneous variables, pairs of ribbons were mounted in several special ways as follows: (1) Two ribbons were cut longitudinally, and the four 0.045×0.002-inch ribbons so formed were mounted with 1-millimeter spacing between the ribbons. (2) Two ribbons were creased longitudinally. (3) Two ribbons were slightly "humped," giving a 1-millimeter spacing between the card and the underside of the ribbons at the center of the card. (4) Two ribbons were mounted in the form of a +, and (5) two in the form of an X.

In each group of data, the "normal" conditions, indicated by ellipses in the last two columns, are the following: 2 lengths of ribbon with no spacing (0 mm) between them oriented parallel (0 deg) to the sides and positioned at the center (C) of the sample mask window; x-ray tube operating potential 50 kv; x-ray tube current for Nb$K\alpha$ and Sn$K\alpha$ 15 and 45 ma, respectively; spectrometer 2θ setting for Nb$K\alpha$ and Sn$K\alpha$ 21.41 and 14.04 deg, respectively.

At each combination of conditions Nb$K\alpha$ and Sn$K\alpha$ intensities were measured on the Nb_3Sn-coated sample card, and the corresponding backgrounds were measured on the uncoated substrate card. From this data the net intensities and their ratio were calculated.

For each combination of variables, Table V gives the Nb$K\alpha$ and Sn$K\alpha$ net intensities, the Nb$K\alpha$/Sn$K\alpha$ intensity ratio, and the niobium concentration. The last two columns give the deviation, in both absolute and relative mole %, of the niobium concentration for a given set of conditions with respect to the concentration for normal conditions.

The data in Table V is self-explanatory, but several features warrant citation. All the variables have substantial effects on the Nb$K\alpha$ and Sn$K\alpha$ net intensities, but in general much smaller effects on their ratio, and thus on the analytical niobium concentration. The exceptions

Table V—Effect of Variables on the Determination of Niobium in Nb_3Sn-Coated Metal Ribbon by the Ratio Method

Variable	Number of Lengths	Spacing Between Ribbons (mm)	Orientation and Position (deg)	Excitation			Spectrometer Setting (2θ)		Net Intensity		Intensity Ratio $\frac{NbK\alpha}{SnK\alpha}$	Nb Concn. (atom %)	Deviation from Nb Concn. Under Normal Conditions[a]	
				(kv)	Nb (ma)	Sn (ma)	$NbK\alpha$ (deg)	$SnK\alpha$ (deg)	$NbK\alpha$ (count/sec)	$SnK\alpha$ (count/sec)			(atom %)	(rel. %)
Potential	2	0	0-C	45	15	45	21.41	14.04	4263	660	6.46	79.9	4.1	5.41
				47.5					4856	885	5.49	77.8	2.0	2.64
				50					5353	1116	4.80	75.8	—	—
				52.5					5746	1286	4.47	74.7	—1.1	—1.45
Current (Constant ratio)	2	0	0-C	50	5	15	21.41	14.04	2040	422	4.83	75.8	0.1	0.13
					7	21			2818	591	4.77	75.7	0	0
					10	30			3960	836	4.74	75.6	—0.1	—0.13
					12	36			4712	984	4.79	75.8	0.1	0.13
					15	45			5717	1197	4.78	75.7	—	—
					17	51			6093	1272	4.79	75.8	0.1	0.13
Current	2	0	0-C	50	13	43	21.41	14.04	5014	1123	4.46	74.7	—1.1	—1.45
					15	45			5635	1177	4.79	75.8	—	—
					17	47			6280	1209	5.19	76.9	1.1	1.45
					13	47			5014	1209	4.15	73.7	—2.1	—2.77
					17	43			6280	1123	5.59	78.0	2.2	2.90
2θ	2	0	0-C	50	15	45	21.31	13.94	5440	1119	4.86	76.0	0.3	0.40
							21.41	14.04	5669	1186	4.78	75.7	—	—
							21.51	14.14	5353	1114	4.80	75.8	0.1	0.13
							21.31	14.14	5440	1114	4.88	76.0	0.3	0.40
							21.51	13.94	5353	1119	4.78	75.7	0	0
Orientation	2	0	0-C	50	15	45	21.41	14.04	5725	1190	4.81	75.8	—	—
			5						5514	1125	4.90	76.1	0.3	0.40
			10						4922	984	5.00	76.4	0.6	0.79
			20						4995	1004	4.98	76.4	0.6	0.79
			45						3365	620	5.43	77.6	1.8	2.37
			90-C						2580	470	5.49	77.8	2.0	2.64

[a] Normal conditions are those for which no data is given in the deviation column.

Table V—Effect of Variables on the Determination of Niobium in Nb_3Sn-Coated Metal Ribbon by the Ratio Method—*Continued*

Variable	Number of Lengths	Spacing Between Ribbons (mm)	Orientation and Position (deg)	Excitation (kv)	Excitation Nb (ma)	Excitation Sn (ma)	Spectrometer Setting (2θ) Nb$K\alpha$ (deg)	Spectrometer Setting (2θ) Sn$K\alpha$ (deg)	Net Intensity Nb$K\alpha$ (count/sec)	Net Intensity Sn$K\alpha$ (count/sec)	Intensity Ratio Nb$K\alpha$ / Sn$K\alpha$	Nb Concn. (atom %)	Deviation from Nb Concn. Under Normal Conditions[a] (atom %)	Deviation from Nb Concn. Under Normal Conditions[a] (rel. %)
Position	2	0	0-C	50	15	45	21.41	14.04	5918	1232	4.80	75.8	—	—
			0-L						5181	1063	4.87	76.0	0.2	0.26
			0-R						5014	1024	4.90	76.1	0.3	0.40
			90-T						2835	515	5.50	77.8	2.0	2.64
			90-C						2580	467	5.52	77.8	2.0	2.64
			90-B						2159	398	5.42	77.6	1.8	2.37
Spacing	2	0	0-C	50	15	45	21.41	14.04	5918	1232	4.80	75.8	—	—
		1							4829	990	4.88	76.0	0.2	0.26
		2.5							5058	1001	5.05	76.5	0.7	0.92
		5							3220	572	5.63	78.0	2.2	2.90
Number of lengths	1	0	0-C	50	15	45	21.41	14.04	2557	525	4.87	76.0	0.2	0.26
	2								5790	1200	4.82	75.8	—	—
	3								6999	1473	4.75	75.6	—0.2	—0.26
	4								8404	1806	4.65	75.4	—0.4	—0.52
	5								8880	1902	4.67	75.4	—0.4	—0.52
Form	Normal		0-C	50	15	45	21.41	14.04	5790	1200	4.82	75.8	—	—
	Cut to half width								3850	795	4.84	75.9	0.1	0.13
	Creased								4708	962	4.89	76.1	0.3	0.40
	Humped								5588	1116	5.01	76.4	0.6	0.79
	+								3777	745	5.07	76.6	0.8	1.06
	×								4552	853	5.33	77.3	1.5	1.98

[a] Normal conditions are those for which no data is given in the deviation column.

are potential, current when the 1 to 3 ratio is not maintained, and orientation. The effect of operating potential is explained by the fact that it determines the effective wavelength of the primary x-ray spectrum. At higher potentials, the shorter effective wavelength results in more efficient penetration and excitation, particularly for the Sn$K\alpha$ line. The effect of x-ray tube current is also readily understood, particularly when it is high for one line, low for the other. The reason for the marked effect of misalignment of the ribbons is not known, but a similar effect was observed in determination of plate metals on plated wires.[5]

The variations in instrument conditions imposed in the measurements just described are much more severe than can reasonably be expected in practice. Moreover, in the tests the variables were imposed only on the test samples. The resulting intensity ratios were applied to a calibration curve established with standards under normal conditions. If both samples and standards were measured under the same conditions, even incorrect ones, much smaller deviations in analytical concentration would result. On the basis of these considerations and the data in Table V, it may be concluded that the ratio technique effectively compensates for reasonable variations in instrumental variables.

Nature of the Sample

When the coating is not infinitely thick for both lines, the most serious limitations are imposed by the nature of the coated samples themselves.

1. *Substrate*

The substrate may affect the value of the Nb$K\alpha$/Sn$K\alpha$ intensity ratio. The effect will be particularly marked if there is enhancement of one or both coating lines by a substrate line, especially if only one coating line is enhanced, or if the two lines are enhanced with substantially different efficiency. Most of the Nb_3Sn-coated samples had three substrates—platinum and platinum-plated nickel-base alloy ribbon and ceramic plates. A set of slurry-coated platinum-ribbon standards served for both types of ribbon sample. Another set of coated ceramic standards was provided for the ceramic samples.

2. *Coating Thickness*

Suppose coating AB is relatively opaque to the spectral line of element A, but relatively transparent to that of B. Then as the coating increases in thickness, but without change in composition, it first becomes infinitely thick for the A line, whereupon intensity I_A becomes

constant. Intensity I_B continues to increase with coating thickness until infinite thickness is reached for the B line, whereupon the I_A/I_B ratio becomes constant. Thus, I_A/I_B may be dependent upon thickness, even though composition is constant. This effect becomes more marked as the difference increases between the mass absorption coefficients of the coating for the spectral lines of its two constituents. The coatings on the ceramic plates were "more than infinitely" thick for both Nb$K\alpha$ and Sn$K\alpha$. The coatings on the metal ribbon were less than infinitely thick for both wavelengths. However, the coating thickness was held sufficiently uniform that coating-thickness errors were avoided.

3. Interfacial Diffusion or Alloying

The ratio method presupposes an abrupt interface between coating and substrate. However, suppose that there is an interfacial zone in which the coating and substrate have interdiffused or alloyed. That part of the Nb$K\alpha$ and Sn$K\alpha$ emission originating in the part of the coating that remains free of substrate is excited and emitted in precisely the same manner as in unalloyed coating. However, that part of the emission originating in the interfacial zone, and the primary radiation which excites it, must pass through a certain concentration of substrate. In doing so, both the primary and secondary radiation undergo absorption different from that which would prevail in pure coating. This phenomenon becomes more pronounced the greater the interfacial penetration and the greater the difference in absorption coefficients of the substrate and coating for the two lines. The effect becomes particularly serious if the substrate has very different absorption for the two coating lines. Fortunately, interfacial interpenetration in the Nb_3Sn-coated ribbon samples, as indicated by photomicrographs of metallographic sections, is minimal.

ACKNOWLEDGMENT

Some of the text on chemical methods is reprinted here by the courtesy of the editor of *Chemist-Analyst*, and some of the text on x-ray methods and Tables IV and V are reprinted here by the courtesy of the editors of *Analytical Chemistry*.

ANOMALOUS RESISTIVITY OF NIOBIUM STANNIDE*†

By

David W. Woodard and George D. Cody

RCA Laboratories
Princeton, N. J.

Summary—*The resistivity of several specimens of niobium stannide has been measured over the range 18° to 850°K. The resistivity rises rapidly up to 200°K and then approaches a linear variation with a considerably smaller slope. Over the entire range the resistivity can be fit to better than 1% by the form* $\rho(T) = \rho_0 + \rho_1' T + \rho_2 \exp\{-T_0/T\}$ *where* $\rho_0 \approx 1 \times 10^{-5}$ *ohm-cm,* $\rho_1' = 4.66 \times 10^{-8}$ *ohm-cm/°K,* $\rho_2 = 7.47 \times 10^{-5}$ *ohm-cm and* $T_0 = 85°K$. *Hall measurements made at 27°, 77° and 300°K, if interpreted on a one-band model, indicate a constant hole density of* $1.77 \times 10^{22}/cm^3$ *and an effective valence of 0.27/atom. The anomalous resistivity can not be explained on the basis of present models of the resistivity of transition metals, although the constancy of the Hall coefficient implies that the scattering probability rather than effective number of carriers is changing with temperature. The relevance of the present results to recent models of the electronic structure of* Nb_3Sn *is discussed.*

Introduction

NIOBIUM STANNIDE, Nb_3Sn, is unique among superconducting materials in having a transition temperature above 18°K.[1] Its superconducting state may also be sustained in very high magnetic fields, and with high current densities.[2] For these reasons there is considerable commercial interest in Nb_3Sn for superconducting devices. Furthermore, a number of other unusual effects of importance to a fundamental understanding of the superconductivity of Nb_3Sn have recently been observed in the related V and Ta compounds having

* This work was supported by the Materials Laboratory, Wright Patterson Air Force Base under Contract AF33(657)11208 and by RCA Laboratories, Princeton, New Jersey.

† Submitted by one of the authors (D.W.W.) in partial fulfillment of the requirements for the degree of Master of Science, Rutgers University (1964).

[1] B. T. Matthias, T. H. Gabelle, S. Geller, and E. Corenzwit, "Superconductivity of Nb_3Sn," *Phys. Rev.*, Vol. 95, No. 6, p. 1435, Sept. 15, 1954.

[2] R. M. Bozorth, A. J. Williams, and D. D. Davis, "Critical Field for Superconductivity in Niobium-Tin," *Phys. Rev. Ltrs.*, Vol. 5, No. 4, p. 148, Aug. 15, 1960.

the same (β-tungsten)[3] crystal structure. Clogston and Jaccarino[4] have shown that there are pronounced anomalies in the temperature dependence of the Knight shift[5] and the susceptibilities in the vanadium compounds V_3X, where X = As, Au, Co, Ga, Ge, Si, Sb, Sn, or Pt. They have also shown that one possible explanation of their results is that a sharp peak exists in the density-of-states curve for the *d*-band, and that the Fermi level intersects this peak in the superconductors. This interpretation seems consistent with the results of the specific heat measurements by Morin and Maita,[6] who found an anomalously high coefficient for the electronic specific heat in Nb_3Sn and V_3Ga. Weger[7] has found an anomaly in the temperature dependence of the nuclear magnetic relaxation time in V_3Si and V_3Ga, and has presented an explanation of this and the above effects in terms of an unusual band structure having essentially one-dimensional properties.

The experiments reported here present yet another anomalous temperature dependence in Nb_3Sn, namely that of the electrical resistivity. The resistivity of several specimens of Nb_3Sn was measured over the range 18° to 850°K. The measurements were made on single-phase stoichiometric Nb_3Sn obtained by chemical reduction from the chlorides of Nb and Sn,[8] as well as on similarly prepared nonstoichiometric material (Nb_4Sn) with the same β-tungsten crystal structure.

The resistivity of all samples measured showed a marked departure from the usual temperature dependence of both transition and nontransition metals (see Figure 2). Rather than a power-law dependence at low temperatures that converges to a linear dependence at high temperatures, as is characteristic of most metals, the resistivity rises rapidly up to about 200°K and then saturates to a relatively shallow linear dependence at high temperatures. An interesting result of the present work is that the resistivity can be described to an accuracy of

---

[3] S. Geller, "A Set of Effective Coordination Number (12) Radii for the β-Wolfram Structure Elements," *Acta. Cryst.*, Vol. 9, p. 885, 1956.

[4] A. M. Clogston and V. Jaccarino, "Susceptibilities and Negative Knight Shifts of Intermetallic Compounds," *Phys. Rev.*, Vol. 121, No. 5, p. 1357, March 1, 1961.

[5] C. H. Townes, C. Herring, and W. D. Knight, "The Effect of Electronic Paramagnetism on Nuclear Magnetic Resonance Frequencies in Metals," *Phys. Rev.*, Vol. 77, No. 6, p. 852, March 15, 1950.

[6] F. J. Morin and J. P. Maita, "Specific Heats of Transition Metal Superconductors," *Phys. Rev.*, Vol. 129, No. 3, p. 1115, Feb. 1, 1963.

[7] M. Weger, "The Electronic Bond Structure of V_3Si and V_3Ga," *Rev. Mod. Phys.*, Vol. 36, No. 1, p. 175, Jan. 1964.

[8] G. W. Cullen, "Preparation and Properties of Niobium Stannide on Insulating Substrates," *Trans. Metallurgical Soc.*, in press; see also J. J. Hanak, p. 161 of *Metallurgy of Advanced Electronic Materials*, edited by G. E. Brock, Interscience Publishers, Inc., New York, 1963.

better than 1% over the entire temperature range 18° to 850°K by the relationship,

$$\rho = \rho_0 + \rho_1' T + \rho_2 \exp\left\{-\frac{T_0}{T}\right\} \tag{1}$$

where ρ_0 and ρ_1' are constants, $\rho_2 \approx 5 \times \rho_1' \times (300°\text{K})$, and $T_0 = 85°\text{K}$.

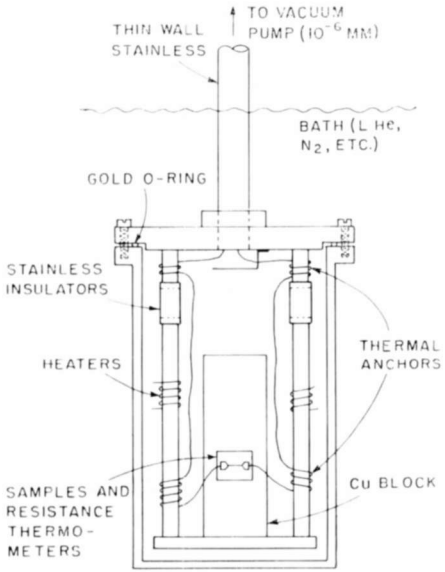

Fig. 1—Diagram of the cryostat.

Experimental Method and Results

Figure 1 shows a schematic diagram of the cryostat used in the measurements from 18° to 373°K. The temperature of the copper block to which the samples were attached was controlled by varying the current in the heaters, the measurements being made after the system reached equilibrium. Measurement in the temperature ranges 18° to 77°K, 77° to 200°K, 200° to 273°K, and 273° to 373°K were made by placing the apparatus in baths of liquid He, liquid N_2, acetone and solid CO_2, and ice, respectively. The pressure, measured at the vacuum pump, was maintained at 10^{-6} mm Hg, and outgassing from the can was found to be low. Radiative heat transfer from the samples to the walls of the can was found to be negligible by noting that the resistance

measured at 77°K with the can in liquid He joined smoothly with the value measured when the samples were dipped directly in liquid N_2.

Temperature measurements in the ranges 18° to 100°K and 100° to 373°K were made using a Minneapolis–Honeywell germanium resistance thermometer, and a platinum resistance thermometer, respectively. The platinum thermometer was a very small unit made by the Rosemount Engineering Company, Minneapolis, Minn., and was found to be excellent for work of this accuracy. It is estimated that below 373°K the accuracy of temperature measurement, including the effects of self-

Table I—Characteristics of Specimens

Specimen	Nb* (wt %)	T_c (°K)	ΔT_c (°K)	Area (cm^2)	Length (cm)
FS 14	70.5 ± 0.3	18.3	0.03	5.1×10^{-2}	1.26
FS 20	70.5 ± 0.3	18.32	0.04	5.2×10^{-5}	0.64
81 (10)	71.2 ± 0.3	18.2**	0.07	1.7×10^{-5}	0.38
87 (1)	70.5 ± 0.3	18.3	0.27	33.6×10^{-5}	0.92
65 (6)	73.4 ± 0.3	15.5	4.0	14.3×10^{-5}	0.355

* Stoichiometric Nb_3Sn contains 70.1 wt % Nb.

** Resistance determination; all others are by a-c permeability.

heating in the samples was about ± .05°K. At temperatures above 373°K the samples were placed in an oven in a helium atmosphere, and the temperature measured with a cromel–alumel thermocouple. Accuracy of temperature measurement in this range was not as great as in the lower range, but was less critical since the resistivity slope is fairly shallow there. Possible error may have been ± 2°K.

The resistance of samples and thermometers was measured by a four-probe d-c technique using a Leeds and Northrup K-3 potentiometer and a quartz-fiber galvanometer. It is estimated that resistance measurements are accurate to about ± 0.7%. Sample resistances at room temperature were typically of the order of 1 ohm.

Table I lists the characteristics of some of the samples measured; all were prepared by vapor deposition[8] on a ceramic substrate with the exception of FS 14, which was a thick deposited film with the support removed. Vapor-deposited material presents several advantages for

research on niobium stannide; perhaps the most important is that the material is single phase and of relatively low impurity content ($\approx 0.2\%$). It is thus considerably better defined than that prepared by the usual metallurgical techniques. For example, vapor-deposited Nb_3Sn with a T_c of 18.3°K can have a transition width as low as .03°K, about a factor of 10 below any width reported in the literature for sintered or arc-melted material. Stoichiometry of the samples was determined by wet-chemical analysis. X-ray and optical examination of anodized material indicates that the material is single phase. Electron-microscope measurements indicate a crystalline size of the order of 2000 Å in diameter, which agrees with the results of low-temperature thermal-conductivity measurements.[9] The transition temperatures and widths were determined by the inductance method except as noted.

Table II—Resistivity Coefficients

Specimen	Nb* (wt %)	ρ_0 (ohm-cm)	ρ_1' (ohm-cm/°K)	ρ_2 (ohm-cm)	T_0 (°K)
FS 14	70.5 ± 0.3	1.08×10^{-5}	4.66×10^{-8}	7.47×10^{-5}	85
FS 20	70.5 ± 0.3	1.08×10^{-5}	4.66×10^{-8}	7.47×10^{-5}	85
81 (10)	71.2 ± 0.3	1.16×10^{-5}	4.66×10^{-8}	7.47×10^{-5}	85
87(1)	70.5 ± 0.3	1.25×10^{-5}	4.66×10^{-8}	7.47×10^{-5}	85
65 (6)	73.4 ± 0.3	4.7×10^{-5}	4.66×10^{-8}	7.47×10^{-5}	85
		4.7×10^{-5}	6.92×10^{-8}	7.68×10^{-5}	105

The samples were polished and then cut to shape by sand blasting. With the exception of sample FS 14, the cross-sectional areas were small and poorly defined due to the rough edges left by the blasting. Thus FS 14 was used to obtain absolute resistivity (to about ± 7%), and effective areas were computed for the others assuming Matthiessen's rule. This was justified since T_0 and the ratio ρ_1'/ρ_2 in Equation (1), which *are* determined by a resistance measurement, were invarient except in the very off-stoichiometric sample 65(6) where the variations were only slight.

Table II summarizes the resistivity coefficients of Equation (1) obtained in this manner. Figure 2 shows the resistivity for samples FS 20 and 87(1) from 18.3° to 850°K. As noted, the other stoichiometric samples show identical behavior except for small differences in "residual" resistivities, ρ_0. The smooth curve represents Equation (1)

[9] G. Cody and R. Cohen, "Thermal Conductivity of Nb_3Sn," *Rev. Mod. Phys.*, Vol. 36, No. 1, p. 121, Jan. 1964.

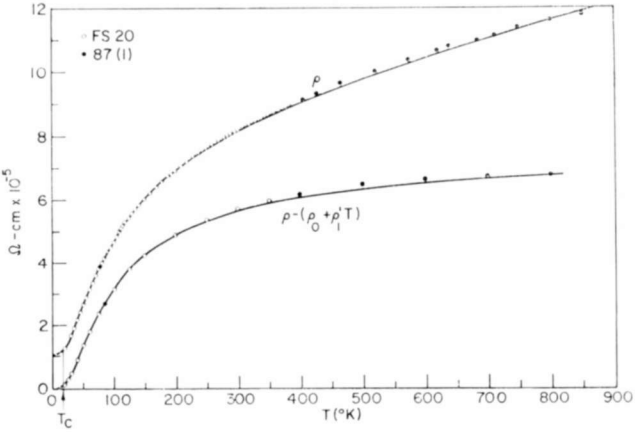

Fig. 2—Upper curve shows resistivity of Nb_3Sn as a function of absolute temperature; lower curve, the measured resistivity minus $(\rho_0 + \rho_1' T)$.

with $\rho_0 = 1.08 \times 10^{-5}$ ohm-cm, $\rho_1' = 4.66 \times 10^{-8}$ ohm-cm/centigrade degree, $\rho_2 = 7.47 \times 10^{-5}$ ohm-cm and $T_0 = 85°K$. This figure and Figure 3 also show the exponential part of Equation (1) compared to the difference between the measured resistivity and the first two terms of Equation (1). One also notes in Table II the relative invariance of ρ_2 and T_0 for sample 65(6) with changes in the residual resistivity by almost a factor of five. This result indicates that there is little deviation from Matthiessen's rule even for large departures from stoichiometry, and that essentially the same mechanism governs the resistivity

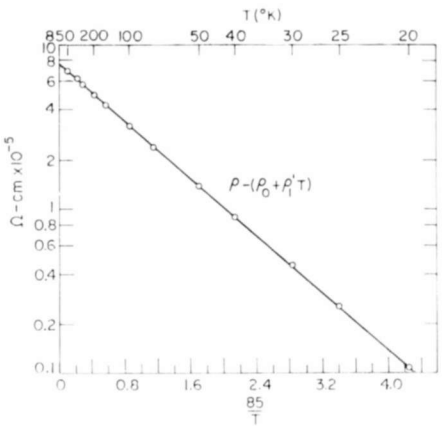

Fig. 3—Measured resistivity minus $(\rho_0 + \rho_1' T)$ as a function of 85/T.

of stoichiometric and nonstoichiometric material. Indeed, previous measurements[10] on sintered Nb_3Sn can be interpreted in terms of Equation (1) using essentially the same value of T_0, although the ratio ρ_1'/ρ_2 differs by about a factor of 1.5 from the value obtained from Table II. The nonstoichiometric sample 65(6) could be fitted by Equation (1) to $\pm 2\%$ using $T_0 = 105°K$, and to $\pm 10\%$ using $T_0 = 85°K$.

Discussion

While departures from the resistivity predicted by the simple theory of metals are to be expected for the transition-metal compound Nb_3Sn, the striking agreement with Equation (1) is unexpected and, as will be shown, is difficult to interpret in terms of the usual modifications of the simple theory.

Mott[11] in 1935 proposed a model for the transition-element metals in which the unfilled d band has a high density of states and a low mobility. It thus acts as a trap into which the conduction s-shell electrons may be scattered. The scattering is proportional to the density of states at the Fermi level in the d band. Mott calculated the changes in resistance that would be produced by the known dependence of the Fermi level upon alloy concentration and temperature. The model has been confirmed in detail by studies of the alloys of transition metals with monovalent metals.[11a] For the temperature dependence, however, Wilson[12] has given a more extensive treatment in which he included the effect of the conservation of momentum in an electron–phonon collision. Thus, if the states at the Fermi level in the s and d bands differ in wave number by at least Δk_{sd}, then only a phonon with wave number $q \geqq \Delta k_{sd}$ can scatter an electron from the s to the d band. The decreasing number of such phonons at low temperatures gives rise to a rapid drop in the resistivity. Wilson assumed that the energy states in both the d and s bands may be treated with the Bloch approximation. Here the energy in each band is a quadratic function of the wave number in the reduced-

---

[10] G. D. Cody, J. J. Hanak, C. T. McConville, "Resistance Anomaly in β-Tungsten Compounds," *Bull. Amer. Phys. Soc.*, Vol. 6, p. 146, 1962.

[11] N. F. Mott, "A Discussion of the Transition Metals on the Basis of Quantum Mechanics," *Proc. Phys. Soc.*, Vol. 47, Part 4, p. 571, July 1, 1935; "The Resistance and Thermoelectric Properties of Transition Metals," *Proc. Royal Soc.*, Vol. 153, p. 368, Aug. 1936; and "The Electrical Conductivity of Transition Metals," *Proc. Roy. Soc.*, Vol. 153, p. 699, Feb. 1936.

[11a] B. R. Coles, "Electronic Structures and Physical Properties in the Alloy Systems Nickel-Copper and Palladium-Silver," *Proc. Phys. Soc.*, Vol. 65, Sec. B, Part 3, p. 221, March 1952.

[12] A. H. Wilson, "The Electrical Conductivity of the Transition Metals," *Proc. Royal Soc.*, Vol. 167, p. 580, Sept. 23, 1938.

zone scheme, and the phonons have a Debye frequency spectrum. The result he obtains for the resistivity is

$$\rho \propto \left(\frac{T}{\theta_D}\right)^3 \int_{\theta'/T}^{\theta_D/T} \frac{z^3 dz}{(e^z - 1)(1 - e^{-z})}, \tag{2}$$

where θ_D is the Debye temperature, and $\theta' (\ll \theta_D)$ is the energy of the phonon with the wave number $q = \Delta k_{sd}$; i.e., $k\theta' = hv(q)$. At high temperatures, Equation (2) becomes

$$\rho \propto \left(\frac{\theta_D^2 - \theta'^2}{2\theta_D^3}\right) T, \tag{3}$$

while at low temperatures ($T \ll \theta'$),

$$\rho \propto \left(\frac{\theta'}{\theta_D}\right)^3 \exp\left\{-\frac{T_0}{T}\right\} \tag{4}$$

Wilson's theory therefore predicts an exponential dependence at low temperatures and a linear dependence at high temperatures, which is highly suggestive of Equation (1). However, if we consider the ratio of coefficients of the linear term and the exponential term,

$$r = \frac{(\theta_D^2 - \theta'^2)/2\theta_D^3}{(\theta'/\theta_D)^3},$$

and substitute the value $\theta_D = 290°\text{K}$ from Reference (6), and $\theta' = 85°\text{K}$ appropriate to our results, we obtain

$$r \cong 7 \times 10^{-2} \ (°K)^{-1}. \tag{5}$$

However, if we compute ρ_1'/ρ_2 from *Table II* for the stoichiometric material, we obtain

$$\frac{\rho_1'}{\rho_2} \cong 7 \times 10^{-4} (°\text{K})^{-1}. \tag{6}$$

The Wilson theory therefore predicts a contribution of the linear term two orders of magnitude larger relative to the exponential term than

we have found experimentally for Nb_3Sn. While Wilson himself admitted that his theory was "at best an indifferent approximation," such poor agreement would indicate that the model is not applicable. Furthermore, a preliminary measurement shows that the Hall coefficient of this polycrystalline material is positive and approximately invarient in the range 27° to 300°K. This would suggest that the number of carriers is not changing, and that the unusual resistivity arises purely from scattering within the conduction band.

Another model with possible applicability to Nb_3Sn was proposed by Elliot[13] to explain the resistance anomalies in some rare-earth metals. For these substances, which have an unfilled f shell, it is believed that a good basic approximation is to consider that all the atomic electrons are tightly bound at the lattice points except three outer electrons per atom which form the conduction electrons. The f electrons interact with the crystalline field producing a Stark splitting of the energy levels. The core potential then depends upon how the split levels in the unfilled shell are populated. Since the inner electrons are tightly bound, they may be considered not to interact with each other from one atom to the next. The occupation in either level is, therefore, randomly distributed around the crystal. We would expect a contribution to the usual resistivity of the form

$$\rho \propto Cx(1-x), \tag{7}$$

where x is the proportion of electrons in one state, and is given by

$$x = \frac{\exp\left\{-\dfrac{\Delta E}{kT}\right\}}{\exp\left\{-\dfrac{\Delta E}{kT}\right\}+1}. \tag{8}$$

Here ΔE is the Stark splitting. The contribution to the resistivity is, therefore,

$$\rho = \frac{1}{4} C \frac{1}{\cosh^2(\Delta E/kT)}. \tag{9}$$

Ziman[14] has also shown that if there is the possibility of inelastic

[13] R. J. Elliot, "Resistance Anomalies in Some Rare-Earth Metals," *Phys. Rev.*, Vol. 94, No. 3, p. 564, May 1, 1954.

[14] J. Ziman, *Electrons and Phonons*, Clarendon Press, 1962, p. 382.

scattering with the split f levels, there is a further contribution of

$$\rho = C' \frac{\Delta E/kT}{\sinh(\Delta E/kT)}. \tag{10}$$

Both of these functions have an exponential dependence at low temperatures and saturate at high temperatures, and can be fitted to the data to within about 10%. The coefficients required for the fit are about an order of magnitude larger than the values estimated by Elliot. However, when one considers that the theory was based on f electrons and

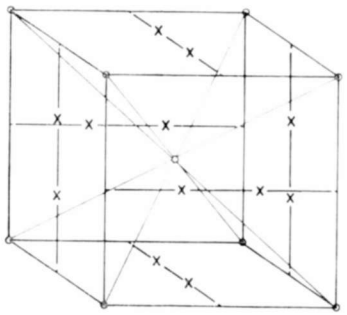

Fig. 4—β-tungsten crystal structure; X = niobium, o = tin.

not d states, the agreement is certainly better than with the Wilson model. Moreover, the energy splitting required to fit the data (ΔE = 160°K) is of the same order as that predicted by Calloway and Edwards[15] for transition metals in bcc or fcc lattices. However, as Callaway and Edwards point out, this is very much less than the width of the d bands in these structures. This suggests that neither the localization nor the splitting of the d levels has much meaning. Nb_3Sn, however, has the unusual β-tungsten crystal structure in which the Nb atoms form chains with much smaller spacing than the other atoms (see Figure 4), and the anomalous temperature dependence of the Knight shift has been interpreted[4] as resulting from a very narrow peak (width ≈ 200°K) in the density of states in the d band. Such a peak has also been calculated theoretically[16] for vanadium compounds with the

[15] J. Callaway and D. M. Edwards, "Cubic Field Splitting of D Levels in Metals," *Phys. Rev.*, Vol. 118, No. 4, p. 923, May 15, 1960.

[16] Mattheiss, "Energy Bands for V_3X Compounds," *Bull. Amer. Phys. Soc.*, Vol. 9, p. 251, March 1964.

β-tungsten structure. The splitting might, therefore, have some meaning in β-tungsten structures.

One final model that could also be offered to explain the anomalous resistivity is the one-dimensional band structure proposed by Weger.[7] According to this model, the niobium $4d$ states form three degenerate bands: the $4d$ states belonging to the close-spaced niobium atoms that form lines in the [100] direction combine to form a band in which the electronic energy $\epsilon(\mathbf{k})$ depends only on k_x, the component of $\mathbf{k}$ in the [100] direction; similarly, states of atoms that form lines in the [010] and [001] directions form bands in which $\epsilon(\mathbf{k}) = \epsilon(k_y)$ and $\epsilon(\mathbf{k}) = \epsilon(k_z)$, respectively. The Fermi surface of each of these bands consists of two parallel planes, perpendicular to the corresponding line of atoms. Assuming (somewhat unrealistically) that the energy has a quadratic dependence upon wave vector, and that there is essentially a Debye phonon spectrum, one can calculate the scattering time of the electrons with the result that

$$\frac{1}{\tau} \propto \frac{1}{\exp\left\{\dfrac{T_0}{T}\right\} - 1}. \tag{11}$$

Here $kT_0 = 2Shk_f$, S is the velocity of sound, and k_f is the Fermi wave vector. If one takes the velocity of sound as 3×10^5 cm/sec, T_0 from the data corresponds to $k_f = 2 \times 10^7$/cm. The free-electron model of Nb_3Sn with the full valence of 4.75 would imply $k_f = 2 \times 10^8$/cm, while a one-dimensional lattice would imply that $k_f = 6 \times 10^7$/cm in somewhat better agreement. A preliminary measurement of the Hall coefficient, however, indicates that the number of carriers is not 4.75 but 0.27 per atom. This would give for the one-dimensional model $k_f = 0.4 \times 10^7$/cm. Since the Hall coefficient is positive, however, it is not possible to place much confidence in any of these numbers without a further knowledge of the mobilities and band structure.

Equation (11) behaves linearly at high temperatures and exponentially at low temperatures. The ratio of linear to exponential coefficients is $1/T_0$, which, for $T_0 = 85°$K, is about a factor of 15 larger than the experimental value. The agreement of this model is thus distinctly better than the Wilson model, and about the same as the Elliot model.

Conclusion

The resistivity of several specimens of Nb_3Sn has been measured over the range 18° to 850°K. The measurements were made on single-

phase stoichiometric material obtained by chemical deposition of the chlorides of Nb and Sn. The resistivity shows a marked departure from the usual temperature dependence of both transition and nontransition metals, and can be described to within 1% over the entire range by the addition of an exponential term to the ordinary resistivity. An off-stoichiometric (excess Nb) specimen was also measured in the range 18° to 373°K and was found to have approximately the same temperature dependence, even though the "residual" resistance was about four times as large. These results imply that the anomalous resistivity is a property of the energy bands of Nb_3Sn in the β-tungsten structure, and that it is relatively independent of small changes in the electron-to-atom ratio and the presence of Nb atoms on Sn sites.

The possible applicability to Nb_3Sn of several models of the electronic structure and the scattering mechanism was discussed. It was shown that the theories of interband scattering in transition metals due to Mott and Wilson are in poor agreement with the experimental results. Somewhat better agreement can be obtained with either the Elliot model in which unfilled $4d$ levels are split by the crystalline field, or the Weger one-dimensional model of band structure.

Acknowledgments

The authors wish to thank G. Cullen and R. Nyman for sample preparation, J. Cooper for transition temperature measurements, and R. Parmenter and Y. Goldstein for numerous discussions.

TRANSITION TEMPERATURE OF NIOBIUM STANNIDE*

By

J. L. Cooper

RCA Laboratories
Princeton, N. J.

Summary—*Transition-temperature measurements have been made by an inductance method on sintered and vapor-deposited samples of niobium stannide. The transitions and transition widths are discussed relative to the chemical and metallurgical state of the samples. The shift in the superconducting transition of vapor-deposited Nb_3Sn for a neutron dosage of 2.7×10^{18} neutrons/cm² is given. Finally, the transition shift with applied external field is examined, and values for the upper critical field for Nb_3Sn are given, based on existing theory.*

Introduction

THE MAGNITUDE AND gross shape of a superconducting transition are microscopic properties that reflect not only the electronic interactions responsible for the superconducting state, but also the history of the material as regards its preparation and chemical and structural homogeneity. In this paper, preliminary results of an investigation of (1) the determination of the critical temperature of niobium stannide (Nb_3Sn) and its dependence on material preparation parameters, (2) the effect of fast neutron irradiation on the magnetic properties of Nb_3Sn, and (3) the upper critical field for Nb_3Sn as estimated from the shift of critical temperature with applied external field are presented.

Procedure

There are two general methods in use to determine the critical temperature (T_c) of a superconductor—the direct measurement of the loss of resistance, and the indirect measurement using inductive or frequency-dependent techniques. We have chosen the latter for several reasons, the most important being the difficulty encountered in applying electrical contacts to small and sometimes irregular specimens. The superconducting material is used as the core of a small copper-wound coil whose output is connected to an Anderson inductance bridge.[1] The

* This work was supported by the Air Force Materials Laboratory, Research and Technology Division, Air Force Systems Command, Wright-Patterson Air Force Base, Ohio, under Contract No. AF33(657)-11208.

[1] B. I. Bleaney, *Electricity and Magnetism*, p. 438, Oxford, Clarendon Press, 1957.

coil and sample are encased in a vacuum-tight can and immersed in liquid helium. As the temperature is varied by electrical heating, the self-inductance of the coil changes in direct proportion to the permeability of the core. The change of self-inductance of the coil plotted against the temperature gives the critical temperature of the specimen. The sensitivity of the Anderson bridge is such that the change of inductance can be measured to a precision of approximately two parts in 10^5. The smallest volume that can be measured is about 1/100 cm^2. The field in the coil is less than 1 gauss. The temperature was measured with a carbon resistor calibrated with respect to the vapor pressure of liquid helium, the superconducting transition of high-purity lead, and a point at 18.13°K given by the transition temperature of a sample of sintered Nb_3Sn. The lead and Nb_3Sn samples were calibrated with a germanium resistance thermometer that was, in turn, calibrated by its manufacturer (Minneapolis Honeywell Co.) from 1.5°K to 100°K and checked in the present work at liquid helium, liquid neon, liquid nitrogen, and room temperature.

The temperature interval (ΔT_c) from the normal to the superconducting state is an indication of the homogeneity of the sample. Thus, it is important to determine ΔT_c as well as T_c for any given sample. While T_c is often defined as the start of the superconducting transition, as in the present paper, it is sometimes given as the mid-point of the transition.

Results

Measurements of T_c and ΔT_c were made on Nb_3Sn samples prepared by metallurgical sintering techniques[2] and by vapor deposition[3] on various substrates. Figure 1 shows the transition curve for a typical sintered specimen. The transition starts at 18.25°K, and ΔT_c is 0.1°K. The transition width for similarly sintered material can be as large as 0.3°K, and is seldom less than 0.1°K. Figure 2 illustrates an early attempt to vapor deposit Nb_3Sn on ceramic substrates.[4] This represents a nonstoichiometric deposit on the niobium-rich side (approx. 73 wt. % Nb) with $T_c = 17.4$°K and $\Delta T_c = 1.65$°K. The material was then vacuum annealed at 1000°C for approximately 15 hours, and the T_c shifted upward by 0.6°K to 18.0°K with a narrowing of ΔT_c to 0.2°K. Metallographic examination suggests that this effect of annealing on

[2] B. T. Matthias, "Empirical Relation between Superconductivity and the Number of Valence Electrons per Atom," *Phys. Rev.*, Vol. 97, p. 74, 1 Jan. 1955.

[3] J. J. Hanak, *Metallurgy of Advanced Electronic Materials*, G. E. Brock, ed., Interscience Publishers, New York, 1963, p. 161.

[4] G. W. Cullen, "Preparation and Properties of Niobium Stannide on Insulating Substrates," *Trans. Metallurgical Soc.*, in press.

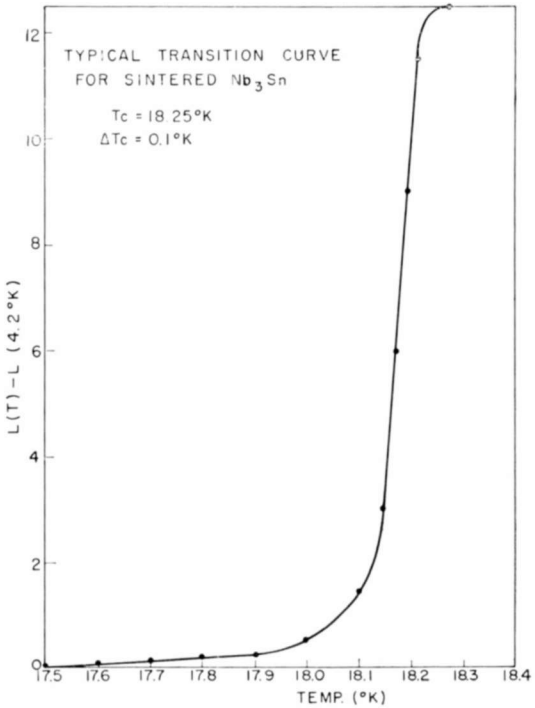

Fig. 1—T_c of sintered Nb_3Sn.

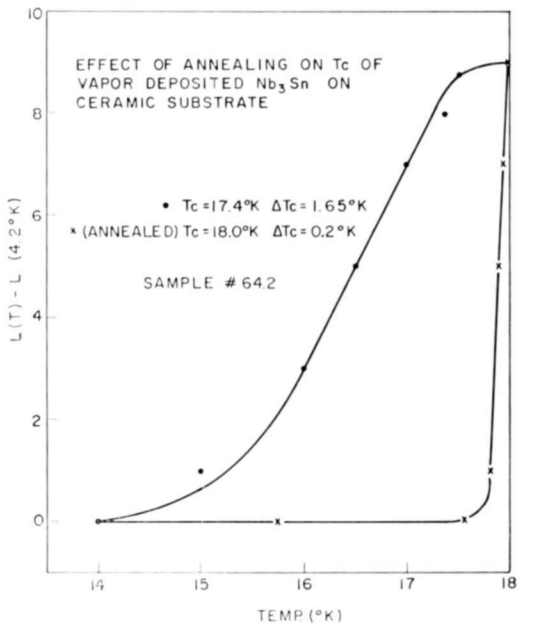

Fig. 2—Effect of annealing on T_c of vapor-deposited Nb_3Sn.

T_c and ΔT_c is associated with the precipitation of Nb or its oxide. It is clear that transition-temperature measurements furnish an important guide to changes in microstructure or phase relationships, as previously noted by Matthias.[5] However, complementary chemical and x-ray analysis are also necessary to ensure that the measurement is one

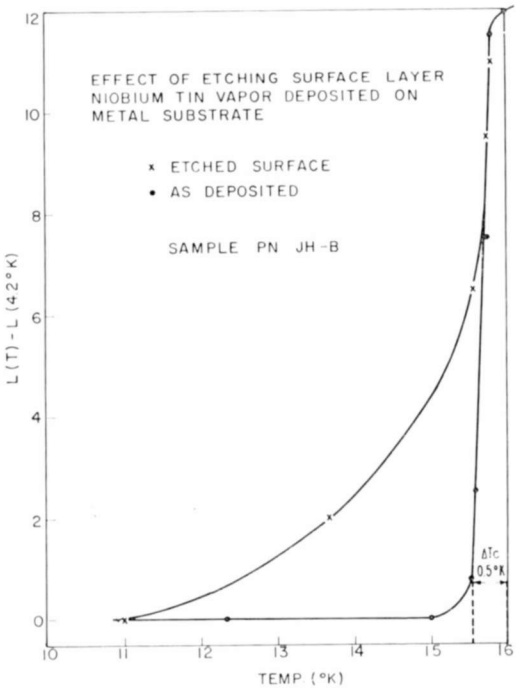

Fig. 3—Effect of etching surface layers on T_c of vapor-deposited Nb_3Sn.

of bulk and not surface properties. For example, Figure 3 shows a sample of Nb_3Sn vapor deposited on metal ribbon with $\Delta T_c = 0.5°K$. Chemical analysis showed the deposit to be beyond the compositional range for Nb_3Sn. The deposit was subsequently etched and T_c remeasured. The result was a broadening of ΔT_c due to compositional variations in sublayers. Higher-T_c material on the surface had prevented flux penetration in the original measurement. R. E. Enstrom of these Laboratories examined oblique sections of similar material with an electron-beam microanalyzer, and discovered the presence of several distinct compositional layers close to the interface between the substrate and the niobium stannide.

---

[5] B. T. Matthias, "Metallurgy of Advanced Electronic Materials," *Superconductors*, M. Tanenbaum and W. V. Wright, ed., Interscience Publishers, New York, 1962, p. 1.

More recent efforts on vapor depositing stoichiometric Nb_3Sn has yielded very high and sharp transition temperatures. A typical example is shown in Figure 4, where $T_c = 18.3°K$, $\Delta T_c = 0.03°K$, and $\Delta T/T_c = 0.2\%$. The sharpness of this transition compares favorably with high-purity, single-crystal specimens of soft superconductors.

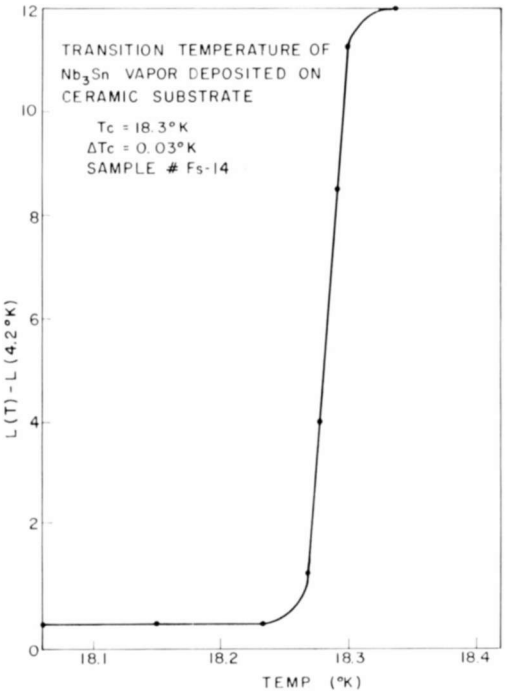

Fig. 4—Transition of narrow width (ΔT_c) vapor-deposited Nb_3Sn.

There has been some interest recently in the effect of fast-neutron irradiation on the magnetic properties of Nb_3Sn.[6] We have irradiated several samples of Nb_3Sn deposited on ceramic plates with medium and heavy doses of fast neutrons, and measured their critical temperature before and after irradiation. With the medium-dose material (4.7×10^{17} neutrons/cm^2), there is no apparent shift in the transition temperature. However, with the high-dose rate (2.7×10^{18} neutrons/cm^2) one observes in Figure 5 a shift of $-0.16°K$ to $-0.20°K$. In Figure 5, sample #1 was measured before and after irradiation, and sample #2

[6] J. P. McEvoy, Jr., R. F. Decell, and R. L. Novak, "Effect of Neutron Radiation on Critical Currents in Hard Superconductors (Nb_3Sn and NbZr)," *Appl. Phys. Ltrs.*, Vol. 4, p. 43, 1 Feb. 1964.

was used as a non-irradiated reference.* Very recently, studies by Swartz et al[7] on arc-cast and diffusion-processed Nb_3Sn indicate a lowering of T_c by 0.10 and 0.08°K, respectively, along with a broadening of ΔT_c for flux densities of 1.5×10^{18} neutrons/cm². In this connection, it is interesting to note that although the T_c of the vapor-deposited Nb_3Sn is also lowered, it does not broaden with neutron irradiation.

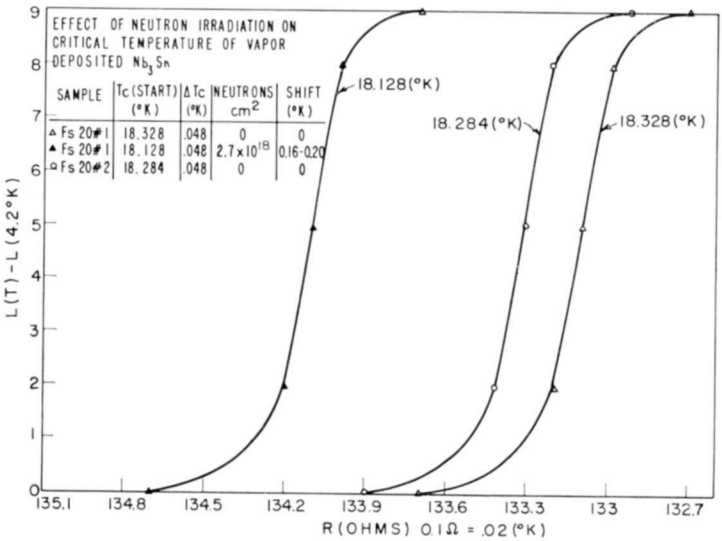

Fig. 5—Effect of neutron irradiation on T_c of vapor-deposited Nb_3Sn.

Measurements were made in the shift of the temperature of the superconducting transition with applied field for various specimens of vapor-deposited Nb_3Sn with different T_c, residual resistivity, and stoichiometry. Such measurements give information on the upper critical field (H_{c_2}). The field was applied longitudinal to a coil containing the specimens. The results of these measurements are given in Table I in terms of the zero-field T_c, transition width (ΔT_c), residual resistivity (ρ_0) (estimated from resistivity ratios), specimen composition, and the measured slope $(dH_{c_2}/dT)_{T=T_c}$. The large uncertainty in $(dH_{c_2}/dT)_{T=T_c}$ results from the low value of the applied field (6,000 gauss

* From Figure 5 it is estimated that uncertainty in temperature determination from run to run is ≈0.04°K.

[7] P. S. Swartz, H. R. Hart, Jr., and R. L. Fleischer, "Effect of Fast Neutron Irradiation on Magnetic Properties and Critical Temperature of Some Type II Superconductors," *Appl. Phys. Ltrs.*, Vol. 4, p. 71, 15 Feb. 1964.

maximum). Despite the low value of the temperature shift ($\approx 0.3°K$), the interpretation of the shift was unambiguous, since the slope of the transition did not change with applied field. On averaging the values in the last column of Table I, one obtains $(dH_{c_2}/dT)_{T=T_c} = (-1.3 \pm 0.2) \times 10^4$ gauss/°K. Significantly $(dH_{c_2}/dT)_{T=T_c}$ for each sample appears insensitive to rather large changes in the residual resistance.

Given $(dH_{c_2}/dT)_{T=T_c}$, one can obtain $H_{c_2}(0)$ and the product, $\kappa_1 H_c(0)$, where $H_c(0)$ is the thermodynamic critical field at $T = 0°K$,

Table I—Properties of Vapor-Deposited Nb_3Sn

Sample	T_c (°K)	ΔT_c (°K)	Composition (Wt. % Nb)	ρ_0 (ohm-cm)	$(dH_{c_2}/dT)_{T=T_c}$ (gauss/°K)
FS-14	18.31	.03	70.5	1.08×10^{-5}	$(-1.4 \pm .2) \times 10^4$
87-2	18.43	.27	70.5	1.25×10^{-5}	$(-1.8 \pm .4) \times 10^4$
86-5	18.40	.40	70.7	——	$(-1.4 \pm .2) \times 10^4$
74	18.20	.30	70.7	1.65×10^{-5}	$(-.9 \pm .1) \times 10^4$
69	18.23	3.00	73.5	3.1×10^{-5}	$(-1.2 \pm .1) \times 10^4$
53	17.90	2.20	72.0	3.1×10^{-5}	$(-1.1 \pm .1) \times 10^4$

and κ_1 is the Landau–Ginzburg parameter at $T = T_c$. We consider two models following Jones, Hulm, and Chandrasekhar.[8] The Abrikosov model for $H_{c_2}(t)$ $(t = T/T_c)$ leads to

$$H_{c_2}(t) = 2\sqrt{2}\kappa_1 H_c(0)\left(\frac{1-t^2}{1+t^2}\right) \tag{1}$$

where the Gorter–Casimir temperature dependence has been used to evaluate $\kappa(t)$. Hence,

$$\left(\frac{dH_{c_2}}{dT}\right)_{T=T_c} = \frac{-2.82\kappa_1 H_c(0)}{T_c}, \tag{2}$$

and

$$H_{c_2}(0) = 2\sqrt{2}\kappa_1 H_c(0). \tag{3}$$

[8] C. K. Jones, J. K. Hulm, and B. S. Chandrasekhar, "Upper Critical Field of Solid Solution Alloys of the Transition Elements," *Revs. Mod. Phys.*, Vol. 36, p. 74, Jan. 1964.

The Gor'kov[8] expression for the temperature dependence of the upper critical field has the same slope at $T = T_c$, but

$$H_{c_2}(0) = 1.25\sqrt{2}\kappa_1 H_c(0). \tag{4}$$

From the averaged data in Table I,

$$\kappa_1 H_c(0) \approx 80 \pm 10 \text{ kilogauss.}$$

For the Abrikosov–Gorter–Casimir form, we thus obtain

$$H_{c_2}(0) \approx 230 \pm 30 \text{ kilogauss,}$$

and for the Gor'kov expression,

$$H_{c_2}(0) \approx 150 \pm 20 \text{ kilogauss.}$$

Goodman[9] has shown that

$$\begin{aligned} \kappa_1 &= \frac{.96\lambda_L(0)}{\xi_0} + \frac{.73\lambda_L(0)}{\Lambda} \\ &= \kappa_0 + \kappa\rho, \end{aligned} \tag{5}$$

where $\lambda_L(0)$ is the London penetration depth at $T = 0°\text{K}$, ξ is the pure metal coherence distance, and Λ is the mean free path. Thus κ_1 should vary linearly with resistivity if we assume that only the mean free path is effected by impurities. The invariance of $(dH_{c_2}/dT)_{T=T_c}$ with ρ (see Table I) is therefore surprising. One explanation is that κ_0 is quite large, and changes in such a way as to compensate the effect of ρ on $\kappa\rho$. Another possible explanation is that the relevant upper critical field is determined by the paramagnetic limit (H_{c_p}) rather than H_{c_2}. In this connection the formula of Clogston[10] leads to $(dH_{c_p}/dT)_{T=T_c} = -3.7 \times 10^4$ gauss/°K, if the full BCS energy gap $2\Sigma_0 = 3.5\, kT_c$ is used.

---

[9] B. B. Goodman, "Type II or London Superconductors," *Revs. Mod. Phys.*, Vol. 36, p. 12, Jan. 1964.

[10] A. M. Clogston, "Upper Limit for the Critical Field in Hard Superconductors," *Phys. Rev. Ltrs.*, Vol. 9, p. 266, 15 Sept. 1962.

[11] Y. Goldstein, "Anomalous Band Gap in Superconducting Nb_3Sn," *Revs. Mod. Phys.*, Vol. 36, p. 213, Jan. 1964.

[12] G. D. Cody and R. W. Cohen, "Thermal Conductivity of Nb_3Sn," *Revs. Mod. Phys.*, Vol. 36, p. 121, Jan. 1964.

If one-half the energy gap were used, a value for which there is some evidence,[11,12] then $(dH_{c_p}/dT)_{T=T_c} = 1.9 \times 10^4$ gauss/°K.

ACKNOWLEDGMENT

The author sincerely acknowledges the helpful discussion with, and valuable suggestions of, G. D. Cody. Appreciation is also extended to G. Cullen for supplying materials on ceramic, to K. Strater for materials on tape, and to R. L. Novak and J. Pellicane for neutron-irradiated specimens.

THE SUPERCONDUCTING PENETRATION DEPTH OF NIOBIUM STANNIDE*

By

G. D. Cody

RCA Laboratories
Princeton, N. J.

Summary—*A review is given of the present theory of the superconducting penetration depth, and its relation to the properties of type-II superconductors. Recent measurements of the penetration depth of Nb_3Sn are discussed in terms of this theory. Finally, a calculation is made of the Bardeen–Schrieffer–Cooper and mixed-state parameters of Nb_3Sn in terms of an effective-mass model.*

Introduction

THE SUDDEN loss of electrical resistance below the critical temperature, T_c, is perhaps the most striking property of a superconductor, but it has long been recognized that the magnetic properties are just as unique and are also more amenable to fundamental analysis. Soon after the discovery of superconductivity, it was found that the normal resistance is restored when the superconductor is inserted in a magnetic field in excess of a critical field, $H_c(T)$. Equally important, later work showed that a pure superconductor expels the magnetic field when cooled to a temperature T in a field less than $H_c(T)$. The reversible nature of magnetic transitions is derived from this observation and permits one to consider the applied field as a thermodynamic variable. From thermodynamic reasoning it can be shown that the maximum free-energy difference between the normal and superconducting state is $H_c^2(T)V/8\pi$, where V is the volume of the superconductor. The critical field is thus shown to be related to the energy stability of the superconducting state.[1]

Further interpretation of the microscopic effect of a field on a superconductor emerges from an analysis of the field distribution. It is apparent that the field cannot drop to zero inside the superconductor

* The research reported in this paper was sponsored by the Air Force Materials Laboratory, Research and Technology Division, Air Force Systems Command, Wright-Patterson Air Force Base, Ohio, under Contract AF33(657)-11208 and RCA Laboratories, Princeton, New Jersey.

[1] For a general background in superconductivity the reader is referred to D. Shoenberg, *Superconductivity*, Cambridge, 1952 and E. A. Lynton, *Superconductivity*, Methuen, 1962.

in an infinitesimal region, but that there must be a finite region of penetration over a distance characteristic of the superconductor. This distance is called the penetration depth, $\lambda(T)$. A schematic diagram of the penetration of a magnetic field at a normal–superconducting boundary is shown in Figure 1. A quantitative definition of λ as shown in Figure 1 is given by

$$\lambda H_0 = \int_{-\infty}^{0} H(x)\,dx. \tag{1}$$

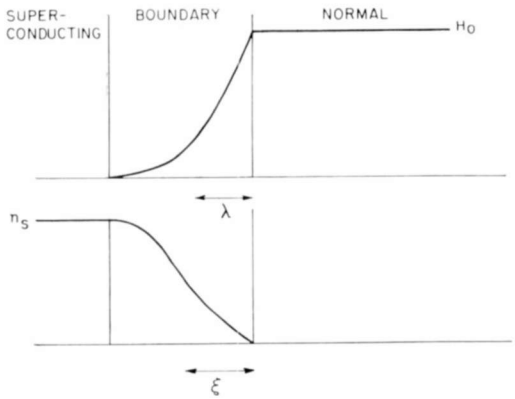

Fig. 1—Superconducting–normal phase boundary.

The first theory to satisfactorily describe the effect of a field on a superconductor was the work of London.[1] Based on the idea of a reversible field transition, and with the model of nondissipative electrons of mass m^*, density n_s, and charge e, London arrived at the following equations to describe a superconductor at low frequencies:

$$\nabla \times \mathbf{j}_s = \frac{-n_s e^2}{m^* c}\,\mathbf{H} \tag{2}$$

and

$$\nabla^2 \mathbf{H} = \frac{4\pi n_s e^2}{m^* c^2}\,\mathbf{H} = \frac{1}{\lambda_L{}^2}\,\mathbf{H}. \tag{3}$$

In Equations (2) and (3), $\mathbf{H}$ is the applied field and $\mathbf{j}_s$ is the current density. Thus, for a plane boundary as in Figure 1,

$$\mathbf{H} = \mathbf{H}_0 \exp\left\{\frac{x}{\lambda_L}\right\}$$

and the field decays exponentially in a characteristic distance, $\lambda_L = [m^*c^2/(4\pi n_s e^2)]^{1/2}$. From Equation (1) we see that $\lambda = \lambda_L$, and a measurement of the penetration depth should give information relative to such fundamental parameters as n_s and m^*. If one substitutes $n_s \approx 5 \times 10^{22}/\text{cm}^3$, $m^* \approx 9 \times 10^{-28}$ gram, and $e = 4.8 \times 10^{-10}$, then $\lambda_L \approx 230$ Å, which is a factor of 2 to 3 less than that observed experimentally for the elemental superconductors at the lowest temperatures. Although the London treatment is in order-of-magnitude agreement, quantitative agreement would require unrealistic values for the ratio of m^* to n_s.

As is often the case, the agreement between theory and experiment is better for the temperature dependence of λ_L than for its absolute value. Given the London interpretation of n_s, one expects λ_L to vary with temperature since n_s presumably goes from a small value at T_c to its full value at $T = 0°\text{K}$. Gorter and Casimir[1] developed a model of the transition that supplied an explicit temperature dependence on the basis of two experimental facts—a second-order transition at T_c, and the essentially T^3 dependence of the specific heat in the superconducting state. Interpreting the order parameter of their two-fluid model as n_s, one has

$$n_s \propto 1 - \left(\frac{T}{T_c}\right)^4,$$

and thus

$$\lambda = \lambda_0 \left[1 - \left(\frac{T}{T_c}\right)^4\right]^{-1/2} = \lambda_0 y. \tag{4}$$

Here λ_0 is the value of the penetration depth at $T = 0°\text{K}$. This temperature dependence is in very good agreement with experimental data for most materials. Small but observable departures from Equation (4) are observed for pure metals as $(T/T_c) \to 0$, and it is one of the successes of the BCS theory of superconductivity[2] that it predicts the observed dependence. Since changes in λ are easier to observe than absolute values, and since the departures from Equation (4) are so small, it is common experimental practice to determine λ_0 from $d\lambda/dy$.*

The good agreement of the temperature dependence of λ with the London–Gorter–Casimir theory would now appear to be fortuitous, since the accepted theory of superconductivity, the BCS theory,[2] is not

---

* For a discussion of this point in which the opposite conclusion is drawn, see J. R. Waldram, "The Surface Impedance of Superconductors," *Advances in Physics*, Vol. 13, p. 1, 1964.

[2] For a review of this theory see J. Bardeen and J. R. Schrieffer, "Recent Developments in Superconductivity," *Progress in Low Temperature Physics* III, C. J. Gorter, Ed., Interscience Publishers, New York, 1961.

a two-fluid model. The BCS theory, however, does lead to a gap in the density of states, and does distinguish between the superconducting electrons and normal "quasiparticles" which, at finite temperature, are excited over the gap. Quantities such as specific heat and thermal conductivity, which are roughly proportional to the number of normal quasiparticles for not too low temperatures, obey an approximate power-law dependence reminiscent of the two-fluid model. However, at very low temperatures they follow an exponential law, which differs significantly.[2] This is perhaps one explanation for the good agreement of $\lambda(T)$ with Equation (4), but its basis is still not completely clear theoretically.

The significance of the BCS theory for the penetration depth, however, does not depend on the temperature dependence alone; it also rigorously accounts for the magnitude of λ_0 and its dependence on mean free path Λ. It is to be noted that apart from its poor numerical agreement with experiment, Equation (3) does not permit any dependence on residual resistivity. From penetration depth measurements on pure metals and alloys where the parameters n_s and m^* were known from resistivity measurements, from anomalous skin-depth measurements, and from measurements of electronic specific heat, Pippard[3] was led to a semi-empirical theory that could account for both the magnitude and mean-free-path dependence of λ_0. His early work was put on a rigorous theoretical basis by the BCS theory, but it remains valid for its quantitative agreement with experiment, and the importance of the physical concepts introduced. Indeed, the idea of second-kind superconductors was implicit in the work of Pippard.

The key concept in this theory is the introduction of a coherence distance for a superconductor. Just as one cannot consider the magnet field at a normal–superconducting boundary falling discontinuously to zero at the interface, one cannot consider the density of superconducting electrons falling discontinuously to zero. Analogous to the penetration depth, a characteristic distance ξ is introduced over which rapid changes in the density of superconducting electrons can occur (Figure 1). It is clear that this distance should play a role in any theory of the electromagnet properties of a superconductor. For example, if an electromagnetic disturbance does not vary greatly over this distance ($\lambda \gg \xi$), one is led to consider a local theory where the response at a point is determined by the field at that point, as in the London equations. Conversely, if the field varies rapidly over the coherence distance,

---

[3] A. B. Pippard, "An Experimental and Theoretic Study of the Relation Between Magnetic Field and Current in a Superconductor," *Proc. Roy. Soc.*, Vol. 216, p. 547, 24 Feb. 1953.

($\lambda \ll \xi$), one is led to consider the response at a point as determined by the field at distance of the order of ξ, since correlations exist over this distance. Rather than the London equations, one emerges with a nonlocal integral equation analogous to the equations of the anomalous skin depth.

On the basis of these ideas and his experimental data on pure metals and alloys, Pippard was led to two forms for the penetration depth. For $\lambda \gg \xi$ (London limit)

$$\lambda = \lambda_L \left(\frac{\xi_0}{\xi} \right)^{1/2}, \tag{5}$$

where

$$\frac{1}{\xi} = \frac{1}{\xi_0} + \frac{1}{0.8\Lambda}, \tag{6}$$

ξ_0 is the pure metal coherence distance, and Λ is the mean free path. For $\lambda \ll \xi$ (Pippard limit),

$$\lambda = 0.65\, \lambda_L \left(\frac{\xi_0}{\lambda_L} \right)^{1/3}. \tag{7}$$

From Equations (5) and (6) we see that the London form is exact for a pure metal such that $\lambda_L \gg \xi_0$. For the other limits, λ is larger than λ_L either because of the short mean free path, or due to the intrinsic ratio of ξ_0 to λ_L.

From an analysis of the data, Pippard was led to the following expression for ξ_0:

$$\xi_0 = \frac{a\hbar v_F}{kT_c}, \tag{8}$$

where v_F is the Fermi velocity, and a is a numerical constant, approximately 0.15. The BCS theory leads[2] to

$$\xi_0 = \frac{\hbar v_F}{\pi \epsilon_0}, \tag{9}$$

where $2\epsilon_0$ is the energy gap at $T = 0°\text{K}$. If $2\epsilon_0 = 3.5\, kT_c$ as predicted by BCS, then

$$\xi_0 = \frac{0.18\hbar v_F}{kT_c}, \tag{10}$$

in quite good agreement.

In this introduction we have discussed the theory of the penetration depth, and have emerged with expressions for λ that depend on fundamental parameters of the normal and superconducting state: n_s, m^*, ξ_0, Λ. One motivation for penetration depth measurements is to test the application of this theory to particular metals. Clearly Nb_3Sn is a good candidate, since it has the highest T_c of any known superconductor (18.3°K) and represents an extreme test for any microscopic theory of superconductivity.

The second motivation arises from the theory of superconductors of the second kind. Let us consider the boundary between a normal and superconducting region as shown in Figure 1. We have approximately

$$F_S = F_N - (V_s - \xi A)\frac{H_c^2}{8\pi} + (V_s - \lambda A)\frac{H_0^2}{8\pi}, \tag{11}$$

where F_s is the free energy of the superconducting region, F_n is the free energy of the same region in the normal state, V_s is the volume of the region and the other quantities have been defined previously. Rearranging Equation (11), we obtain

$$F_S - F_N = -V_s\left(\frac{H_c^2}{8\pi} - \frac{H_0^2}{8\pi}\right) + A\left(\frac{\xi H_c^2}{8\pi} - \frac{\lambda H_0^2}{8\pi}\right). \tag{12}$$

The first term on the right-hand side represents the depression of the energy below that of the normal state arising from bulk properties; the second term represents the surface energy of the interface. Clearly if $\xi > \lambda$, the surface energy is positive and the homogeneous superconducting state is stable relative to the normal state. If $\xi < \lambda$, for $H_0 > (\xi/\lambda)^{1/2}H_c$, the surface energy is negative, and the sample would tend to break up into small domains with a net gain in energy. The magnetization would then not be proportional to $-H_0/4\pi$ up to H_c, but would drop off from $H_L \approx (\xi/\lambda)^{1/2}H_c$. Furthermore, if we suppose the drop-off to be linear up to some upper field H_u, we obtain from energy considerations $H_u H_L \approx H_c^2$; hence, $H_u \approx (\lambda/\xi)^{1/2}H_c$. Thus, one is led to consider the possibility of broad magnetic transitions extending over an order of magnitude or more in field. The work of Abrikosov[4] and others is a more rigorous treatment, and shows that at $T \approx T_c$,

[4] For a review of these theories see T. G. Berlincourt and R. R. Hake, "Superconductivity at High Magnetic Fields," *Phys. Rev.*, Vol. 131, p. 140, 1 July 1963; B. B. Goodman, "Type II or London Superconductors." *Rev. of Mod. Phys.*, Vol. 36, p. 12, Jan. 1964; and T. G. Berlincourt, "Type II Superconductivity," *Rev. of Mod. Phys.*, Vol. 36, p. 19, Jan. 1964.

$$H_L = H_{c1} \approx H_c \frac{\ln(\kappa) + .08}{\sqrt{2\kappa}}, \tag{13}$$

and

$$H_u = H_{c2} = \sqrt{2}\kappa H_c. \tag{14}$$

Here

$$\kappa = 0.96 \frac{\lambda_L}{\xi_0} + 0.73 \frac{\lambda_L}{\Lambda}$$
$$= \kappa_0 + \kappa_\rho. \tag{15}$$

Equation (15) is based on the approximate treatment of Goodman.[4] Furthermore, the work of Abrikosov[4] and others shows that the thermodynamic and magnetic properties of second-kind superconductors in the mixed state are largely a function of the penetration depth and ξ, in the form of Equation (15). Measurements of the penetration depth and their analysis thus permit comparison of the properties of the mixed state of second kind superconductors with current microscopic theories.

The present paper concerns the first measurements of the penetration depth of Nb_3Sn. The following section discusses the experiment and the results. A shorter version of this work was presented at the Eighth Low Temperature Physics Conference at London in September 1962.[5] The last section of the paper examines the results of these measurements with respect to the simplified theory described in this introduction.

Experimental Procedure and Results

Measurements were made of the change in penetration of a longitudinal magnetic field of variable peak amplitude and frequency into specimens of Nb_3Sn over the temperature range 4.2° to 18.2°K. The specimens consisted[6] of platinum wires coated with a chemically deposited layer of Nb_3Sn. Chemical and metallurgical analysis of the individual wires showed the deposit to have the form of a smooth (to $\approx 10^{-4}$ cm) circular cylinder of single-phase Nb_3Sn oriented with the (200) planes parallel to the wire axis. The sample discussed in

[5] G. D. Cody, J. J. Hanak, and M. Rayl, "Magnetic Field Penetration in Nb_3Sn," *Proc. Eighth International Conf. on Low Temperature Physics*, Butterworths, 1964.

[6] J. J. Hanak, p. 161 in *Metallurgy of Advanced Electronic Materials*, ed. by G. E. Brock, Interscience Publishers, New York, 1963.

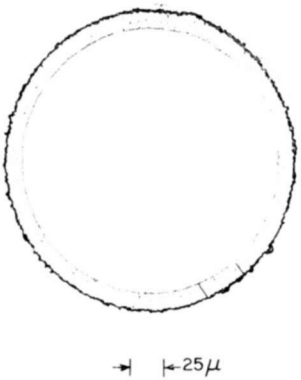

Fig. 2—Cross section of deposited Nb_3Sn sample 43-4 (×400).

detail below (43-4) consisted of 71 wires of length of 2.1 ± .4 cm. The substrate radius was 8.98×10^{-3} cm; the deposit thickness was 10.8×10^{-4} cm. The transition temperature (T_c) of this sample was 17.8°K with a transition width of the order of 1% of T_c. Figure 2 is a photomicrograph of a cross section of the wire. Figure 3 is a larger magnification of the wire. As noted by Hanak[6] these materials have properties similar to those of the sintered materials previously available ($T_c = 18.1$°K; $\Delta T_c / T_c \approx 3\%$), except for the narrow transitions.

The wires were encapsulated in a glass tube with a molybdenum base, and the tube was closed in an atmosphere of 600 torrs of helium gas to ensure thermal equilibrium among the wires. A 0.1-watt, 56-ohm carbon resistor was cemented with GE 7031 adhesive into a hole in the molybdenum base 3 mm below the bottom of the wires. The base fitted

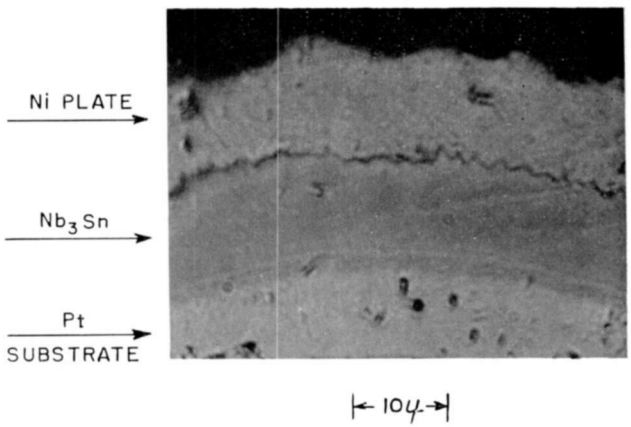

Fig. 3—Cross section of deposited Nb_3Sn sample 43-4 (×2300).

snugly into a hole in a copper block which was kept in good thermal contact with a gas thermometer by Apiezon N grease. A schematic of the apparatus is shown in Figure 4. A 41-mh coil, 1.5 cm long, consisting of 4600 turns of No. 40 copper wire, was placed around the glass tube and grounded thermally to the copper block. The coil and sample were isolated from the bath by a vacuum of about 4×10^{-6} torr. The inductance of this coil was measured as a function of temperature with a high-sensitivity Anderson bridge[7] where changes of inductance and

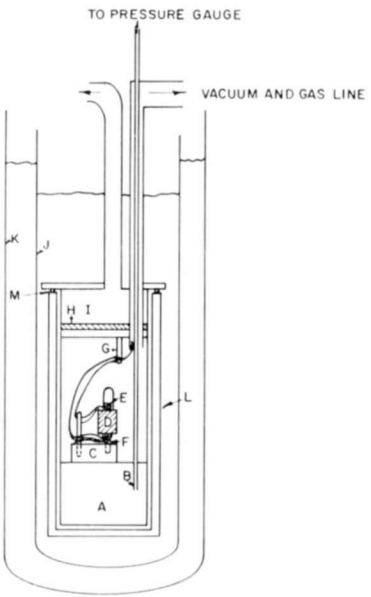

Fig. 4—Schematic of penetration-depth apparatus.

equivalent resistance for the coil could be measured to a precision of about two parts in 10^5 and one part in 10^3, respectively. A schematic diagram of the bridge is shown in Figure 5. The temperature was measured with the carbon resistor calibrated with respect to the vapor pressure of liquid helium and a point at 18.21°K determined by the gas thermometer, which in turn was calibrated with respect to the vapor pressures of liquid helium, nitrogen, and oxygen. The thermometer calibrations did not change during the three days required to obtain the data shown; the liquid-helium calibration points differed by less than 2×10^{-3}°K and temperatures in the range 17° to 18°K

[7] Bleaney and Bleaney, *Electricity and Magnetism*, p. 438, Oxford, 1957.

differed by no more than 2×10^{-2}°K, the limit of the measuring sensitivity, from day to day. The absolute uncertainty in temperature (distinct from the relative uncertainty) is of the order of 1/2%.

The inductance of the coil as a function of temperature was measured; at 200 cps, $H_{max} = 0.57$ oe, at 2000 cps, $H_{max} = 0.28$ oe, and at 2000 cps, $H_{max} = 0.10$ oe. In the course of a run, the temperature was varied at a slow enough rate (<0.10°K/hr), so that the sample was in quasi-static equilibrium with the carbon resistor and the gas thermometer. The change of inductance with temperature $L(T) - L$ (4.2°K) is shown in Figure 6. The curves at the right show the full

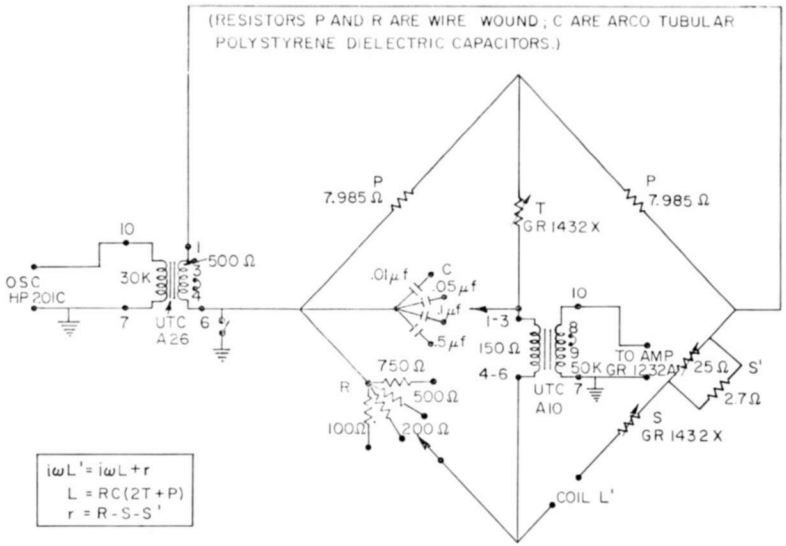

Fig. 5—Anderson inductance bridge.

transitions to the limit of the precision in temperature measurement (some inductance points have been omitted for clarity); the inset curve shows the approach of the sample to the transition to the limit of the precision in measuring the inductance of the coil. The temperature near the horizontal arrows are the transition temperatures obtained from one half the total inductance change in the transition. The inductance change between 4.2° and 18.2°K agrees with that calculated from the geometry of the coil and the total volume of the sample.

The measured inductance of the sample coil for each of the three runs changed by 2.5×10^{-5} from 4.22° to 13°K, by 4.5×10^{-3} from 13° to 17.65°K, by 7×10^{-2} from 17.65° to 17.93°K (the superconducting-to-normal transition), and by 4×10^{-3} from 17.93° to 79.0°K.

It should be noted in Figure 6 that up to 17.65°K the data at 200 cps and 2000 cps are in very good agreement, but above 17.65°K there is a systematic difference. The 2000-cps data are displaced by .02°K and .06°K from the 200 cps data. This difference is outside the temperature

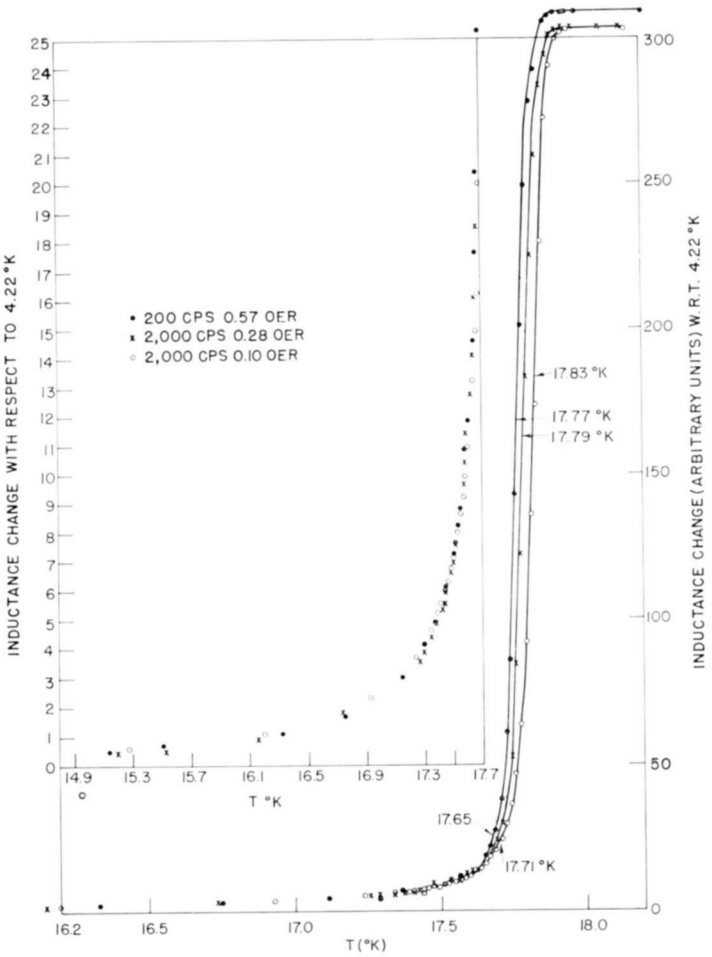

Fig. 6—Inductance change with respect to 4.22°K versus T.

uncertainty, and it appears that it is a secondary effect of the intermediate state properties of this material.

The nature of the intermediate state is shown in Figure 7, where the a-c resistance of the sample coil is plotted as a function of temperature. One notes a small temperature dependence of the resistance below 17.65°K, which is due to the copper losses in the coil. At 17.65°K

there is a clear indication of a sharp rise in the resistance, which reaches a maximum within 0.01°K of the midpoints of the transitions of Figure 6. The a-c resistance above the transition falls to a value close to that below 17.65°K. Such a resistance curve is expected on the basis of eddy-current losses occurring in the intermediate state. Below 17.65°K the sample is superconducting, and there are no losses; above 17.93°K the high resistivity of Nb_3Sn and the substrate reduce the eddy-current losses to a value comparable to the copper losses. The

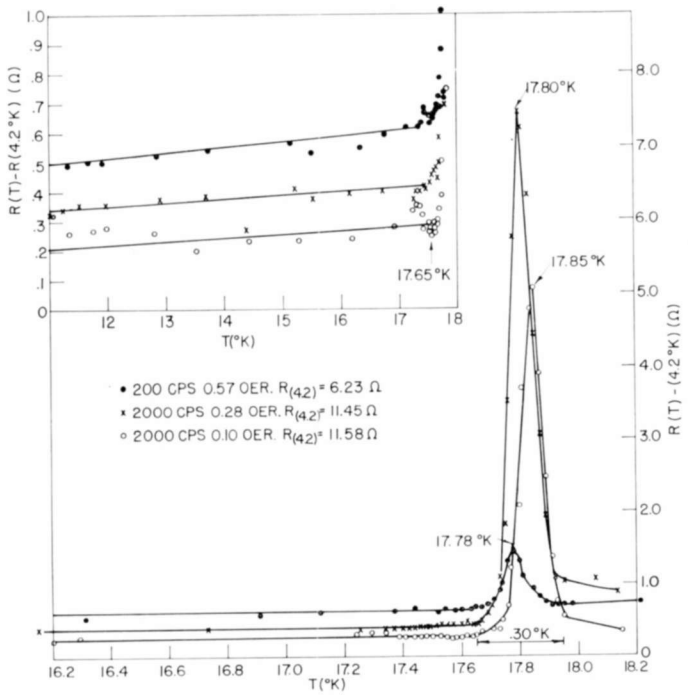

Fig. 7—A-C resistance versus T.

small difference between the 200-cps data and the 2000-cps data above 17.93°K can be accounted for by a slight degree of eddy-current shielding of the sample.

The resistance data shown in Figure 7 can be used to correct for the inductance change introduced through eddy currents on the inductance change associated with the pure superconducting state. It is clear from Figure 7 that, to the accuracy of the present experiment, no such correction is required below 17.65°K, and that below this value the sample appears to be completely superconducting. The large eddy currents in the sample in the intermediate state should have an appreciable

effect on the shape of the inductance curve in this region and, as noted above, are thought to be the cause of the shifts in temperature of the midpoints of the transition. It is apparent that the effect of the eddy currents is to reduce the inductance change at a given temperature and to shift the midpoint of the transition region to higher temperatures. In principle this contribution to the transition curves shown in Figure 6 could be calculated using the data of Figure 7; however, the present accuracy permits only a qualitative treatment.[8,9]

The present measurements are in fair agreement with previous, less accurate measurements on other Nb_3Sn-coated wires. In general, it has been shown in these measurements that there is a region of rapid field penetration that is proportional to the number of wires in the sample, is independent of the thickness of the deposit, and cannot be associated with intermediate-state phenomena. It is a reasonable interpretation of the present data to associate the change of inductance with temperature with a change in the penetration depth of the magnetic field in the superconducting state.

The superconducting penetration depth $\lambda(T)$ can be shown to modify the inductance change for $T < T_c$ in the following manner:

$$\Delta L(T) = \frac{2}{r} (\Delta L)(\lambda(T) - \lambda(0)), \tag{16}$$

where $L(T)$ = measured inductance at temperature T,

$\Delta L(T) = L(T) - L(0)$,

$\Delta L = L(>T_c) - L(0)$,

$\lambda(T)$ = penetration depth at temperature T,

r = radius of a single wire.

It is assumed that the inductance change is proportional to the volume of wires. It has been shown experimentally and theoretically that, to a good approximation,[1,3,10]

$$\lambda = \lambda_0 y \tag{17}$$

---

[8] E. Laurmann and D. Shoenberg, "Penetration of Magnetic Field Into Superconductors. II. Measurement by the Casimir Method," *Proc. Roy. Soc.*, Vol. A198, p. 560, Sept. 1949.

[9] J. E. Zimerman, "Measurement of Electrical Resistivity of Bulk Metals," *Rev. Sci. Inst.*, Vol. 32, p. 402, April 1961.

[10] A. L. Shawlow and G. E. Devlin, "Effect of Energy Gap on the Penetration Depth of Superconductors," *Phys. Rev.*, Vol. 113, p. 120, 1 Jan. 1959.

where

$$y = \left(1 - \left(\frac{T}{T_c}\right)^4\right)^{-1/2}, \tag{18}$$

and

λ_0 = penetration depth at $T = 0°\text{K}$.

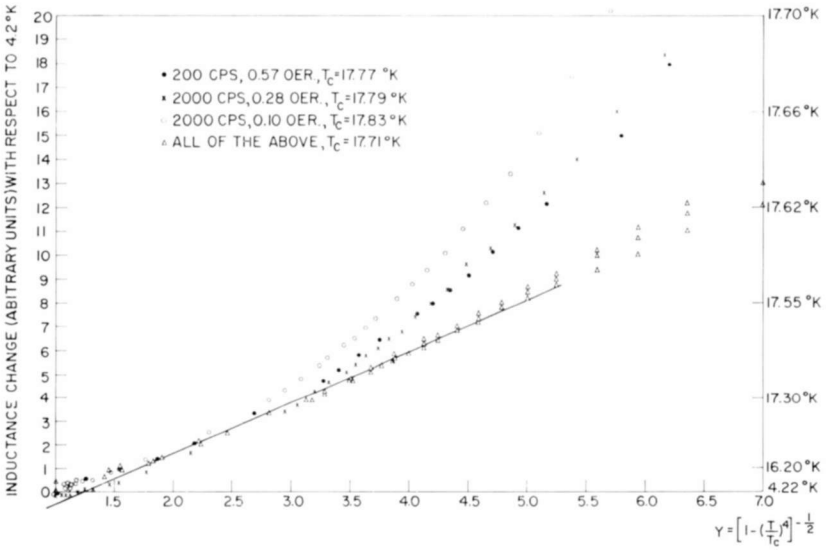

Fig. 8—Inductance change versus y for Nb_3Sn.

From Equations (16) and (17),

$$\frac{d}{dy}\left[\Delta L(T)\right] = \frac{2}{r}(\Delta L)\,\lambda_0, \tag{19}$$

and this expression can be used unambiguously to derive λ_0 if $d(\Delta L(T))/dy$ can be shown to be constant.

The transition width of the present Nb_3Sn sample is approximately 1% of T_c, a factor of three larger than the percentage transition width found for such soft superconductors as tin, lead, and mercury. The value of T_c is relatively unambiguous for such material, and is usually somewhat arbitrarily chosen as the midpoint of the transition curve.[10] In the present experiment the value of T_c is less clear-cut and, as can be seen in Figure 8, is somewhat critical.

Figure 8 shows the inductance changes obtained from Figure 6 plotted against y for two sets of values of T_c. Since the inductance change can be used to construct a temperature scale for each point, this scale has been drawn on the right-hand side of the figure. The first set of points on this graph is based on values of T_c for the midpoints of the transition curve in Figure 6. One notes that these points diverge considerably from a straight line for temperatures in excess of 17.40°K, whereas one would expect such behavior only above 17.65°K. One explanation of the discrepancy is an incorrect choice of T_c, and the second set of points shows the effect of referring all points to $T_c = 17.71$°K. For this value all three runs follow a straight line that joins smoothly to the previous data at $y = 3.3$ (17.4°K), and deviations occur only above $y = 7$ (17.64°K). This functional dependence is what one would expect from Figure 6. The value of λ_0 obtained is 4,040 Å, which is within the uncertainty of preliminary measurements on samples 43-4 and 45-3.

The sources of random error in the determination of λ_0 are uncertainties in temperature, the sensitivity limitation of the bridge, the choice and slope of the line $\lambda(y) = \lambda_0 y$, and the measurement of the radius of the wires. The estimate of the error in λ_0 due to all of these sources is less than 10%. The chief sources of systematic error that have not yet been resolved are surface roughness on a scale less than 10^{-4} cm and a broader intermediate state than assumed. Photomicrographs indicate that, to the limit of resolution of optical microscopy, the average parameter is larger than $2\pi r$ by about a factor of 1.4 (Figure 4), but electron microscopy is required to resolve this point. The experimental value for λ_0 is thus $\lambda_0 \approx 2900$ Å.

Figure 9 shows the results of penetration-depth measurements made on a sample of lead. One notes that for the polished state, the value of λ_0 is in good agreement with literature values[11] of 3.9×10^{-6}. In the etched specimen the penetration depth rose by a factor of 2.5, an effect of the same order of magnitude as was noted previously by Laurmann and Shoenberg[8] on tin.

Discussion

One can compare the present value of the penetration depth with the BCS theory on the basis of a formula originally derived by Pippard from a semi-empirical treatment which is derived from Equations (5), (6), and (10).

---

[11] J. M. Lock, "Penetration of Magnetic Field Into Superconductors. III. Measurement on Thin Films of Tin, Lead, and Indium," *Proc. Roy. Soc.*, Vol. A208, p. 391, Sept. 1951.

$$\lambda_0 = \left(\frac{0.18\hbar c^2}{4\pi (0.8)\sigma k T_c} \right)^{1/2} \tag{20}$$

where σ is the conductivity. With $T_c = 18°\text{K}$ and a resistivity of 3×10^{-5} ohm-cm,[12] Equation (20) gives $\lambda_0 = 1500$ Å, compared to the experimental value of 2900 Å. This may be considered good agreement considering possible systematic errors and theoretical uncertainties, but for the present discussion we will examine the discrepancy in terms of a possible inconsistency in the theory.

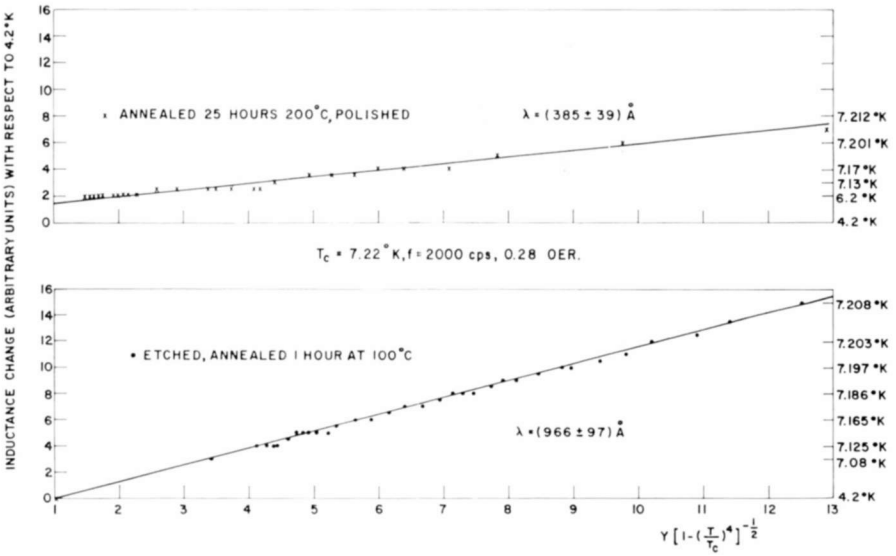

Fig. 9—Inductance change versus y for etched and unetched lead.

Unfortunately, the presently available data make it impossible to use anything but an effective-mass model in a comparison of theory with experiment. The four experimental parameters available are the penetration depth, the electronic specific heat,[13] the transition temperature, and the normal-state resistivity. The unknown quantities are the effective mass, m^*, and the number of electrons per unit volume, νn_0, where n_0 is the atomic density and ν is the valence.

[12] D. W. Woodard and G. D. Cody, "Anomalous Resistivity of Nb_3Sn," *Phys. Rev.*, in press; G. D. Cody, J. J. Hanak, and G. T. McConville, "Resistance Anomaly in β-Tungsten Compounds," *Bull. Amer. Phys. Soc.*, Vol. 6, p. 146, 1961.

[13] F. J. Morin and J. P. Maita, "Specific Heats of Transition Metal Superconductors," *Phys. Rev.*, Vol. 129, p. 1115, 1 Feb. 1963.

One can use the electronic specific heat (γT) to obtain m^* $(\nu n_0)^{1/3}$ from the expression,

$$\gamma T = \frac{\pi m^* k^2}{3\hbar^2}\left(\frac{3\nu n_0}{\pi}\right)^{1/3} T. \tag{21}$$

Hence, if a value of γ is given, m^* is determined for a choice of ν. Given m^* again for a choice of ν one can then determine the London penetration depth,

$$\lambda_L = \left(\frac{m^* c^2}{4\pi \nu n_0 e^2}\right)^{1/2}, \tag{22}$$

and the Fermi velocity, v_F

$$v_F = \frac{\hbar k_F}{m^*} = \frac{\hbar (3\pi^2)^{1/3} (\nu n_0)^{1/3}}{m^*}. \tag{23}$$

From the Fermi velocity and the transition temperature one can determine the Pippard coherence distance ξ_0 from Equation (9). Furthermore, one can then determine the mean free path Λ from the relation

$$\sigma = \frac{n_0 \nu e^2 \Lambda}{m^* v_F}. \tag{24}$$

Finally, one has the BCS[2] relation

$$\frac{H_0^2}{8\pi} \approx \frac{\pi m^* k^2}{3\hbar^2}\left(\frac{3\nu n_0}{\pi}\right)^{1/3} \frac{T_c^2}{4} \tag{25}$$

to determine H_0, the critical field at absolute zero (Equation (25) is based on $2\epsilon_0 = 3.5kT_c$). If one used the following values:

$$\gamma = 150 \times 10^{-4} \text{ cal/mole deg}^2$$

$$= 14.1 \times 10^3 \text{ ergs/cm}^3 \text{ deg}^2 \text{ (Ref. (13))}$$

$$\sigma = 3 \times 10^{16} \text{ ohm}^{-1} \text{ cm}^{-1} \text{ gaussian units (Ref. (12))}$$

$$n = 5.45 \times 10^{22} \text{ atoms/cm}^3 \text{ (based on lattice constant of 5.28 Å) (Ref. (5))}$$

one obtains the data of Table I for various choices of energy gap and valence.

The calculated values of Table I represent a consistent set of free-

Table I—Computed Free-Electron Values of Normal-State, Superconducting-State, and Mixed-State Parameters for Nb_3Sn as a Function of Valence (ν) and Energy Gap ($2\epsilon_0$)

	$\nu = 4.75$		$\nu = 1.00$		$\nu = 0.27$	
$2\epsilon_0(kT_c)$	3.5	1.8	3.5	1.8	3.5	1.8
λ_0[a] (Å)	1500	2120	1900	2400	3000	3380
m^*/m	14	14	23	23	36	36
λ_L(Å)	390	390	1100	1100	2630	2630
Λ(Å)	10	10	28	28	68	68
ξ_0(Å)	125	250	44	88	18	36
v_F(cm/sec)	1.7×10^7	1.7×10^7	6×10^6	6×10^6	2.4×10^6	2.4×10^6
k_F(cm^{-1})	2.0×10^8	2.0×10^8	1.2×10^8	1.2×10^8	7.6×10^7	7.6×10^7
H_c(gauss)	5400	2700	5400	2700	5400	2700
κ_0[b]	3	1.5	24	12	140	70
κ_p[b]	28	28	28	28	28	28
κ[b]	31	29.5	52	40	168	98
H_{c1}(gauss)	415	220	320	197	123	105
H_{c2}(kilogauss)	280	140	490	190	1600	460

[a] Based on Equations (5) and (6).

[b] Based on Equation (15).

electron parameters based on the electronic specific heat data of Morin and Mata, and the residual resistivity. The motivation for the various valences chosen is simply that $\nu = 4.75$ corresponds to the total number of electrons available, $\nu = 1$ corresponds to the usual electron-theory-of-metals value, and $\nu = 0.27$ is a value "derived" from a one-band treatment of the measured Hall coefficient for Nb_3Sn. Two values of the energy gap were used—the BCS value and one half of it. The lower energy gap was chosen in an attempt to raise the computed value of the penetration depth. The data of Table I may be compared with the present penetration depth measurements, upper critical field measurements of Cherry,[14] estimates made by Hecht[15] of the lower critical field, and measurements of dH_{c2}/dt by Cooper.[16] In general, these measure-

[14] W. L. Cherry, "Surge-Magnetic-Field and Pulse-Current Effects in Niobium Stannide," *RCA Review*, Vol. XXV, p. 510, Sept. 1964 (this issue).

[15] R. Hecht, "Lower Critical Field of Niobium Stannide," *RCA Review*, Vol. XXV, p. 453, Sept. 1964 (this issue).

[16] J. L. Cooper, "Transition Temperature of Niobium Stannide," *RCA Review*, Vol. XXV, p. 405, Sept. 1964 (this issue).

ments imply that $H_{c2} \approx 160$-180 kg, $H_{c1} \approx 190$ g, and $\lambda_{exp} = 2900$ Å. The relevant data would thus seem to support the possibility of a small energy gap for Nb_3Sn compared to the BCS value, and indeed the best agreement is for an effective valence of about unity with an energy gap 1/2 that predicted by BCS. It is noteworthy that the table shows that it is possible for κ_0 to be as large, or larger than, κ_ρ due to the high effective mass and high T_c of Nb_3Sn. It is thus possible for the upper critical field to be less sensitive to the conductivity than such second-kind superconductors as Pb-Tl, Pb-Bi, Pb-In, etc. Such insensitivity has been observed by Cherry[14] and Cooper.[16] Moreover, the extremely high value of H_{c2} for some entries in the table would imply that the observed H_{c2} is possibly determined by paramagnetic effects as noted by Clogston[17] and Chandrasekar,[18] rather than mixed-state phenomena.

Thermal conductivity measurements have been shown to be in excellent agreement with the predictions of the BCS theory if one assumes largely impurity limited, electronic conduction, and an energy gap of $2\epsilon_0 = 3.56kT_c$.[19] Tunneling data[20] indicate an energy gap about 1/3 that of the BCS value, but it is possible to interpret this result in terms of a fall-off in the band gap as one approaches the surface, and the restriction of tunneling electrons to those within a mean free path of the surface. The tunneling data is in excellent agreement with this theory if one assumes the energy gap to be at least $1.75kT_c$ in the body of the specimen.

---

[17] A. M. Clogston, "Upper Limit for the Critical Field in Hard Superconductors," *Phys. Rev. Letters*, Vol. 9, p. 266, 1 Oct. 1962.

[18] B. S. Chandrasekhor, "A Note on the Maximum Critical Field of High-Field Superconductors," *Appl. Phys. Letters*, Vol. 1, p. 7, 1 Sept. 1962.

[19] G. D. Cody and R. W. Cohen, "Thermal Conductivity of Nb_3Sn," *Rev. Mod. Phys.*, Vol. 36, p. 121, Jan. 1964.

[20] Y. Goldstein, "Anomalous Band Gap in Superconductive Nb_3Sn," *Rev. Mod. Phys.*, Vol. 36, p. 213, Jan. 1964.

THE SUPERCONDUCTING ENERGY GAP OF NIOBIUM STANNIDE*

By

R. W. Cohen, G. D. Cody, and Y. Goldstein

RCA Laboratories
Princeton, N. J.

Summary—*Measurements of the thermal conductivity of Nb_3Sn in the superconducting and normal states are analyzed in terms of the BCS theory of the superconducting state applied to thermal transport by Bardeen, Rickayzen, and Tewordt. The data lead to a value of $2\epsilon_0 = 3.56\ kT_c$ for the energy gap at $T = 0°K$, in excellent agreement with the BCS theory. The experimental basis for the analysis is discussed and several material parameters of Nb_3Sn are derived. Tunneling measurements of the superconducting density of states of Nb_3Sn are analyzed in terms of two models. The first ignores the role of the surface in the tunneling process and differs from the BCS theory in two basic aspects—a finite density of states in the gap, and a value for ϵ_0 approximately 1/3 that predicted by BCS. The second model is based on the idea that the surface can dominate tunneling in a short-mean-free-path material, such as Nb_3Sn. With the assumption that the energy gap goes to zero at the Nb_3Sn–insulator interface, an excellent fit is obtained for the tunneling characteristics and their temperature dependence. The model implies that the energy gap in the bulk of the specimen is the same as that obtained from the thermal conductivity data, but it drops by a factor of two within one mean free path of the surface.*

Introduction

NIOBIUM STANNIDE is an intermetallic compound that has the A-15 (β-tungsten) structure and possesses a range of compositions from about Nb_3Sn to Nb_4Sn.[1] The stoichiometric compound Nb_3Sn has a transition temperature of 18.3°K, which is the highest transition temperature of any known superconductor. The magnetic transition of Nb_3Sn is characteristic of superconductors of the second kind, and starts at about 200 gauss at 4.2°K,[2] and continues to about 220 kilogauss.[3]

* This work was supported by the Air Force Materials Laboratory, Research and Technology Division, Air Force Systems Command, Wright-Patterson Air Force Base, Ohio, under Contract No. AF33(657)-11208 and by RCA Laboratories.

[1] J. J. Hanak, K. Strater, and G. W. Cullen, "Preparation and Properties of Vapor-Deposited Niobium Stannide," *RCA Review*, Vol. XXV, p. 342, Sept. 1964 (this issue).

[2] R. Hecht, "Low Critical Field of Niobium Stannide," *RCA Review*, Vol. XXV, p. 453, Sept. 1964 (this issue).

[3] W. H. Cherry, "Surge-Magnetic-Field and Pulse-Current Effects in Niobium Stannide," *RCA Review*, Vol. XXV, p. 510, Sept. 1964 (this issue).

Relatively little is known about the normal-state properties of Nb_3Sn. Specific-heat measurements indicate a Debye temperature (θ) of about 300°K, and an electronic specific heat considerably larger than the calculated free-electron value.[4] The electrical resistivity of Nb_3Sn is high ($\approx 10^{-4}$ ohm-cm at room temperature) and displays an anomalous temperature dependence.[5] The Hall coefficient is positive, and if interpreted on a one-band model indicates 0.27 hole per atom, considerably different from the average valence[5] of 4.75. Presumably the transport properties are dominated by light holes in an *s* band, with the balance of the valence electrons occupying high mass states in the *d* band.

Intermetallic compounds of the same crystal structure as Nb_3Sn show low-temperature anomalies in the Knight shift,[6] paramagnetic susceptibility,[6] and nuclear relaxation time, T_1.[7] The proper explanation of these effects awaits a fundamental understanding of the band structure. Qualitative explanations are based on a peak in the density of states at the Fermi level, which manifests itself in the unusual normal-state behavior and the high T_c of many of these compounds. It would appear that a similar peak in the density of states should be expected for Nb_3Sn.

Fundamental information on the superconducting properties of Nb_3Sn is also scarce. Until recently, samples were restricted to those obtained either by sintering or by arc melting, and were not suitable for many measurements. The chemical deposition technique for the preparation of Nb_3Sn led to well-defined specimens of high homogeneity[1] and has made a variety of experiments possible for the first time, including measurement of penetration depth in the superconducting state,[8] and electrical resistivity and Hall measurements in the normal state.[5] As part of a systematic study of the superconducting properties of Nb_3Sn we discuss here the results of two measurements on chemically deposited Nb_3Sn—the thermal conductivity of Nb_3Sn at

---

[4] F. J. Morin and J. P. Maita, "Specific Heats of Transition Metal Superconductors," *Phys. Rev.*, Vol. 129, p. 1115, 1 Feb. 1963.

[5] D. W. Woodard and G. D. Cody, "Anomalous Resistivity of Niobium Stannide," *RCA Review*, Vol. XXV, p. 393, Sept. 1964 (this issue).

[6] A. M. Clogston and V. Jaccarino, "Susceptibilities and Negative Knight Shifts of Intermetallic Compounds," *Phys. Rev.*, Vol. 121, p. 1357, 1 March 1961; A. M. Clogston, A. C. Gossard, V. Jaccarino and Y. Yafet, "Orbital Paramagnetism and the Knight Shift in Transition Metal Superconductors," *Revs. Mod. Phys.*, Vol. 36, p. 170, Jan. 1964.

[7] M. Weger, "The Electronic Band Structure of V_3Si and V_3Ga," *Revs. Mod. Phys.*, Vol. 36, p. 175, Jan. 1964.

[8] G. D. Cody, "The Superconducting Penetration Depth of Niobium Stannide," *RCA Review*, Vol. XXV, p. 414, Sept. 1964 (this issue).

temperatures below 27°K,[9] and the superconducting density of states of Nb_3Sn determined by tunneling experiments.[10] In principle, both of these measurements give information on the superconducting energy gap and its temperature dependence. However, the results of the two measurements differ considerably. The thermal conductivity can be interpreted in terms of an energy gap in excellent agreement as to magnitude and temperature dependence with that predicted by the BCS theory;[11] the tunneling data can be interpreted in terms of an energy gap about a factor of three less, with an anomalous temperature dependence.

The explanation of these results could be based on possibly unique superconducting properties for Nb_3Sn which, as noted above, does exhibit unique normal-state properties. We have chosen, instead, to resolve the differences in a manner that maintains the structure of the BCS superconducting state for Nb_3Sn. The basic idea is that while the thermal conductivity is determined by the bulk properties of the material, and should give an energy gap characteristic of a massive specimen, the tunneling experiment probes the surface of the specimen, and can, under circumstances to be described, give an energy gap considerably different from that of the bulk.

Thermal Conductivity of Nb_3Sn

Normal-State Data

At low temperatures[12] two carriers contribute to the thermal conductivity, κ. If we denote the electronic contribution by κ_e and the phonon or lattice contribution by κ_g,

$$\kappa = \kappa_e + \kappa_g. \tag{1}$$

For each carrier, in turn, several processes contribute to the thermal resistivity, and upon assuming the independence of scattering probabilities, one obtains

---

[9] G. D. Cody and R. H. Cohen, "Thermal Conductivity of Nb_3Sn," *Revs. Mod. Phys.*, Vol. 36, p. 121, Jan. 1964.

[10] Y. Goldstein, "Anomalous Band Gap in Superconducting Nb_3Sn," *Revs. Mod. Phys.*, Vol. 36, p. 213, Jan. 1964.

[11] J. Bardeen, L. N. Cooper, and J. R. Schrieffer, "Theory of Superconductivity," *Phys. Rev.*, Vol. 108, p. 1175, 1 Dec. 1957.

[12] An excellent review of the thermal conductivity of metals and alloys at low temperatures is given by K. Mendelsohn and H. M. Rosenberg in *Solid State Physics*, Vol. 12, p. 223, ed. by F. Seitz and D. Turnball, Academic Press, New York, 1961.

$$\frac{1}{\kappa_{e,g}} = \sum_i W^i_{e,g}. \tag{2}$$

The terms $W^i_{e,g}$ denote the thermal resistance arising from a particular scattering process for either phonons or electrons.

The relative complexity of Equations (1) and (2) would appear to lessen the usefulness of the thermal conductivity for the examination of either the normal or superconducting state. Fortunately, in certain temperature regions only one carrier and one scattering mechanism contributes to κ. In this case the thermal conductivity can be used to furnish fundamental information on the material. The problem is then to evaluate the dominating term $W^i_{e,g}$ as a function of temperature and the constants of the material. Unfortunately, the available analysis of the various scattering mechanisms is based on a free-electron model[13] of doubtful validity for an intermetallic compound such as Nb_3Sn. Despite this fact, the existing theory has been very successful for a wide variety of elemental metals and alloys, and there are some grounds for supposing that Nb_3Sn should be no exception. A more serious problem connected with Equations (1) and (2) is that, even within the framework of the theory, there is little justification for the separation of the total thermal resistance for a particular carrier into various scattering mechanisms. However, the approximation inherent in Equation (2) is a fairly good one when one scattering mechanism dominates; as will be seen, such a condition usually holds in the present experiment.

The theory of the electronic thermal conductivity at low temperatures leads to the following expression[12] for κ_e:

$$\frac{1}{\kappa_e} = \frac{A}{\kappa_\infty \theta^2} T^2 + \frac{\rho_0}{LT}, \tag{3}$$

where κ_∞ is the high-temperature limit of the electronic thermal conductivity, ρ_0 is the residual resistivity, and L is the Lorentz number (2.45×10^{-8} ohm-watt/°K^2). In Equation (3) the first term represents the thermal resistance due to scattering of electrons by phonons; the second term represents electron-impurity scattering. The theoretical value of A is $70N^{2/3}$, where N is the number of free electrons per atom. Experimentally, $A \approx 15$ for a wide variety of metals.[13]

Figure 1 is a plot of T/κ versus T^3 for $T > T_c$ for a vapor-deposited

[13] P. G. Klemens in *Handbuch der Physik*, Vol. 14, p. 245, ed. by G. Flugge, Springer-Verlag, Berlin, 1956.

specimen of Nb_3Sn (FS14).* Although the temperature range is limited (18°-29°K), there is fair agreement with Equation (3). From the intercept of the straight line one obtains $\rho_0 = 1.4 \times 10^{-5}$ ohm-cm. This is in reasonable agreement with the value of 1.1×10^{-5} ohm-cm obtained by direct measurements on a similar sample when one considers the geometrical uncertainties involved in comparing the two resistivities. The slope of the line shown in Figure 1 yields $A/(\kappa_\infty \theta^2) = 1.38 \times 10^{-2}$ cm/watt °K. To obtain κ_∞, an additional measurement

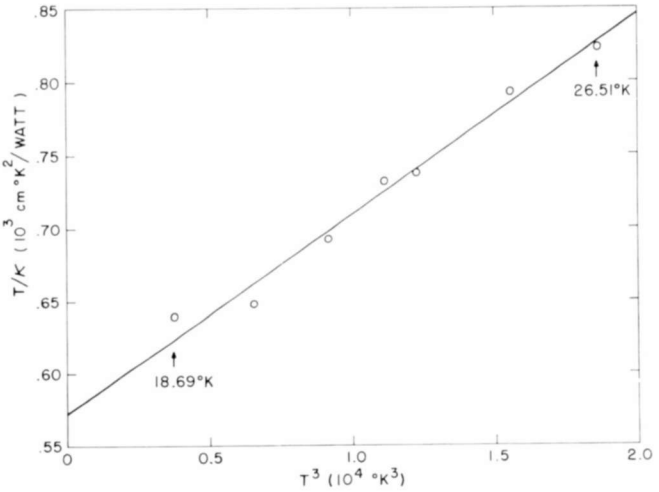

Fig. 1—T/κ as a function of T^3 for Nb_3Sn sample FS14 from 18°K to 27°K.

was taken at 90°K which yielded $\kappa = 36 \times 10^{-3}$ watt/cm °K. The ratio between the phonon-limited thermal resistance at 23°K and 90°K is 0.33. Using the theory of Wilson[14] (of which Equation (3) is the low-temperature limit), one can estimate from this ratio the effective Debye temperature if a value is assumed for N. For the full valence of 4.75, one obtains $\theta = 330$°K, in reasonable agreement with the value of Morin and Maita.[4] From the above value for θ and $A = 15$, one obtains $\kappa_\infty \approx 10 \times 10^{-3}$ watt/cm°K. The anomalous resistivity of Nb_3Sn makes it difficult to determine κ_∞ directly from an extrapolation of the electrical resistivity to high temperatures.[5] The linear term in the electrical resistivity would lead to $\kappa_\infty \approx 300 \times 10^{-3}$ watt/cm°K. This value would be consistent with the above values for θ and $A/(\kappa_\infty \theta^2)$ if A were about

* The details of sample preparation and measurement are given in Ref. (9).

[14] A. H. Wilson, *Electron Theory of Metals*, p. 286, University Press, Cambridge, 1953.

30 times larger than the estimate quoted previously. The estimate of A and κ_∞ is given here for completeness; only the quantity $A/(\kappa_\infty\theta^2)$ occurs in future analysis.

Superconducting State Data

From the analysis of the data in Figure 1, at T_c the ratio of the thermal resistance due to phonon scattering to the thermal resistance due to impurity scattering is 0.09. If we assume the thermal conductivity in the normal state to be electronic in origin one can thus use the simple treatment of Bardeen, Rickayzen, and Tewordt (BRT)[15,16] to determine the temperature variation of the thermal conductivity in the superconducting state, $\kappa_s(T)$. In terms of $\kappa_s(T_c)$, one obtains

$$\kappa_s(T) = \kappa_s(T_c)\frac{T_c}{T}\left\{-0.608\int_{\epsilon/kT}^{\infty} y^2\frac{df}{dy}\,dy\right\} \tag{4}$$

In Equation (4), ϵ is one-half the temperature-dependent energy gap, and

$$f(y) = (e^y + 1)^{-1} \tag{5}$$

is the Fermi distribution function. For $0.95\ T_c \geq T \geq 0.25\ T_c$, an excellent approximation to Equation (4) is

$$\kappa_s(T) \propto \exp\left\{\frac{-b\epsilon_0}{kT}\right\} \tag{6}$$

Here the BCS temperature dependence for $\epsilon(T)$ is assumed, $2\epsilon_0$ is the energy gap at $T = 0°$K, and $b = 0.901$. Figure 2 shows a semi-log plot of $\kappa(T)$ as a function of T_c/T, which yields a straight line from $T = T_c$ to $T_c/T = 2.7$ ($T = 6.9°$K), in agreement with Equation (6). The slope of this line yields $2\epsilon_0 = 3.56\ kT_c$, in striking agreement with the BCS value of $2\epsilon_0 = 3.52\ kT_c$ and the BCS temperature dependence for $\epsilon(T)$.

Figure 3 shows the measured thermal conductivity on a linear scale as a function of temperature from 26.5° to 2.62°K. Also shown in the figure are the computed curve for κ_n (normal state conductivity) obtained from Figure 1 and the theoretical curve obtained from the BRT

[15] J. Bardeen, G. Rickayzen, and L. Tewordt, "Theory of Thermal Conductivity of Superconductors," *Phys. Rev.*, Vol. 113, p. 982, 15 Feb. 1959.

[16] L. P. Kadanoff and P. Martin, "Theory of Many-Particle Systems. II. Superconductivity," *Phys. Rev.*, Vol. 124, p. 670, 1 Nov. 1961.

expression (Equation 4), κ_{BRT}, which is normalized to agree with the data at 18.3°K. Below 6°K the temperature dependence is less rapid than the BRT expression. As discussed below, the low-temperature points are associated with a phonon contribution to the thermal conductivity which is boundary limited.

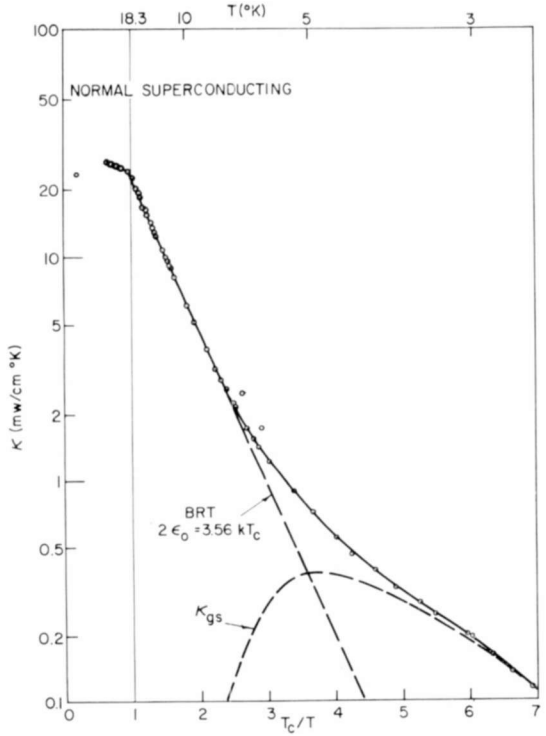

Fig. 2—Semi-log plot of the total thermal conductivity as a function of T_c/T. The linear curve corresponds to the BRT expression for electronic thermal conductivity (impurity limited) with the energy gap given by $2\epsilon_0 = 3.56kT_c$. The dashed curve labeled κ_{gs} is the lattice contribution to the thermal conductivity.

Lattice Thermal Conductivity

If we insert in Equation (2) theoretical values[12] for the lattice thermal conductivity, we obtain for $T \leq 0.1\ \theta$,

$$\frac{1}{\kappa_g} = \frac{E}{T^2} + \frac{D}{T^2} + \frac{B}{T^3} + \frac{P}{T} + UT^n \exp\left\{-\frac{\theta}{mT}\right\}, \qquad (7)$$

where the various terms correspond to phonon scattering by electrons,

dislocations, boundaries, point defects, and umklapp process. It can be shown that in the temperature range of interest, and for reasonable values of the material constants of Nb_3Sn, one can neglect all but the first term on the right-hand side of Equation (7) for the *normal* state thermal conductivity κ_{gn}. This term, $1/\kappa^E_{gn}$, corresponds to electron scattering, and is given by

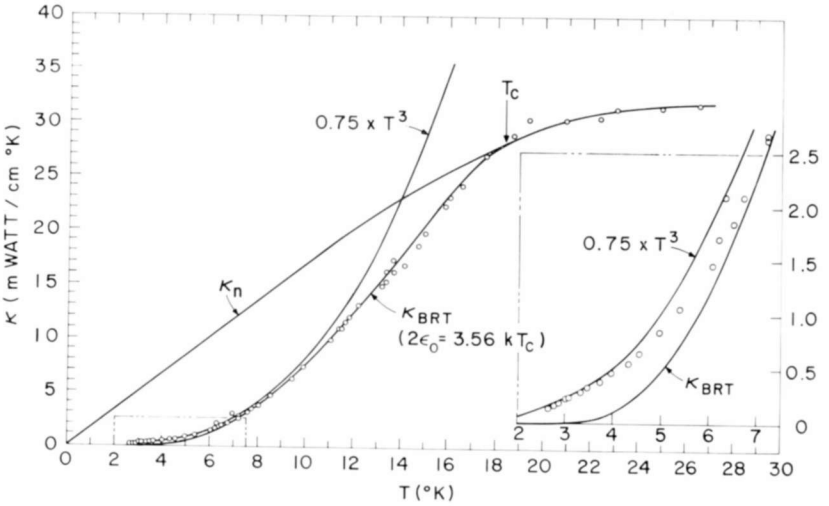

Fig. 3—The total thermal conductivity on a linear scale from 2.62°K to 26.5°K. The estimated value for the normal electronic conductivity, Equation (3), is also shown over this range, as well as the BRT expression for the thermal conductivity in the superconducting state, Equation (4), and the low-temperature limit of the phonon thermal conductivity, Equation (10). The insert shows on an expanded scale the low-temperature points.

$$\kappa^E_{gn} = \frac{\kappa_\infty \theta^2}{3.2 \times 10^{-3} A} \frac{T^2}{\theta^4 N^{4/3}}. \tag{8}$$

If we substitute into Equation (8) the values of $\kappa_\infty \theta^2/A$ and θ obtained previously,

$$\kappa_{gn} = \kappa^E_{gn} = \frac{1}{N^{4/3}} \left(\frac{T}{724} \right)^2. \tag{9}$$

For reasonable values of $N (5 \geq N \geq 1)$ one can neglect κ_{gn} with respect to κ_{en} below 30°K. For $T \ll T_c$, however, κ_{es} becomes very small and one expects κ_g to be observable. Indeed, as the number of "normal"

electrons is reduced in the *superconducting* state, $1/\kappa^E{}_{gs}$ approaches zero. However, one expects boundary-limited phonon scattering ($\kappa^B{}_g$, the third term on the right hand side of Equation (7)) to eventually dominate κ_{gs}. Since this term should be unaffected by the state of the material, we expect at the lowest temperatures

$$\kappa \approx \kappa^B{}_{gs} = \kappa^B{}_{gn} = 0.6\, l_g T^3, \tag{10}$$

where the data of Morin and Maita[4] have been used to evaluate the low-temperature lattice specific heat, and l_g is the mean free path of the phonons, presumably of the order of the grain size of the specimen. The experimental data at low temperatures is in fair agreement with a T^3 dependence as shown by the expanded plot in the insert of Figure 3. The computed value of l_g is of the order of 1000 Å, in fair agreement with electron microscopic estimates made by M. Coutts of these Laboratories of the grain size in vapor-deposited Nb_3Sn.

Prior to the boundary limitation one expects the phonon contribution to rise exponentially as the "normal" electrons (quasi particles) condense. Indeed, from the BRT theory[15] one expects $\kappa^E{}_{gs}/\kappa^E{}_{gn} \approx 200$ at $T/T_c \approx 0.33$. From the experimental data at 6°K, one estimates $\kappa^E{}_{gs} \approx 0.3 \times 10^{-3}$ watt/cm°K; hence, $\kappa^E{}_{gn} \approx 1.5 \times 10^{-6}$ watt/cm°K. From Equation (9) with $N = 4.75$, $\kappa^E{}_{gn} \approx 9 \times 10^{-6}$ watt/cm°K; the discrepancy is about a factor of 6. The data of Laredo[17] and Hulm[18] would indicate that BRT overestimate $\kappa^E{}_{gs}/\kappa^E{}_{gn}$, which is a possible explanation of this discrepancy. Unfortunately, it is difficult to estimate the uncertainty in $\kappa^E{}_{gs}$ for the present experiment. In the temperature region around 6°K, both boundary scattering and electronic scattering are of similar magnitude; the relationship according to Equation (2) is probably no longer valid.

Thermal Conductivity in a Magnetic Field

The thermal conductivity in a longitudinal magnetic field was measured at 15.0°K and 17.5°K in a field of 6500 gauss. The change in thermal conductivity with field can be estimated in two ways. The first follows Dubeck *et al*[19] and assumes that the energy gap is a linear function of the field from the lower critical field, H_{c1}, to the upper

[17] S. J. Laredo, "The Thermal Conductivity of Tin at Low Temperatures," *Proc. Roy. Soc.*, Vol. A229, p. 473, 24 May 1955.

[18] J. K. Hulm, "The Thermal Conductivity of Tin, Mercury, Indium and Tantalum at Liquid Helium Temperatures," *Proc. Roy. Soc.*, Vol. A204, p. 98, 22 Nov. 1950.

[19] L. Dubeck, P. Lindenfeld, E. A. Lynton, and H. Rohrer, "Thermal Conductivity of Superconductors of the Second Kind," *Phys. Rev. Ltrs.*, Vol. 10, p. 98, 1 Feb. 1963.

critical field, H_{c2}. The second assumes that the number of quasi-particles is a linear function of the field.[20,21] This latter dependence may be due, for example, to a layered or vortex structure that has an essentially normal core, and where the number of such cores increases linearly with field. If it is assumed that there is no other effect of a field beyond the above possibilities, we obtain the results of Table I. The values of H_{c2} used in the calculation are also given in Table I.

The data are in better agreement with a linear variation in the number of quasi particles with field, but is inconclusive. Experiments are in progress with a larger magnetic field than 6500 gauss, and at temperatures where greater sensitivity is to be expected.

Table I—Estimate of the Effect of a Longitudinal Field of 6500 Gauss on κ $\kappa_s(H,T)/\kappa_s(0,T)$

T	a	b	c	H_{c2}[d]
15°K	≤ 1.01	1.04	1.02	53,000
17.5°K	≤ 1.02	1.01	1.01	8,500

(a) Present work.
(b) From linear variation of energy gap and Equation (4).
(c) From linear variation of number of quasi particles and Figure 3.
(d) Unpublished data, G. W. Cullen and G. D. Cody (field at which resistance appears at $\approx 10^2$ amp/cm^2).

Tunneling Measurements

The samples for the tunneling measurements were chemically[1] deposited in strip form into grooves cut previously in ceramic plates. After the deposition process, the ceramics, with the Nb_3Sn strip on it, were ground and polished to a flat smooth surface. To remove the damaged surface layer the samples were subsequently electropolished cathodically in a mixture of 10% HF, 40% HNO_3 and 50% H_2SO_4 at 12 volts. This usually resulted in a fairly smooth surface. The samples were oxidized by exposure to air for a period of several hours at room temperature. After the oxidation two metallic strips, usually lead or indium, were evaporated across the Nb_3Sn strip to make up two tunnel

[20] B. Rosenblum, M. Cardona, and G. Fischer, "Microwave Studies of Niobium Stannide," *RCA Review*, Vol. XXV, p. 491, Sept. 1964 (this issue).

[21] C. Caroli, P. G. de Gennes, and J. Matricon, "Bound Fermion States on a Vortex Line in a Type II Superconductor," *Physics Letters*, Vol. 9, p. 307, 1 May 1964.

junctions. Samples polished only mechanically were also tried, but the junctions were invariably found shorted.

The current–voltage (I–V) characteristics and the conductance, dI/dV, of the junctions were measured by a four-contact[22] method. The I–V curves were recorded continuously by an X-Y recorder, using a variable constant-current source. The conductance was measured point by point in the following manner. The current was increased slowly until the voltage across the tunnel junction reached a value of ΔV. At this point the current scale of the recorder was adjusted to zero, and

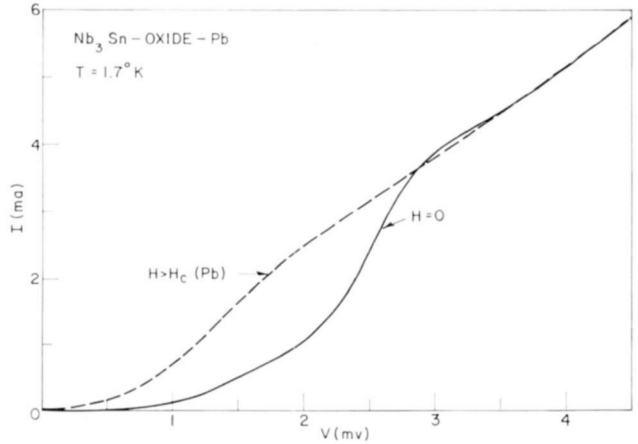

Fig. 4—Typical I–V curves for Nb_3Sn tunnel junctions with superconducting ($H = 0$) and normal ($H > H_c$) lead at 1.7°K.

then the current through the junction increased to yield a voltage of $2\Delta V$. By repeating this procedure one obtains a series of ΔI values as a function of the total voltage V across the tunnel junction. Because the voltage steps are constant (ΔV), the current increments ΔI are proportional to $\Delta I/\Delta V$. To get a good approximation to the derivative dI/dV, the voltage steps were kept down to a value of 0.1 millivolt.

Figure 4 shows two typical I–V curves for Nb_3Sn–Pb junctions at 1.7°K. The one for $H = 0$ corresponds to the lead being superconducting, while the curve for $H > H_c$(Pb) was taken with an applied magnetic field above the critical field of lead and corresponds to normal lead. The essentially zero current up to 0.5 millivolt for the superconductor–superconductor junction shows that one may rule out the possibility of a short across the oxide layer. In junctions where such a short was

[22] I. Giaver and K. Megerle, "Study of Superconductors by Electron Tunneling," *Phys. Rev.*, Vol. 122, p. 1101, 15 May 1961.

present it always showed up as superconducting, that is a high current with a zero voltage drop across the junction. Such a superconducting short could be quenched either by a magnetic field or by passing high currents through the junction. Moreover, these shorts were found in most cases to exhibit nonlinear behavior even to the extent of discontinuities in the I–V characteristics. Figure 5 shows such an erratic behavior for an Nb_3Sn–In junction at a temperature below the transition temperature of indium. In Figure 4, there are two striking features in the I–V curves. First, the curve for $H = 0$ does not show any

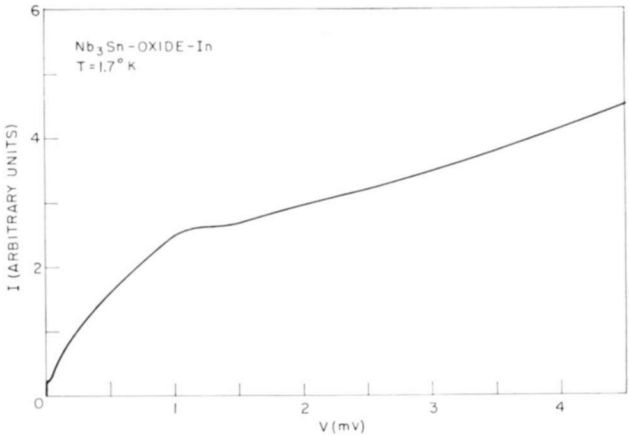

Fig. 5—An I–V curve for an Nb_3Sn–In tunnel junction at 1.7°K, showing the erratic behavior in the presence of a metallic short across the oxide layer.

negative-resistance region. Assuming the BCS ratio[11] to hold for Nb_3Sn (as evidenced by the thermal conductivity data), the energy gap of Nb_3Sn should be more than twice as large as that of lead. The curve for $H = 0$ was taken with both sides of the junction superconducting, and one would expect on theoretical grounds a broad region of negative resistance.[23] The other feature of interest is the finite initial slope of the I–V curve for normal lead. At 1.7°K (about 0.1 of the transition temperature of Nb_3Sn), one would expect an initial slope of virtually zero regardless of whether the other metal is normal or superconducting. That the value of the conductance (dI/dV) at $V = 0$ is high above the expected theoretical value is most readily seen from Figures 6 and 7. In Figure 6 the conductance values for two Nb_3Sn tunnel junctions

[23] See, e.g., S. Shapiro, P. H. Smith, J. Nicol, J. L. Miles, and P. L. Strong, "Superconductivity and Electron Tunneling," *IBM Jour. Res. and Dev.*, Vol. 6, p. 34, Jan. 1962.

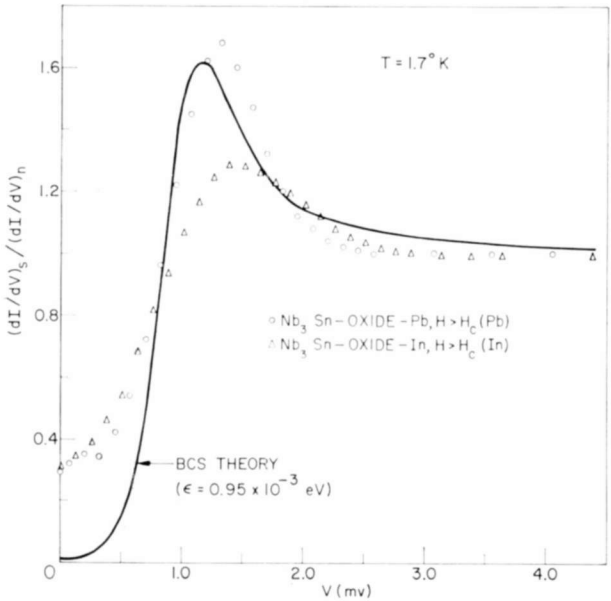

Fig. 6—Conductance values relative to the normal-metal–normal-metal conductance for two tunnel junctions at 1.7°K together with the theoretical curve.

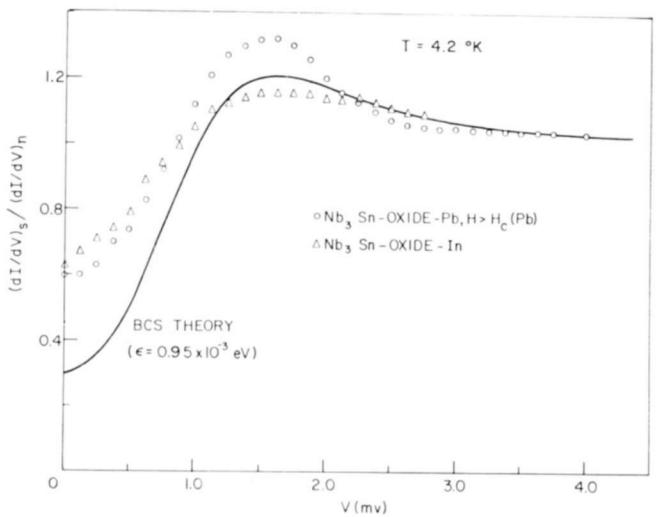

Fig. 7—Relative conductance values for two tunnel junctions at 4.2°K together with the theoretical curve.

(one with lead and one with indium, both in normal state) at 1.7°K are plotted as a function of the applied voltage. The theoretical curve was calculated as usual[24-26] from the BCS theory.[11] To obtain any reasonable fit with the experimental data, the value of $2\epsilon = 1.9$ meV was chosen for the (temperature dependent) energy gap of Nb_3Sn. As noted, at low voltages there is a serious discrepancy between the experimental and theoretical values of the tunneling conductance, the former converging to about 0.3 at $V = 0$. This value was found to be reproducible from sample to sample. The situation is similar at 4.2°K, as shown in Figure 7. To calculate the theoretical curve, the BCS temperature dependence was assumed for the energy gap of Nb_3Sn, and accordingly again the value of $\epsilon = 0.95$ meV was used. (In the temperature range 1.7° to 4.2°K the variation of $\epsilon(T)$ is negligible.) The agreement between the experimental data and the theoretical curve is considered worse than for 1.7°K. The experimental values of the tunneling conductance at low voltages lie again above the theoretical values, and converge to the value of 0.6 at $V = 0$. In addition, the sharp rise in the conductance occurs at lower voltages than the rise in the theoretical curve. This latter feature can be fitted somewhat better by assuming a value of 0.75 meV for $\epsilon(T)$ at 4.2°K.

The value of the energy gap at 1.7°K ($\approx 0.1T_c$) is a good approximation to its value at $T = 0$°K, $2\epsilon_0$. Using the value of 1.9 meV, the ratio of $2\epsilon_0$ to kT_c would seem to be 1.3—much lower than the theoretical[11] ratio of ≈ 3.5. The data at 4.2°K imply a strongly temperature-dependent gap at low temperatures, contrary to the BCS theory. Moreover, the experimental data cannot be really fitted by the usual simple model of tunneling and the BCS density of states. This would indicate an anomalous superconducting state for Nb_3Sn. On the other hand, the results can be interpreted on the basis of a surface effect, as discussed in the next section.

Because the energy gap of Nb_3Sn appeared to be so small and quite close to that of lead, the possibility arose that this may be the reason for the absence of a negative-resistance region in the I–V curves of Nb_3Sn–Pb junctions. To check this, measurements were taken at temperatures close to the transition temperature of lead, where the energy gap of lead decreases rapidly. No evidence of a negative-resistance

---

[24] J. Nicol, S. Shapiro, and P. H. Smith, "Direct Measurement of the Superconducting Energy Gap," *Phys. Rev. Ltrs.*, Vol. 5, p. 461, 15 Nov. 1960.

[25] J. Bardeen, "Tunneling from a Many-Particle Point of View," *Phys. Rev. Ltrs.*, Vol. 6, p. 57, 15 Jan. 1961; "Tunneling Into Superconductors," Vol. 9, p. 147, 15 Aug. 1962.

[26] M. H. Cohen, L. M. Falicov, and J. C. Phillips, "Superconductive Tunneling," *Phys. Rev. Ltrs.*, Vol. 8, p. 316, 15 April 1962.

region was found. Similarly, no negative-resistance region was found in the I–V curves of Nb_3Sn–In junctions. Below the transition temperature of indium ($\approx$3.4°K) there appeared a small hump around 0.5 millivolt, as can be seen in Figure 8. The voltage where this hump appears corresponds roughly to half the energy gap of indium, where one would expect a sharper rise were Nb_3Sn normal. Upon applying a magnetic field higher than H_c(In), this hump disappeared and the whole curve shifted slightly.

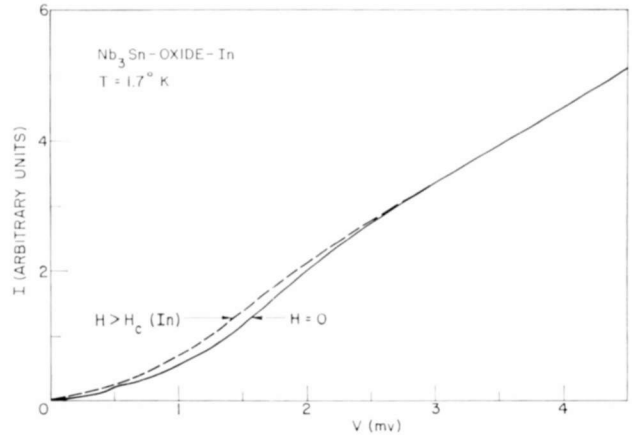

Fig. 8—Typical I–V curves for Nb_3Sn tunnel junctions with superconducting ($H = 0$) and normal ($H > H_c$) indium at 1.7°K.

No change in the tunneling characteristics of Nb_3Sn due to applied magnetic fields up to 7500 gauss was observed. Once the critical field of the other metal (lead or indium) was exceeded, the curves did not change by increasing the field further.

Discussion

The present work presents a fairly complete picture of the low-temperature thermal conductivity of Nb_3Sn. In the normal state, below 90°K, the thermal conductivity is electronic in origin, and largely impurity limited. Assuming the full valence of 4.75, the effective Debye temperature is 330°K, in fair agreement with specific-heat data.[4] The values for electron–phonon interaction constants are in reasonable agreement with present theories of metallic thermal conductivity, and the value of the residual resistivity derived from the thermal conductivity data is in good agreement with independent measurements. Below T_c the agreement with the BRT theory[15] is excellent, and the

energy gap at $T = 0°K$ is in excellent agreement with the BCS relation,[11] $2\epsilon_0 = 3.52\ kT_c$. At the lowest temperatures there is evidence for a boundary-limited phonon contribution with a distance between boundaries of $\approx$1000 Å. This is of the same order as that obtained from Coutts' substructure studies by electron microscopy. Rather than indicating anomalous behavior, the present data furnish additional evidence for the wide applicability of the BCS theory of the superconducting state, and support the BRT expression for the impurity-limited electronic thermal conductivity in the superconducting state of Nb_3Sn.

It is clear that the value of the superconducting energy gap obtained from the tunneling experiments disagrees markedly with the BCS value and the results of the thermal conductivity measurements. The difference cannot be accounted for by any experimental error; it is, therefore, natural to conclude that the two experiments measured different quantities. Considerable effort was put into examining certain schemes and models that seemed to offer some promise of reconciling the results of the two experiments. These models fell into two categories—bulk effects and surface effects. All of the bulk effects were subsequently eliminated on the basis of the failure of each model to explain one or more of the experimental features. It was then found that a very simple model of the surface can satisfactorily explain the main features of the tunneling curve while maintaining an energy gap in agreement with the BCS theory and confirmed by the thermal conductivity experiments.

The basis of any explanation of the experimental results must involve a drastically reduced energy gap. It is reasonable to assume that only those particles within essentially an electronic mean free path (l) of the surface are able to contribute to the tunneling current. Thus, if the energy gap at the surface is reduced over a region roughly equal to l, the effective gap observed in a tunneling experiment will be correspondingly small. In order to explain at the same time the results of the thermal-conductivity experiment, it is necessary for the gap to rise to a value of $3.56kT_c$ in the bulk material. The authors believe that this is the most likely explanation of the experimental results. There are several possible mechanisms that can account for such a reduced gap at the surface. The behavior of the gap in the neighborhood of an ideally sharp insulator–superconductor interface has been treated before.[27] It has been found that the value of the gap at the interface can be only a few per cent less than the bulk value. However, the oxide–superconductor interface is certainly far from ideal when examined over distances of 10 Å. There may be a small region of oxygen-saturated

[27] R. H. Parmenter, "Theory of Superconducting Contacts," *Phys. Rev.*, Vol. 118, p. 1173, 1 June 1960.

Nb_3Sn in concentrations large enough to suppress superconductivity, but not large enough to display the electrical properties of an insulator. This layer would probably be formed by the diffusion of oxygen atoms into a few monolayers of Nb_3Sn during the normal growth of the oxide. The effect of these impurity atoms is to drastically reduce the energy gap in the vicinity of the surface.[28] Moreover, these tunneling measurements were performed on bulk samples and not, as is the usual case in tunneling experiments, on evaporated layers. It is conceivable that the chemical preparation left the surface with a thin impurity layer of foreign particles which may likewise contribute to the reduction of the energy gap. This was probably evidenced by tunneling measurements on bulk samples of niobium.[29]

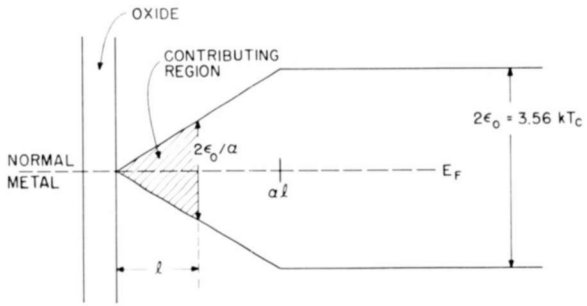

Fig. 9—Schematic diagram illustrating the model used to explain the results of the tunneling experiments.

Assuming[8] that the Pippard coherence length, ξ, is of the same order as the mean free path, l, the energy gap at a distance l from the surface will still be below its bulk value. To demonstrate how such a reduced energy gap near the surface can effectively explain the results of the tunneling experiments, let us consider a simple model illustrated in Figure 9. The energy gap rises linearly from zero at the surface to its bulk value of $3.56kT_c$ in a distance αl, α being a parameter determined from experiment. The linear variation was chosen to simplify the calculation. The model also assumes that all particles within a mean free path l of the surface have equal tunneling probabilities, and that all those located beyond l have a zero tunneling probability. An exponential decrease in tunneling probability with the distance from the

[28] P. G. de Gennes, "Boundary Effects in Superconductors," *Revs. Mod. Phys.*, Vol. 36, p. 225, Jan. 1964.

[29] P. Townsend and J. Sutton, "A Study of Superconducting Niobium by Electron Tunneling," *Proc. Phys. Soc.* (London), Vol. 78, p. 309, Aug. 1961.

surface would be closer to the truth, but the effect of such a function is essentially to introduce a cutoff at l. Under the above assumptions, the expression for the tunneling conductivity normalized to unity for the normal metal is

$$\frac{(dI/dV)_s}{(dI/dV)_n} = \frac{1}{l}\int_0^l dx \int_{\epsilon_0 x/\alpha l}^{\infty} \frac{y\,dy}{\sqrt{y^2 - (\epsilon_0 x/\alpha l)^2}} \frac{\partial}{\partial y}[f(v-y) - f(v+y)] \tag{11}$$

where f is given by Equation (5), $2\epsilon_0$ is the full energy gap (in units of kT) as determined by the thermal conductivity measurements and $v = eV/kT$. The parameter α is the only one that can be varied to fit the experimental data.

Figures 10 and 11 show graphs of the normalized tunneling conductivity versus voltage bias for $T = 1.7°K$ and $4.2°K$, respectively. The experimental points for the Nb_3Sn–oxide–In sandwich are shown for comparison. The parameter α has been chosen to be 2.0 ± 0.05, so that the maximum occurs at a voltage bias of 1.4 millivolts at 1.7°K. The data for 1.7°K are fit very well by the theoretical curve with the exception of a somewhat smaller predicted conductivity at very small voltage biases. The fit at small biases could be improved by extending a tail on the energy-gap function near the surface. The fact that the magnitude of the conductivity maximum is reproduced so well by the theory is probably somewhat fortuitous, since the model under consideration is so crude.

The theoretical curve for 4.2°K, using the same value for α, reproduces both the magnitude and position of the maximum. The fit, however, is not as good as that at 1.7°K, most of the deviation again coming at small biases. It is noteworthy that, while the simple BCS theory for a band gap chosen to give the best fit at 1.7°K predicts a shift in the position of the maximum of 0.6 millivolt when the temperature is raised from 1.7° to 4.2°K, the theory presented here predicts the experimentally observed shift of only 0.2 millivolt.

Because this model implies that at the Nb_3Sn surface there is a thin region that is essentially normal, one would expect a faster rise in the I–V characteristics when the other metal (In or Pb) is superconducting, at voltage biases approximately equal to ϵ/e of the appropriate metal. This is observed in fact both with In and Pb in the superconductor–superconductor characteristics at 0.5 and 1.4 millivolts, respectively (see Figures 4 and 8, $H = 0$), which are the right values for

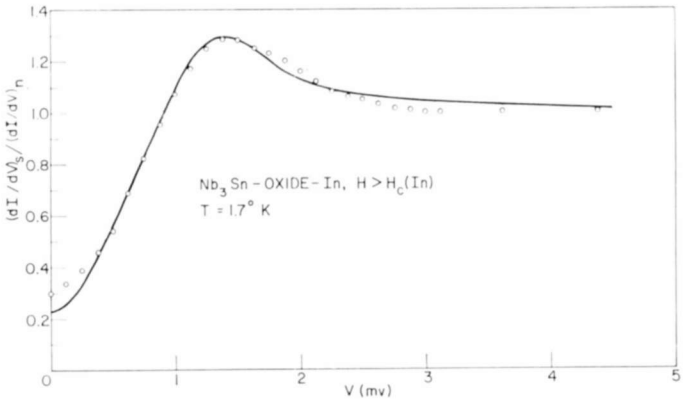

Fig. 10—The conductance values of the Nb_3Sn–In junction from Figure 6 and the theoretical curve calculated from Equation (11) with $\alpha = 2.0$.

indium and lead. At lower voltage biases the model predicts a larger current than for a truly superconductor–superconductor junction, which is likewise observed.

It is appropriate at this point to summarize briefly the above considerations. If the energy gap is assumed to fall off linearly from its bulk value of $3.56kT_c$ to zero at the surface over a distance of $2l$, the main features of the tunneling curves for the Nb_3Sn–oxide–In sandwich are explained. The large conductivity at low voltage biases, the magnitude of the conductivity maximum, and the temperature dependence of

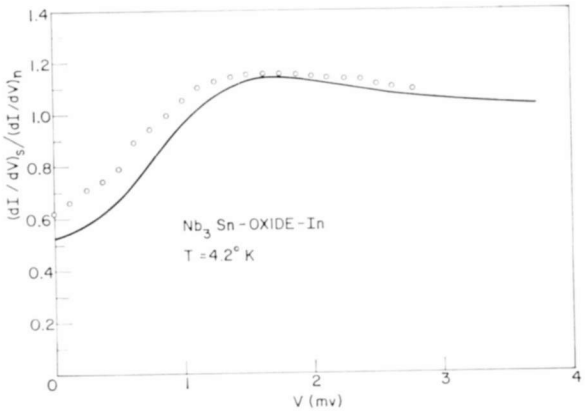

Fig. 11—The conductance values of the Nb_3Sn–In junction from Figure 7 and the theoretical curve calculated from Equation (11) using the same value for α as in Figure 10.

the position of the maximum are reproduced by this model. It also explains semiquantitatively the detailed shape of the I–V characteristics of the superconducting–superconducting junctions. None of these can be explained by the simple BCS theory. It is thought that the mechanism responsible for the small energy gap near the surface involves the presence of an impurity layer at the surface and/or diffused impurity atoms—possibly oxygen—in a region of the order of $\approx$10 Å bordering the surface. The theory, in its present stage, does not account for the small difference in the tunneling characteristics when different metals, such as Pb, are used as electrodes. Apparently the proximity of different metals alters the behavior of the energy gap function near the surface of Nb_3Sn. The reason for this is not yet understood.

LOWER CRITICAL FIELD OF NIOBIUM STANNIDE

By

R. Hecht

Summary—*The lower critical field H_{c1} in Nb_3Sn has been measured by identifying it with the threshold field for flux trapping. It is observed that the trapped moment increases quadratically with increasing field above the threshold. To account for this behavior, a model has been constructed which predicts an average critical current density J_c^* near H_{c1} given by $J_c^*=cH_{c1}/(4\pi\lambda)$. The temperature variation of H_{c1} is observed to be $H_{c1} \approx 200\ [1-(T/T_c)^2]$ gauss, indicating a constant Ginzburg–Landau parameter κ. On combining the observed value of H_{c1} with the reported value of $(\delta H_{c2}/\delta T)_{T=T_c}$, it is found that $\kappa \approx 34$, and that the thermodynamic critical field is about 2600 gauss. The corresponding BCS band gap is unusually low, consistent with reported values obtained from tunneling and penetration-depth experiments.*

Introduction

HIGH-FIELD superconductors, such as Nb_3Sn, have magnetic properties that differ markedly from those of soft superconductors, such as lead or tin. In particular, applied magnetic fields will penetrate a high-field superconductor without destroying its ability to support supercurrents; for Nb_3Sn this penetration occurs at an applied field strength perhaps one hundredth of that required for the complete destruction of superconductivity. It should be stressed that this penetration is not related to the occurrence of the intermediate state in soft superconductors; the latter effect only arises in samples shaped so as to distort the applied field.

The kind of magnetic behavior exhibited by the superconductor depends, as do the other thermodynamic properties, on the value of the Ginzburg–Landau parameter, $\kappa = \lambda_L(0)/\xi$, where $\lambda_L(0)$ is the London penetration depth at $T = 0$, and ξ is the coherence length of the superconducting electron pairs. Superconductors of $\kappa > 1/\sqrt{2}$ are denoted as type-II superconductors; Nb_3Sn is an extreme example, with $\kappa > 40$ for some samples.

Abrikosov[1] has shown that a type-II superconductor in an applied magnetic field greater than a lower critical field H_{c1} will enter a "mixed state," which is characterized by a uniform distribution of current vortices threading the sample. The theory shows the mixed state to

[1] A. A. Abrikosov, "On the Magnetic Properties of Superconductors of the Second Group," *Zh. Eksperim. i. Teor. Fiz.*, Vol. 32, p. 1442, June 1957; translation in *Soviet Physics, JETP*, Vol. 5, p. 1174, 15 Dec. 1957.

be the state of minimum free energy, but gives no prediction as to the time required for its establishment. This problem of the dynamics of flux penetration has been considered by Anderson,[2,3] and his conclusions are supported by the extensive experimental results of Kim and coworkers.[4,5] In brief, their findings are that whenever the gradient α of magnetic pressure is less than a critical value α_{crit} in a given region of a type-II superconductor, the rate of flux passage through this region will be immeasurably slow. Thus, when H_{c1} is exceeded, flux enters the surface of the superconductor rapidly at first, driven by a magnetic pressure gradient $\alpha > \alpha_{crit}$; as α decreases, the flux finally penetrates to a depth such that $\alpha = \alpha_{crit}$ from the surface to the flux boundary, and $\alpha = B = 0$ beyond. The critical magnetic pressure gradient α_{crit} depends on the particular superconductor considered (it is structure-sensitive as well), on the temperature, and in principle on the field. Because of this temperature dependence, α_{crit} may also be affected by rapidly changing applied fields and by local thermal fluctuations. Unfortunately, the theory is too crude to permit an exact derivation of α_{crit}, and it must be considered at best an experimentally defined quantity.

Since flux will only partially penetrate a superconductor with a high value of α_{crit}, such as Nb_3Sn, the magnetization does not drop sharply at H_{c1} as predicted by Abrikosov.[1] On the contrary, the magnetization increases almost linearly with field well beyond H_{c1}, has a broad maximum, and then falls off slowly toward zero at the upper crtical field, H_{c2}. However, if flux has difficulty entering the superconductor, it will have difficulty getting out as well, and it will be seen that this permits a determination of H_{c1}.

A frequently employed formulation of the Kim–Anderson theory[2,5] relates α_{crit} to the magnetic induction, B, and to a field-dependent critical current density, J_c. Kim[4] *et al* have closely fitted their magnetization data by assuming $\alpha_{crit} = J_c\ (B + B_0)$, where B_0 is a constant somewhat larger than H_{c1}. However, the physical justification for this expression is unclear. Cody[6] *et al* suggest that J_c in current-carrying wires is self-field limited; by assuming a uniform current density near quenching, they derive an expression that reduces to Kim's for small

---

[2] P. W. Anderson, "Theory of Flux Creep in Hard Superconductors," *Phys. Rev. Ltrs.*, Vol. 9, p. 309, 1 Oct. 1962.

[3] P. W. Anderson and Y. B. Kim, "Hard Superconductivity: Theory of the Motion of Abrikosov Lines," *Rev. Mod. Phys.*, Vol. 36, p. 39, Jan. 1964.

[4] Y. B. Kim, C. F. Hempstead, and A. R. Strnad, "Flux Creep in Hard Superconductors," *Phys. Rev.*, Vol. 131, p. 2486, 15 Sept. 1963.

[5] Y. B. Kim, C. F. Hempstead, and A. R. Strnad, "Resistive States of Hard Superconductors," *Rev. Mod. Phys.*, Vol. 36, p. 43, Jan. 1964.

[6] G. D. Cody, G. W. Cullen, and J. P. McEvoy, Jr., "Field and Angular Dependence of Critical Currents in NB_3Sn II," *Rev. Mod. Phys.*, Vol. 36, p. 95, Jan. 1964.

transverse fields, and in which B_0 depends both on α and on the wire thickness. Friedel[7] *et al* postulate that $\alpha_{\text{crit}} = (1/c)\,|\mathbf{J}_c \times \mathbf{B}|$, and further derive from thermodynamic considerations that $\mathbf{J}_c = (c/4\pi)$ curl $\mathbf{H}(B)$. Here $\mathbf{H}(B)$ is that applied field which would produce the magnetic induction B at thermodynamic equilibrium (i.e., in the Abrikosov mixed state). The simplest of all proposals is that J_c is constant; with this assumption, Bean[8] has been able to account for the magnetization of sintered V_3Ga and of Pb in porous glass in moderate fields.

It is evident that in any of these descriptions, the magnetization of a type-II superconductor with finite α_{crit} cannot be expected to be reversible above H_{c1}. If flux only moves when α_{crit} is exceeded, then reducing the applied field must generate a second flux front, ascending from the surface inward. This is a field configuration that is unobtainable while the applied field is only increasing. Alternatively, one can suppose that a counter-current density J_c is generated at the surface on reducing the applied field. When the applied field is completely removed, there remain inner and outer current layers of opposite sense; the fields generated by these will cancel deep inside the superconductor. Clearly, flux remains "trapped" between the layers.

In this paper, the results of measurements of such flux trapping in vapor-deposited particles of Nb_3Sn is reported. Fields in the neighborhood of H_{c1} are applied, removed, and the remanent magnetic moment of the sample is detected with a vibrating-coil magnetometer.[9] Each point is taken with the sample virgin; i.e., any trapped flux is initially destroyed by heating the sample above T_c and cooling in zero field. By plotting the remanent magnetic moment against the applied field, the threshold field for flux penetration is found by extrapolation (see Figure 2), and this field is identified with H_{c1}. Furthermore, the curvature of this plot near the threshold field is determined by the critical current density at the surface. The measurements extend over the temperature range from 4.2° to 17.1°K ($T_c = 18.3$°K).

Apparatus and Measurements

The magnetometer (see Figure 1) is contained in a chamber in a liquid helium cryostat, and can be thermally isolated from the helium

---

[7] J. Friedel, P. G. deGennes, and J. Matricon, "Nature of the Driving Force in Flux Creep Phenomena," *Appl. Phys. Ltrs.*, Vol. 2, p. 119, 15 Mar. 1963.

[8] C. P. Bean, "Magnetization of Hard Superconductors," *Phys. Rev. Ltrs.*, Vol. 8, p. 250, 15 Mar. 1962.

[9] A thorough discussion of this device is given by D. O. Smith, "Development of a Vibrating Coil Magnetometer," *Rev. Sci. Instr.*, Vol. 27, p. 261, May 1956.

bath by evacuating the chamber wall. Surrounding the chamber is a niobium solenoid, suitable for generating the low fields ($\sim$ 200 gauss) required for measurements near H_{c1} in Nb_3Sn. High-field solenoids have been employed in other applications of the magnetometer, but the niobium solenoid has the advantage of stability and of reproducibly low residual fields.

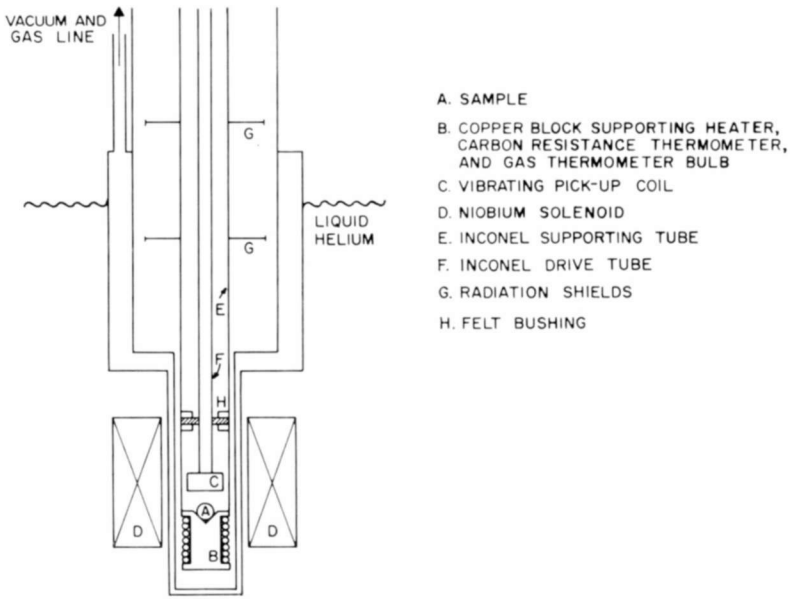

Fig. 1—Cryostat and magnetometer.

Within the chamber is an annular copper cylinder with a hollow wall. A 400-ohm manganin heater is noninductively wound on the cylinder, and power is fed back to the heater in response to the imbalance of a Wheatstone bridge, one arm of which is a 57-ohm 0.1-watt resistor buried in the cylinder wall. The absolute temperature is monitored by a helium gas thermometer, the hollow cylinder wall serving as a bulb. The estimated temperature stability is better than .01°K. Samples are mounted in copper rods which fit the cylinder annulus tightly; when in position, the copper rods are clamped to the cylinder by set screws.

Immediately above the cylinder is a vibrating pick-up coil. It is 20 mm in diameter and 6 mm thick, and contains about 20,000 turns of #50 Formvar-coated copper wire potted in silicone rubber. The coil

is driven up and down at 50 cps with a peak-to-peak displacement of 2 mm. Its output thus contains a strong 50 cps component proportional to the sample magnetic moment; the output is then filtered and amplified by a tuned phase-sensitive detector. As a refinement, the coil is tapped so as to provide three concentric sections. The output voltages from these sections are combined so as to cancel any background signal due to gradients in the applied field. Since the sample is just below the coil ($\sim$ 5 mm below), its moment couples only weakly to the outer

Table I — Characteristics of Nb_3Sn Sample FS-14*

T_c (inductive measurement)		18.3°K†
$\triangle T_c$ (inductive measurement)		.04°K†
Band Gap (thermal conductivity)		$3.56kT_c$‡
Electrical Resistivity:	(300°K)	8.1×10^{-5} ohm-cm‡
	(77°K)	3.9×10^{-5} ohm-cm‡
	(27°K)	1.5×10^{-5} ohm-cm‡
$\left(\frac{\partial H_{c2}}{\partial T}\right)_{T=T_c}$		-1.4×10^4 gauss/°K†
Kim–Anderson α		2.0×10^6 kilogauss-amp A/cm²#

* FS-14 is single-phase, vapor-deposited material of nearly ideal stoichiometry.
† See Ref. (16).
‡ See Ref. (19).
# This value of α is the best value for sample FS-20, which has an almost identical T_c and $\triangle T_c$ as FS-14, and is also single-phase, vapor-deposited and nearly stoichiometric material.

sections of the coil. Thus, the signal from the sample is not greatly reduced in this arrangement. The sensitivity of the magnetometer is 10^{-3} e.m.u.

Since the amount of flux trapped in fields just above H_{c1} will be proportional to the sample surface area, it was advantageous in this experiment to use powdered specimens obtained by grinding vapor-deposited Nb_3Sn films. The Nb_3Sn sample chosen, FS-14, had a high transition temperature and narrow transition width, and considerable information about it had been previously obtained (see Table I). The material was ground and sifted between #230 and #325 sieves, so that the particle diameters ranged between 0.0017 and 0.0024 inch. Microscopic examination showed the particles to be angular. About 0.4 gram of powder was pressed into a roughly spherical shape using a copper die and plunger, and the assembly was then fitted into the copper

cylinder (gas-thermometer bulb) described above. The packing factor is estimated at 0.7.

To observe flux trapping, a magnetic field is applied and the resulting signal is recorded for calibration purposes. The field is then reduced to zero and the signal recorded. Finally, a heat pulse is applied which drives the sample normal. The sample then cools in zero field, and the signal is again recorded. The difference between the signals observed before and after the heat pulse is proportional to the quantity of flux trapped, and can be normalized to the much larger signal observed in the applied field. This procedure avoids background error.

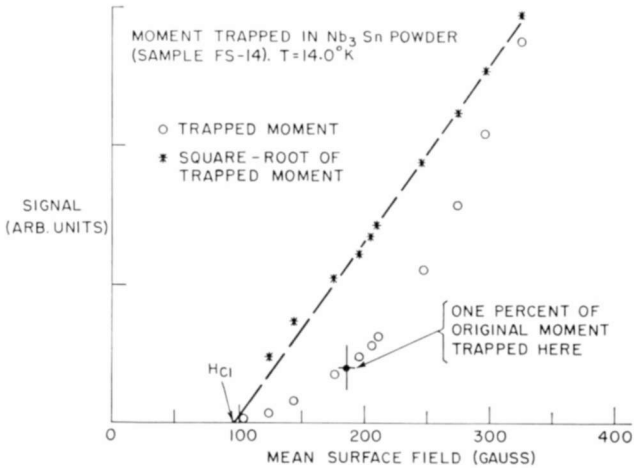

Fig. 2—Trapped moment in Nb_3Sn powder. The mean surface field is an estimate, and is a factor $4/\pi$ greater than the applied field.

Figure 2 shows typical data obtained at 14.0°K. The threshold field for flux trapping is well-defined; the amount of flux trapped increases quadratically with the field excess over the threshold field. It was observed that the amount of flux trapped after repeated cycling between zero field and some fixed field is no greater than that trapped in a single cycle. This is consistent with the mechanism for flux trapping outlined in the introduction. Evidently, flux lines move into the superconductor when H_{c1} is first exceeded, and are left behind when the field is reduced to zero. Thus, on subsequent cycling α_{crit} is never again exceeded, and further motion of flux does not occur.

Powder Statistics

It is necessary to relate the field at the surface of the particles to

the field supplied by the solenoid. If it could be assumed that the particles are truly spherical, we could immediately obtain an expression for the effective magnetic susceptibility of the powder. Considering only the perfectly diamagnetic limit, each particle would acquire a magnetic moment,

$$m = -\frac{a^3}{2}\left(H + \frac{4\pi}{3}nm\right), \tag{1}$$

where a is the particle radius, n is the number of particles per unit volume, H is the average internal field (treating the powder as a continuous medium), and $4\pi nm/3$ is the so-called Lorentz field (cavity field). H is given by

$$H = H_0 - 4\pi Dnm, \tag{2}$$

where H_0 is the field supplied by the solenoid, and D is the demagnetizing coefficient of the entire powder pellet (e.g., $D = 1/3$ for a spherical pellet). Combining Equations (1) and (2), one obtains for the magnetization of the pellet

$$M = nm = -\frac{3}{8\pi}\frac{4}{3}\pi a^3 n\left[1 - \left(\frac{3}{2}D - \frac{1}{2}\right)\left(\frac{4}{3}\pi a^3 n\right)\right]^{-1} H_0. \tag{3}$$

It is seen that as the packing factor $4\pi a^3 n$ approaches unity, $4\pi M$ approaches $H_0/(D-1)$. This limit is identical with the expression for the magnetization of a solid pellet. Hence, we can expect Equation (3) to be exact for densely packed spherical particles. It can be seen that Equation (3) should be a close approximation to the magnetization of a pellet of irregularly shaped particles, since Equation (3) really depends only on the packing factor and the pellet demagnetizing factor. Because $D \approx 1/3$ for the powder pellet used, the denominator in Equation (3) is close to unity. Thus, each particle should acquire the magnetic moment it would have if isolated and subjected to the solenoid field, H_0.

An isolated particle in a field H_0 will, of course, have different fields at different parts of its surface, due to demagnetizing effects. Since flux is trapped at the surface only, the flux trapped by the particle will be determined by the distribution of field weighted by surface area. Actually, the component of trapped flux transverse to H_0 will cancel out, so the distribution must be further weighted according to the angle the surface normal makes with H_0. This distribution is readily com-

puted for spherical particles, for which $H = (3/2)\ H_0 \sin\theta$. An element dA_{II} of effective area has the value

$$dA_{II} = 2\pi a^2 \sin^2\theta d\theta. \tag{4a}$$

Thus, the normalized distribution of field H over the effective area in an applied field H_0 is given by

$$\rho(H, H_0)\,dH = \frac{4}{\pi}\left(\frac{2H}{3H_0}\right)^2\left(1-\left(\frac{2H}{3H_0}\right)^2\right)^{-1/2} d\left(\frac{2H}{3H_0}\right) \tag{4b}$$

over the interval, $0 < H < (3/2)\ H_0$. The significant feature of the distribution of Equation (4b) is the sharp peak at $H = (3/2)\ H_0$. The distribution for irregular particles will have a similar peak, and the addition of a tail extending to fields above $(3/2)\ H_0$ should not be too important since a protuberance at which H is large will not have much surface area. It is true that to some extent the threshold signal may be smeared. However, by extrapolating from higher fields, we should be able to fix the threshold field within reasonable limits of error. To test this conclusion, identical flux-trapping measurements were made on a sample consisting of a number of lengths of Nb_3Sn-coated steel ribbon packed side by side, parallel to the field. Here the geometry was ideal, each ribbon surface being uniformly exposed to the solenoid field H_0. No significant difference in the shape of the flux trapping curves (see Figure 2) was found for the ribbon. This confirms the lack of smearing of the data obtained with the powdered sample FS-14.

Finally, since each surface element of a particle acquires a trapped moment proportional to $(H-H_{c1})^2$, it follows from the small variance of the distribution of Equation (4b) that the total moment trapped by the particle will be proportional to $(\bar{H}-H_{c1})^2$, where $\bar{H} = \int H\rho dH = (4/\pi)\ H_0$. Thus, the "mean surface field," which is the abscissa of Figure 2, was obtained by multiplying the solenoid field by $4/\pi$. It also follows from Equation (4a) that each particle of radius a has an equivalent plane surface area given by π^2a^2. This is the same plane surface area which, if parallel to the mean field H, would acquire the same trapped moment as the particle.

Classical Model of Flux Trapping

To account for the shape of the trapped moment versus field plot, particularly near H_{c1} where the trapped flux consists of a few Abrikosov

vortices confined to a surface region comparable to the penetration depth, a classical model of flux trapping is proposed. The fields and currents inside the superconductor will be thought to be smoothed out, as if the particles were superimposed. As justified in the preceding section, we will for simplicity suppose the superconductor to have an infinite plane surface parallel to an applied field, H.

If $H < H_{c1}$, the field inside the superconductor will then have the form, $B = H \exp\{-z/\lambda\}$, where λ is the experimental penetration depth. It is now postulated that no matter what the applied field, H, any change δH will at first induce in the superconductor an incremental field, $\delta B = \delta H \exp\{-z/\lambda\}$, and that subsequently the field configuration is changed by the motion of flux wherever α_{crit} is exceeded. It seems clear that if H is not too much greater than H_{c1}, reducing H to zero will nowhere cause α_{crit} to be exceeded. Thus, the final field distribution within the superconductor will be the difference between the original distribution (after H was applied) and the field, $B = H \exp\{-z/\lambda\}$.

For the original distribution, we suppose that in an applied field $H_{c1} + \delta H$, the field within the superconductor decreases monotonically from a value $B = H_{c1} + \delta H$ at the surface to a value $B = H_{c1}$ at $z = t$; and beyond this point it is given by $B = H_{c1} \exp\{(t - z)/\lambda\}$. In order that the amount of flux trapped be positive, it is necessary that $t \geqq \lambda \ln(1 + \delta H/H_{c1})$. We define the average critical current density by $J_c^* = cH/(4\pi t)$. It should also be emphasized that we have smoothed out the actual current distribution. Only in sufficiently large applied fields, where $t \gg \lambda$, will J_c^* be identical to the critical current density, J_c, discussed earlier.

After subtracting from the original distribution the field $(H_{c1} + \delta H) \exp\{-z/\lambda\}$, generated on reducing the applied field to zero, we integrate the remanent field from $z=0$ to $z=\infty$. This integral is the flux trapped per unit length of surface, Φ. To second order in δH,

$$\Phi = \lambda\left(\frac{c}{4\pi J_c^*\lambda} H_{c1} - 1\right)\delta H + \frac{\lambda}{2}\left(\frac{c}{4\pi J_c^*\lambda}\right)^2 H_{c1}(\delta H)^2, \qquad (5)$$

where

$$\frac{c}{4\pi J_c^*\lambda} H_{c1} \geqq 1.$$

The trapped moment per unit area of surface, μ, is then given by $\mu = (1/4\pi)\,\Phi$.

The observed trapped moment (see Figure 2) is very nearly quadratic in δH. In fact, the departures from quadratic dependence are

such as to make the observed moment near threshold approach zero more slowly than $(\delta H)^2$. This is to be expected when a distribution ρ of finite width is folded over the threshold. Therefore, by setting the first term on the right in Equation (5) equal to zero, one obtains

$$\frac{4\pi J_c^* \lambda}{c} \approx H_{c1} \tag{6a}$$

and

$$\mu = \frac{\Phi}{4\pi} \approx \frac{\lambda}{8\pi} \frac{(\delta H)^2}{H_{c1}}. \tag{6b}$$

Note that Equation (6a) implies a linear decrease of B from a value $H_{c1} + \delta H$ at the surface to a value H_{c1} at $z = t$. Hence J_c^* is constant up to $z = t$. If we identify J_c^* with J_c and apply Kim's formulation, $\alpha_{\text{crit}} = J_c\ (B + B_0)$, then on setting both B and B_0 equal to H_{c1} and using the available values $\alpha_{\text{crit}} \approx 2 \times 10^6$ kilogauss-amp/cm (at 4.2°K)[10] and $\lambda \approx 3000$ Å,[11] we obtain from Equation (6a), $H_{c1} \approx 200$ gauss. The observed threshold is 190 gauss (the actual solenoid field $H_0 = 140$ gauss, and we estimate from Equation (4b) that $\overline{H} = (4/\pi)\ H_0$). This agreement is admittedly contrived, but it lends support to the model presented above. A better test can be made by inferring the moment trapped per particle from the relative magnitudes of the signal obtained on first applying the field and that obtained from the trapped flux. The former signal results from a perfectly diamagnetic moment of $(1/2)$ $a^3 H_0$ per particle, the latter from a trapped moment of $(\pi a)^2\ \mu(H)$ per particle. On comparing the signal strengths and using Equation (6b) for $\mu(H)$, one finds that $a \approx 100\lambda$. The powder particles have an average radius of 2.5×10^{-3} cm and $\lambda \approx 3000$ Å.[11] This again gives good agreement.

Results

Figure 3 shows the observed values of H_{c1} plotted against the square of the absolute temperature. It is seen that $H_{c1} \approx 200\ [1 - (T/T_c)^2]$ gauss, which is the temperature dependence to be expected for the thermodynamic critical field H_c. This same temperature dependence

---

[10] G. D. Cody and G. W. Cullen, "Critical Currents and the Lorentz Force Model in Niobium Stannide." *RCA Review*, Vol. XXV, No. 3, p. 466, Sept. 1964 (this issue). Also, see Table I.

[11] G. D. Cody, "The Superconducting Penetration Depth of Niobium Stannide," *RCA Review*, Vol. XXV, No. 3, p. 414, Sept. 1964 (this issue).

for H_{c1} has been reported for Mo-Re alloys[12] and for In-Bi alloys.[13] The implication is that for these materials the Ginzburg–Landau parameter κ is largely temperature independent, since the Abrikosov[1] theory expresses the ratio H_{c1}/H_c as a function of κ only. For $\kappa \gg 1$, as in Nb_3Sn,

$$\frac{H_{c_1}}{H_c} = \frac{\ln \kappa + 0.08}{\sqrt{2}\kappa}. \tag{7}$$

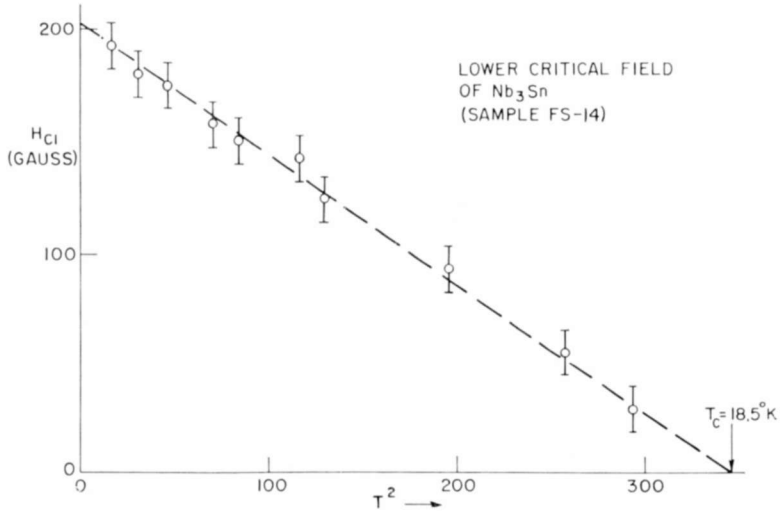

Fig. 3—Temperature dependence of H_{c1}. The precise value of T_c obtained by inductance measurements is $T_c = 18.3°$K, with $\triangle T_c = .04°$K.

It should be noted that Gor'kov[14] predicts only a 25 per cent variation in κ from $T = 0$ to $T = T_c$.

A numerical relation between κ and $H_0 = H_c(T = 0)$ can be obtained from the measured values of $(\partial H_{c_2}/\partial T)_{T=T_c}$, where H_{c_2} is the upper critical field. Abrikosov,[1] Gor'kov,[14] and Ginzburg[15] each have given

[12] W. C. H. Joiner and R. D. Blaugher, "Magnetic and Resistive Transitions of Some Mo-Re Alloys," *Rev. Mod. Phys.*, Vol. 36, p. 67, Jan. 1964.

[13] T. Kinsel, E. A. Lynton, and B. Serin, "Magnetic and Thermal Properties of Second-Kind Superconductors. I. Magnetization Curves," *Rev. Mod. Phys.*, Vol. 36, p. 105, Jan. 1964.

[14] L. P. Gor'kov, "Theory of Superconducting Alloys in a Strong Magnetic Field Near the Critical Temperature," *Zh. Eksperim. i. Teor. Fiz.*, Vol. 37, p. 1407, Nov. 1959; (translation in *Soviet Physics, JETP*, Vol. 10, p. 998, May 1960).

[15] V. L. Ginsburg, "Some Remarks Concerning the Macroscopic Theory of Superconductivity," *Zh. Eksperim. i. Teor. Fiz.*, Vol. 30, p. 593, March 1956; (translation in *Soviet Physics, JETP*, Vol. 3, p. 621, Nov. 1956).

expressions for H_{c_2} as a function of temperature, all of which reduce to

$$\left(\frac{\partial H_{c_2}}{\partial T}\right)_{T=T_c} = 2\sqrt{2}\,\kappa\,\frac{H_0}{T_c} \tag{8}$$

provided $H_c = H_0\,[1 - (T/T_c)^2]$ near T_c. Using the value $(\partial H_{c2}/\partial T)_{T=T_c} = -1.4 \times 10^4$ gauss/°K obtained for sample FS-14 by inductance bridge measurements[16] of T_c, we find $2\kappa H_0 \approx 1.3 \times 10^5$ gauss. It then follows from Equation (7) together with the value $H_{c_1}(0) \approx 200$ gauss obtained in this experiment that $\kappa \approx 34$ and $H_0 \approx 2600$ gauss.

This value of H_0 can be tested by the BCS relation,[17]

$$\frac{2\epsilon_0}{kT_c} = \frac{4\pi}{\sqrt{3}}\sqrt{\frac{H_0^2}{8\pi\gamma T_c^2}} \tag{9}$$

where $\gamma = 1.5 \times 10^{-2}$ cal/mole-deg is the coefficient of electronic specific heat measured in Nb_3Sn by Morin and Maita,[18] and $2\epsilon_0$ is the BCS band gap. It is found that $2\epsilon_0 \approx 1.9kT_c$, in poor agreement both with the value $2\epsilon_0 = 3.56kT_c$ inferred from thermal conductivity measurements[19] on sample FS-14, and with the BCS prediction of $2\epsilon_0 = 3.5kT_c$ experimentally substantiated for other materials. Probably the agreement is even poorer, since one expects γ for sample FS-14 ($T_c = 18.3$°K) to be larger than the Morin and Maita[18] value, which was obtained from a sample with $T_c = 17.3$°K. It is also discouraging that the value of $\kappa \approx 34$ is several times larger than the Goodman[20] prediction, $\kappa = \kappa_0 + 7.5 \times 10^3\gamma^{1/2}\rho \approx 10$, where κ_0 is assumed to be of order unity as for most type-II superconductors, γ is in cgs volume units, and $\rho \approx 10^{-5}$ is the residual resistivity in ohm-cm. On the other hand, there is some evidence that the band gap in Nb_3Sn might, in fact, be unusually small. Both tunneling measurements[21] and penetration-depth measurements[11]

---

[16] J. L. Cooper, "Transition Temperature of Niobium Stannide," *RCA Review*, Vol. XXV, No. 3, p. 405, Sept. 1964 (this issue).

[17] See, for example, E. A. Lynton, *Superconductivity*, Methuen, London; John Wiley, New York, 1962, p. 125.

[18] F. J. Morin and J. P. Maita, "Specific Heats of Transition Metal Superconductors," *Phys. Rev.*, Vol. 129, p. 1115, 1 Feb. 1963.

[19] G. D. Cody and R. W. Cohen, "Thermal Conductivity of Nb_3Sn," *Rev. Mod. Phys.*, Vol. 36, p. 121, Jan. 1964.

[20] B. B. Goodman, "The Magnetic Behavior of Superconductors of Negative Surface Energy," *IBM Jour. Res. and Dev.*, Vol. 6, p. 63, Jan. 1962.

[21] Y. Goldstein, "Anomalous Band Gap in Superconducting Nb_3Sn," *Rev. Mod. Phys.*, Vol. 36, p. 213, Jan. 1964.

are consistent with this possibility. In this connection, it may be significant that both these latter measurements, as well as the present work, depend on the surface properties of Nb_3Sn, whereas measurements of specific heat, electrical resistivity, and thermal conductivity reflect bulk properties.

ACKNOWLEDGMENTS

The author is indebted to G. D. Cody for many helpful discussions of this experiment and its interpretation, and to J. J. Halloran for his able assistance.

CRITICAL CURRENTS AND LORENTZ-FORCE MODEL IN NIOBIUM STANNIDE*

By

G. D. Cody and G. W. Cullen

RCA Laboratories
Princeton, N. J.

Summary—*An extensive study has been made of the angular and field dependence of the critical current in vapor-deposited Nb_3Sn. The results indicate excellent agreement with the Lorentz-force model of flux creep described by Anderson and Kim. In the present work, the model has been generalized to include the case where the applied field and current are not perpendicular, and to include the presence of a self field. For all samples there is a sharp rise in the critical current density at low longitudinal fields, which is associated with a transition from an inhomogeneous to homogeneous current distribution. The value of the high-field longitudinal current can be related to the self field produced by the current. Results indicate that the longitudinal current can be essentially field independent from 10 to 100 kilogauss.*

Introduction

FOR THE practical application of second-kind superconductors, two aspects of their behavior are important. The first is the upper critical field (H_{c_2}) defined for the present as that field at which the longitudinal critical current density (J_c) and the magnetization go to zero. The second is the absolute magnitude of the critical current density and its field dependence. As is well known, the upper critical field depends on certain microscopic properties of the superconductor. In a free-electron approximation,[1] H_{c_2} depends on the density of electrons (n), the effective mass (m^*), the mean free path (Λ), and the energy gap, ($2\epsilon_0$). It is not a constant for a given material, but is a linear function of the residual resistivity as long as resistivity changes do not affect the other properties of the superconductor.[1] On the other hand, large and apparently independent changes in the critical current density at a given field are observed for materials whose residual resistivities differ by less than 20%. Moreover, one can show that the critical current density is quite

* The research reported in this paper was sponsored by the Air Force Materials Laboratory, Research and Technology Division, Air Force Systems Command, Wright-Patterson Air Force Base, Ohio, under Contract AF33(657)-11208.

[1] B. B. Goodman, "Type II or London Superconductors," *Rev. Mod. Phys.*, Vol. 36, p. 12, Jan. 1964.

sensitive to cold working and, in certain materials, to neutron irradiation, whereas the change in residual resistivity and H_{c_2} from such treatment is quite small. Finally, the critical current density at a given field has been shown to vary approximately linearly at low temperatures, while at the same low temperatures H_{c_2} exhibits very little temperature dependence.

From the above discussion it is clear that as the residual resistivity permits one to decouple the upper critical field from its proportionality to the transition temperature, a different mechanism permits one to decouple the magnitude of the critical current density from the upper critical field. From the experimental fact that high current density, second-kind superconductors are generally multiphase or highly cold worked, one is led to the view that extended defects are responsible for the magnitude of the critical current density and its field dependence. Annealing experiments also support this view.[2] For example, negligible changes are observed in the residual resistivity after annealing, while the critical current density varies by as much as a factor of two.

The above discussion, while suggestive, offers little guidance for either the analysis of experiment or the optimization of the critical current density. A meaningful analysis of the current-carrying state in second-kind superconductors became possible after the experiments of Kim, Hempstead, and Strnad,[3] and the flux-creep theory of Anderson.[4] Before we discuss the work of these authors, let us consider the current-carrying mixed state of second-kind superconductors.

It is well known that the magnetic transition for second-kind superconductors (the mixed state) can be extremely broad. For example, for Nb_3Sn at 4.2°K the field starts penetrating at about 200 gauss,[5] whereas the sample approaches the normal state at about 200 kilogauss.[6] At fields above about 10 kilogauss for Nb_3Sn one obtains a sample with almost uniform field penetration. The magnetic microstructure of the mixed state has, up to the present, not been directly observed. Present

---

[2] G. W. Cullen, R. L. Novak, and J. P. McEvoy, "Effect of Neutron Induced Defects on the Current-Carrying Behavior of Niobium Stannide," *RCA Review*, Vol. XXV, p. 479, Sept. 1964 (this issue).

[3] Y. B. Kim, C. F. Hempstead, and A. R. Strnad, "Magnetization of Critical Supercurrents," *Phys. Rev.*, Vol. 129, p. 528, 15 Jan. 1963.

[4] P. W. Anderson, "Theory of Flux Creep in Hard Superconductors," *Phys. Rev. Ltrs.*, Vol. 9, p. 309, 1 Oct. 1962.

[5] R. L. Hecht, "Lower Critical Field of Niobium Stannide," *RCA Review*, Vol. XXV, p. 453, Sept. 1964 (this issue).

[6] W. H. Cherry, "Surge Magnetic Field and Pulse Current Effects in Niobium Stannide," *RCA Review*, Vol. XXV, p. 510, Sept. 1964 (this issue).

theories in the absence of a transport current suggest either a layer[7] or vortex[8] model. In both cases, below H_{c_2} the microstructure is described in terms of a periodic variation on the superconducting order parameters (n_s) and the local magnetic field. The local field is at its maximum, and the order parameter at its minimum value in regions of the order of ξ, the coherence distance (≈ 100 Å for Nb_3Sn). For $H > H_{c_1}$ (the penetration field), these regions are separated by distances of the order of the superconducting penetration depth λ ($\approx 3{,}000$ Å for Nb_3Sn). Since $\lambda \gg \xi$, the bulk of the material is completely superconducting. At $H = H_{c_2}$, the separation of high-field regions becomes of the order of ξ, and the superconducting regions go rapidly to zero. In the vortex model, flux quantization plays a dominant role;[8] but this is not so in the layer model. In the layer model the high-field region contains a normal core; at present, it is not clear whether such a core exists in the vortex model.[8]

Neither of these models includes the case where the specimen is carrying a net current. It is clear that for $H \gg H_{c_1}$ the current distribution is uniform across the specimen, unlike the case of a first-kind superconductor where it is confined to within a penetration depth of the surface. It was pointed out quite early by Gorter[9] that the domain structure described above is unstable under the action of the net magnetic pressure on the specimen. Consider a wire with a current density **j** in a transverse field **H**. The magnetic pressure across the specimen is proportional to the Lorentz force **F**, where

$$\mathbf{F} = \frac{(\mathbf{j} \times \mathbf{H})}{c} V . \tag{1}$$

Here V is the volume of the flux element (core of the vortex or the normal layer). If the domains could move without friction, a net electromotive force (EMF) would appear across the length of the wire, which in the steady state would exactly compensate the applied EMF, and which would reduce the applied current to zero. If the domain structure is restricted by frictional forces to a limiting velocity, the EMF across the specimen would be equal to the work done by the applied EMF against the viscous or frictional forces. In either case,

[7] B. B. Goodman, "Simple Model for the Magnetic Behavior of Superconductors of Negative Surface Energy," *Phys. Rev. Ltrs.*, Vol. 6, p. 597, 1 June 1961.

[8] P. G. DeGennes and J. Matricon, "Collective Modes of Vortex Lines in Superconductors of the Second Kind," *Rev. Mod. Phys.*, Vol. 36, p. 45, Jan. 1964.

[9] C. J. Gorter, "Magnetic Properties of Superconductors," *Nuovo Cimento*, Vol. 6, Suppl. 3, p. 1168, 1957.

although the current continues to pass through the superconducting regions, an EMF appears across the specimen, and it appears resistive for a measurement at any current level.

Second-kind superconductors such as Nb_3Sn and NbZr do support high densities at high fields with no sign of a steady voltage up to the critical current density.[10,11] It is plausible that the extended defects discussed above are responsible for this fact, since they would present an obstacle to flux motion. The first quantitative treatment of the problem was due to Anderson,[4] who explained the magnetization measurements of Kim et al[3] in terms of a model involving flux pinning by extended defects, a critical Lorentz force that can just overcome the pinning defect, and eventual flow of the flux at a limiting velocity dependent on the applied force and the "viscosity" of the medium.

At $T = 0°K$, the flux in the low-order-parameter regions is pinned by potential barriers, and no motion is possible until a critical Lorentz force is exceeded. At this value a finite voltage appears across the specimen. If sufficient heat is generated in the medium, the temperature rise can be enough to catastrophically quench the superconducting state. At higher temperatures, thermally activated creep under the action of the Lorentz force is always possible, but the critical current is defined in terms of the smallest voltage across the specimen that is experimentally detectable. If catastrophic quenching due to local heating does not occur, a reversible voltage can be observed that is proportional to the velocity of flux motion and the applied magnetic field.

The Lorentz force model leads to the following expression for the critical current density in a transverse field $H \gg H_{c_1}$:

$$J_c = \frac{\alpha}{H}, \tag{2}$$

where α is a material constant that is a measure of the effectiveness of the pinning centers and their density and distribution.[4,12] Ander-

[10] C. K. Jones, J. K. Hulm, and B. S. Chandrasekhar, "Upper Critical Field of Solid Solution Alloys of the Transition Elements," *Rev. Mod. Phys.*, Vol. 36, p. 74, Jan. 1964.

[11] G. W. Cullen, G. D. Cody, and J. P. McEvoy, Jr., "Field and Angular Dependence of Critical Currents in Nb_3Sn," *Phys. Rev.*, Vol. 132, p. 557, 15 Oct. 1963; G. D. Cody, G. W. Cullen, and J. P. McEvoy, Jr., "Field and Angular Dependence of Critical Currents in Nb_3Sn II," *Rev. Mod. Phys.*, Vol. 36, p. 95, Jan. 1964.

[12] J. Friedal, P. G. DeGennes, and J. Matricon, "Nature of the Driving Force in Flux Creep Phenomena," *Appl. Phys. Ltrs.*, Vol. 2, p. 119, 15 Mar. 1963; J. Silcox and R. W. Rollins, "Hysterises in Hard Superconductors," *Appl. Phys. Ltrs.*, Vol. 2, p. 231, 15 June 1963.

son[4] has shown further that

$$\alpha = a[H_c(T)]^2 - bT, \tag{3}$$

where $H_c(T)$ is the thermodynamic critical field, and a and b are temperature-independent constants which depend on the density of pinning defects, the size of a flux element, and the magnitude of the pinning force.

In the region where $JH > \alpha$, motion of the domain structure is possible, leading to power dissipation

$$P = I^2\left(\frac{lH}{c}\right)^2 \frac{1}{KN} = V^2 KN\,. \tag{4}$$

where l is the length of the specimen, I, the total current, N is the number of flux elements, V is the velocity of the flux motion, and KV is the frictional force exerted on one flux element. From Equation (4) it is clear that the additional work done by the current source goes into the work done by the flux elements against the frictional forces. Equation (4) is equivalent to the expression of Kim et al[13] if one assumes flux quantization and sets $K = d/\eta$, where d is the thickness of the specimen and η is the viscosity coefficient introduced by Kim et al.[13]

Qualitatively and quantitatively the above theory has been shown[3,11] to be in excellent agreement with experiment, particularly the tube magnetization experiments of Kim et al.[3] Its weakness is in the failure to account quantitatively for the constants a, b, and η in terms of specific material parameters. The experimental work reviewed in the present paper represent an extension of the measurements of Kim et al[3] to configurations where the current is externally supplied, and where the field and current axis are at a controlled angle. In general, these results support the interpretation of Kim et al[3] and Anderson,[4] and have led to a modest generalization of the theory to include non-perpendicular fields. More important, the results to be discussed give strong support for the application of the Lorentz-force model to currents in a longitudinal field. Finally the present results represent the first step in a systematic correlation of the parameters of the Lorentz-force model with the material properties of a practical high-field, high-current superconductor, Nb_3Sn.

---

[13] Y. B. Kim, C. F. Hempstead, and A. R. Strnad, "Resistive States of Hard Superconductors," *Rev. Mod. Phys.*, Vol. 36, p. 43, Jan. 1964.

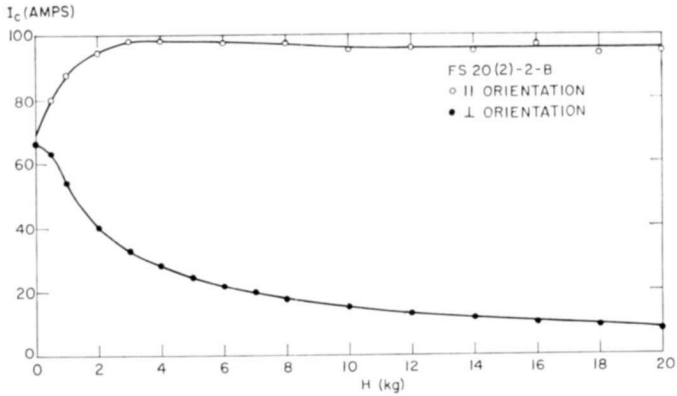

Fig. 1—Longitudinal and transverse critical currents in sample FS20(2)-2-B as a function of field

Experimental Results

In previous papers[11] we have presented the field and angular dependence of the critical current density of Nb_3Sn for a variety of samples. The samples were all obtained by hydrogen reduction of the chlorides of niobium and tin on a ceramic substrate.[14] The critical current was determined by the first sign of voltage on the potential contacts to the specimen, and at low fields a quenching of the superconducting state usually followed immediately. Figures 1 and 2 show

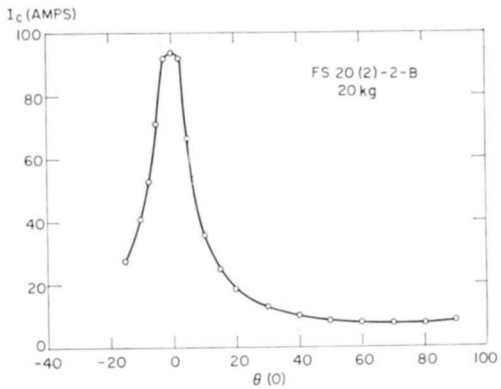

Fig. 2—Angular variation of critical current in sample FS20(2)-2-B at 20 kilogauss.

[14] G. W. Cullen, "Preparation and Properties of Niobium Stannide on Insulating Substrates," *Trans. Metallurgical Soc.*, in press.

typical data up to 20 kilogauss. One notes in Figure 1 that the critical current in a longitudinal field rises rapidly at low fields and then saturates to an essentially constant value. The transverse current, on the other hand, drops continuously. Figure 2 shows the sharp angular dependence at 20 kilogauss with a maximum at $\theta = 0°$, and a minimum at 90°. The theory to be discussed implies that for $H\sin\theta \gg 1$

$$\frac{1}{I_c} = \frac{H\sin\theta}{\alpha A}, \tag{5}$$

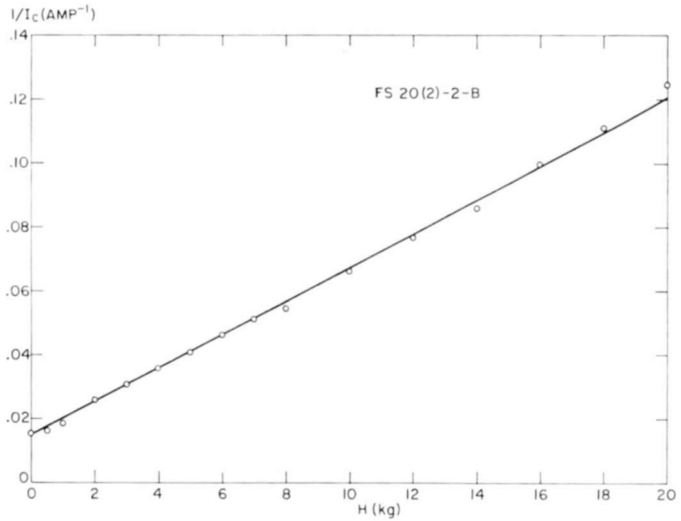

Fig. 3—$1/I_c$ as a function of field for sample FS20(2)-2-B.

where α is the constant introduced by Kim et al,[3] and A is the cross-sectional area of the specimen. Figures 3 and 4 show the data of Figures 1 and 2 plotted in this manner, and one notes agreement with Equation (5) to within about 10%. For example, the α values determined from Figures 3 and 4 agree within about 10%. The example shown represents about the widest divergence observed. Several samples give agreement to better than 2% over a range in field about five times that shown in Figures 3 and 4.[15] The results of low-field ($H < 20$ kilogauss) experiments for a variety of specimens are given in Table I. One notes that T_c, but not α, correlates well with the residual resistivity.

[15] G. D. Cody and G. W. Cullen (to be published).

Discussion

If one considers the Lorentz force as determining the first sign of voltage across the specimen, we have

$$\mathbf{J}_c \times \mathbf{H} = \alpha.$$

Here $\mathbf{H} = \mathbf{H}_0 + \mathbf{H}_I$, where H_0 is the external field, and H_I is the self field due to the current. If we consider a long isotropic bar, and assume that the current flows uniformly along the aris, one obtains for the maximum Lorentz force[11]

$$J_c H_0 \sin\theta + J_c H_I = \alpha, \tag{6}$$

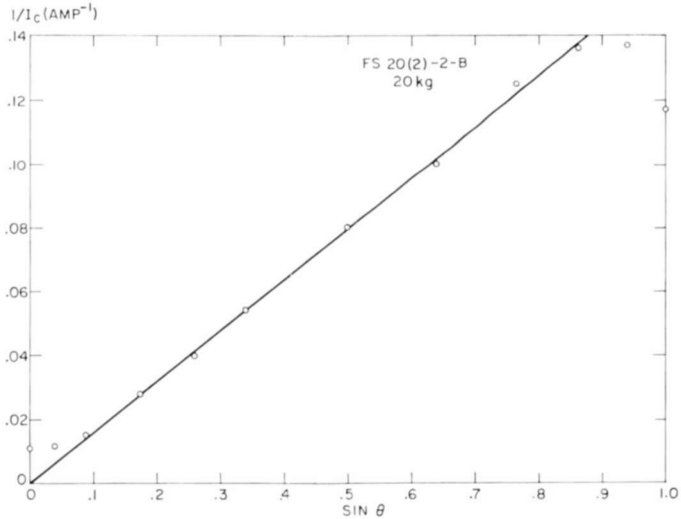

Fig. 4—$1/I_c$ as a function of $\sin\theta$ for sample FS20(2)-2--B at 20 kilogauss.

where θ is the angle between the applied field and the axis of the bar. If we suppose

$$H_I = KJ_c, \tag{7}$$

$$J_c^2 + \frac{J_c}{K} H_0 \sin\theta - \frac{\alpha}{K} = 0, \tag{8}$$

and

$$J_c = \frac{\dfrac{-H_0 \sin\theta}{K} + \left[\dfrac{H_0^2 \sin^2\theta}{K^2} + \dfrac{4\alpha}{K}\right]^{1/2}}{2}. \tag{9}$$

For $H_0^2 \sin^2\theta \gg 4\alpha K$,

$$J_c \approx \frac{\alpha}{H_0 \sin\theta}. \tag{10}$$

For $H_0^2 \sin^2\theta \ll 4\alpha K$,

$$J_c \approx \left(\frac{\alpha}{K}\right)^{1/2} = J_c\,(\theta = 0). \tag{11}$$

The constant K in Equation (11) can be approximated by $2\pi A/(10d)$, where A is the cross-sectional area of the strip and d is a dimension of the order of the thickness of the bar. Thus,

$$J_c(\theta = 0) \approx \left(\frac{5\alpha d}{\pi A}\right)^{1/2}$$

and

$$I_c(\theta = 0) \approx \left(\frac{5\alpha d A}{\pi}\right)^{1/2} \tag{12}$$

From a similar argument, one can estimate the current at $H = 0$ when the current density is confined to within a penetration depth (λ) of the perimeter;

$$I_c\,(H = 0) \approx \left[\frac{10\alpha\,\lambda\,d}{\pi}\,(d + w)\right]^{1/2}, \tag{13}$$

where w is the width of the strip. From Equations (12) and (13) we see that

$$\frac{I_c(H = 0)}{I_c(\theta = 0)} \approx \left(2\,\lambda\,\frac{(d + w)}{A}\right)^{1/2} < 1. \tag{14}$$

The present model leads to the following predictions. (1) The critical current in a longitudinal field should rise rapidly from its zero-field value. This rise should reflect the magnetization curve, with the current saturating to a constant value when $B \approx H$ in the sample. The longitudinal current is proportional to $\alpha^{1/2}$, and the ratio between it and the zero-field value is independent of α, and depends only on the

geometry of the sample. (2) For all other orientations $1/J_c$ is linear with $H\sin\theta$ when $H\sin\theta > 2\,\alpha/J_c$ $(\theta = 0)$. The slope of such a plot is $1/\alpha$.

As can be seen from Figures (3) and (4), and from similar curves for other specimens, the broad features of the field and angular dependence of the critcial current are in good agreement with the above model. The longitudinal current for all samples appears to be essentially constant from about 4 to 20 kilogauss; the reciprocal of the critical current is linear with $H \sin\theta$, and the longitudinal current in the high-field region is about twice the zero-field value, and is independent of α. Recent work at fields as high as 104,000 gauss further supports the above model, including the relative constancy of the critical current in a longitudinal field.[15] Indeed, it appears that if one can achieve angular resolution to better than 0.2°, homogeneous samples would have a longitudinal critical current independent of field up to 104 kilogauss.

The magnitude of the maximum longitudinal current predicted by Equation (12) is about a factor of three less than that observed for the samples shown in Table I. However, since Equation (12) is based on a naïve estimate of the field distribution in the strip, the numerical disagreement is not significant. More crucial tests of the α dependence of Equation (12) can be obtained by the variation of the longitudinal critical current with temperature[11] and neutron irradiation,[16] where the α dependence is clearly established and the quantities d and A are constants. Table II shows the maximum longitudinal current $I_c\ (\theta = 0)_{\max}$ and the quantity α obtained from a neutron-irradiated specimen. $(I_c\ (\theta = 0)_{\max})^2/\alpha$, which should be a constant if the longitudinal current is self limited, is also shown. Table III shows the results obtained from the temperature variation of the critical current.

From the data in Tables II and III it is apparent that Equation (12) is verified in that $I_c\ (\theta = 0) \approx \alpha^{1/2}$ for varations in α from 30% to 200%.

Equation (14) predicts $I(H = 0) \approx 0.2\, I(\theta = 0)$ for representative geometries, and the measured penetration depth of Nb_3Sn.[17] As shown in Table I the measured values of this ratio are of the order of 0.6, but again the failure to calculate exact field distributions probably can account for the discrepancy. The data in Table I do show that

---

[16] G. W. Cullen and R. L. Novak, "Effect of Fast-Neutron-Induced Defects on the Current Carrying Behavior of Superconducting Nb_3Sn," *Appl. Phys. Ltrs.*, Vol. 4, p. 147, 15 April 1964.

[17] G. D. Cody, "The Superconducting Penetration Depth of Niobium Stannide," *RCA Review*, Vol. XXV, p. 414, Sept. 1964 (this issue).

Table I—Superconducting Properties of Vapor-Deposited Nb_3Sn Strips

	FS20	FS20B	69(6)-1-2	74(6)-1-0	75(3)-3-1	80(7)-2	78(5)-2-0
Composition (Wt% Nb)	70.5±.3	70.5±.3	73.5±.3	70.4±.3	71.3±.3	70.7±.3	71.3±.3
T_c (°K)[a]	18.3	18.3	17.9	17.3	16.5	18.0	17.7
$\triangle T_c$ (°K)	0.04	0.04	2.2	0.8	0.8	.07	0.10
ρ_n (Ω-cm)[b]	1.05×10^{-5}	1.05×10^{-5}	3.10×10^{-5}	1.60×10^{-5}	2.20×10^{-5}	1.80×10^{-5}	1.50×10^{-5}
A (cm)[c]	4.9×10^{-5}	6.1×10^{-5}	5.3×10^{-5}	2.3×10^{-5}	2.7×10^{-5}	3.1×10^{-5}	4.0×10^{-5}
d (cm)	34×10^{-4}	32×10^{-4}	29×10^{-4}	20×10^{-4}	36×10^{-4}	22×10^{-4}	30×10^{-4}
w (cm)	1.5×10^{-2}	1.9×10^{-2}	1.8×10^{-2}	1.1×10^{-2}	1.4×10^{-2}	1.4×10^{-2}	1.4×10^{-2}
l (cm)	62×10^{-2}	74×10^{-2}	38×10^{-2}	50×10^{-2}	40×10^{-2}	38×10^{-2}	91×10^{-2}
J_c (amp/cm²)[d]	15×10^5	16×10^5	17×10^5	32×10^5	18×10^5	22×10^5	28×10^5
J_c (amp/cm²)[e]	7.6×10^5	11×10^5	7.5×10^5	18×10^5	8.4×10^5	14×10^5	14×10^5
J_c (amp/cm²)[f]	0.66×10^5	1.3×10^5	1.5×10^5	7.6×10^5	1.9×10^5	3.9×10^5	2.1×10^5[g]
α (kG amp/cm²)	1.5×10^6	3.0×10^6	3.7×10^6	23×10^6	4.9×10^6	9.4×10^6	2.2×10^6

(a) mid point of transition
(b) estimated from resistance ratios
(c) nonrectangular cross section
(d) 20-kilogauss parallel field
(e) zero field
(f) 20-kilogauss perpendicular field
(g) data at 10 kilogauss perpendicular field

Table II—Neutron Irradiation Results, Sample 75(3)-3-1

Dosage	α (kilogauss-amp/cm^2)	$I_c(\theta = 0)_{max}$ (amp)	$(I_c(\theta = 0)_{max})^2/\alpha$ (amp-cm^2/kilogauss)
0	6.52×10^6	48.8	3.65×10^{-4}
3.4×10^{17}	12.10×10^6	58.0	2.78×10^{-4}
6.6×10^{17}	15.6×10^6	66.0	2.78×10^{-4}

the ratio is independent of α for wide ranges in the value of this parameter.

While the above theory is oversimplified, it has been shown to be in semiquantitative agreement with experiment. Unfortunately its simplicity tends to obscure a detailed picture of the current distribution in the longitudinal field. Rather than the naïve picture of a uniform current distribution along the sample axis, a more plausible view is that of a force-free current distribution.[18] For a simple conducting fluid, one could readily derive the conditions for such a distribution, but for the second-kind superconductor, the vortex[8] or layer[7] structure presents a far more difficult problem. In terms of the vortex model, a possible picture is that of vortex drifting with a net velocity down the conductor.

At sufficiently high fields, irrespective of the zero Lorentz-force condition, one would expect a decrease in the longitudinal current since less and less superconducting volume is avaliable due to the crowding of the quantized fluxoids[8] or the normal layers.[7] For simplicity we restrict ourselves to the vortex model, and use the relation[8]

$$H \approx n\phi_0 , \tag{15}$$

Table III—Temperature Data, Sample FS 20

T (°K)	α (kilogauss-amp/cm^2)	$I_c(\theta = 0)_{max}$ (amp)	$(I_c(\theta = 0)_{max})^2/\alpha$ (amp-cm^2/kilogauss)
2.1	1.58×10^6	80.6	4.12×10^{-3}
4.2	1.28×10^6	70.6	3.90×10^{-3}

[18] S. Chandrasekhar, *Proc. of Nat. Acad. of Sciences*, Vol. 42, p. 1, 1956; C. J. Bergeron, Jr., "Simple Model for Longitudinal Force-Free Current Flow in Superconductors of the Second Kind," *Appl. Phys. Ltrs.*, Vol. 3, p. 63, 15 Aug. 1963.

where n is the number of fluxoids per cm^2 and $\phi_o = 2 \times 17^{-7}$ gauss/cm^2. At 200 kilogauss, $n \approx 10^{12}$/cm^2. Hence, the distance between the fluxoids is of the order of 100 Å. If one assumes the coherence distance to be of the order of the mean free path for Nb_3Sn (≈ 50 Å), we see that the effective "superconducting volume" has been reduced by about 25% from its value at low fields; at 100 kilogauss the reduction is of the order of 12%. It is clear that the longitudinal current cannot be constant for fields close to H_{c_2}, although detailed calculations have yet to be made.

ACKNOWLEDGMENTS

We are grateful to J. Cooper for transition-temperature measurements and F. Dougherty for assistance in sample preparation.

EFFECT OF NEUTRON-INDUCED DEFECTS ON THE CURRENT-CARRYING BEHAVIOR OF NIOBIUM STANNIDE

By

G. W. Cullen,* R. L. Novak,* and J. P. McEvoy†

Summary—*The current-carrying characteristics of niobium-stannide cylindrical and strip deposits on ceramic substrates have been measured before and after exposure to fast neutron fluxes. Changes in the flux shielding properties of cylindrical samples demonstrated qualitatively that the* α *of the samples is increased by neutron irradiation. More quantitative measurements were possible on the strip samples, where the current was supplied externally. On one strip, the* α *more than doubled after exposure to a flux of* 6.9×10^{17} *neutron/cm*^{2}*. The increase in the critical currents subsequent to irradiation is associated with the action of defects, introduced by the neutron damage, which pin fluxoids and thus stabilize the applied currents.*

Introduction

In early investigations on the high-field current-carrying capacity of Nb_3Sn, Kunzler and coworkers[1] noted that samples cut from Nb_3Sn ingots carried significantly less current than samples made of sintered cores clad with niobium. The difference was associated with preparative techniques that led to a structure containing a large number of "filaments" in the clad material. Subsequent work[2] on clad material revealed that the current density is strongly related to the sintering heat treatment, with optimum densities occurring in material containing unreacted niobium particles. High-temperature treatment that results in more homogeneous material degrades the current densi-

The research reported in this paper was supported in part by the Air Force Materials Laboratory, Research and Technology Division, Air Force Systems Command, Wright-Patterson Air Force Base, Ohio, under Contract AF33(657)-11028.

* RCA Laboratories, Princeton, N. J.

† RCA Defense Electronic Products, Camden, N. J.

[1] J. E. Kunzler, E. Buehler, F. S. L. Hsu, and J. H. Wernick, "Superconductivity in Nb_3Sn at High Current Density in a Magnetic Field of 88 KGauss," *Phys. Rev. Ltrs.*, Vol. 6, No. 3, p. 89, Feb. 1, 1961.

[2] E. Buehler, J. H. Wernick, K. M. Olsen, F. S. L. Hsu, and J. E. Kunzler, p. 105 in *Metallurgy of Advanced Electronic Materials*, G. E. Brock, ed., Interscience Publishers, N. Y., 1963.

ties. At about the same time it was found[3,4] that mechanical deformations appreciably enhance the high-field characteristics of the more malleable 3Nb:Zr alloy. These observations indicated that physical defects play an important role in determining the high-field characteristics of hard superconducting materials.

In the realm of soft superconductors, Shaw and Mapother[5] showed that the superconducting properties of pure single-crystal Pb can be influenced only by low-temperature deformation. This work, however, provided more insight into the relationship between superconducting properties and crystal lattice defects. More recently Hauser and Buehler[6] established a similar relationship in hard superconducting materials with their annealing and room temperature deformation studies on polycrystalline and single-crystal Nb and Re. Effects were seen in both poly- and single-crystal material.

The work of Kim and coworkers[7] and Anderson[8] have given a basis for the quantitative treatment of the influence of physical defects on superconducting properties. Kim derived an expression for the field-dependent current density, J_c, as a function of the field, H;

$$J_c = \frac{\alpha}{H + B_0}, \tag{1}$$

where α and B_0 are constants that depend on the nature of the material and the temperature. This expression establishes the role of the Lorentz force in determining the critical current density. When critical values of J or H are exceeded, "flux creep," as described by Anderson,[8] sets in to re-establish the critical state. In Anderson's model, physical defects serve to act in opposition to the Lorentz-force-aided flux creep by pinning flux bundles in free-energy barriers. Thermally activated flux creep explains the temperature dependence of the

---

[3] J. E. Kunzler, "Superconductivity in High Magnetic Fields at High Current Densities," *Revs. Mod. Phys.*, Vol. 33, No. 4, p. 501, Oct. 1961.

[4] J. E. Kunzler, "Superconducting Materials and High Magnetic Fields," *Jour. Appl. Phys.*, Vol. 33, p. 1042, March 1962.

[5] R. W. Shaw and R. E. Mapother, "Irreversibility in the Superconducting Transition of Lead," *Phys. Rev.*, Vol. 118, No. 6, p. 1474, June 15, 1960.

[6] J. J. Hauser and E. Buehler, "Effect of Plastic Deformation and Annealing Temperature on Superconducting Properties," *Phys. Rev.*, Vol. 125, No. 1, p. 142, Jan. 1, 1962.

[7] Y. B. Kim, C. F. Hempstead, and A. R. Strnad, "Magnetization and Critical Supercurrents," *Phys. Rev.*, Vol. 129, No. 2, p. 528, Jan. 15, 1963.

[8] P. W. Anderson, "Theory of Flux Creep in Hard Superconductors," *Phys. Rev. Ltrs.*, Vol. 9, No. 7, p. 309, Oct. 1, 1962.

critical current. Subsequent calculations[9,10] have introduced the effect of defects on the high-field current density into the Abrikosov model.

The brittle nature of Nb_3Sn precludes a study of the superconducting properties as a function of plastic deformation in this material. To date the only indication of the influence of defects on the properties of Nb_3Sn is included in the previously mentioned work of Kunzler and coworkers that was carried out on sintered polyphase material. The present work is concerned with a study of the influence of neutron-induced defects on the superconducting properties of single-phase polycrystalline Nb_3Sn. The material is prepared by the simultaneous hydrogen reduction of niobium and tin halides.[11] The deposits are formed on ceramic substrates.[12] A firm background for a quantitative treatment has been provided by the observation[13,14] that the current-carrying characteristics of vapor-deposited material are in excellent agreement with the Lorentz-force expression of Kim and coworkers.

Experimental

The influence of neutron-induced defects on the current-carrying characteristics of vapor-deposited Nb_3Sn has been studied by two methods. In the first method, the flux-shielding properties of cylindrical samples were measured before and after irradiation.[15] The shielding properties are measured in the manner described by Kim and coworkers.[7] The currents induced by the applied field are derived from the magnitude of the shielded field. This induced-current method has the advantage that electrical contact to the sample is not necessary. This is of particular convenience in radiation-damage studies because

---

[9] J. Friedel, P. G. de Gennes, and J. Matricon, "Nature of the Driving Force in Flux Creep Phenomena," *Appl. Phys. Ltrs.*, Vol. 2, No. 6, p. 119, March 15, 1963.

[10] J. Silcox and R. W. Rollins, "Hysteresis in Hard Superconductors," *Appl. Phys. Ltrs.*, Vol. 2, No. 12, p. 231, 15 June 1963.

[11] J. J. Hanak, p. 161 in *Metallurgy of Advanced Electronic Materials*, G. E. Brock, ed., Interscience Publishers, N. Y., 1963.

[12] G. W. Cullen, "Preparation and Properties of Niobium Stannide on Insulating Substrates," *Trans. Metallurgical Soc.*, in press.

[13] G. W. Cullen, G. D. Cody, and J. P. McEvoy, Jr., "Field and Angular Dependence of Critical Currents in Nb_3Sn," *Phys. Rev.*, Vol. 132, No. 2, p. 577, Oct. 15, 1963.

[14] G. D. Cody, G. W. Cullen, and J. P. McEvoy, Jr., "Field and Angular Dependence of Critical Currents in Nb_3Sn II," *Revs. Mod. Phys.*, Vol. 36, No. 1, p. 95, Jan. 1964.

[15] J. P. McEvoy, Jr., R. F. Decell, and R. L. Novak, "Effect of Neutron Irradiation on Critical Currents in Hard Superconductors (Nb_3Sn and NbZr)," *App. Phys. Ltrs.*, Vol. 4, No. 3, p. 43, 1 Feb. 1964.

most contact materials such as Pb-Sn and In solders are highly radioactive subsequent to exposure to neutron fluxes. On the other hand the flux jumping experienced in these samples rendered it impossible in most cases to establish critical-state curves. Thus, quantitative changes in the constants of Equation (1), α and B_0, as a function of irradiation could not be made, although it is clear that α increased. In the second method,[16] the current was directly applied to thin strips of Nb_3Sn. Flux jumps do not interfere, and quantitative evaluations of α and B_0 as a function of damage may be made. Previous studies[13,14] on non-irradiated samples have shown excellent agreement in the data obtained by the two methods. Results obtained from each of the procedures is presented in the following sections.

Induced-Current Method

The samples are in the form of 10-100 micron thick single-phase polycrystalline Nb_3Sn deposits on 0.57 cm outside diameter ceramic tubes. These samples are placed in a longitudinal field at liquid-helium temperature. The internal field (H') is measured with a sensitive Hall probe[17] located in the center of the tube. As the applied field, H, is increased, the superconductor shields the flux from the interior until the critical current is reached. At this point, uniform penetration begins and the shielded field decreases monotonically as the applied field is increased. The shape of the resulting "critical-state" curve, H' versus H, can be used to determine the critical current density, J_c, in the manner first proposed by Bean.[18] In all cases J_c obeyed the relationship Equation (1) derived by Kim and coworkers.[7]

Cylinders for which accurate critical-state curves had been obtained (see Table I) were irradiated for 40 hours at 50°C using the RCA facilities at the Industrial Reactor Laboratories. The specimens were cadmium shielded to eliminate any effects produced by thermal neutrons. The fast neutron flux was measured utilizing the $Ni^{58}(n,p)Co^{58}$ reaction which has an effective threshold near 5 mev. The total integrated flux was approximately 10^{18} neutrons/cm^2. The samples were

---

[16] G. W. Cullen and R. L. Novak, "Effect of Fast-Neutron-Induced Defects on the Current Carrying Behavior of Superconducting Nb_3Sn," *Appl. Phys. Ltrs.*, Vol. 4, No. 8, p. 147, 15 April 1964.

[17] J. P. McEvoy, Jr. and R. F. Decell, "Accurate Low Magnetic Field Measurements on Superconducting Coils," *Rev. Sci. Instr.*, Vol. 34, No. 8, p. 914, Aug. 1963.

[18] C. P. Bean, "Magnetization of Hard Superconductors," *Phys. Rev. Ltrs.*, Vol. 8, No. 6, p. 250, March 15, 1962.

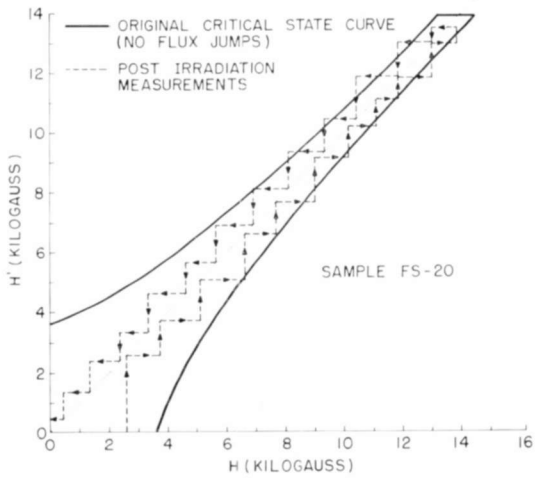

Fig. 1—Flux-shielding characteristics of sample FS-20 before and after irradiation.

kept at room temperature for about 24 hours before the post-irradiation flux shielding measurements were made.

The results shown are typical of all the samples that were irradiated. Figure 1 shows the H' versus H curves before and after irradiation for sample FS-20. The effect of the neutron irradiation was twofold. First, at the same temperature (4.2°K) and rate of change of applied field ($dH/dt \sim 10$ gauss/sec) as in the pre-irradiation tests, it was not possible to induce the critical current in the sample due to the occurrence of flux jumps. Second and more significant, even though the

Table I—Pre-Irradiation Sample Data

Sample No.	Composition (Wgt. %Nb ±.2%)	T_c (°K)	ΔT_c (°K)	α (kilogauss-amp/cm²)	B_0 (kilogauss)	Thickness (w) (μ)	Cross-Section (A) (cm²)
FS-20 (cyl)	70.5	18.3	.04	1.54×10^6	0.7	50	
77 (cyl)	71.3	17.9	.14	6.35×10^6	3.5	18	
75 (strip)	71.2	16.1	.80	6.52×10^6	6.0		2.0×10^{-5}
79 (strip)	70.2	18.0	.14	5.7×10^6	12.1		2.7×10^{-5}

post-irradiation critical current was not attained, the magnetic shielding and, consequently, the current density were increased above their pre-irradiated critical value.

The increase in critical current density is demonstrated more clearly in Figure 2. In this sample (No. 77) it was possible to reach the post-irradiated critical current density value at a few points, as indicated in the figure. By interpolation, we draw a new critical-state curve that indicates that α, and consequently J_c, have increased by at least 50%.

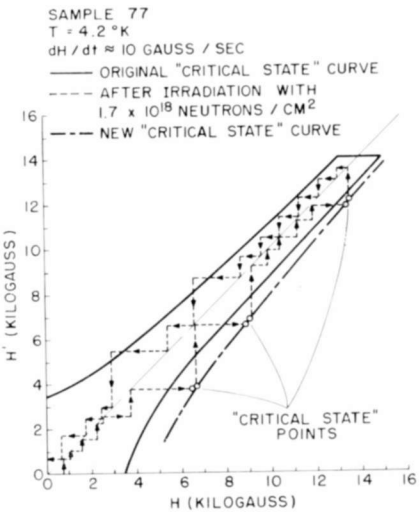

Fig. 2—Flux-shielding characteristics of sample 77 before and after irradiation.

Sample 77 was annealed in an He atmosphere for 1 hour at 800°C, and allowed to cool with the furnace. After this treatment, the shielded field is within 300 gauss of the original shielded field at any given applied field. Thus, it appears that the influence of the neutron damage at this level of irradiation may be essentially removed by annealing. More complete annealing studies are in progress.

Applied-Current Method

The samples used in the applied-current method are thin strips on ceramic substrates, approximately 1 cm long and 2×10^{-5} cm^2 in cross section. Current and potential contacts are established by indium soldering to nickel-plated regions on the strip. Critical currents are

determined by the first sign of voltage drop across the sample using an amplifier with a noise level of 0.2 μvolt.

Neutron irradiation was carried out in the manner previously described for the cylindrical samples. The only difference was that subsequent to irradiation, the strip samples were allowed to stand at room temperature for two weeks in order to allow the induced radioactivity to decay to a point where the specimens could safely be mounted and measured. This precaution was necessary due to the presence of the radioactive contact materials.

Table II—Influence of Irradiation on Strip Sample Characteristics

Sample No.	Flux (Neutrons/cm^2)	Critical Current (I_c) (Amp.) 0 Field	12 kilogauss ∥	12 kilogauss ⊥	α $\left(\frac{\text{kilogauss-amp}}{\text{cm}^2}\right)$	B_0 (kilogauss)
	0	22.5	48.0	7.0	6.52×10^6	6.0
75	3.3×10^{17}	28.0	57.5	12.0	12.1×10^6	7.8
	6.9×10^{17}	31.0	67.0	14.9	15.6×10^6	10.0
79	0	20	32.3	9.5	5.70×10^6	12.1
	3.6×10^{17}	22.5	50.5	14.3	8.62×10^6	13.8

The influence of irradiation of two samples is presented in Table II. Sample 75 is niobium rich, whereas sample 79 is stoichiometric material (see Table I).

The results of two successive irradiations of sample 75 are shown in Figure 3. The critical current carried by the specimen is shown as a function of the externally applied magnetic field. Two cases are shown—one in which the current-carrying axis of the specimen is normal to the field, and the other with the axis parallel to the field. The maximum value of the external field used after irradiation was limited by the capability of the available magnet. Table II tabulates the changes produced by the neutron bombardment. The changes in I_c are relatively large, particularly for the case where the current in the specimen is normal to the applied field.

The effects are best described by changes in α, since this parameter is independent of the applied field strength. Rearrangement of Equation (1),

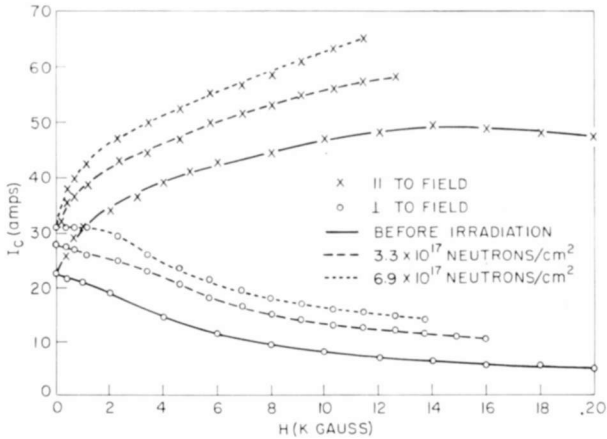

Fig. 3—Current-carrying characteristics of sample 75(3)-3-1 before and after irradiation.

$$\frac{1}{I_c} = \left(\frac{1}{A\alpha}\right) H + \frac{B_0}{A\alpha}, \tag{2}$$

(A is the sample cross-sectional area) shows that α may be derived from the slope of a $1/I_c$ versus H plot. Thus, the clear changes of slope (Figure 4) are indicative of increases in α. Results are given in Table II. It is evident from the data that defect saturation has not been achieved. Further irradiations of this sample are in progress.

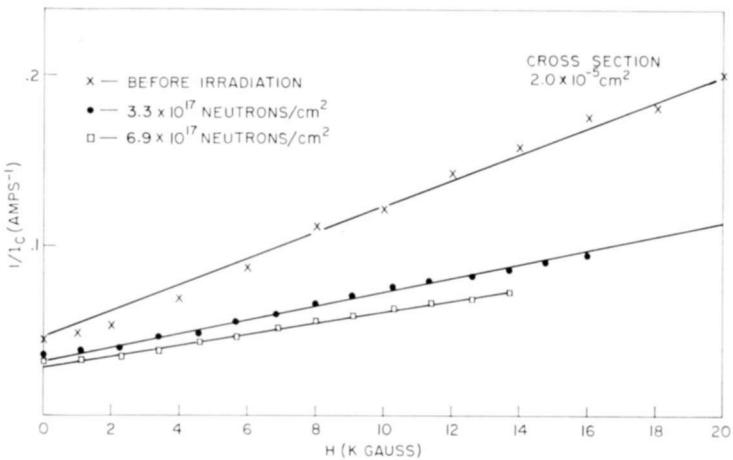

Fig. 4—Reciprocal of the current versus perpendicular applied field for sample 75(3)-3-1 before and after irradiation.

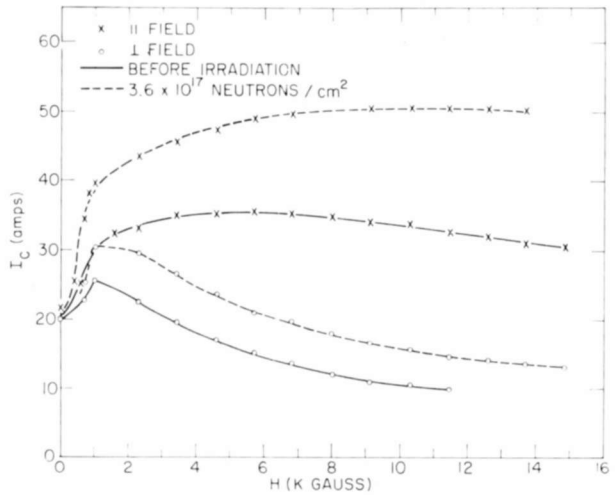

Fig. 5—Current-carrying characteristics of sample 79(9)-2-1 before and after irradiation.

Subsequent to irradiation B_0 is also found to increase (Table II). However, this parameter is measured less accurately than α, since the sample behavior is less ideal near zero field than at higher fields, as may be seen in the I_c versus H plots.

Results obtained from a single irradiation of sample 79 are presented in Figures 5 and 6. Unfortunately, this sample was destroyed when the radioactive contact material was being removed after the first irradiation.

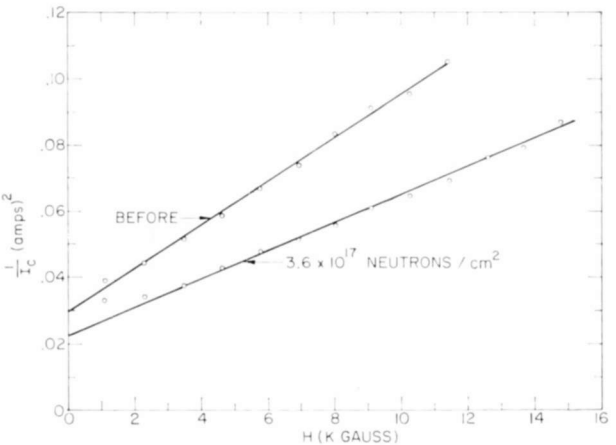

Fig. 6—Reciprocal of the current versus perpendicular applied field for sample 79(9)-2-1 before and after irradiation.

Resistivity Changes

The resistivity of the material was measured at 300°K and 77.4°K both before and after irradiation. Recent work of Woodard and Cody[19] has shown that the temperature-dependent contribution to resistivity in Nb_3Sn can be described in the range 18°-850°K by the empirical expression,

$$\rho(T) = \left(4.66 \times 10^{-3} T + 7.47 \exp \left\{ -\frac{85}{T} \right\} \right) \times 10^{-5}. \qquad (3)$$

Table III—Resistivity Ratio and Residual Resistance Changes in Nb_3Sn Produced by Neutron Bombardment

Sample	Flux (Neutrons/cm²)	$\frac{R(300°K)}{R(77°K)}$	ρ_0 (ohm-cm)	$\frac{d\rho_0}{d\phi}$ $\left(\frac{\text{ohm-cm}^3}{\text{neutron}}\right)$
75	0	1.824	21.8×10^{-6}	———
	3.3×10^{17}	1.794	23.7×10^{-6}	5.8×10^{-24}
	6.9×10^{17}	1.768	25.6×10^{-6}	5.5×10^{-24}
	10.1×10^{17}	1.730	27.8×10^{-6}	5.9×10^{-24}
79	0	2.029	12.2×10^{-6}	———
	3.6×10^{17}	1.962	15.0×10^{-6}	7.8×10^{-24}

Thus, it may be shown that the residual resistivity, which is a function only of the purity and perfection of the crystal lattice, can be expressed by

$$\rho_0 = \rho(77°K) \left\{ \left[\frac{\rho(300°K)}{\rho(77°K)} - 1 \right] \frac{1}{\frac{R(300°K)}{R(77°K)} - 1} - 1 \right\} \qquad (4)$$

The ratios of the sample resistance at 300°K to the resistance at 77°K were measured before and after irradiation. These ratios and the residual resistivities calculated by Equation (4) are given in Table III.

[19] D. W. Woodard and G. D. Cody, "Anomalous Resistivity of Niobium Stannide," *RCA Review*, Vol. XXV, p. 393, Sept. 1964.

Discussion

The above work demonstrates that neutron irradiation is capable of producing significant increases in the critical current density of both stoichiometric and nonstoichiometric Nb_3Sn. The defect configuration and the interaction between the structural defects and the field penetrating the superconductor is complex and not completely understood at the present time.

Calculations of Silcox and Rollins[10] give a quantitative relationship between the flux density within the specimen and the density of defects that can act as pinning points for the flux bundles or fluxoids. Their calculations, which treat the effects of pinning due to a precipitate or pore, show a direct proportionality between α and the defect density. Using their method, we estimate the defect concentration to be about 1.5×10^{16} defects/cm^3 in the material before irradiation. This would lead to an average distance between defects of 400 Å. If grain boundaries can act as pinning centers for stabilizing transport current, the distance between defects may be the grain size of the Nb_3Sn deposit. The increases in α after irradiation are undoubtedly due to defects, produced by atomic displacements, that are capable of pinning fluxoids. The damage may consist of many small dislocation loops that have formed due to vacancies collapsing in the cluster of displaced atoms that resulted from a neutron collision and subsequent secondary events. The Silcox–Rollins treatment would be applicable if the effect of the dislocation loop is similar to a pore or precipitate. We estimate the number of defect clusters to be about 5.6×10^{16}/cm^3 and 10.9×10^{16}/cm^3 for two successive irradiations of sample 75. If a linear relationship is assumed between α and the density of defects present, a value $\sim 10^6$ defects/cm^3 is obtained for the pre-irradiated material. This is in very good agreement with the value calculated using the Silcox and Rollins procedure. Therefore, we conclude that the neutron-induced defects exert pinning forces comparable to the defects already present in vapor-deposited Nb_3Sn.

The flux jumping observed in the irradiated cylinders is probably the result of the increase in α. Anderson[8] has shown that the power dissipation due to flux creep increases exponentially with α, and can lead to thermal instabilities. The absence of flux jumping in the strip samples subsequent to irradiation may be attributed to a geometry that is more efficient for dissipation of power.

It is evident that relatively large changes can be produced in the residual resistivity of Nb_3Sn after moderate neutron exposures. It should be noted that sample 79, whose lower residual resistivity indicated a more perfect structure and/or less impurities than that of 75, showed a larger increase in the resistivity than sample 75.

The close agreement in the ρ_0 change per unit flux of sample 75 after three successive irradiations indicates that the neutron-induced defect concentration present has not yet increased sufficiently to saturate the changes occurring in the nonsuperconducting properties.

The influence of neutron irradiation on the transition temperature of Nb_3Sn is described by J. Cooper.[20]

It is informative to consider the effect of similar irradiations on other hard superconductors. Cylinders of 25% cold-worked 3Nb:Zr alloy were irradiated with the Nb_3Sn cylinders. No measurable increase in J_c was detected. Swartz and coworkers[21] have recently observed changes in the magnetization curves of various compound superconductors (Nb_3Sn, Nb_3Al, V_3Ga, V_3Si) subsequent to fast-neutron irradiation, but noted no changes in the properties of elemental Nb or the $Nb_{.7}Ta_{.3}$ alloy. It has been previously demonstrated, on the other hand, that further cold working of 3Nb:Zr, and room-temperature deformation of Nb, does alter the superconducting properties.[3,6] While the alloys can be both mechanically deformed and irradiated, unfortunately this dual treatment cannot be imposed on the brittle compounds. A further understanding of these apparent anomalies await electron microscopic structural studies. Such studies have, to date, been carried out[22] only on deformed and annealed 3Nb:Zr.

Conclusion

It has been demonstrated that neutron-induced damage in Nb_3Sn results in large changes in the current-carrying characteristics and residual resistivity. The increase in the current density with introduction of damage is in quantitative agreement with the calculations of Silcox and Rollins.[10] The influence of higher flux densities on the material characteristics, and more detailed annealing studies, are in progress.

Acknowledgment

The authors are appreciative of the support of F. C. Dougherty for sample preparation, J. Pellicane for sample irradiation, and R. F. Decell for flux-shielding measurements. J. Cooper has been responsible for the transition-temperature measurements, and B. Goydish for the chemical analyses.

---

[20] J. L. Cooper, "Transition Temperature of Niobium Stannide," *RCA Review*, Vol. XXV, p. 405, Sept. 1964 (this issue).

[21] P. S. Swartz, H. R. Hart, Jr., and R. L. Fleischer, "Effect of Fast Neutron Irradiation on Magnetic Properties and Critical Temperature of Some Type II Superconductors," *Appl. Phys. Ltrs.*, Vol. 4, p. 71, 15 Feb. 1964.

[22] M. S. Walker, R. Stickler, and F. E. Werner, p. 49 in *Metallurgy of Advanced Electronic Materials*, G. E. Brock, ed., Interscience Publishers, N. Y., 1963.

MICROWAVE STUDIES OF NIOBIUM STANNIDE

By

Bruce Rosenblum,* Manuel Cardona,‡ and Gaston Fischer†

Summary—*The microwave surface resistance of Nb_3Sn has been studied as a function of temperature from 1.5°K to above the transition temperature and in magnetic fields up to 2×10^4 oersteds. These measurements have been used to determine several properties of the material such as $H_{c2}(T)$. The variation of the surface resistance with magnetic field and temperature is not yet explained theoretically. We discuss several conceivable absorption mechanisms and point out that one, with which certain features of the mixed state can be explained most readily (e.g., the temperature independence of the surface resistance at low temperatures), results in a model of the mixed state where the flux tubes have esentially normal cores. A large anisotropy in the surface resistance is observed, depending on the relative orientation of the d-c and microwave magnetic fields. An explanation in terms of a laminar model of the mixed state is given and its extension to flux tubes suggested. A hysteretic effect observed in the surface resistance is believed due to an effective surface barrier for the creation and destruction of flux tubes. An appendix is included in which observations on some earlier and nonstoichiometric samples of Nb_3Sn are reported.*

Introduction

MICROWAVE MEASUREMENTS have provided a great deal of experimental information upon which our ideas of the superconducting state are based. It is to be expected that such techniques can also provide information as to the nature of the mixed state. When the real part of the surface impedance, R, is measured as a function of magnetic field, H, and temperature, T, for several type-II superconductors,[1] the results follow a simple and consistent pattern. For a given value of the Ginsburg–Landau parameter, κ, the form of $R(H,T)$ is largely independent of the particular material. Therefore $R(H,T)$ appears to be characteristic of the mixed state and not of the chemistry or metallurgy of the material. With microwave measurements one can determine $H_{c1}(T)$, $H_{c2}(T)$, $H_{c3}(T)$, and several

* RCA Laboratories, Princeton, N. J.

† Laboratories RCA Ltd., Zurich, Switzerland.

‡ RCA Laboratories, Princeton, N. J.; present address, Physics Department, Brown University, Providence, R. I.

[1] M. Cardona, G. Fischer, and B. Rosenblum, "Microwave Surface Impedance of Superconductors of the Second Kind: In-Bi Alloys," *Phys. Rev. Letters*, Vol. 12, p. 101, 1964; M. Cardona and B. Rosenblum, *Phys. Letters*, Vol. 8, p. 308, 1964; B. Rosenblum and M. Cardona, "Evidence for Normal Regions at Low Temperatures in the Superconducting Mixed State," *Phys. Rev. Letters*, Vol. 12, p. 657, 1964.

properties of the Bean–Livingston barrier.[2] This can be done with no assumption as to the nature of the absorption mechanism in the mixed state. Some of the models proposed for the detailed nature of the mixed state do not yield the form of absorption that is observed.[1] A recent theoretical treatment[3] modifies the picture of this state, and appears to be in agreement with the microwave observations.

The reflection of electromagnetic waves at the surface of a medium in free space is completely characterized by the surface impedance of the material, $Z = R + iX$, where R is the real part of the surface impedance (surface resistance) and X is the imaginary part (surface reactance). The ratio of the electric field in the reflected wave to that in the incident wave at the boundary is $\gamma = (Z_0 - Z)/(Z_0 + Z)$, where Z_0 is the impedance of free space. For a metal $Z \ll Z_0$, and one readily finds that the fraction of the power absorbed by the metal, $1 - \gamma^2$, is proportional to R, and the phase change of the reflected wave is proportional to X.

In Nb_3Sn the microwave penetration depth, δ, is much larger than the mean free path, l, in the normal state or the coherence length, ξ, in the superconducting state; the equations governing the current at a given point are local, and the surface-impedance problem is much simpler than in the general case. We can, therefore, treat the problem in the local limit with no concern for the anomalous skin effect. All of the following discussion is restricted to this local limit in both the normal and superconducting states.

In the normal state if $l \ll \delta$ and $\omega\tau \ll 1$ (ω is the angular frequency and τ the scattering time), the real part of the conductivity, σ_1, is much larger than the imaginary part, σ_2. The normal-state surface resistance R_n is proportional to $\sigma_n^{-1/2}$, where σ_n is the normal-state conductivity. In the superconducting state the surface resistance[4] depends on a rather complicated combination of σ_1 and σ_2.

$$\frac{R}{R_n} = \left\{ \frac{\left[\left(\frac{\sigma_1}{\sigma_n} \right)^2 + \left(\frac{\sigma_2}{\sigma_n} \right)^2 \right]^{1/2} - \frac{\sigma_2}{\sigma_n}}{\left[\left(\frac{\sigma_1}{\sigma_n} \right)^2 + \left(\frac{\sigma_2}{\sigma_n} \right)^2 \right]} \right\}^{1/2} \tag{1}$$

[2] C. P. Bean and J. D. Livingston, "Surface Barrier in Type-II Superconductors," *Phys. Rev. Letters*, Vol. 12, No. 1, p. 14, 1964.

[3] C. Caroli, P. G. de Gennes, and J. Matricon, "Bound Fermion States on a Vortex Line in a Type II Superconductor," *Phys. Letters*, Vol. 9, No. 4, p. 307, 1 May 1964.

[4] M. Tinkham, *Low-Temperature Physics*, edited by G. DeWitt, B. Dreyfus, and P. G. de Gennes, Gordon and Breach, New York, New York, 1962, p. 157.

The conductivity, $\sigma = \sigma_1 - i\sigma_2$, has been introduced here in a purely phenomonological way; no specific mechanism has yet been implied for the interaction of the electromagnetic wave with the superconductor. After a brief description of the experimental technique used and of $R(T,H)$, we choose what appears to be a most likely absorption mechanism; in this framework we discuss what the surface resistance tells us about the mixed state.

Experimental Method

The measurements were made with a standard microwave bridge. The sample formed one wall or part of one wall of an undercoupled TE_{011} rectangular cavity. The actual measured quantity was the change in microwave power reflected from the sample cavity. For small changes the increase in reflected power is proportional to the variation in the Q of the cavity. This in turn is proportional to the change in R of the sample, if that is the only material in the cavity whose R varies with T and H. Care was taken that this be true or else a correction was made. It was always the change in R/R_n with temperature or magnetic field that was determined. In reporting and plotting the data we always assume that $R(H = 0) = 0$ at the lowest temperatures of measurement ($T \approx 1.5°K$). Since the changes are large fractions of R_n and since the measurements clearly show $R(H = 0, T \approx 1.5°K) \ll R_n$, this is an excellent approximation.

The frequency of the klystron was stabilized to that of the experimental cavity. This ensures that the reflected power changes only with the change in R and is insensitive to changes in X. Actually, the frequency shift caused by the changing penetration depth is very small.

The sample cavity was in two halves joined on a plane across which no microwave currents flow. This made the cavity Q much less sensitive to the contact between the two halves. This technique was necessary in order to minimize spurious signals produced by the torque exerted by the magnetic field on the superconducting sample. The cavity half containing the sample was in good thermal contact with a germanium resistance thermometer. The other half was brazed to a section of guide to which was affixed a manganin wire heater completely enclosed in a copper block. The cavity assembly was enclosed in a double-walled evacuable can. The arrangement is shown in Figure 1.

Sample Preparation

All the samples of Nb_3Sn were grown by the simultaneous reduction of the halides of niobium and tin on steatite substrates,[5] and were

[5] G. Cullen, "Preparation and Properties of Niobium Stannide on Insulating Substrates," *Trans. Metallurgical Soc.*, in press.

approximately 0.001 inch thick. Since the as-grown samples were very rough (on the scale of penetration depths), they were mechanically polished [first with Linde "A" (0.3 micron) and then with Linde "B" (0.05 micron)]. After polishing, the samples had an almost perfect surface as observed with an optical microscope. Admittedly, mechanical polishing is not a desirable surface treatment for microwave studies; however, the electron mean free path is already so small in Nb_3Sn that the surface damage that might be introduced could not reasonably be

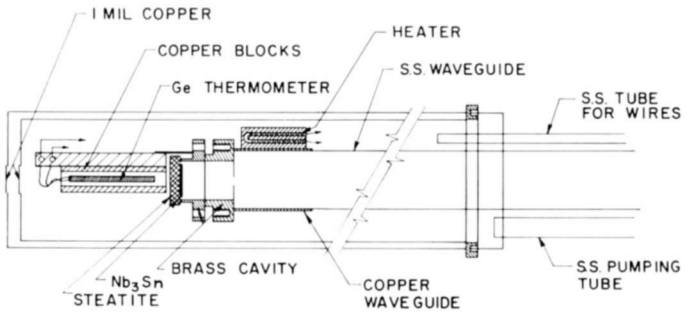

Fig. 1—Diagram of sample mounting, microwave cavity, and temperature-controlling arrangement.

expected to decrease it further. To verify the negligible effect of the surface damage, an unusually smooth sample was obtained and studied without surface treatment. The results were the same as the polished samples in every respect. Samples etched with acid also showed no change in microwave properties. The samples were fastened to the cavity with an epoxy resin to form one wall. The joint was then painted with a silver paint.

To obtain greater sensitivity, or to work with smaller samples, a much smaller piece of Nb_3Sn on steatite (approx. 0.100×0.150 inch) was polished. The steatite was then ground away and the reverse side also polished. The sample was then mounted in the microwave cavity on top of a sheet of Mylar. The size and orientation of this small sample could be adjusted until it formed a strip line resonator within the TE_{011} cavity. The sensitivity in this configuration could be more than an order of magnitude greater than when the sample formed the entire bottom of the cavity. A disadvantage of this mounting system is that the resulting current distribution over the sample is not uniform. Since the surface impedance shows a large dependence on the direction of the magnetic field with respect to the microwave current, this mounting is not completely satisfactory for measurements in a magnetic field.

Experimental Results

One can experimentally determine the field H_{c2} at which the surface resistance becomes independent of magnetic field, and thus measure H_{c2} as a function of temperature. This, of course, involves no assumptions about the absorption mechanism in the mixed state. As discussed below, there is no complication with surface superconductivity[1] in Nb_3Sn. Table I gives dH_{c2}/dT near T_c and T_c for six samples determined with magnetic fields up to 2×10^4 oersteds. Also listed are values of $H_{c2}(T = 0)$ calculated using either the Gor'kov[6] temperature depend-

Table I

Lot No.	T_c°K	ΔT°K	$\frac{dH_{c2}}{dT}$ kOe/°K	$H_{c2}(0)$kOe Gor'kov	$H_{c2}(0)$kOe $H_{c2}(t) \sim 1 - t^2$	ρ_0 ohm-cm
FS20	18.3	0.04	19.5 ± 1	224	178	1×10^{-5}
80	17.9	0.10	19.7 ± 1	222	177	1.5×10^{-5}
80*[a]	17.4	—	21 ± 1	229	183	$\sim 2.4 \times 10^{-5}$
79	18.0	0.14	18.6 ± 1	210	167	1×10^{-5}
58	17.4	0.7	22 ± 2	238	191	$0.9 \rightarrow 1.4 \times 10^{-5}$
53	14.8	2.0	———	—	—	4×10^{-5}

[a] 80* was another piece of lot 80 which was irradiated with 1.5×10^{18} neutrons/cm^2. The resistivity was computed assuming $\Delta\rho_0 = 6 \times 10^{-24} \times$ (neutron flux) [see Reference (14)].

ence $H_{c2}(t) = H_{c2}(0)\,(1 - 1.24t^2 + 0.28t^4 - 0.04t^6)$ or $H_{c2}(t) = H_{c2}(0)\,(1 - t)^2$, which is obtained if κ is temperature independent; t is the reduced temperature T/T_c. The last column in Table I lists the residual resistances ρ_0 for these specimens.[7] The lack of dependence of dH_{c2}/dT (and therefore $H_{c2}\,(0)$) on ρ_0 indicates either that $l > \xi_0$ and hence Nb_3Sn is an intrinsic type-II superconductor, or that H_{c2} is limited by spin paramagnetism.[8] In this latter case $H_{c2}(t)$ should have a $(1 - t^2)$ temperature dependence.

We will now describe the dependence of the surface resistance on

[6] L. P. Gor'kov, "The Critical Supercooling Field in Superconductivity Theory," *Zh. Eksperim. i. Teor. Fiz.*, Vol. 37, p. 833, Sept. 1959 (translation in *Soviet Phys. JETP*, Vol. 10, p. 593, March 1960).

[7] G. D. Cody and D. W. Woodard, "Anomalous Resistivity of Niobium Stannide," *RCA Review*, Vol. XXV, p. 393, Sept. 1964 (this issue).

[8] A. M. Clogston, "Upper Limit for the Critical Field in Hard Superconductors," *Phys. Rev. Letters*, Vol. 9, p. 266, 15 Sept. 1962.

the magnetic field and temperature for highly stoichiometric material, which shows little variation from sample to sample. The data presented in the figures are for a sample of particularly low ρ_0 labeled FS20. We then give the interpretation of these data and discuss some older data on nonstoichiometric samples in Appendix A.

Figure 2 shows the surface resistance, R, versus the applied mag-

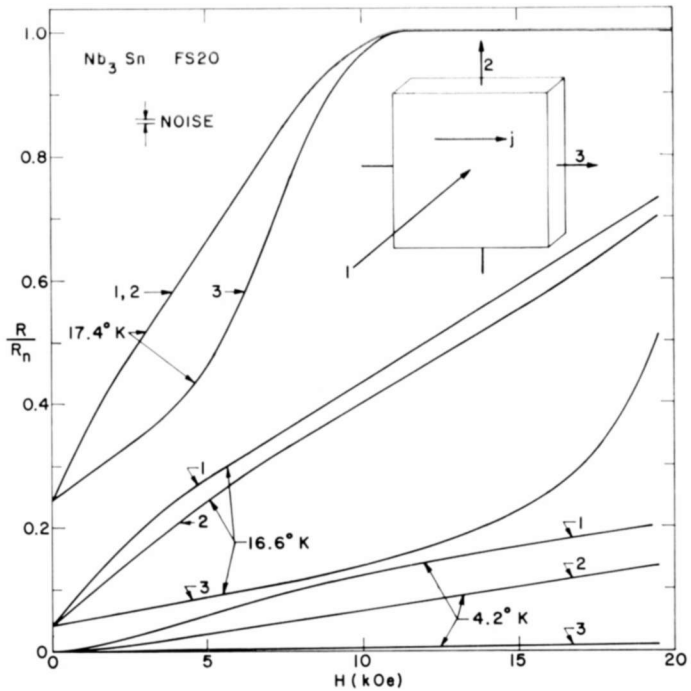

Fig. 2—Microwave surface resistance at 23 gc versus magnetic field for a polished Nb_3Sn sample (Lot FS20) at different temperatures.

netic field, H, for three orientations of the magnetic field. In the low-temperature region—from about 9°K to the lowest temperature of measurement 1.5°K—the surface impedance is almost independent of temperature. At these temperatures when the magnetic field in the plane of the sample and perpendicular to the microwave current j was increased, R did not perceptibly increase until a field H_{c1}^* was reached, and then it rose almost linearly to about $0.14R_n$ at 2×10^4 oersteds. A linear extrapolation would yield $R = R_n$ at 14×10^4 oersteds, which is close to the calculated H_{c2}. In the Pb-Tl and In-Bi alloys studied,[1] the rapid rise in R began at the value of H_{c1} determined from magneti-

zation studies. However, because of the hysteresis effect discussed below and the flux trapping measurements of Hecht,[9] we do not necessarily make this identification in Nb_3Sn. H_{c1}^* ($T = 4.2°K$) $\approx 10^3$ oersteds and varies with temperature as expected for H_{c1}. When the magnetic field is parallel to the microwave current, the absorption is at least an order of magnitude smaller. When the magnetic field is perpendicular to the sample, the absorption is about forty per cent greater at moderately high fields. However, this percentage difference appears to decrease as the field increases. Depolarization effects should not be important even in this configuration, since the field almost completely penetrates the sample. At temperatures near T_c all anisotropy disappears.

At temperatures at which the available field is sufficient to bring the material to the normal state, the surface resistance, R, reaches R_n at the same field for orientations both parallel and perpendicular to the surface. In Nb_3Sn we thus observed none of the surface superconductivity effects that have been seen up to $H_{c3} \simeq 1.7\ H_{c2}$ in several alloys.[1] This is not surprising, since the thickness of the superconducting surface layer is the coherence distance, ξ, which is much smaller than the microwave penetration depth (about 10^4 Å near H_{c2}). Such a thin superconducting layer would not significantly change the surface resistance. The depth of the region of serious surface damage due to polishing may also be larger than ξ. The surface would, therefore, not be parallel to the field on this scale.

Figure 3 shows a plot of R as a function of temperature for $H = 0$ and 19.5×10^3 oersteds. With zero magnetic field R drops rapidly as the temperature is reduced below T_c. The shape of the curve is very much like that predicted with the Gorter–Casimir two-fluid model and Equation (1). However, the width $\Delta T = 0.3°K$, where $\Delta T = T_c - T$ ($R = 1/2\ R_n$), is about four times greater than expected for Nb_3Sn. Since the width measured with a low-frequency inductance bridge is only $0.03°K$, the excess width at 23 gc cannot easily be explained by sample inhomogeneity. In other lots the width was larger; e.g., lot 80 gave widths about four times larger than FS20 both in the inductance bridge and at microwave frequencies.

When a magnetic field is applied in the plane of the sample parallel to the microwave current (curve 3), the transition temperature is reduced and the width of the transition is slightly greater, but now there is a long tail to the curve. The surface resistance does, however, get very small when $T \ll T_c$. For a magnetic field perpendicular to

[9] R. Hecht, "Lower Critical Field of Niobium Stannide," *RCA Review*, Vol. XXV, p. 453, Sept. 1964 (this issue).

the microwave current and either perpendicular (curve 1) or parallel (curve 2) to the sample surface, the width of the transition is considerably increased by the magnetic field. Moreover, the surface resistance no longer goes to zero as T approaches zero, but instead appears to saturate at a value R/R_n of the order of $H/H_{c2}(t = 0)$. Indeed, the temperature dependence of R/R_n is much like that of H/H_{c2}. The dashed line shows the temperature dependence of H/H_{c2} for $H_{c2} \propto (1 - t^2)$.

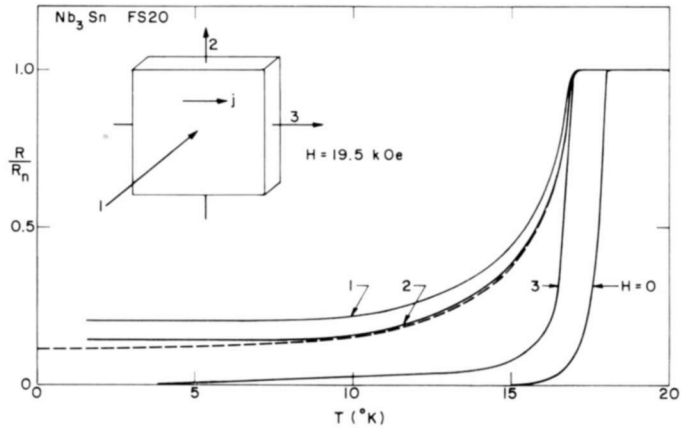

Fig. 3—Microwave surface resistance of Nb_3Sn (Lot FS20) at 23 gc versus temperature for $H = 0$ and $H = 19.5 \times 10^3$ oersteds (full curves). The dashed curve represents the function H/H_{c2} $(t = 0)$ $[1 - t^2]$.

In examinations of other type-II superconductors with moderately high κ, $R(H)/R_n = H/H_{c2}$ is also approximately true. This apparently rules out the attractive possibility of making high-Q microwave cavities that could operate in high magnetic fields.

The data shown are all due to measurements at 23 gc. Preliminary and less complete studies at 55 gc show that $R(H,T)/R_n$ at low temperatures is not strongly dependent upon frequency. The width of the transition is about twice as large at the higher frequency, but at low temperatures $R(H)/R_n$ is the same at both frequencies. The frequency-dependence studies are continuing, and are to be extended to the ten- and one-gigacycle ranges.

Hysteretic Behavior

The measurement in Figure 2 was performed by increasing the field from zero to 19.5×10^3 oersteds at each given temperature. When

the direction of change of magnetic field is reversed, a hysteretic effect is observed in all stoichiometric samples. For H in the plane of the sample and perpendicular to the microwave current, there are two R-versus-H curves—one for increasing field and one for decreasing field. When the direction of the change of the magnetic field was reversed, R changed quite abruptly between the "H increasing" and "H decreasing" curves. The general character of the effect is shown in Figure 4. When the magnetic field was perpendicular to the plane of

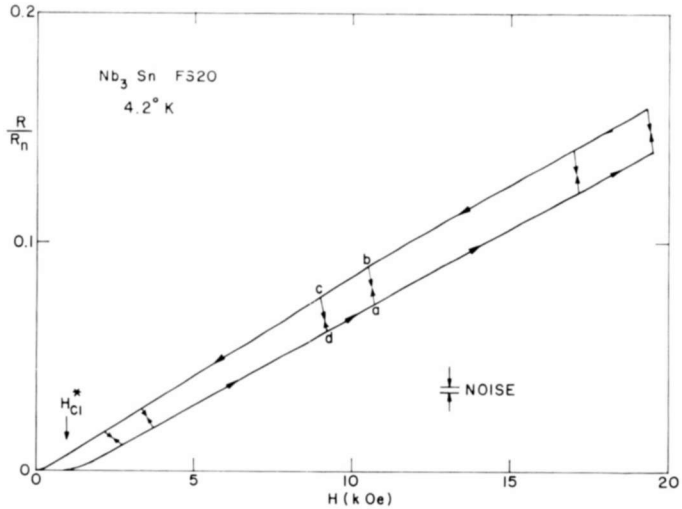

Fig. 4—Surface resistance at 23 gc versus magnetic field showing hysteretic behavior of Nb_3Sn (lot FS20) at 4.2°K.

the sample the effect disappeared. (Very little flux trapping was evident—a sample cooled in zero field showed almost the same $R(H)$ on the first increase of magnetic field as on subsequent runs.) The hysteretic effect is believed due to the existence of an effective barrier to the entrance and exit of flux tubes, in part related to the barrier of Bean and Livingston.[2] When the field is increased to point "a" and then decreased, the flux tube density within the microwave penetration depth increases. This increases the loss until a critical point is reached at "b" whence the flux tubes begin to disappear at the surface, and R decreases on the "H decreasing" curve. If at "c" the field is increased, the flux tubes are repelled from the surface, but no new ones are created until point "d".

The surface resistance should start rising as soon as flux tubes are created in the material. This might be expected to occur at $H = H_{c1}$.

However, if the barrier causing the hysteresis inhibits initial penetration of the field, $H_{c1}^* > H_{c1}$. The values of H_{c1} measured by Hecht[9] are considerably smaller than H_{c1}^*. The hysteretic effect is being studied in more detail and will be published shortly.

Discussion

There are several conceivable mechanisms for power absorption in the mixed state. By a process of elimination we will tentatively attribute the microwave loss to absorption by quasi particles or normal electrons existing in the mixed state. We will then try to determine some features of the mixed state from the dependence of the microwave surface resistance on magnetic field and temperature.

Flux Flow

At very low frequencies and at current densities below a critical value, superconductors in the mixed state exhibit almost no power absorption. Direct currents persist in closed loops with little decay for long periods. At currents above a critical value, the Lorentz force is sufficiently great that the pinning centers can no longer restrain the motion of the flux tubes. The tubes then move over the pinning centers, and in this "viscous state" there is considerable loss.[10] In the Nb_3Sn samples, the critical current densities for the start of flux flow is given by[11] $J \approx 3 \times 10^9/H_\perp$ amp/cm^2, where $H_\perp$ is the field in oersteds, perpendicular to the current. The microwave current densities in the skin depths of our samples are lower than 100 amp/cm^2. For the fields of several thousand oersteds at which absorption is observed, we are four orders of magnitude below the critical current for flux flow. In the study of low-frequency a-c losses in the mixed state, the losses[12] have been attributed to flux tubes jumping over pinning centers. The power loss divided by the square of the current (i.e., the effective resistance) increases with current and frequency. In our case the effective resistance is largely independent of the current and frequency. We therefore conclude that flux tube flow is not responsible for the observed microwave absorption. A related mechanism—flux-tube vibration—will now be discussed.

---

[10] P. W. Anderson and Y. B. Kim, "Hard Superconductivity: Theory of the Motion of Abrikosov Flux Lines," *Rev. Mod. Phys.*, Vol. 36, p. 39, Jan. 1964.

[11] G. D. Cody and G. W. Cullen, "Critical Currents and the Lorentz Force Model in Niobium Stannide," *RCA Review*, Vol. XXV, p. 466, Sept. 1964 (this issue).

[12] T. A. Buchhold, "The Nature of the Surface Losses of Superconductors at Low Frequencies," *Cryogenics*, Vol. 3, p. 141, Sept. 1963.

Flux-Tube Vibrations

The Lorentz force due to an alternating current flowing perpendicular to the flux tubes can move (vibrate) the flux tubes even though the current is far less than the critical value for flux flow. It has been suggested by de Gennes and Matricon[13] that superconductors in the mixed state may absorb high-frequency radiation through the excitation of the normal modes of vibration of the system of flux tubes. The actual loss mechanism envisaged was the creation of eddy currents in the "hard cores" of the flux tubes by the $\partial B/\partial t$ due to the motion of the tubes. Another possible dissipation mechanism is the creation of phonons by the pinning centers, which are vibrated by the forces exerted on them by the flux tubes. At present there is no theory of flux-tube vibration that is complete enough for us to compare with experimental results. There are, however, several properties that a theory of flux-tube vibration would be expected to yield. The loss through this mechanism should be fairly strongly dependent on the frequency of the incident wave, ω. When $\omega \gg \omega_0$, where ω_0 is the natural vibration frequency, the loss would be small and would decrease with increasing frequency. The loss would also be expected to depend on the nature of the pinning.

The observed loss at low reduced temperatures is largely independent of frequency and whether the material is weakly pinned (small α_c, e.g., Pb-Tl alloys) or strongly pinned (large α_c, e.g., Nb_3Sn). Material from a relatively weakly pinned lot of Nb_3Sn (FS20, $\alpha_c = 10^9$ oersted-amp/cm^2) and from a moderately strongly pinned (lot 80, $\alpha_c = 11.7 \times 10^9$ oersted-amp/cm^2) gave similar results. It has been found[14] that fast-neutron irradiation with an integrated flux of about 10^{18}/cm^2 increases α_c by a substantial amount. The density of pinning centers in such irradiated material is believed to be about 3×10^{17}/cm^3. This means that the distance along flux tubes between pinning centers is much less than the penetration depth, and even less than the spacing of the flux tubes. A sample from lot 80 was studied before and after irradiation with a flux of more than 10^{18}/cm^2; no change in $R(H,T)$ was found. In view of the independence of $R(H,T)$ on the pinning and an independence of $R(H)$ at low temperatures on frequency, flux-tube vibration is not believed to play a major role in the microwave absorption.

---

[13] P. G. de Gennes and J. Matricon, "Collective Modes of Vortex Lines in Superconductors of the Second Kind," *Rev. Mod. Phys.*, Vol. 36, p. 45, Jan. 1964.

[14] G. W. Cullen, R. L. Novak, and J. McEvoy, "Effect of Neutron-Induced Defects on the Current-Carrying Behavior of Niobium Stannide," *RCA Review*, Vol. XXV, p. 479, Sept. 1964 (this issue).

Across-the-Gap Excitation

The highest frequency used in the present study was very small compared to the energy gap at zero field; but in a magnetic field the order parameter varies periodically to zero, and excitations with lower energies exist. The connection between the order parameter and the minimum energy needed to excite quasiparticles is not clear, and the contributions of this mechanism cannot yet be assessed. However, one would expect the contribution to increase rapidly with frequency. The small frequency dependence at low temperatures found experimentally indicates that this mechanism is relatively unimportant in this region. Near the transition temperature there is some temperature dependence, and across-the-gap excitations may be playing a role.

Absorption by Quasi Particles

In the pure superconducting state (type I, or type II below H_{c_1}) the absorption at frequencies well below the energy gap is due to the quasi particles present in thermal equilibrium. At these frequencies it is reasonable to treat this absorption in terms of the two-fluid model. At zero magnetic field we use the Gorter–Casimir temperature dependence of the normal carrier concentration, $N_n \sim t^4$. Since for Nb_3Sn the scattering time for normal electrons is of the order of 10^{-13} second, $\omega\tau \ll 1$, where $\omega \sim 10^{11}$ sec^{-1} is the angular frequency of the microwave field. It is thus a very good approximation to attribute the real part of the conductivity to the normal carriers and the imaginary part to the superconducting carriers. Since the normal-state mean free path, l, is small compared to the penetration depth, we need not be concerned with anomalous skin effects. Thus

$$\frac{\sigma_1}{\sigma_n} = \frac{N_n e^2\tau/m}{Ne^2\tau/m} = \frac{N_n}{N} = t^4, \tag{2}$$

where N, e, τ, and m are, respectively, the number, charge, scattering time, and mass of the conduction electrons in the normal state. For σ_2 we cannot assume a London two-fluid model, but instead must use the local limit of the Pippard integral.[15]. This yields

$$\frac{\sigma_2}{\sigma_n} = \frac{N_s e^2/m\omega}{Ne^2\tau/m}\frac{\xi}{\xi_0} = \frac{N_s}{N\omega\tau}\frac{\xi}{\xi_0} = \frac{1-t^4}{\omega\tau}\frac{\xi}{\xi_0}, \tag{3}$$

and the coherence distance ξ is given by $1/\xi = 1/\xi_0 + 1/(\alpha l)$, where

[15] M. Tinkham (see Ref. (4), p. 162).

ξ_0 is the intrinsic coherence distance, N_s the density of superconducting carriers, and α a constant of the order of unity. According to BCS, $\xi_0 = 0.18\,\hbar v_F/(kT_c)$ where v_F is the Fermi velocity, T_c is the transition temperature, and k is Boltzmann's constant. For an extrinsic type-II superconductor ($l \ll \xi_0$),

$$\frac{\xi}{\xi_0} = \frac{\alpha l k T_c}{0.18 \hbar v_F} = \frac{\alpha}{0.18}\,\frac{kT_c}{\hbar}\,\tau. \tag{4}$$

Substituting this result into Equation (3),

$$\frac{\sigma_2}{\sigma_n} = \frac{\alpha}{0.18}\,\frac{kT_c}{\hbar\omega}\,(1 - t^4). \tag{5}$$

For an intrinsic (pure) type-II superconductor $\xi = \xi_0$, and

$$\frac{\sigma_2}{\sigma_n} = \frac{1 - t^4}{\omega\tau}. \tag{6}$$

Equations (2) and either (5) or (6) are then substituted into Equation (1) to give a theoretical R/R_n. As pointed out earlier, the width of the $R(T, H = 0)$ curve obtained by using Equations (1), (2), and (5) or (6) is about four times smaller than found experimentally.

At this point it may be mentioned that a small density of superconducting carriers is enough to effectively "short out" the normal carriers, and cause the surface resistance to be much smaller than the normal-state value. The coefficient of $(1 - t^4)$ in Equation (5) is approximately 100 for Nb_3Sn. Setting $\tau = l/v_F$ and choosing reasonable values[16] for l and v_F, one obtains about the same coefficient for the intrinsic case. These values yield $R/R_n \sim 1/2$ for only 1 per cent of the carriers being superconducting. (Using the *experimental* $R(T)/R_n$ curve and $N_n \sim t^4$, we would conclude that only 6 per cent of the carriers are superconducting when $R(T)/R_n = 1/2$). Thus if the normal carriers are not concentrated in almost normal regions, their effectiveness in absorbing microwaves is greatly reduced.

If the normal carriers are concentrated in nearly normal regions so that $\sigma_1^2 \gg \sigma_2^2$ for such regions, R/R_n is independent of frequency, which is approximately true experimentally. If, on the other hand, $\sigma_2^2 \gg \sigma_1^2$ and the normal carriers are present in largely superconducting regions, $R/R_n \sim \omega^{3/2}$.

[16] G. D. Cody, "The Superconducting Penetration Depth of Niobium Stannide," *RCA Review*, Vol. XXV, p. 414, Sept. 1964 (this issue).

The model of the mixed state with which we can most simply explain our data has normal regions of finite extent at the centers of the Abrikosov flux tubes. In referring to these regions as being "normal" we do not wish to exclude the possibility that the regions do have finite gaps. However, the lack of temperature dependence of R at low temperature strongly suggests that any energy gap in the regions at the centers of the flux tubes must be small compared to thermal energies. We assume that at low temperature the extent of the normal regions is of the order of the coherence distance. This model readily accounts for the linear increase with H and the temperature independence of the absorption at low temperature.

If, instead, the assumption is made that the normal carriers are somehow uniformly distributed over the material rather than concentrated at the centers of the flux tubes, an extremely small average order parameter would be required to give the observed absorption. This would be in disagreement with the average order parameter predicted by the Abrikosov theory and found so successful in the analysis of thermal conductivity in In-Bi alloys.[17] Another even stronger argument for the localization of the normal carriers at the centers of the flux tubes is the observed anisotropy discussed below.

By extrapolating Abrikosov's solution of the Ginzburg–Landau equations in the vicinity of H_{c2} to lower magnetic fields, one would not conclude that the flux tube centers were normal. This extrapolation could be done by identifying the order parameter with an energy-gap parameter.[18] The excitation energy for quasi particles would then be finite everywhere or perhaps everywhere except on "lines of zero volume." Such a model for the individual flux tube would not yield a temperature-independent absorption at low temperatures. With such a model one would predict that the absorption in a magnetic field would continue to decrease with temperature, approaching *zero* as $T \rightarrow 0$. At a given low temperature one would not expect a linear rise in R with H, but rather that R would remain very small until $H \sim H_{c2}$.

Although we cannot accept the above model of the individual flux tube which might be obtained from an extrapolation of the Abrikosov

---

[17] L. Dubeck, P. Lindenfeld, E. A. Lynton, and M. Rohrer, "Thermal Conductivity of Superconductors of the Second Kind," *Phys. Rev. Letters*, Vol. 10, p. 98, Feb. 1963.

[18] L. P. Gor'kov, "Microscopic Derivation of the Ginzburg-Landau Equations in the Theory of Superconductivity," *Zh. Eksperim. i. Teor. Fiz.*, Vol. 36, p. 1918, June 1959 (translation in *Soviet Phys. JETP*, Vol. 9, p. 1364, Dec. 1959).

theory, Abrikosov's expression for the magnetization[19] near H_{c2} has been experimentally shown to hold even at low temperatures. This expression is

$$-4\pi M = (H_{c2} - H)\,a \qquad (7)$$

$$\text{where } a = \frac{1}{1.18\,(2\kappa^2 - 1)}.$$

From the experimental magnetization one concludes that Equation (7) can be used without large error for $H > H_{c1}$, provided H is not very close to H_{c1}.

The number of single quantum flux tubes per unit area n is given by

$$n = \frac{B}{\phi_0} = \frac{1}{\phi_0}(H + 4\pi M) = \frac{1}{\phi_0} H(1 + a) - \frac{a}{\phi_0} H_{c2}, \qquad (8)$$

where $\phi_0 = hc/(2e)$, the flux quantum, and B is the average flux density within the superconductor.

We can now write

$$H_{c2} = \sqrt{2}\,\kappa\, H_c = \sqrt{2}\,\kappa\, H_c(t = 0)\,(1 - t^2), \qquad (9)$$

and set[20]

$$\kappa = 0.96\,\frac{\lambda_L(t = 0)}{\xi_0} = 0.96\left[\frac{mc^2}{4\pi N_s(0)\,e^2}\right]^{1/2}\frac{1}{\xi_0}, \qquad (10)$$

and

$$H_c(t = 0) = \sqrt{2\pi N(\epsilon_F)}\;\epsilon_0(0) = \sqrt{2\pi N(\epsilon_F)}\;\frac{\hbar v_F}{\pi\xi_0}. \qquad (11)$$

Here H_c is the thermodynamic critical field, λ_L is the London penetration depth, $N(\epsilon_F)$ is the density of states at the Fermi surface, v_F is the Fermi velocity, and we have assumed that Nb_3Sn is an intrinsic type-II superconductor. From Equations (9), (10), and (11),

$$H_{c2} = 0.17\,\frac{\phi_0}{\xi_0^2}\,(1 - t)^2. \qquad (12)$$

---

[19] A. A. Abrikosov, "On the Magnetic Properties of Superconductors of the Second Group," *Zh. Eksperim. i. Teor. Fiz.*, Vol. 32, p. 1142, June 1957 (translation in *Soviet Phys. JETP*, Vol. 5, p. 1174, Dec. 1957).

[20] B. B. Goodman, "The Magnetic Behavior of Superconductors of Negative Surface Energy," *IBM Jour. Res. and Dev.*, Vol. 6, p. 63, Jan. 1962.

For a very impure superconductor with $\xi_0 \gg l$, ξ_0^2 must be replaced[20] by $1.3\xi_0 l$ in Equation (12). The fraction of volume F_n that we assume to be normal is, in the spirit of the recent calculation by Caroli *et al*,[3] proportional to $n\xi^2$. We take the proportionality coefficient such that $F_n = 1$ at $H = H_{c2}(t = 0)$. Then

$$F_n = \frac{H(1 + a) - aH_{c2}}{H_{c2}\ (t = 0)}. \tag{13}$$

For Nb_3Sn, aH_{c2} is not much different from H_{c1}*, and Equation (13) correctly gives the low-temperature dependence of R on H if $R/R_n = F_n$ for the magnetic field perpendicular to the microwave current. The reason for choosing this orientation is discussed below.

Since $a \ll 1$ for Nb_3Sn, Equation (13) is almost temperature independent. One could modify Equation (13) by replacing $H_{c2}(t = 0)$ by $H_{c2}(t)$, so that the fraction of normal material $F_n(t) = 1$ at $H = H_{c2}(t)$. The temperature dependence of $R/R_n = F_n$ would then agree remarkably well with our experiments. The dashed line in Figure 3 corresponds to Equation (13) putting $H_{c2}(0)[1 - t^2]$ for the denominator. Almost as good agreement is obtained by using the Gor'kov temperature dependence[6] of H_{c2}. One can see physically why $R(H \neq 0)$ should show a more gradual increase with temperature than $R(H = 0)$. Although we postulate that there is a core of essentially normal material of finite extent at the centers of the flux tubes, the gap must rise gradually outside this normal core. As the temperature is raised quasi particles are excited in the region around the core, and hence the volume of essentially normal material grows.

Ratios of surface resistance $R_\perp/R_\parallel$ larger than 20 have been observed for Nb_3Sn samples, where $R_\perp$ and $R_\parallel$ are, respectively, the surface resistances with H perpendicular and parallel to the microwave current but in the plane of the sample. Smaller anisotropies have been observed in other materials; the anisotropy is approximately proportional to the κ of the material. Anisotropy is expected for the model of flux tubes with normal cores* and, indeed, is strong evidence for the existence of a spacially modulated order parameter in the mixed state (if any such evidence is needed at this date). We will tentatively assume that the anisotropy is a classical phenomenon due to an array of tubes of normal conductivity σ_n imbedded in a medium of conduc-

* One would also expect a large anisotropy of this form (but not necessarily the κ dependence) for a flux tube vibration mechanism of power absorption.

tivity $i\sigma_2$. This boundary value problem has not yet been solved, but such an anisotropy could be expected.

It is much simpler to consider a one-dimensional problem of normal laminae in a superconducting medium rather than the two-dimensional array of normal flux-tube cores. We assume that the applied magnetic field is in the planes of these laminae, and that the laminae are in planes perpendicular to the sample surface. Clearly, a direct current driven by a constant-current generator would show an infinite anisotropy, since with the current in the plane of the laminae the superconducting regions would completely short out the laminae. When the current is perpendicular to the laminae, the loss would be proportional to the fraction of normal material.

For normal laminae thin compared to the microwave penetration depth, one might expect a similar result. When the microwave current is perpendicular to the laminae, the loss should be proportional to the volume that is normal. When the current is parallel to the laminae, a magnetic induction effect—the same one that keeps the current in the skin depth in the usual electromagnetic wave reflection problem—reduces the current in the normal region and thus reduces the loss in this configuration. It is important to note that if the width of the normal and superconducting regions were large compared to a skin depth (as in an intermediate state), one would observe no anisotropy. The loss in a region of the surface can only be affected by a region of a different conductivity if the two regions are within a penetration depth of each other.

Some of these qualitative ideas have been confirmed by Fischer,[21] who has recently calculated the microwave surface impedance of a medium with a complex conductivity periodically modulated in one direction (laminae). He assumed a sinusoidally modulated conductivity with a wavelength d. For $d \gg \delta$, the microwave penetration depth, no anisotropy is obtained. For $d \ll 4\pi\delta$, he obtains the same value for the surface resistance $R_\parallel$ that one would obtain for a uniform material with the average complex conductivity. In the case in which the aver-

[21] G. Fischer, "Microwave Surface Impedance of a Periodic Medium," *Jour. Math. Phys.*, Vol. 5, p. 944; "Microwave Surface Impedance of Superconductors of the Second Kind," *Phys. Rev.*, Vol. 135 p. A1202, 1964. (The definition of surface impedance in these papers was incorrectly stated as $Z \equiv E\ (z = 0)/\int_0^\infty j_\parallel(z)dz$. In the present case the denominator is not independent of coordinates. The definition $Z \equiv E\ (z = 0)/B_\parallel\ (z = 0)$ is more appropriate and was, in fact, used. No results are changed by this correction.)

age number of superconducting carriers N_{s0} is of the same order of magnitude as the number of normal carriers, an isotropy is obtained where

$$\frac{R_\perp}{R_\parallel} = \sqrt{2}\,\frac{3N_0 - N_{s0}}{N_0 - N_{s0}},$$

where N_0 is the total carrier density. The normal carrier density is assumed to be sinusoidally modulated between N_0 and $N_0 - 2N_{s0}$, while the superconducting carrier density is modulated between zero and $2N_{s0}$.

The maximum possible value of $R_\perp/R_\parallel = 7$ takes place for $N_0 = 2N_{s0}$. Hence, a sinusoidal conductivity modulation does not quite explain the large values of $R_\perp/R_\parallel$ obtained in Nb_3Sn and other materials (a Pb-Tl alloy with 30 at.% Tl gives $R_\perp/R_\parallel = 13$). On the other hand, higher anisotropies would presumably result if one took into account more than one sinusoidal component of the periodic conductivity modulation.

Fischer's calculation applies only to a one-dimensional conductivity modulation (laminae). Whether anisotropies as high as observed experimentally can be obtained with a flux tube model remains a question.

Acknowledgment

We are indebted to H. Hanson for taking much of the experimental data and for his assistance throughout the course of the work. We wish to thank G. W. Cullen for supplying the Nb_3Sn samples and information concerning them. We have profited greatly from many discussions with G. D. Cody, R. H. Parmenter, and A. Rothwarf.

Appendix A—Nonstoichiometric Materials

The microwave measurements on Nb_3Sn were started before the procedure for making highly stoichiometric material was perfected. Consequently, several lots of not very stoichiometric material were also examined. The results did not vary much from lot to lot (lot 53 was typical), but were quite different from those consistently obtained with the more highly stoichiometric material discussed above.

A typical plot of R versus H for this earlier material is shown in Figure 5. When a sample was cooled in zero field and the field then increased, R increased extremely rapidly (solid curve). Noise prevented studying R closer to the origin than about 20 oersteds, but at this field this initial increase of R with H was still rapid. The form of

the curve was $R \sim H^{1/2}$. The anisotropy was typically about two. The absorption for $H = 2 \times 10^4$ oersteds perpendicular to the microwave current but in the plane of the sample was somewhat more than half the value for the more stoichiometric material. When the magnetic field was reduced to zero with the sample still cold, the dashed curve was followed and was repeatable for all succeeding runs. On this curve there was little or no hysteresis of the type shown in Figure 4. Only when the material was warmed to the normal state and then recooled in zero field was the solid curve retraced.

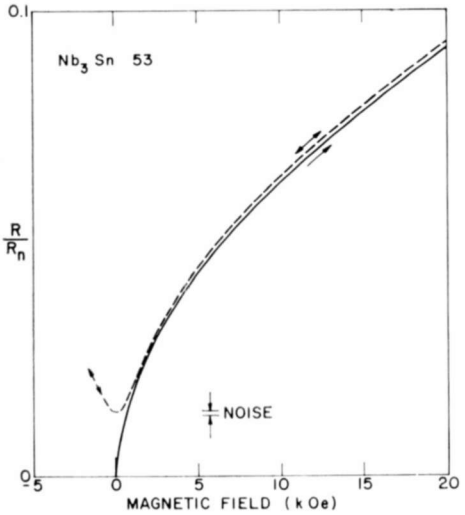

Fig. 5—Microwave surface resistance at 23 gc versus magnetic field at 4.2°K for a nonstoichiometric Nb_3Sn sample (Lot 53).

This behavior can be qualitatively explained if we assume that the nonstoichiometric material is microscopically magnetically inhomogeneous. The inhomogeneity is taken to be great enough that (1) a large fraction of the flux tubes within a microwave penetration depth is parallel neither to the applied field nor to the sample surface when the applied field is parallel to the surface; (2) in some regions the magnetic field can penetrate in fields as low as about 20 oersteds.

With such inhomogeneity, enough flux trapping would be expected to explain the rapid increase of R for the virgin curve. Since the flux tubes are both parallel and perpendicular to the microwave current, only a small anisotropy would be expected. Since the hysteresis of Figure 4 is only observed for the magnetic field parallel to the surface, this effect would now be too small to be seen, the flux tubes having large components perpendicular to the surface.

SURGE-MAGNETIC-FIELD AND PULSE-CURRENT EFFECTS IN NIOBIUM STANNIDE

By

William H. Cherry

RCA Laboratories
Princeton, N. J.

Summary—*Equipment is described capable of generating surge magnetic fields up to 250 kilogauss longitudinally and 165 kilogauss transversely with a useful crest duration of 1 millisecond, and capable of generating test current pulses up to 500 amperes with up to 5 milliseconds duration. Critical field and current characteristics of superconducting niobium stannide (Nb_3Sn) were obtained with this equipment and suitable measuring techniques. As compared with d-c methods, the surge methods are very laborious and less exact, but achieve great economies in apparatus. Of greater importance, they disclose the extensive range of electrodynamic transient phenomena that appear in Nb_3Sn superconductors. These phenomena were surveyed and are reported here in terms of (1) inductive effects of current, (2) effects of Joulean heat generated by current, (3) transient magnetic field effects, and (4) interactions between current and field. Examples are given of the oscilloscope traces through which these effects became evident.*

Introduction

ENGINEERING STUDIES concerning the application of hard superconductors such as niobium stannide in various practical devices, and research studies concerning a fundamental understanding of superconductivity, both require testing of superconductive material under conditions of applied magnetic field and conduction current. Such tests are not merely to ascertain at what values the superconductivity of a given material quenches and normal resistivity appears, but also to study the very complex behavior of the superconductor both before and during this transition.

The currents involved in such tests are sufficiently large to create serious technical problems. In addition, the magnetic field intensities required are extraordinarily high, and apparatus to achieve these fields of from 100 to 250 kilogauss on a direct-current basis is extremely expensive and massive. Surge-discharge equipment to achieve the same peak fields can be built on a far smaller and less expensive scale. It must not be supposed, however, that the surge equipment is merely a substitute for a d-c solenoid. Rather, the two complement each other. The determination of simple, steady-state critical field and current curves can be carried out much more easily and precisely with the d-c equipment. On the other hand, the surge equipment brings into evidence

many transient processes unrecognizable under steady-state conditions, and permits discrimination between different kinds and different causes of transition. Results from the use of surge equipment on superconductors have also been reported by others.[1,2]

Testing Apparatus and Technique

The surge apparatus used in the present work consists of four main parts* interrelated as shown in Figure 1, and illustrated separately in Figures 2-5. The magnetic field surge, effected by the discharge of a capacitor bank through an ignitron into the copper solenoid magnet within the cryostat, is initiated by pressing a button after the camera

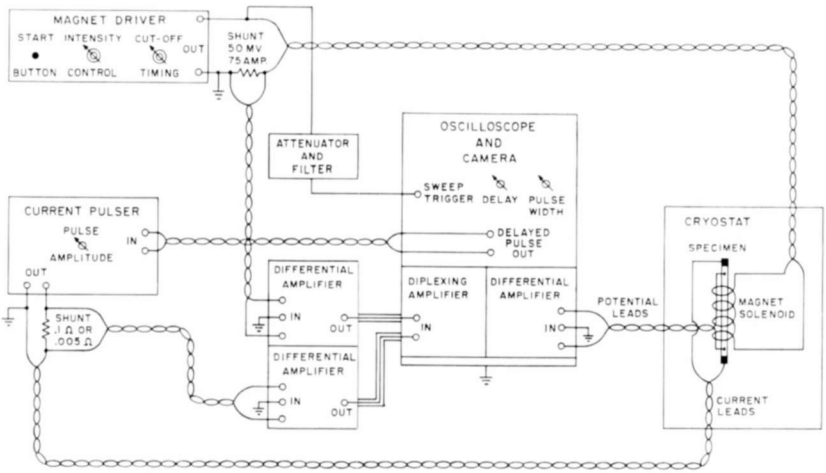

Fig. 1—Surge-magnetic-field and pulse-current equipment.

shutter on the oscilloscope has been opened. The beginning of the surge serves to trigger the prompt sweep of the oscilloscope, while associated with the delayed sweep a rectangular pulse is produced of up to 5 milli-

[1] H. R. Hart, Jr., I. S. Jacobs, C. L. Kolbe, and P. E. Lawrence, *High Magnetic Felds*, (H. Kohn, B. Lax, F. Bitter, and R. Mills, editors), John Wiley and Sons, New York, N. Y., 1961, p. 609.

[2] T. G. Berlincourt, R. R. Hake, and A. C. Thorsen, "Pulsed Magnetic Field Studies of the Negative Magnetoresistivities of Dilute Ti-Mn and Cu-Mn Alloys at Low Temperatures," *Phys. Rev.* Vol. 127, p. 710, 1 Aug. 1962; also T. G. Berlincourt and R. R. Hake, "Superconductivity at High Magnetic Fields," *Phys. Rev.*, Vol. 131, p. 140, 1 July 1963.

* These elements of equipment are suitable only for research purposes since many of the components are stressed far beyond proper commercial ratings.

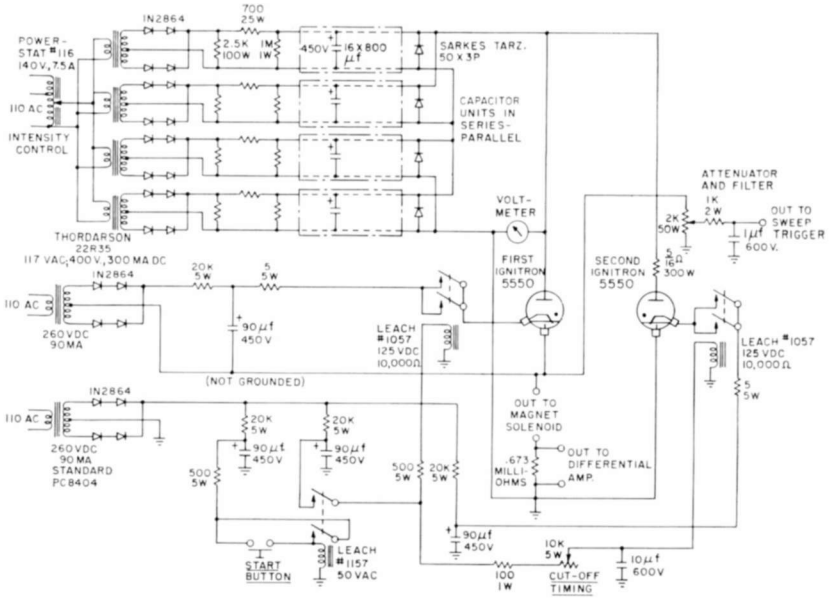

Fig. 2—Magnet driver.

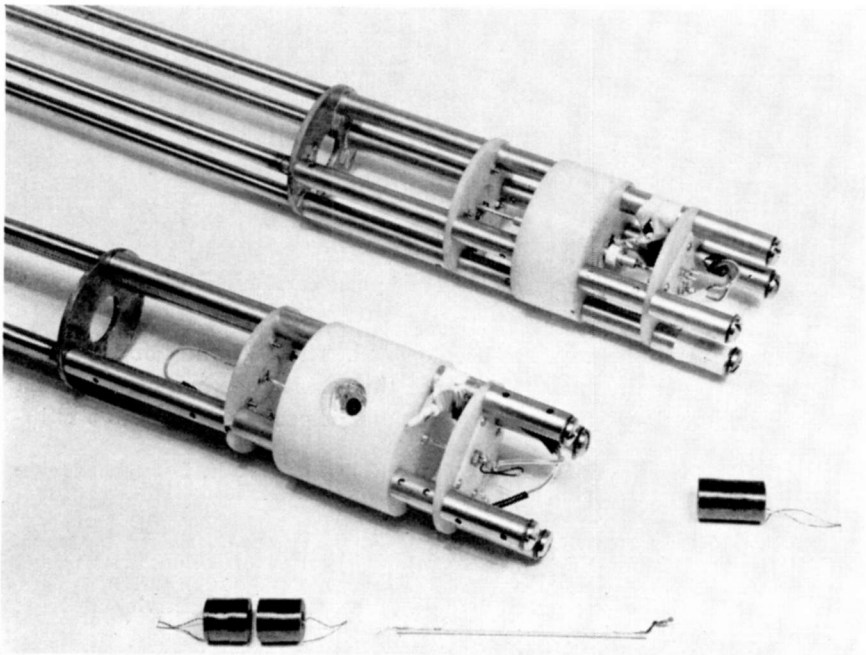

Fig. 3—Magnet solenoid and specimen assembly, showing transverse and longitudinal arrangements, with extra solenoids and specimen mount.

seconds duration. This is amplified in either the hard-tube circuit of Figure 4, which is reliable up to 60 amperes output, or in the thyratron circuit of Figure 5, which provides currents of from 50 to 500 amperes. The rectangular current pulse is imposed as conduction current on the superconductive specimen, with the delay and pulse duration

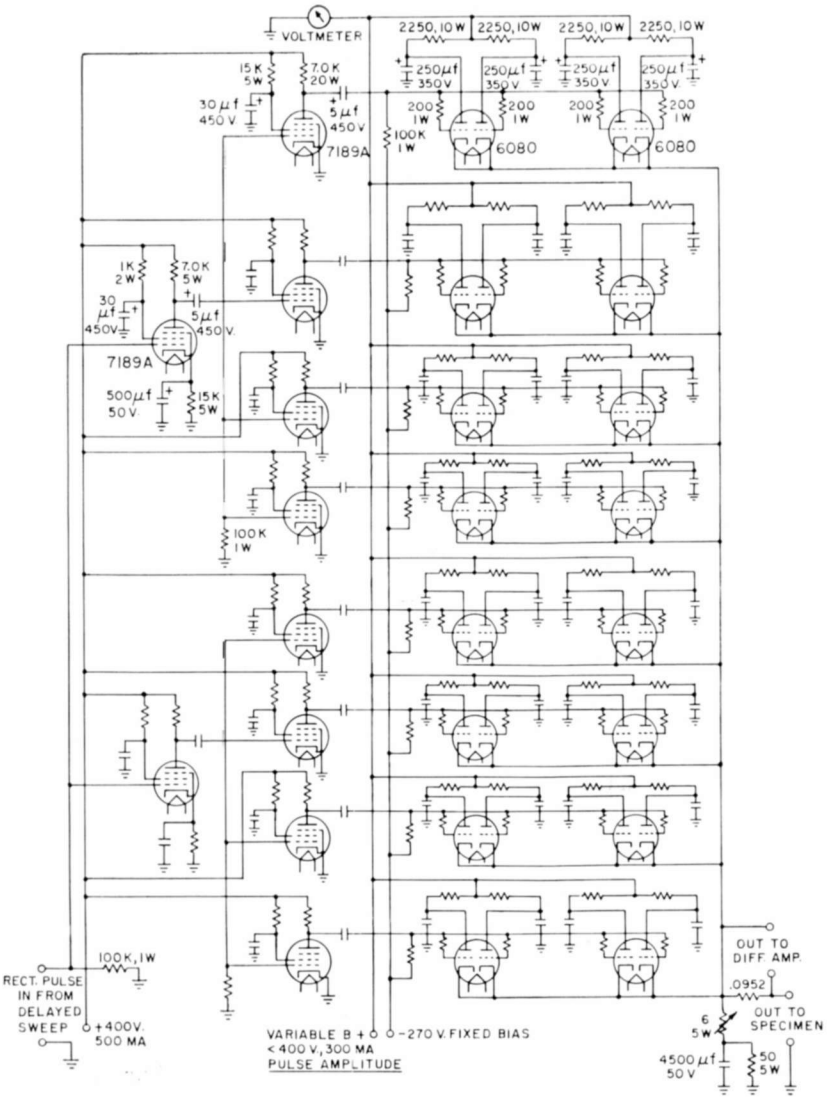

Fig. 4—Vacuum-tube current pulse amplifier (conventional a-c filament supplies and d-c power supplies not shown).

adjusted to coincide with that part of the magnetic field surge, very often the crest, appropriate to the measurement being made. The oscilloscope, which uses two beams and a diplexing amplifier deflecting one of them, has effectively three independent traces. These record on one photograph the magnet current surge (which is proportional to the field intensity), the current pulse through the specimen, and the voltage generated across the specimen and appearing on two potential leads.

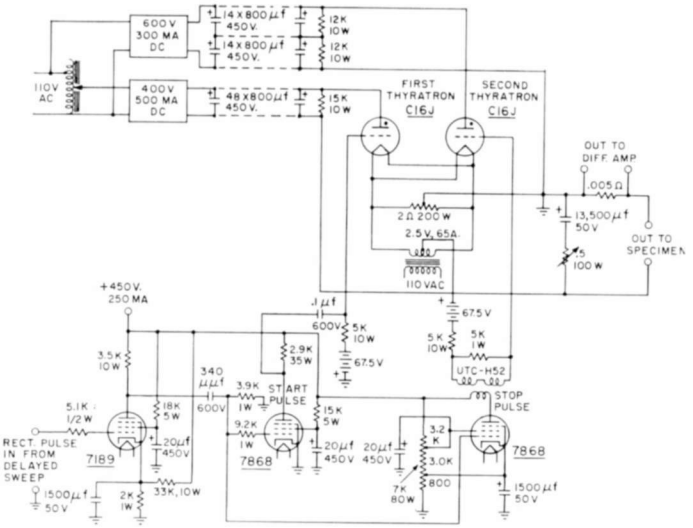

Fig. 5—Thyratron pulse generator (conventional a-c filament supplies and d-c power supplies not shown).

The Surge Magnet System

The magnet driver, diagrammed in Figure 2, is controlled by a series of relays. The manual starter button was found to be noisy and given to making successive multiple contacts, and could not be used in the circuit directly. Therefore it is followed by a self-holding relay with delayed release. This relay closes two others—one immediately, which energizes the ignitor of the first ignitron, and one after an adjustable delay, which fires the second ignitron. The electrolytic capacitor bank consists of four 450-volt units, each of 12,800 μf, insulated from the others and possessing its own power supply. All four supplies are energized from a common, variable autotransformer. Thus, a variety of series and parallel hookups can be used to adjust the magnet surge duration and magnitude. Each of these power supplies is rated in excess

of 300 milliamperes at 450 volts. A considerable resistance is placed in series to avoid parts damage and to avoid blowing fuses when recharging the capacitors under full voltage after they have been discharged. There is also a rather small shunt load resistance of high wattage to give a short time constant for ease of adjusting the capacitor voltage and hence the surge magnitude. Moreover, it permits the safe, early discharge of the capacitors after the power is turned off. Each electrolytic capacitor unit is shunted by a 500-volt, 200-ampere silicon diode in opposing polarity. This prevents reverse voltage charging, either from inductive swing by the solenoid magnet or through discharging unequal capacitances in series. In the discharge process, the solenoid magnet is heated so rapidly that, except for the lowest field values, the coil resistance becomes sufficient to overdamp the discharge circuit by the time the surge has passed its crest. The subsequent discharge of the capacitors would thus be both long and powerful, so that the latter half of the capacitor energy would heat up the solenoid further and waste the liquid helium coolant. By firing the second ignitron just after the crest, this energy is shorted out of the coil and is dissipated with much less harm by being dumped into the circuit resistor of 5/16 ohm.

The magnet itself is an arrangement of air-core, copper-wire solenoids. In the photograph of Figure 3, the transverse-field apparatus is in the foreground and the longitudinal-field apparatus is in the back. Typical solenoids, unencapsulated, are also shown. Iron and other ferromagnetic materials are of no use at the level of field intensity generated here. Moreover, since the field changes rapidly with time, highly conductive metals must also be avoided to prevent field distortion and loss by eddy currents.

The solenoid magnet is immersed in the liquid helium bath with the specimen. Separate arrangements of coil and specimen are of course possible, e.g., the coil can be cooled in a separate helium bath, the surrounding nitrogen bath, or even in the air outside the cryostat. The choice made here is the most economical, because the volume of space occupied by the field is a minimum and because the helium cooling permits the highest possible current density in the copper for a specified field duration. Thus, for a given field magnitude, the energy requirements and, hence, the size of the circuit components are least. This arrangement makes alignment of field and specimen comparatively easy in both the longitudinal and the transverse field assemblies shown in Figure 3. Eddy-current problems are minimal, as compared with structures where Dewar flasks and other elements must intervene between coil and specimen. On the other hand, in this arrangement, the

specimen needs protection from heat radiation from the coil. This is provided by a tube wound of several layers of paper sprayed with a nonconducting aluminum paint. The paper, in turn, must be protected from implosion by the shock wave from the coil, which occurs at the moment of the surge. This is done with a loose-fitting glass tube inserted in the coil and taped on both ends to prevent its being subsequently forced out while in the cryostat. Unfortunately, coil failure occurs rather frequently, usually by fatigue of the copper. This necessitates dismounting of both coil and specimen. It can be seen that there are advantages to placing the magnet outside of the specimen coolant chamber, even though it is electrically a less economical arrangement.

The solenoids used here are similar in form to those of Olsen[3] with an inside diameter of 8 mm and an outside diameter of 18 mm. They were wound of #26 Formex insulated copper wire* covered with a thermosetting layer which, after baking, made the coils conveniently self supporting for further encapsulation in epoxy. Each of these were subsequently enclosed in a large, press-fitted nylon sleeve, which is necessary to prevent explosion of the coil at highest field strengths. Examples of these solenoids include (1) a longitudinal-field coil, 30 mm long with 752 turns, capable of reaching 250 kilogauss, and (2) a transverse-field, split coil of 92 turns and 42 mm length with a 4 mm gap between the two halves, capable of reaching 165 kilogauss. These coils, unencapsulated, are shown in the foreground of Figure 3. At peak field levels it was found that twenty minutes cooling time was required between single surges, and after one or two dozen firings a coil would fail because of fatigue.

Specimen Holder and Mount

In the specimen holders (shown in Figure 3) the mount for the superconductive material is held compressively between two conical center holes in two nylon discs. These discs and the nylon sleeve containing the solenoid are supported and aligned by four thin stainless steel tubes. Stainless sleeves of appropriate lengths and slightly larger diameter are slipped over the tubes to space the nylon pieces and help in their alignment. The tubes also serve as conduits for the (#10 to #18) tapered copper leads to solenoid and specimen. The specimens were either thin niobium-stannide cylinders deposited on a ceramic rod substrate, or niobium-stannide-coated ribbon or wire. For the latter it was necessary to further support the ribbon or wire on a ceramic or

[3] J. L. Olsen, "Liquid Helium Cooled Coils for Making Intense Transient Magnetic Fields," *Helvetica Physica Acta*, Vol. 26, p. 798, 1953.

* 0.0405-cm-diameter copper.

sapphire mounting rod to which the specimen was tied every 1/8 inch lengthwise with 0.006-inch-diameter monofilament nylon. The 0.080-inch-diameter mounting rod had a flat ground lengthwise, on which the specimen was laid to minimize the crushing effect of the ties. The purpose of this mounting was to hold the specimen rigid at high magnetic fields to avoid spurious signals, and at the same time expose the niobium stannide directly to the liquid helium. Covering with cement as an alternative to the nylon filament ties led to erroneous values of critical field and current. Indium was used as a solder after nickel plating of the niobium stannide.

Specimen Current System

Figures 4 and 5 show a hard-tube pulse amplifier and a thyratron pulse generator, respectively, either of which is used to supply a rectangular current pulse as conduction current for the superconductive specimen. Both of these circuits depend on the sudden expenditure of some of the energy stored in a capacitor bank, and the magnitude of the pulse output is controlled by controlling the voltage to which the output capacitor bank is charged. As in the case of the magnet driver, it is desirable for the power supplies to have a low impedance with a low-resistance shunt. Thus, the capacitor voltages can be raised and lowered quickly during adjustments. In shunt with the output circuit of either pulser is an R-C circuit that can be adjusted to largely compensate for the discharge of the capacitor bank during the pulse output. This discharge would otherwise lead to a falling off or ramping of the pulse amplitude. In the hard-tube pulser the type 6080 vacuum tubes deliver in excess of 2 amperes per cathode for 5 milliseconds. Such a current is considerably higher than rating and moreover the pulse length is much greater than in the usual pulse operation. This tube type compared very favorably with others which were tried. However, it is necessary to check the operation frequently for poisoned cathodes, which sometimes occur when a tube flashes over momentarily. The equipment is warmed up prior to a test run, using a dummy load, in order to avoid damage to the niobium-stannide specimen from a tube flashover. A negative grid bias of 270 volts was found optimum, and plate voltages must be held less than 400.

The thyratron pulse generator depends on the application of strong starting pulses on the thyratron grids at the right times. These must be free of other signals that might cause prefiring or multiple firing. The circuit accomplishing this is shown in Figure 5. The second thyratron causes the first to turn off under full plate voltage, and then turns off itself with the discharge of its plate supply capacitor. The

circuit was found operative for currents in excess of 500 amperes. However, for currents much in excess of 300 amperes an uneven voltage drop was sometimes noted across the first thyratron, possibly the result of a different form of discharge plasma for the higher current.

Experimental Observations and Discussion

Each datum initially appears in a photograph of three single, concurrent sweeps of the three signal channel inputs to the oscilloscope. Examples of these photographs, for which relevant calibration data are given in Table I, are shown* in Figures 7-12. The upper two traces in each photograph show (with positive values directed downward) the rectangular pulse of current through the specimen and the overdamped sinusoidal amplitude or surge of the applied magnetic field, if these are present. In most cases, the relevant zero-signal horizontal base lines have been introduced to help in the measurement. With appropriate calibration, the instantaneous values of current and field throughout the sweep can thus be determined. The lowest trace shows the potential drop in that major part of the specimen that lies between the potential lead contacts. The occurrence of resistivity leads to a voltage in this lowest trace during the time when the specimen current is flowing. In addition, many other voltage patterns appear between the potential leads as the result of electrodynamic processes in the superconductor, sometimes associated with the magnetic field. Nevertheless, the systematic correlation of a continuous voltage of proper polarity with the interval of nearly constant current conduction is taken to signify the partial quenching of superconductivity. With the current pulse timed to appear during the magnetic field crest of about 1 millisecond duration, the mean current density just sufficient to show discernible quenching is considered the critical value. A plot of these values is given in Figure 6. The fields were either longitudinal, or transverse and perpendicular to the face of the ribbon. The specimen was vapor-deposited niobium stannide[4] on a flat ribbon substrate of nonsuperconducting metal 0.066 cm wide and 4.3×10^{-3} cm thick. The niobium stannide was 6×10^{-3} cm thick and the cross section was 0.9×10^{-4} cm^2. In this case it was plated with 6×10^{-3} cm of copper.

For some niobium stannide specimens it was found that the largest

* Some of these photographs have been retouched in order to compensate for deficiencies in their subsequent reproduction. Some have had to be overexposed in certain areas in order to bring out detail in other areas.

[4] J. J. Hanak, *Metallurgy of Advanced Electronic Materials*, G. E. Brock, editor, Interscience Publishers, Inc., New York, 1963, p. 161.

current that could be carried without quenching in a given magnetic field depended on the current and field settings of the immediately preceding measurements and on whether quenching then occurred. This "memory" or hysteresis effect appeared as follows. Successive attempts to produce quenching were made at the same peak field but beginning at low currents where the material easily remained superconducting. As the current pulse amplitude was raised in small steps, a quench value was eventually reached. On the next trial, the current pulse was re-

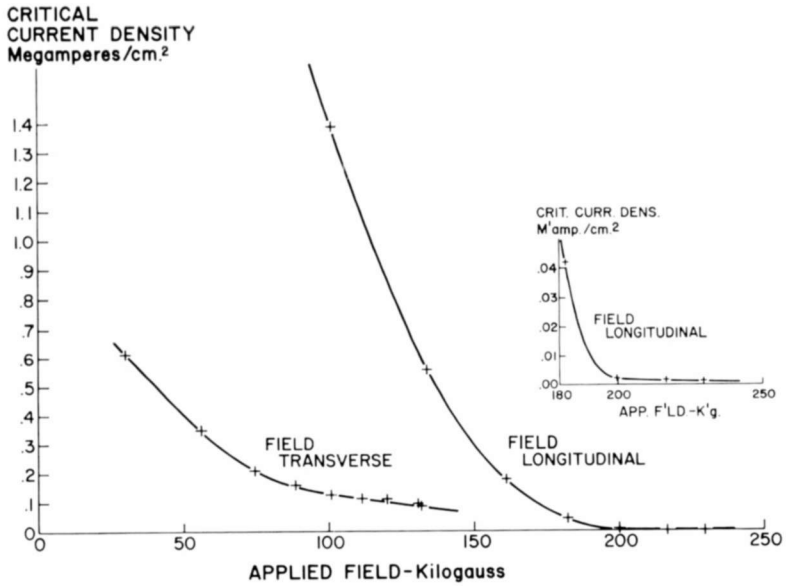

Fig. 6—Mean-critical-current density versus transverse and longitudinal fields for niobium stannide (critical current density at zero field 3.5 megamp/cm^2).

duced, but quenching was again observed. Then at successively smaller values of current, quenching was still observed. A considerable amplitude reduction was required before superconduction could again be sustained during the current pulse. Now with a sufficiently low current so no quenching appeared, it was possible to raise the current amplitude gradually, as before, until the high critical value was again reached. This cycle could be repeated. The effect was most noticeable around 90 kilogauss, amounting to about 25% in the critical current, and disappeared for fields above 150 kilogauss. It has not yet been investigated for low-field values; it does not seem to occur in transverse fields in the hundred-kilogauss range.

The low-frequency impedance of a short length of superconducting

wire or ribbon forming part of a simple closed circuit is primarily inductive. Consequently, the application of a rectangular pulse of current generates across the potential contacts of the specimen a positive-going inductive voltage kick when the current is turned on, and a negative-going kick when the current is turned off. If the top of the pulse is not flat, there is also a corresponding rate-of-change-of-

Table I—Calibration Data for Figures 7 through 12

Figure	Potential-Leads Sensitivity‡ (millivolts per cm*)	Sweep Speed # (milliseconds per cm*)	Peak† Field (kilogauss)	Peak Current (amperes)
7A	.5	1.5	0.	5.7
7B	.5	1.5	0.	40.
7C	1.0	1.5	0.	42.
7D	2.5	1.5	0.	33.
7E	—.5	1.0	0.	6.1
8A	—100.	1.5	0.	56.
8B	—1.3	1.5	0.	69.
8C	3.3	1.0	159.	21.
8D	33.	1.0	136.	59.
9A	—1.0	1.4	88.	17.
9B**	2.	2.	40.	0.
9C	—2.0	2.0	17.(t)	0.
9D	1.0	5.0#	68.(t)	0.
9E	10.	2.0#	107.	0.
9F	10.	2.0#	107.	0.
10A	—10.	1.4	116.	17.
10B	—5.0	1.4	149.	0.
10C	10.	2.0	138.	34.
10D	10.	1.0	168.	3.6
11A	—3.3	1.4	0.	29.
11B	—3.3	1.4	88.	28.
11C	—20.	2.0	68.(t)	1.0
11D	—20.	2.0	69.(t)	1.3
11E	—5.0	2.0	15.(t)	2.1
12A	5.0	1.0	109.(t)	6.2
12B	10.	2.0	65.(t)	7.0
12C	1.0	1.0	65.(t)	6.1
12D	5.0	1.0	66.(t)	15.

* Per cm refers to the division size on the original graticule.

\# The sweep speeds for all three traces in any one figure are the same, excepting that the trace for potential-lead voltage has the speeds .5, .02 and .05 milliseconds per cm in Figures 9D, 9E, and 9F, respectively.

† Fields are longitudinal except where they are marked (t), denoting transverse, normal to principal surface.

** Calibration data for Figure 9B are only roughly estimated.

‡ Negative values indicate that the polarity is positive downward.

current signal during the pulse. However, if the pulse is flat and the material is fully superconducting, there is no perceptible voltage even at such high amplification that the inductive kicks are far off scale. Both situations for a 0.051-cm-diameter lead (Pb) wire with 4.73 cm between potential leads are illustrated by the two sets of traces in Figure 7A.

A transition from the superconducting to the normal state can be induced if the current is sufficient that its magnetic field at the surface of the superconductor exceeds the critical field. For currents just strong enough to begin this process, the wire will go into an intermediate state while still preserving some superconducting path. Under transient conditions it is thought that such an intermediate state might fluctuate or oscillate, with attendant fluctuations in the distribution of

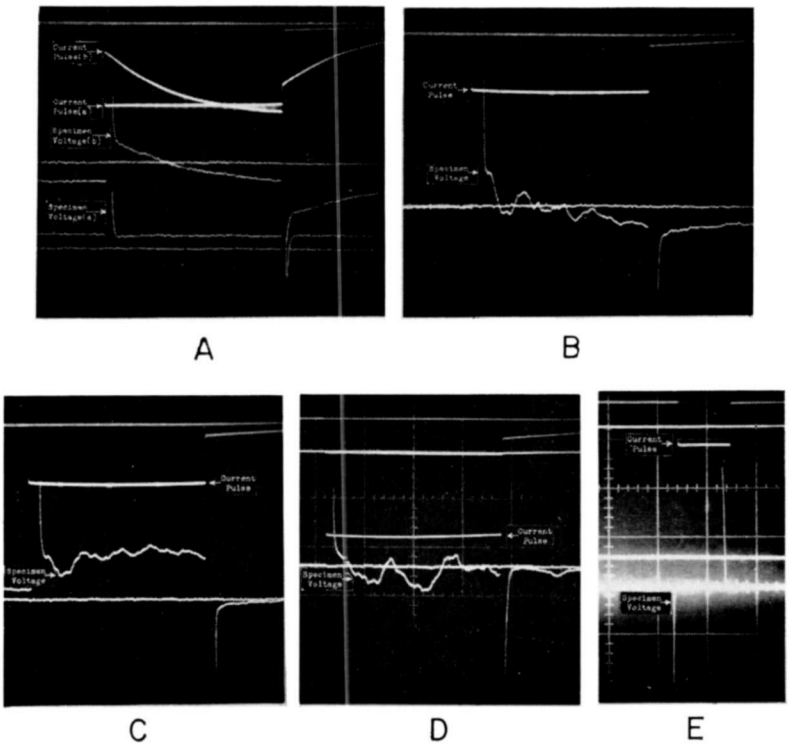

Fig. 7—Inductive effects of current: (A) inductive response to rectangular current pulse (a) and nonrectangular pulse (b), superconducting Pb wire; (B) fluctuating, nonresistive intermediate state, Pb wire; (C) fluctuating, resistive intermediate state, Pb wire; (D) fluctuating, nonresistive "intermediate state," Nb_3Sn wire; (E) inductive response to rectangular current pulse, superconducting Nb_3Sn wire.

magnetic field produced by the current and consequently with voltages induced in the potential leads. Figure 7B shows such a voltage from a fluctuating intermediate state in the lead wire. Figure 7C shows the appearance of some resistance, but a fluctuating intermediate state still seems to have been present. In Figure 7D the specimen was a vapor-deposited niobium-stannide wire of 0.020 cm diameter with a 0.018-cm-diameter platinum core, and apparently a fluctuating intermediate state could likewise occur in this material. In Figure 7E, in a similar specimen at lower current, only the inductive kicks were present.

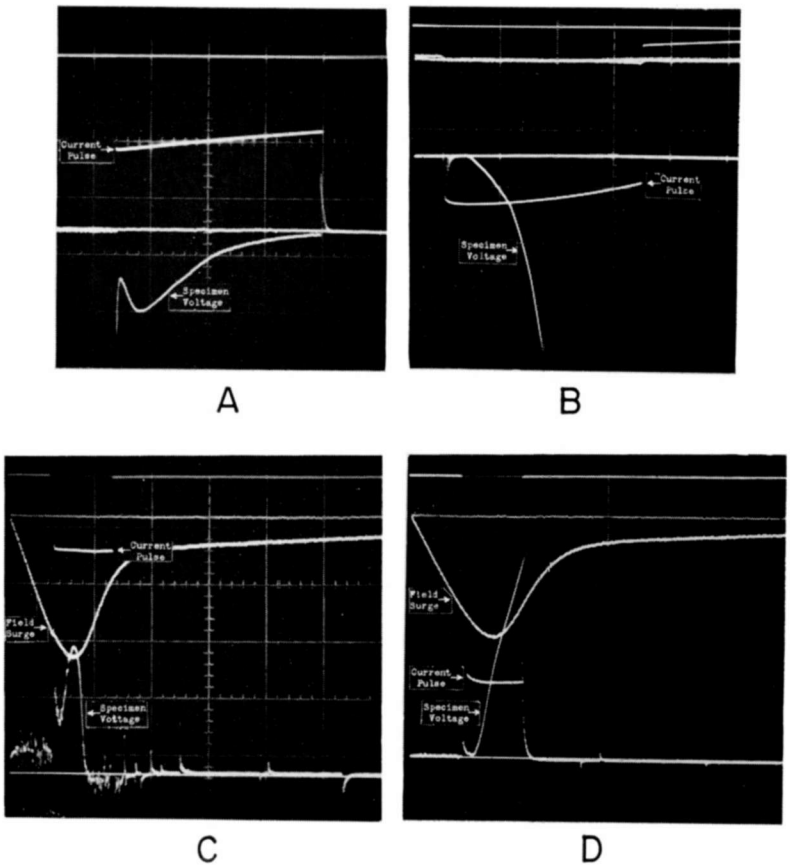

Fig. 8—Effects of current-generated Joulean heat: (A) reversal of Joulean-heat-propagated transition, Pb wire; (B) Joulean-heat-propagated transition plus overheating, Nb_3Sn wire; (C) current and field transition and reversal, Nb_3Sn ribbon; (D) current and field transition sustained by Joulean heat, Nb_3Sn ribbon.

Effects of Current-Generated Joulean Heat

Once resistance is induced in a short segment of a current-carrying, superconducting wire by inhomogeneous temperature or field conditions or an inhomogeneity in the wire itself, Joulean heat is generated in this segment by the current flow. This heat flows into neighboring segments and, if sufficient, will there induce a transition into the normal state.

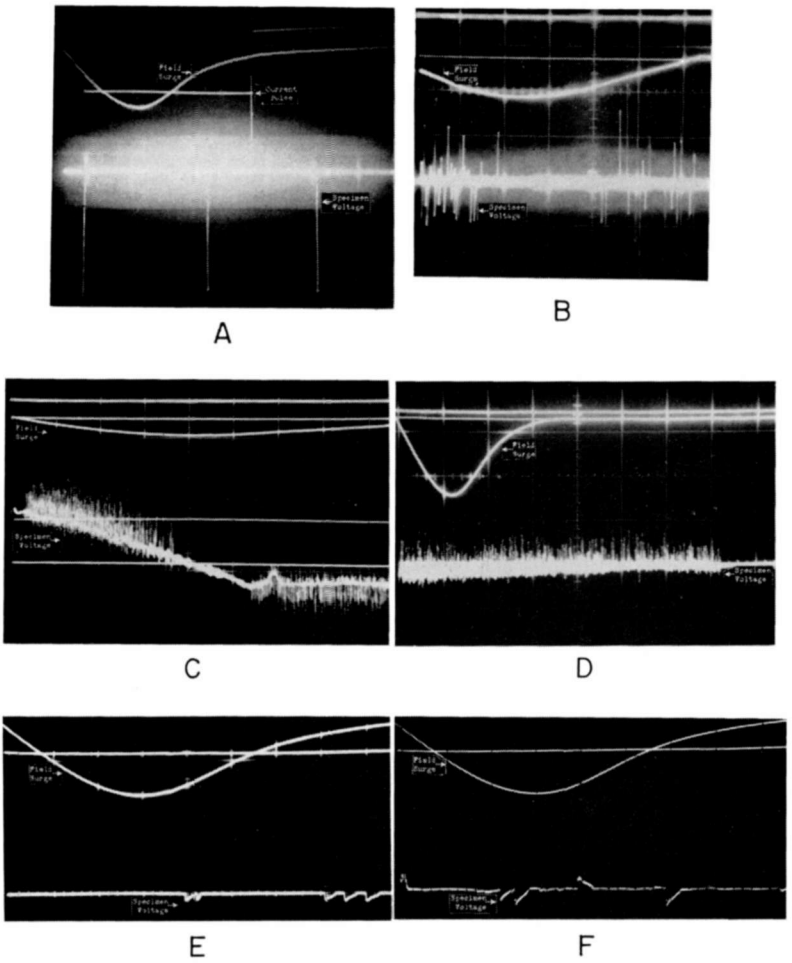

Fig. 9—Transient magnetic field effects: (A) flux redistribution voltage spikes, longitudinal field; (B) ambipolarity of flux spikes, longitudinal field; (C) flux spikes, transverse field; (D) termination of flux spikes at zero field, transverse field; (E) flux spike pattern repetition, longitudinal field; (F) spike pattern repetition and ambipolarity, longitudinal field.

Thus a transition can be propagated along a wire under the impetus of Joulean heat.[5] If this transition is then subjected to a decline in the imposed current and hence in the Joulean heat, the transition may reverse its direction. This starting propagation and later reversal is shown in Figure 8A for a lead (Pb) wire. In Figure 8B the sample was vapor-deposited niobium stannide 2.5×10^{-3} cm thick on a platinum

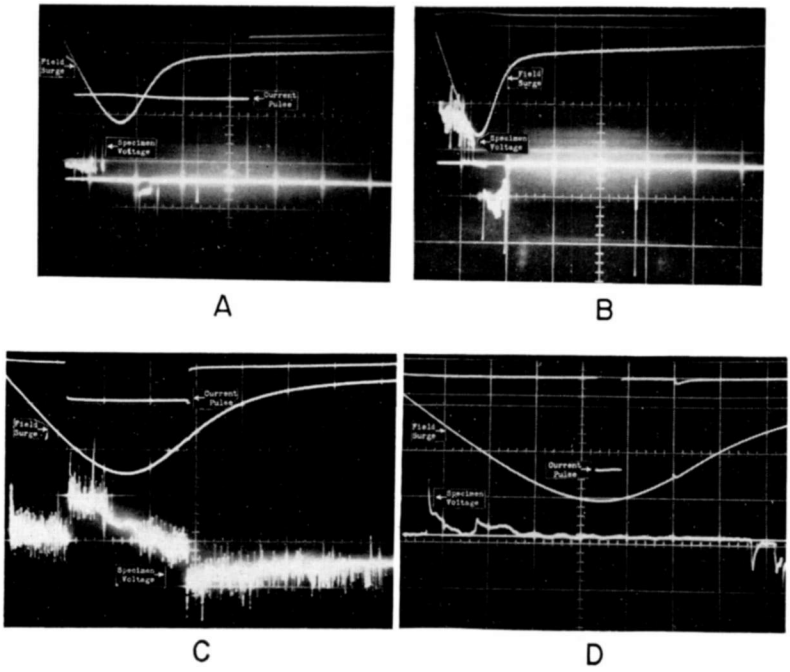

Fig. 10—Further transient magnetic field effects: (A) semicontinuous flux redistribution voltages with current, longitudinal field; (B) semicontinuous flux redistribution voltages without current, longitudinal field; (C) flux spikes, longitudinal field, Nb_3Sn cylinder; (D) pattern in longitudinal field, near-stoichiometric Nb_3Sn cylinder.

ribbon 0.076 cm wide. It had a potential-lead separation of 6.6 cm Here the Joulean heat propagation with its characteristic straight-line segmented signal began an appreciable interval of time after the current pulse began. (The initial inductive kick was complicated by oscillations—the result of transformer coupling). This straight line seg-

[5] W. H. Cherry and J. I. Gittleman, "Thermal and Electrodynamic Aspects of the Superconductive Transition Process," *Solid-State Electronics*, Vol. 1, p. 287, Pergamon Press, Great Britain, 1960.

ment was followed by a steeper line segment and then the curve of voltage drop moved to larger voltages and eventually off scale. The initial time interval is probably the result of the transition being started in the region of the current contact by contact heating. Not only does this heating take time, but the transition, once started, must propagate into the region between the potential leads. The second

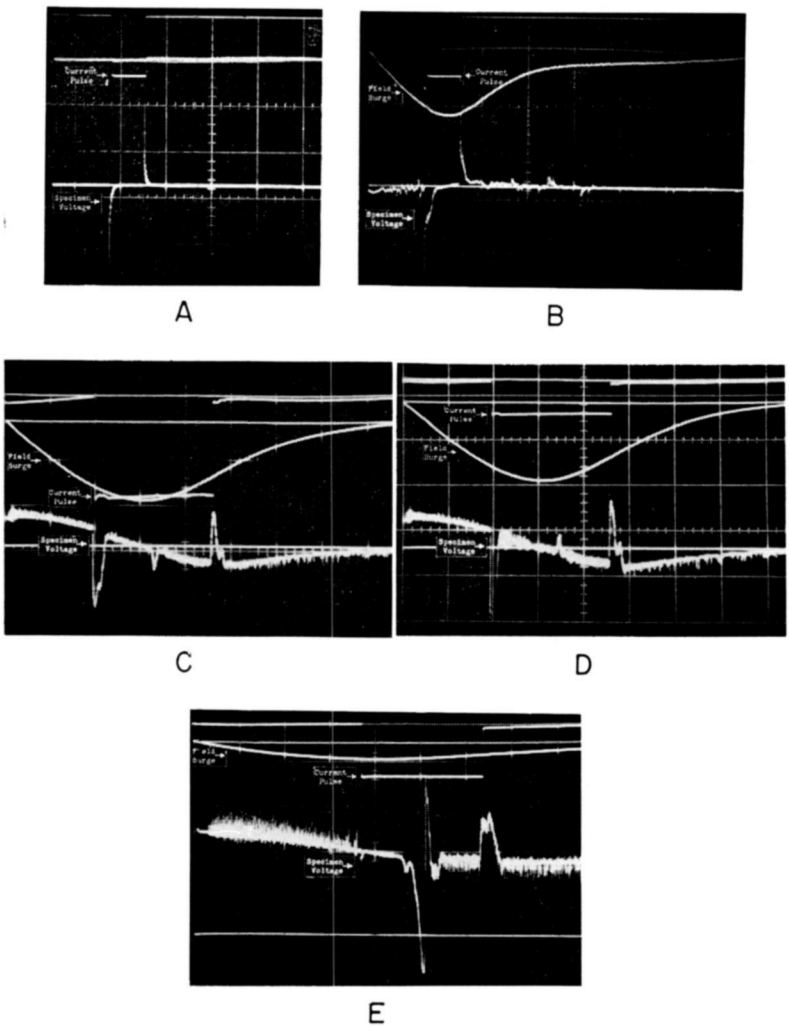

Fig. 11—Interactions between current and magnetic field: (A) inductive kicks without field; (B) inductive kicks showing shoulder broadening, longitudinal field; (C) flux gating by current, central peak positive, transverse field; (D) flux gating by current, central peak negative, transverse field; (E) flux gating by current, central peak bipolar, transverse field.

break upwards is the result of a transition coming in from the opposite contact. This doubles the line slope, as is to be expected. However, the final great increase of voltage, even under current diminution, must be the result of overall severe heating of the niobium stannide and platinum, which radically increases the resistance over the residual values appearing during propagation of the transition. It is to be noted that

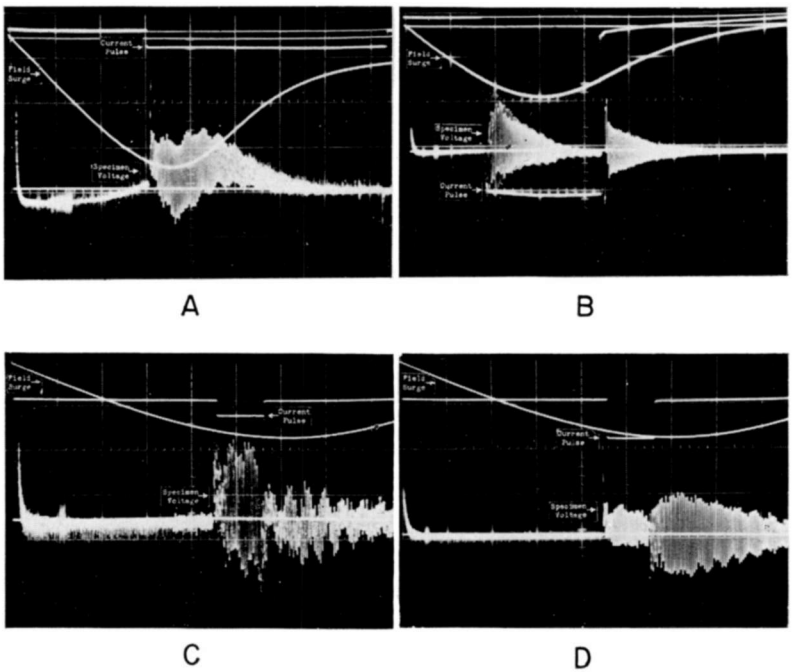

Fig. 12—Oscillatory interactions between current and magnetic field: (A) oscillations with current on, diminishing with transverse field; (B) oscillations with current on and with current off, transverse field; (C) oscillations stronger with current on, transverse field; (D) oscillations stronger with current off, transverse field.

contact heating is a serious source of error in d-c measurements, because it may nucleate a transition that would otherwise not occur; and yet this cannot be so identified because the characteristic time delay is not discernible with the d-c technique.

In Figure 8C, the combination of high magnetic field and conduction current produced resistance and consequent voltage-drop in a similar niobium-stannide ribbon. However, the current level was so low that there was insufficient Joulean heat to sustain the transition. The material reverted to superconduction as the magnetic field declined, even

though the current remained undiminished. At a lower field and higher current the same ribbon was also partially quenched as shown in Figure 8D. Here, however, the current produced sufficient Joulean heat to sustain the transition. The heated specimen then became even more resistive although the magnetic field declined heavily.

Transient Magnetic-Field Effects

If a magnetic field of substantial magnitude is applied to or withdrawn from a specimen of niobium stannide, sudden spikes of voltage are produced across the potential leads, comparable in size but unrelated to the inductive kicks of the current pulse previously described. This can be seen in Figure 9A for a niobium stannide ribbon in a longitudinal field. These voltage spikes may well be flux redistribution spikes, for, as shown in Figure 9B for a ribbon in a longitudinal field, they must be the result of the magnetic field moving into and out of the specimen. Thus, they occur during the rise and fall of the field, and not during the semistatic crest. Figure 9C shows that for a ribbon in a transverse field these flux redistribution spikes began only after the applied field had risen to 2.5 kilogauss; Figure 9D, also for a ribbon in transverse field, shows that their occurrence terminated sharply. Other data, since the sweeps were not synchronous in this figure, showed the termination was obtained when the declining field reached zero. Figure 9C also shows characteristically that there were two orders of magnitude more spikes occurring in the transverse field than in the longitudinal. In addition, their amplitudes were five to ten times smaller, and there was a markedly preferred polarity, which reversed with field change. There can be seen in the spectral distribution of spike amplitudes in Figure 9C a clear preference for certain levels. Within the distribution there were, in several instances, identically reproducible forms. This is shown for a ribbon in a longitudinal field in Figure 9E at a sweep speed of 20 μsec/cm, and in Figure 9F for the same specimen and field at 50 μsec/cm. The ribbon specimen used in Figure 9D was plated with approximately 0.005 mm of copper and had a Hastelloy substrate, while the one in Figure 9C was unplated and had a platinum substrate. Since the amplification in Figure 9D was twice that in Figure 9C, it appears that the flux redistribution spikes were about half size in the case of the copper-plated material. The area of a single spike ranges from 2×10^{-9} to 1×10^{-7} volt-second or, in terms of flux increments, from 2×10^{-1} to 10 gauss cm^2.

The occurrence of the flux redistribution spikes is not noticeably affected by the presence of conduction current. Illustration of this, for a niobium stannide ribbon in a longitudinal field, is obtained by com-

parison of Figures 10A and 10B. The spike pattern in the presence of current in Figure 10A did not differ significantly from that without current and at somewhat higher field in Figure 10B. Moreover, the ambivalent polarity of the spike voltages in the presence of current (Figure 10A) shows that no resistance appeared in the current path as a result of their action.

The photographs of Figures 10A and 10B illustrate another effect—the appearance of more or less continuous voltages during parts of the rise and fall periods of the field. These continuous voltage patterns may be the result of avalanches of flux redistribution spikes, or at least may follow from flux redistribution processes. This is supported by their independence of the presence of current, their alternate polarities, and their noncontribution to overall resistance.

In Figure 10C the pattern of flux redistribution spikes is shown for a specimen of niobium stannide, 50 microns thick and 3.2×10^{-3} cm^2 cross section, vapor deposited on a cylindrical ceramic substrate of 0.203 cm diameter.[6] This hollow superconducting cylinder had the same longitudinal dimensions as the ribbon specimens and was situated in a longitudinal field, yet the number of flux redistribution spikes was more nearly comparable to the transverse field tests on the ribbon. On the other hand, the amplitude spectrum of the spikes was about the same as in the case of the ribbon in a longitudinal field. There were two orders of magnitude advantage in size of internal cross-sectional area of the hollow cylinder over the ribbon (also hollow because of its substrate), and there was a factor of twenty advantage in the bulk of niobium stannide exposed to the magnetic field. Therefore, this equality of spike amplitude suggests that the mechanism that produces the spike and determines its size and time dependence is characteristic of the intrinsic properties of the material, and is not related to the geometrical shape or size of the specimen. The number of spikes, however, is probably proportional to either the internal volume of the specimen or its bulk of niobium stannide. It should be pointed out that if the potential differences observed in this form of spikes are directly produced by flux motions, whatever the cause of these motions,[7,8] the longitudinal symmetry of the tests in longitudinal field must be upset by skew

---

[6] G. W. Cullen, "Preparation and Properties of Niobium Stannide on Insulating Substrates," *Trans. Metallurgical Soc.* (in press).

[7] Y. B. Kim, C. F. Hempstead, and A. R. Strnad, "Magnetization and Critical Supercurrents," *Phys. Rev.*, Vol. 129, p. 528, 15 Jan. 1963; also *Phys. Rev. Ltrs.*, Vol. 9, p. 306, 1 Oct. 1962.

[8] C. P. Bean, "Magnetization of Hard Superconductors," *Phys. Rev. Ltrs.*, Vol. 8, p. 250, 15 March 1962; also C. P. Bean, M. V. Doyle, and A. G. Pincus, "Synthetic High-Field, High-Current Superconductor," *Phys. Rev. Ltrs.*, Vol. 9, p. 93, 1 Aug. 1962.

processes. These must be of approximately equal probability in either direction if spikes of either polarity are to be equally probable. Symmetrical flux motions could not produce voltages in the potential leads since the leads were connected to closed, superconducting segments or caps of the material located outside the field.

Another important aspect in the generation of these flux redistribution spikes is shown in Figure 10D. Here the spikes disappeared altogether, and only a few sharp surges of an entirely different form were present. The specimen was of the same cylindrical form as in Figure 10C, but in this case the niobium–tin composition was within one per cent of stoichiometric Nb_3Sn and the specimen displayed a thermal transition range of only 0.03°K in contrast to the other specimens where the range was about 2°K.

Interactions between Current and Magnetic Field

Perhaps the most important result of the combined application of current and field is the quenching of superconductivity at values of current and field far smaller than would be required for either operating by itself. When the field is nearly static, as during the crest of the surge, the results are as discussed in connection with Figure 6. During the rise and fall of the field, the required quench current has been observed to be as much as an order of magnitude less than during the crest. If some of this rate-of-change-of-field effect carries over to the crest interval, even the crest field values of current may be too low by comparison with d-c field tests.

In addition to the foregoing, surge-field and pulse-current tests display a number of field and current interaction effects that appear significant in terms of the fundamental nature of the superconducting processes in niobium stannide. Figure 11A shows the positive and negative inductive kicks produced by a rectangular current pulse on a niobium stannide ribbon. These are to be compared with the corresponding kicks in Figure 11B on the same specimen with the same current but in the presence of a longitudinal magnetic field of 85 kilogauss, where a large widening of the bases of the kicks, amounting in area to about 3×10^{-7} volt-second, is quite evident. This effect occurred only for current pulses in excess of ninety per cent of the quench current at the given magnetic field intensity. An estimate of the additional flux—produced by the conduction current—which would link the potential-lead circuit if the flux could thread through the niobium stannide layer instead of being forced around it, gave about 2×10^{-7} volt-second (or weber). Thus, a model of the process suggests itself: For low currents, the field produced by the current is excluded from the

superconductor, except for a penetration depth, as is observed in type-I superconductors. Correspondingly, the current is also confined to the surface of the superconductor. For the current values near quench, the field produced by the current slowly (in 2×10^{-4} sec) penetrates the superconductor, with the current becoming more uniformly distributed over the superconducting cross section. When the current is cut off, this internal flux is momentarily trapped, and then slowly pushed out.

When the magnetic field is applied transverse to the current and normal to the face of a niobium-stannide ribbon, an effect that is similar to, but much larger than, the one previously discussed occurs upon the start and stop of the conduction current. A great amplification and broadening of the inductive kick takes place, as shown in Figure 11C, where the area of the first kick (positive voltage downward) is about 1.2×10^{-5} volt-second. The enlargement at the stop or end of the current pulse is negative in voltage. Hence, the effect cannot be explained by the appearance of resistance. The simplest assumption is that again magnetic flux movement was responsible for the induced voltage in the potential circuit, and also in the current circuit itself. Indeed, close inspection of the current pulse shows that the induced voltage was sufficient to appreciably affect the current passing through the specimen. The amount of flux involved was far too large to be supplied by the current. In this transverse-field arrangement, the length of ribbon exposed to the field is about 1.0 cm. Thus, the flux density change, averaged over half the width of the ribbon, was approximately 30 kilogauss in a still rising field of 60 kilogauss. At this stage, there was roughly a fifty per cent flux exclusion. In addition, the opposite polarity of the last large voltage peak indicates a flux movement in the opposite direction, both the ingress and egress of flux being controlled or triggered by the conduction current. The central, positive (downward) potential peak in Figure 11C might be the result of resistance appearing in the specimen just after the peak of the magnetic field. However, with slightly higher current the same specimen showed, in the same time position in the surge, a negative potential peak (see Figure 11D), and at much lower transverse field a potential peak of alternating polarity (see Figure 11E). Resistance cannot account for the latter two examples, and it is reasonable to suppose that all three are the result of the movement in the superconductor of flux originating in the applied magnetic field.

The forms of the foregoing voltage signals and their dependence on current and field are difficult to explain in terms of mechanical motion of the specimen or leads in the magnetic field. In the case of the oscillations shown in Figure 12, the possibility of mechanical motion of the

specimen was eliminated—particularly the possibility of vibration of its support under the impact of the magnetic field on the sample current. By loosening the centering discs at the ends of the ceramic or sapphire rod, the specimen was left virtually floating on its own leads. While the orientation of the specimen in the field was then almost uncontrollable, it was still possible to generate samples of the typical oscillatory voltage under consideration. Since these were of the same frequency as before, it was concluded that mechanical motion was not a factor.

In Figure 12A the application of conduction current and a transverse magnetic field to a copper-plated niobium stannide ribbon produced strong oscillatory voltages in the potential leads at approximately 20 kc. The current pulse was held long enough to show the damping of the oscillations, seemingly with the decay of the magnetic field. However, with almost the same current but considerably lower field, the damping of these oscillations was shown in Figure 12B to be not entirely dependent on the field decay. An example is given in Figure 12C of the start of the current being followed by oscillations of larger amplitude than those following the stop. For higher current (see Figure 12D) the oscillations following the stopping of the current were the larger. The significance of these relative amplitudes is not known, beyond further supporting the view that mechanical movement is not involved. Clearly, however, a state far from equilibrium is manifest. This copper-plated specimen also showed interaction effects similar to those in Figure 11 obtained with a nonplated specimen.

It is noteworthy that in spite of the apparent irregularity of the patterns that have been illustrated, resettings of the current, field, and timing parameters to the same values led to the essentially exact reproduction of the patterns.

Conclusions

Techniques of surge-magnetic-field and pulse-current testing of superconductors permit the determination of critical-current–critical-field properties of the specimens. The higher ranges of magnetic field and current density are reached more easily than with d-c methods. However, flux redistribution and inductive pick-up create in the measurement signals a very high noise level as compared with d-c; this leads to a much lower sensitivity. In addition, pulse measurements are in general of much lower accuracy. The relative fragility of equipment and specimens and the required waiting times between surge measurements lead to a much slower data acquisition rate.

The surge-field and pulse-current techniques bring into evidence a wide range of transient phenomena that are inaccessible to d-c methods.

These transient processes have a direct bearing on d-c results because they often determine, as in cases of flux trapping and irreversible heating, what steady-state conditions will be realized by the specimen under test. Some of these processes are at least qualitatively understandable in terms of known principles, such as Joulean heat or intermediate-state effects. Others are interpretable phenomenologically in terms of ingress and egress of magnetic flux and changes in the distribution of current density.

The results have shown a close and complex interaction between field and current in addition to the interrelationship of their critical values. The current is able to gate in and out of the superconducting material large quantities of magnetic flux. In the presence of copper plating on the niobium stannide this gating is very often turned into a large-scale oscillation of the flux into and out of the material.

In some niobium-stannide specimens the movement of flux is characterized by sudden, discrete events of rather uniform magnitude. These sudden movements involve quantities of flux of the order of 10^7 times the so-called elementary fluxoid quantum, and thus cannot be given an elementary quantum explanation of their discreteness. If a domain explanation can be invoked, the domain size must have a mean cross-sectional diameter of the order of 0.01 cm.

Acknowledgments

My thanks are given to J. J. Hanak, G. W. Cullen, and E. R. Schrader who provided the niobium-stannide specimens, and to R. L. Juliano, K. R. Keller, and S. Bozowski for technical assistance at various periods during the work.

CRITICAL-STATE PHENOMENA AND FLUX JUMPING IN NIOBIUM STANNIDE

By

J. P. McEvoy

RCA Defense Electronic Products,
Camden, N. J.

Summary—*Tube magnetization has been used to study the critical current density of vapor-deposited Nb_3Sn. The results can be described by a model in which the magnetization is derived from an induced current density, $J_c = \alpha/(B_0 + H)$, where H is the transverse magnetic field. This relationship has been verified for a series of single-phase Nb_3Sn films deposited on hollow ceramic tubes. Although large variations in the material constants, α and B_0, have been observed, correlation of these variations with other material properties is uncertain at this time. Discontinuities in the magnetization (flux jumps) resulting from instabilities in the induced currents have been observed. The dependence of flux jumping on magnetic field, rate of change of field, and temperature is qualitatively explained in terms of Anderson's flux-creep model.*

Introduction

RECENT developments in the vapor-phase deposition of niobium stannide (Nb_3Sn) has produced coatings on a variety of insulating substrates.[1] Continuous, adherent films exhibiting high transition temperatures (18°K) and the beta-tungsten crystal structure have been deposited on ceramic plates and hollow cylinders (tubes). Since this material has an unusually high transition temperature, critical magnetic field, and current-carrying capacity, its electrical and magnetic properties are interesting from a practical, as well as fundamental, viewpoint.

An experiment to measure the shielding (or trapping) of magnetic fields by tubular samples yields information regarding the field penetration into hard superconductors and the critical current density, J_c. In addition, the behavior of these tubes in slowly varying magnetic fields is useful in studying the stability of the induced supercurrents. Unfortunately, since the range of temperature and magnetic field is so low, this measurement does not uncover any properties relating specifically to type II superconductivity. Rather, this technique affords the experimenter a simple method for determining the field and temperature dependence of J_c and the characteristics of the sample when

[1] G. W. Cullen, "Preparation and Properties of Niobium Stannide on Insulating Substrates," *Trans. Metallurgical Soc.*, in press.

it is current saturated; i.e., in the so-called critical state.[2] Since J_c is so strongly dependent on the defect structure of the material, tube magnetization can be used to study the effect of mechanical deformation[3] and neutron irradiation[4] on superconducting alloys and compounds. In this paper, data on the critical current density of Nb_3Sn as deposited[1] are reported.

Before considering the experimental results in detail, it is instructive to review briefly the theory of the static magnetization of hard superconductors. The basic premise of the model due to Bean[5] is that there exists a limiting macroscopic superconducting current density J_c that a hard superconductor can carry. Furthermore, any electromotive force will induce this full current to flow locally. The critical current is thus a consequence of the gradient of flux lines that is set up as flux is driven into an inhomogeneous mixed-state[6] superconductor. Thus, the flux penetrates into the superconductor to a distance at which its density vanishes ($B = 0$). Under the condition of complete field penetration (which, of course, depends on the size of the sample), the notions of Kim and Anderson[7] are appropriate; namely, that the critical current density is determined by the Lorentz force $\mathbf{J} \times \mathbf{B}$ acting on the individual "bundles" of flux that result from the inhomogeneous distribution of lattice imperfections in the material. The lattice imperfections act as localized flux-pinning sites and provide a rigid matrix against the action of $\mathbf{J} \times \mathbf{B}$. Although mainly of conceptual value, there are two important results of the Kim–Anderson treatment: First, J_c should be proportional to the reciprocal of the transverse magnetic field (which is almost correct); and second, the critical state is one of nonequilibrium in which the flux is continually in motion due to thermal activation aided by the Lorentz force. This latter concept has been helpful in explaining power dissipation in hard superconductors.

---

[2] Y. B. Kim, C. F. Hempstead, and A. R. Strnad, "Magnetization and Critical Supercurrents," *Phys. Rev.*, Vol. 129, p. 528, 15 Jan. 1963.

[3] J. P. McEvoy, Jr., and R. F. Decell, "Magnetization of Superconducting Niobium-Zirconium Alloys," *Jour. Appl. Phys.*, Vol. 35, p. 982, March 1964.

[4] J. P. McEvoy, Jr., R. F. Decell, and R. L. Novak, "Effect of Neutron Irradiation on Critical Currents in Hard Superconductors (Nb_3Sn and NbZr)," *Appl. Phys. Ltrs.*, Vol. 4, p. 43, 1 Feb. 1964.

[5] C. P. Bean, "Magnetization of Hard Superconductors," *Phys. Rev. Ltrs.*, Vol. 8, p. 250, 15 March 1962.

[6] A. A. Abrikosov, "On the Magnetic Properties of Superconductors of the Second Group," *Zh. Eksperim i Teor. Fiz.*, Vol. 32, p. 1442, June 1957 (translation in *Soviet Physics*, JETP, Vol. 5, p. 1174, 15 Dec. 1957).

[7] Y. B. Kim, C. F. Hempstead, and A. R. Strnad, "Critical Persistent Currents in Hard Superconductors," *Phys. Rev. Ltrs.*, Vol. 9, p. 306, 1 Oct. 1962; P. W. Anderson, "Theory of Flux Creep in Hard Superconductors," *Phys. Rev. Ltrs.*, Vol. 9, p. 309, 1 Oct. 1962.

Critical-State Phenomena

A thin cylindrical shell of a hard superconductor is placed on the axis of a superconducting solenoid, as shown schematically in Figure 1. As the applied field H builds up, the tube interior is shielded by the induced current until the flux front reaches the inner wall of the tube. At this point every region of the superconductor is carrying critical current, and field penetration is incipient. The internal field H' is

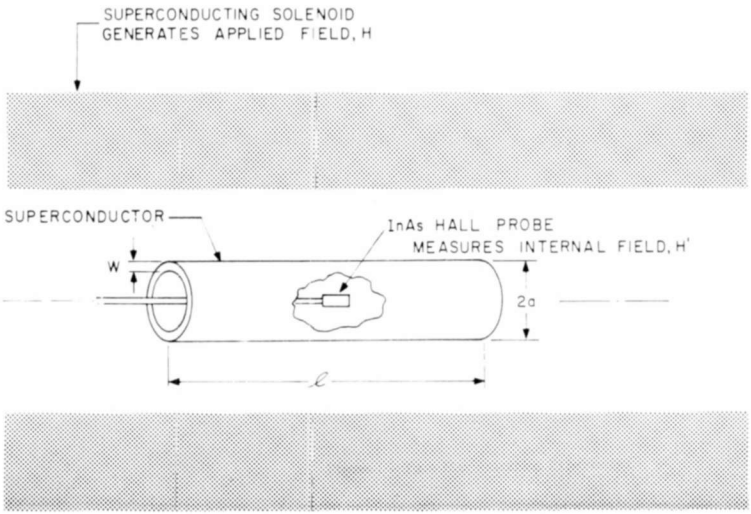

Fig. 1—Tube magnetization experiment.

measured by a Hall probe located at the tube center. A simple analytical approach has been used to derive $J_c(B)$ from the shape of the resulting H' versus H curve.

Consider a uniform magnetic field H applied parallel to the axis of a long hollow cylinder of outer radius a and wall thickness w. The magnetic flux density at any radius r is then given by

$$\mathbf{B}(r) = \mathbf{H} + 4\pi\,\mathbf{m}(r) = \mathbf{H} + c_1 \int_r^a J(x)\,dx, \tag{1}$$

where J is the uniform current density in the tube wall, $\mathbf{m}(r)$ is the magnetization, x and r are radial variables in centimeters, and $c_1 = 0.4$ gauss cm/amp.

It is easily shown that Equation (1) reduces to the scalar integral equation

$$c_1 w = \int_H^{H+M} \frac{dB}{J(B)} = \int_H^{H'} \frac{dB}{J(B)}, \tag{2}$$

where $M = H' - H$, the difference in gauss between the internal and external fields, and H' is $\mathbf{B}(r)$ evaluated at the center of the tube. Using the relation deduced by Kim et al[6],

$$J_c = \frac{\alpha}{B_0 + H}, \tag{3}$$

where α and B_0 are constants depending on the temperature and properties of the medium. Equation (2) becomes

$$\alpha c_1 w = (H' - H)\left[B_0 + \frac{H' + H}{2}\right], \tag{4}$$

or

$$\alpha c_1 w = M\,(B_0 + H^*).$$

Here H^* is the average field in the tube wall. From Equation (4) the reciprocal of M should be linear in H^*, since α and B_0 are both constant at a given temperature. Thus, Equation (4) provides a test for the validity of Equation (3), and in addition allows one to evaluate α and B_0 from an experimental plot of H' versus H. Figure 2a presents the experimental data obtained from such a measurement on a typical Nb_3Sn sample. Critical-state points are recorded at 4.2° and 2.5°K. The flux jumping shown in the curve, which occurred only at the lower temperature, is discussed in the next section. Note the linearity of the $1/M$-versus-H^* curves in Figure 2b. Some thirty vapor-deposited Nb_3Sn tubes have been studied by this method, although only about one-third gave useful data. In general, the measurement is tedious, and great care must be taken to avoid flux jumps that destroy the critical state. In a majority of the samples these instabilities are impossible to eliminate, even when the applied field is varied very slowly. Table I presents the experimental results.

Flux Jumping

Flux jumps, which are actually discontinuities in the magnetization resulting from momentary destruction of the superconducting state, are important in the study of Nb_3Sn and other hard superconductors. These phenomena are manifestations of instabilities in the supercurrent caused by power dissipation in the body of the superconductor. These

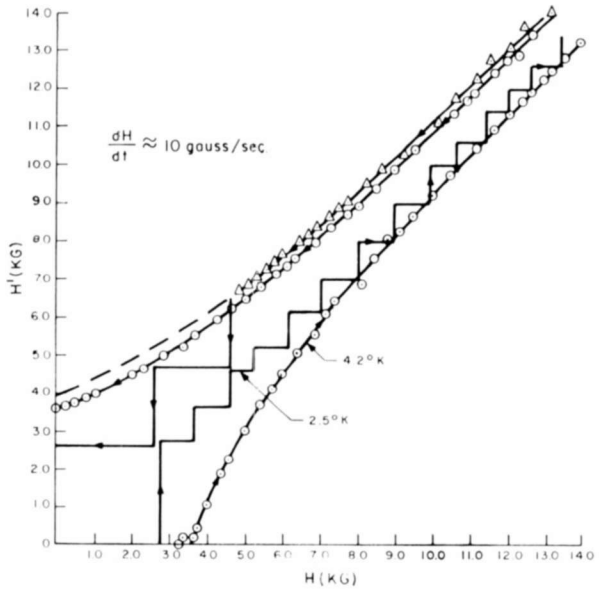

(a)

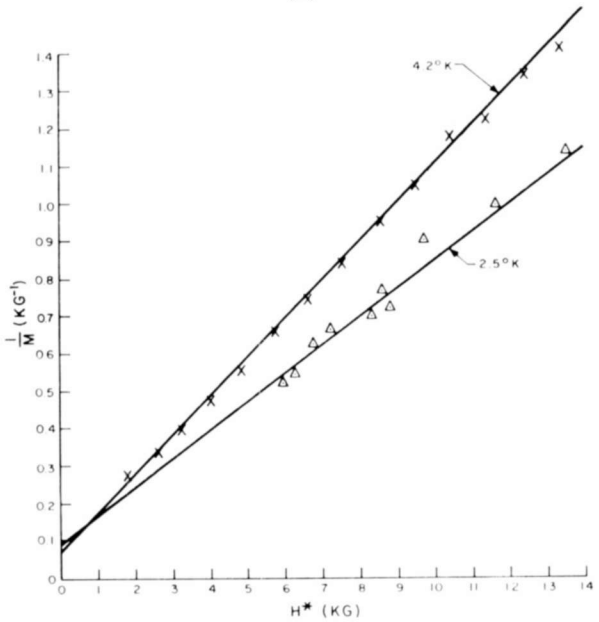

(b)

Fig. 2—Critical state data on Nb_3Sn tube. The measured critical state points are denoted in Figure 2(a). Note the increased flux jumping at 2.5°K. Figure 2(b) shows the reciprocal of M as function of H^*.

instabilities are thought to have a large effect on the operation of superconducting solenoids.[8]

Anderson has developed a phenomenological theory[7,9] that accounts for the power dissipation as a consequence of the moving flux. Very

Table I—Critical-State Data for Nb_3Sn Vapor Deposited on Ceramic Tubes

Sample #	% wt. Nb	w (μ)	T_c(°K)	α (kilogauss-amp/cm^2)	B_0(kilogauss)
66	74.1	40.0	—	8.35×10^6	5.42
69	72.3	63.5	—	1.90×10^6	4.5
77	70.7	17.7	17.55	6.35×10^6	3.5
79	70.3	14.0	17.68	19.0×10^6	3.0
80	71.9	17.8	17.63	13.5×10^6	6.5
FS-5	—	25.4	—	4.9×10^6	2.34
FS-6	—	76.2	—	2.2×10^6	0
FS-8	—	12.7	—	17.0×10^6	3.61
FS-9	—	290.0	—	1.07×10^6	0
FS-20	—	50.0	—	1.54×10^6	0.78
FS-22	—	75.0	—	3.33×10^6	2.16

simply, if flux bundles are in motion one can visualize localized time variations of the flux density B in the superconducting material. This leads to regions of finite electric fields by the relation.

$$c(\nabla \times \mathbf{E}) = -\frac{\partial \mathbf{B}}{\partial t}. \tag{5}$$

[8] M. S. Lubell, B. S. Chandrasekhar, and G. T. Mallick, "Degradation and Flux Jumping in Solenoids of Heat-Treated Nb-25% Zr Wire," *Appl. Phys. Ltrs.*, Vol. 3, p. 79, 1 Sept. 1963.

[9] P. W. Anderson and Y. B. Kim, "Hard Superconductivity: Theory of the Motion of Abrikosov Flux Lines," *Rev. Mod. Phys.*, Vol. 36, p. 39, Jan. 1964.

Power dissipation follows from

$$P = \mathbf{J} \cdot \mathbf{E}, \tag{6}$$

where J is the supercurrent density. Using the fundamental notions described in Equations (5) and (6), and by considering the thermal properties of the superconductor, it is possible to account qualitatively for the dependence of flux jumping on the magnitude of the applied field H, the rate of change of H, and the temperature.

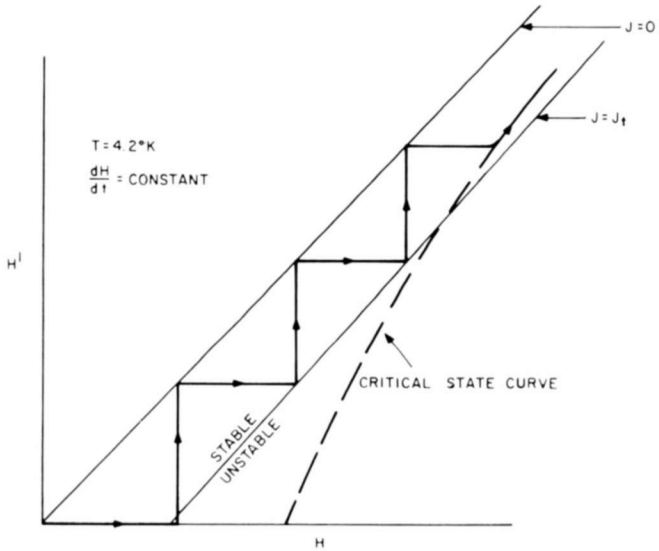

Fig. 3—Effect of magnetic field on flux jumping.

To a first approximation, one can assume that if dH/dt is constant and small, then $\partial B/\partial t$ is constant, or at least field independent, and the power will vary as the current density.* For the moment, assume that a flux jump occurs when the power dissipation exceeds some critical value P_t corresponding to a value of current density J_t. Hence, for $P > P_t$ thermal conduction lags the power dissipation, and the sample becomes thermally unstable, and no longer superconducting. Thus, the tube will shield the external field until J reaches $J_t < J_c$, at which point a flux jump occurs. As the average field H^* in the tube wall increases, J_c decreases until $J_c < J_t$. When this occurs, the tube enters the critical state before J reaches J_t, and the field begins to penetrate uniformly, without flux jumps. The sketch in Figure 3 shows how the critical-

* In a more detailed analysis, Anderson has shown the $P = C\,Je\alpha/\alpha_1$.

state curve moves inside the line $J = J_t$ as the field is increased. This field dependence of flux jumping has been observed on a number of samples, and in general the behavior is as shown in Figure 3.

One of the first observations made on tube shielding was that the degree of flux-jumping is dependent on $|dH/dt|$, i.e., higher values of $|dH/dt|$ cause more frequent flux jumping. This dependence follows naturally from the flux-creep theory.[7,9] As the applied field is increased at some finite rate of change, excessive values of α build up locally in the microstructure. This is due to the slow diffusion of the magnetic flux lines, the diffusion being impeded by the structural irregularities of the material. Since Anderson's analysis shows power to increase exponentially with α, it is easy to see that if flux is being generated at a rate greater than the relaxation rate of the fluxoids in the superconductor, the sample will reach the critical power level at a lower value of J. Thus, the jumps are smaller and more frequent.

Finally, consider the influence of the bath temperature on flux jumping. Figure 2a indicates the difficulties encountered at lower bath temperatures. The sample shown here (FS-20) is completely stable at 4.2°K. At 2.5°K, however, flux jumping commences at low values of J. This is unusual, since in general, superconducting properties improve at lower temperatures. However, this behavior can be explained at least qualitatively by close inspection of the thermal diffusion Equation (9):

$$\frac{dQ}{dt} = C\frac{dT}{dt} = -k\nabla^2 T + P, \tag{7}$$

where k is the thermal conductivity, C is the specific heat, P is the input power defined by Equation (6), and Q is the quantity of heat. If one considers a small temperature fluctuation $\delta T(r, t)$ produced by the phenomena discussed above, then Equation (7) becomes

$$C\frac{d}{dt}(\delta T) = -k\nabla^2(\delta T) + \frac{\partial P}{\partial T}\delta T. \tag{8}$$

If the sample is to remain superconducting, the left side of Equation (8) must be negative; i.e., the temperature fluctuation must decay. Anderson[9] shows that if the fluctuation occurs on a scale of size r, then for stability it is necessary that

$$\frac{k}{r^2} > \frac{\partial P}{\partial T}, \tag{9}$$

and, using experimental data, he concludes that the increase in temperature of a given region caused by the power input P is

$$\Delta T \approx \frac{Pr^2}{k} \approx T \times 10^{-3}. \tag{10}$$

Clearly, P in Equation (10) is P_f as previously defined, i.e., the power density level at which the sample becomes thermally unstable. Thus, since

$$P_f \sim \text{constant} \times kT \tag{11}$$

and k decreases exponentially with T, it is not surprising that Nb_3Sn cylinders become unstable at lower temperatures.

Conclusions

Tube magnetization measurements on hard superconductors provide a convenient method for investigating the field-dependent critical current density $J_c(B)$. The Lorentz-force model of Kim and Anderson can be used to describe the experimental data on vapor-deposited Nb_3Sn for values of α between 2×10^6 and 18×10^6 kilogauss-amp/cm^2 and values of B_0 between 0 and 6 kilogauss at 4°K. Correlation of the variation in these parameters with material properties, such as relative atomic composition and/or transition temperature, is uncertain at this time.

A study of the conditions under which flux jumps occur has shed light on the quenching of hard superconductors at current values considerably below the critical value. Induced currents in Nb_3Sn tubes are more stable for higher values of the applied field, for a slower rate of build-up of the field, and at higher temperatures. It is interesting to note that the "degradation effect" in superconducting solenoids, which arises from the instability of induced persistent currents, is less severe when the coil is operated in a magnetic field[10] or at a slower rate of field build-up. It seems logical, therefore, to investigate the operation of superconducting solenoids at elevated temperatures.

Acknowledgment

The author would like to express his gratitude to G. W. Cullen and R. Nyman for sample preparation, to R. F. Decell for assistance in the measurements, and to G. D. Cody and Y. B. Kim for helpful discussions.

[10] E. R. Schrader, N. S. Freedman, and J. C. Faken, "High Field Nb_3Sn Superconducting Magnets by Magnetic Field Stabilization," *Appl. Phys. Ltrs.*, Vol. 4, p. 105, 15 March 1964.

MAGNETIC FIELD PENETRATION INTO NIOBIUM-STANNIDE DISCS

By

K. G. Petzinger and J. J. Hanak

RCA Laboratories
Princeton, N. J.

Summary—*The internal field and current distributions in superconducting Nb_3Sn discs have been measured for the first time. Under stable transport current conditions (8-ring discs) both the manner of flux penetration and the field and current distributions are found to be in reasonable accord with the predictions of Bean.*[4] *In disc geometries having both very large and very small film widths (1-, 4-, and 20-ring discs) there arise opposing superconducting currents that diminish field shielding and trapping. The opposing currents are formed by an unsymmetrical penetration of the flux toward the center of a disc. Similar effects may be related to the current degradation in superconducting solenoids.*

Introduction

RECENTLY, MAGNETIZATION measurements on Nb_3Sn discs stacked in a cylindrical geometry have been made by Hanak[1] in a manner similar to that used by Kim *et al*[2] on hollow cylinders. The discs, which consisted of 2.25-μ-thick Nb_3Sn film vapor-deposited on both sides of a platinum foil, had a 2.5-cm outside diameter and a 0.5-cm-diameter inner hole. The Nb_3Sn film was subdivided into a varying number of concentric rings. Although the amount of Nb_3Sn on each disc was comparable, it was found that discs subdivided into 8 rings had a significantly greater shielded and trapped fields (H_s and H_t)* than did those in 1-, 4-, or 20-ring configurations.

In order to explain this behavior, measurements of the internal field distribution $B(r)$ have been made on discs of various geometries as a function of applied field H, perpendicular to the plane of the discs as described below. The resulting data are useful in determining the current distribution in each type of disc and the mechanism responsible for degradation in the 1-, 4-, and 20-ring discs.

---

* The definition of H_s and H_t is similar to that used by Kim *et al*,[2] namely, $H_s = H_t = H - B(r = 0)$, when the entire structure is entirely penetrated, i.e., it is in the critical state. H_s is obtained when $B(r = 0) = 0$, and H_t when $H = 0$.

[1] J. J. Hanak, "Magnetization of Niobium Stannide Films in Transverse Fields," *RCA Review*, Vol. XXV, No. 3, p. 551, Sept. 1964 (this issue).

[2] Y. B. Kim, C. F. Hempstead, and A. R. Strnad, "Magnetization of Critical Supercurrents," *Phys. Rev.*, Vol. 129, p. 528, 15 Jan. 1963.

Experimental

Two methods of field measurement were used. The first involved the use of a bismuth magnetoresistance probe that consisted of a 2-cm-long section of 0.03-cm-thick bismuth wire to which 15 copper wires were soldered at intervals of 0.125 cm. The finished probe was encased in a 0.05-cm-thick epoxy disc with the bismuth wire extending radially out from the center. When in use, two Nb_3Sn discs were laid flat on each side of the probe, and a constant current was passed through the bismuth wire. The potential between adjacent copper wires was measured as a function of the applied field. This potential indicates the average value of B in that interval of the radius r. A continuous trace of $B(r)$ versus H was made on an X-Y recorder throughout the cycle 0 to 7 to 0 to -7 to 0 to 7 kilogauss for each pair of copper wires. Prior to each new cycle the samples were heated to destroy any persistent currents.

The second method of field measurement utilized Faraday rotation of light passed through cerium phosphate glass. This technique has been used by De Sorbo and Healy[3] to study domain structure in soft superconductors. It has the advantage that the field profile can be observed over the entire disc instead of only along a particular radial direction. In our experiment a 0.45-mm-thick circular wafer of cerium phosphate glass, aluminized on one side, was placed on a stack of Nb_3Sn discs with its aluminized side facing the discs. Plane-polarized green light from a mercury arc was reflected off the glass and analyzed with a crossed Polaroid. Regions of high or low field intensity were visible as light or dark areas, respectively, on a photograph of the discs. All measurements were done at 4.2°K.

Results and Discussion

The data of $B(r)$ versus H obtained with the bismuth probe were replotted as a family of B versus r curves for various values of H. The following observations can be made:

(1) For the 8-ring discs B versus r curves (Figure 1) indicate that $B(r)$, as well as the penetration mechanism, is in accord with the model proposed by Bean[4] for a superconducting slab. As the field is initially increased to a value less than H_s on a virgin sample, the field penetrates from the outer edge inward but only up to a point r deter-

[3] W. De Sorbo and W. A. Healy, General Electric Research Laboratory, Report No. 61-RL-2723M, 1961 (unpublished).

[4] C. P. Bean, "Magnetization of High-Field Superconductors," *Rev. Mod. Phys.*, Vol. 36, No. 1 (Pt. 1), p. 31, Jan. 1964.

mined by H and J_c. When the field penetrates to the inner edge of the disc, B increases throughout the entire disc with a nearly constant slope dB/dr at a given r. Upon the reversal of the applied field, B first decreases near the outer edge (again only up to a point $r(J_c, H)$) and

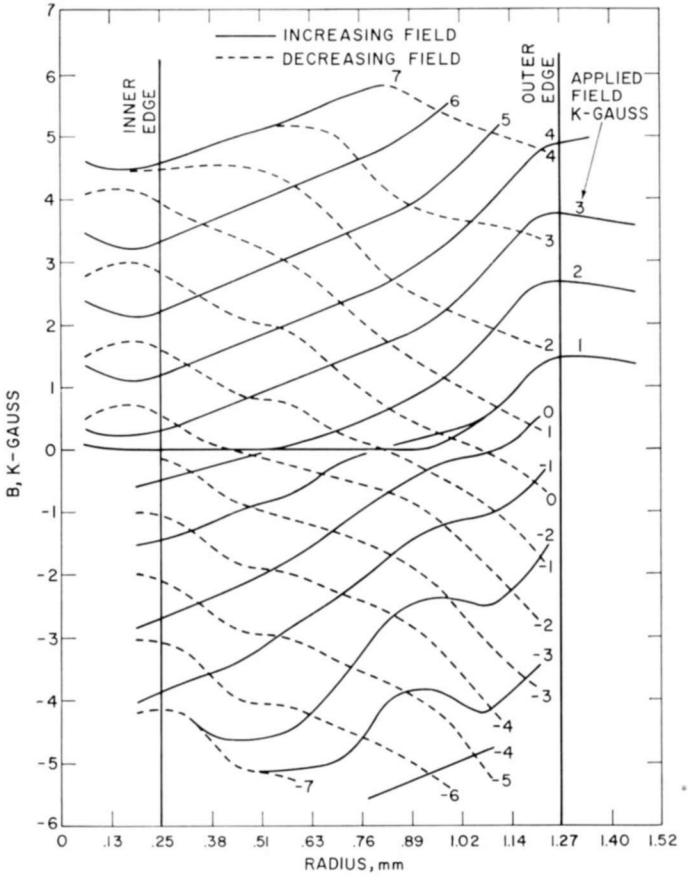

Fig. 1—Radial magnetic field distribution in a stack of four 8-ring discs.

the slope dB/dr at this point changes sign abruptly, while retaining approximately the same absolute value as in the first part of the cycle. When the external field has been decreased by an amount approximately equal to H_s or H_t, B begins to decrease throughout the disc and the sign of dB/dr is changed everywhere.

(2) One significant difference between these results and the Bean model is that $B(r)$ at the outer edge is higher than H during the part of the cycle of increasing fields and vice versa. In the Bean model

$B(r) = H$ for both cases. These results are understandable when the discs are thought of as solenoids. The radial field distribution in the winding of a solenoid (see, for example, Boom and Livingston[5]) is very similar to the analogous case of field trapped in a disc after H has been decreased to zero. In both cases $B(r) = 0$ within the body of each structure and not on the periphery.

(3) The Bean model is not obeyed for disc geometries other than the 8-ring discs. Figure 2 shows B versus r curves for four 1-ring

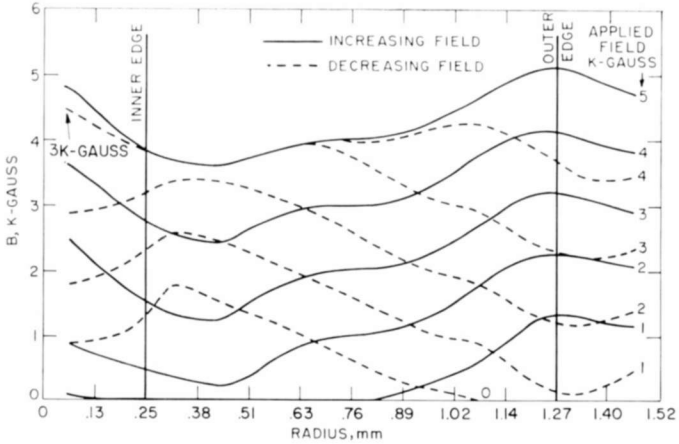

Fig. 2—Radial magnetic field distribution in a stack of four 1-ring discs.

discs during the first two parts of the cycle. The field initially penetrates in the same manner as for 8-ring discs; however, between 1 and 2 kilogauss the field in the hole starts rising faster than in some parts of the disc walls, thereby creating a minimum in the B versus r curves. When the field is reversed, B begins changing in a manner similar to that shown in Figure 1; however, the minimum in B eventually becomes a maximum.

(4) Some idea of the current distribution in the discs can be obtained by calculating $\nabla \times \mathbf{B}$, which is proportional to $\mathbf{J}_c$. With only a J_θ component, the curl reduces to $\partial B_r/\partial z - \partial B_z/\partial r$. Assuming that $\partial B_r/\partial z \ll \partial B_z/\partial r$, which is not unreasonable in our experimental setup since $B_z \gg B_r$, we obtain $\partial B_z/\partial r \approx dB/dr \propto J_c$. A plot of dB/dr versus r for the 8-ring discs taken from the shielding portion of the cycle at $H = 4$ kilogauss is shown by the dashed curve in Figure 3. This result

[5] R. W. Boom and R. S. Livingston, "Superconducting Solenoids," *Proc. I.R.E.*, Vol. 50, p. 274, March 1962.

indicates that the current is in the same direction around the center hole and that J_c has the largest value near the outer edge of the discs where $B(r)$ is also largest. Evidently, the relationship $J_c = \alpha/(B + B_0)$ proposed by Kim *et al*[2] is not obeyed, possibly because of a drastic departure from the ideal geometry of a long, thin tubular specimen or the assumptions made regarding dB/dr.

The presence of maxima and minima in $B(r)$ for the one-ring discs (Figure 2) means that dB/dr, and hence J_c, changes sign at those points as shown by the full curve in Figure 3 taken from the shielding

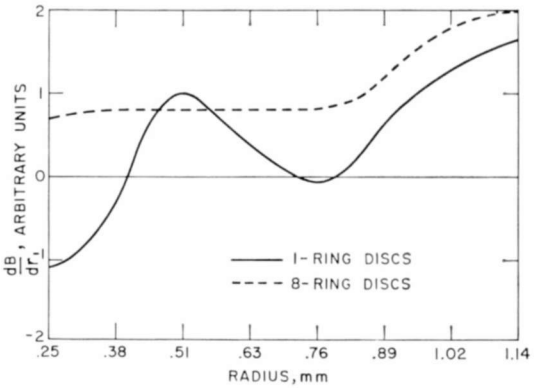

Fig. 3—Radial distribution of superconducting current in 8-ring discs (dashed curve) and 1-ring discs (solid curve) at $H = 4$ kilogauss.

portion of the cycle at $H = 4$ kilogauss. Therefore, the lower H_s or H_t with these discs is due to opposing currents around the center hole as suspected in the initial results.

For the 4- and 20-ring discs, B versus r curves also contain maxima and minima thereby indicating the presence of opposing currents (Figures 4 and 5).

Some results of the Faraday rotation experiments are shown in Figures 6 and 7, which contain sequences of photographs of the surface of the discs for fields varying over indicated cycles. In each photograph about a half of a disc is visible. The wavy structure, identical for each sequence, is due to inhomogeneities in the cerium phosphate glass, which was also cracked as seen in the photographs. The pictures were taken with Polaroids crossed at 90°; therefore, dark regions represent low-field regions, and vice versa. In the sequence shown in Figure 6 for four 8-ring discs, a rather symmetrical penetration is observed for fields increasing from 0 to 5.1 kilogauss (Figures 6a to e). As the field

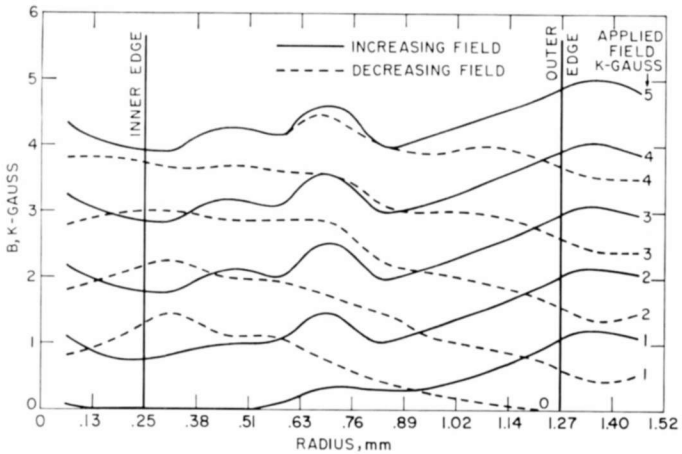

Fig. 4—Radial magnetic field distribution in a stack of four 4-ring discs.

is lowered to zero (f to h), flux leaves the specimen again in a symmetrical fashion. At zero field (h) the discs have trapped a field in and around the center hole, as shown by the bright region. In the same photographs a dark band of $B = 0$ can be observed in the disc wall, as well as a faint band of negative field near the outer edge. As the applied field is made progressively more negative (i to l) the band of $B = 0$ moves inward. In the sequence h to l the individual rings in the discs are distinguishable, thereby showing expected discontinuities of the current at the etch lines and giving some idea of the resolution. Thus,

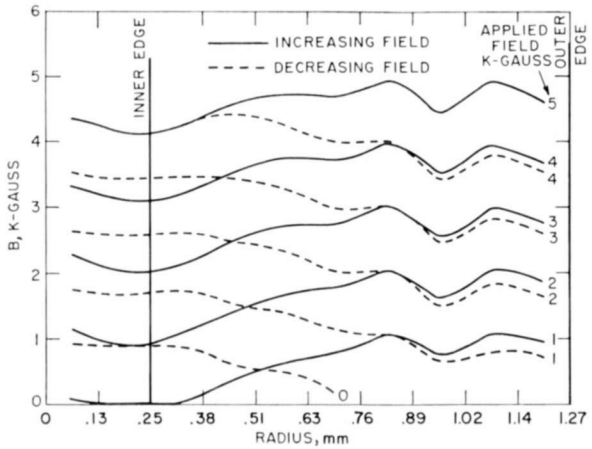

Fig. 5—Radial magnetic field distribution in a stack of four 20-ring discs.

it is seen that the Faraday rotation experiments are in agreement with the magnetoresistance data shown in Figure 1.

In the sequence shown in Figure 7 for four 1-ring discs, the field penetration is radially nonsymmetrical. After the initial uniform field

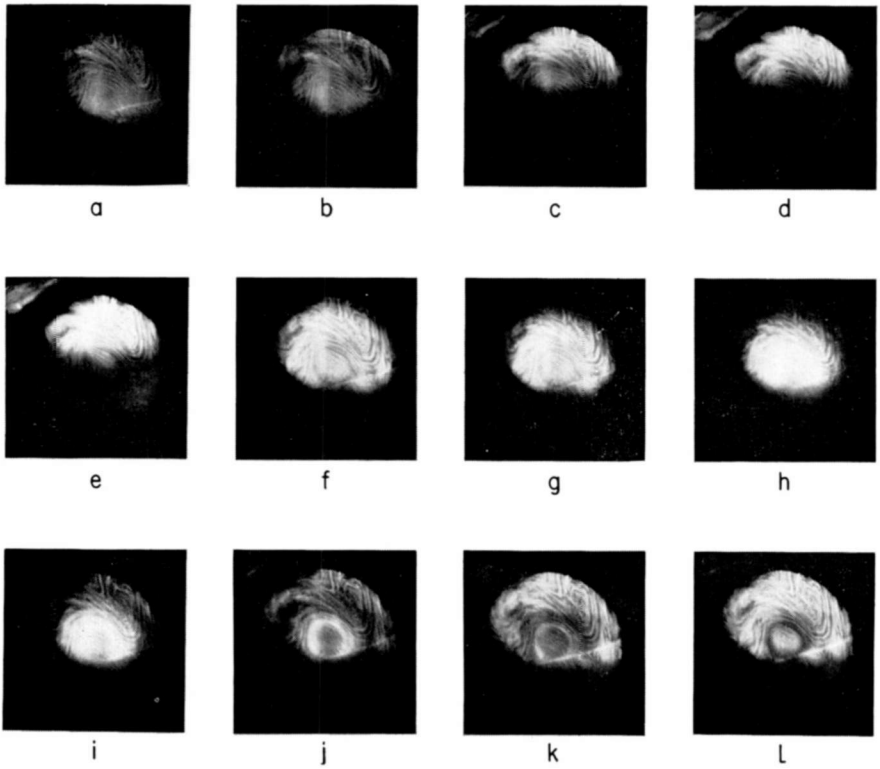

Fig. 6—Faraday rotation photographs of magnetic field penetration into four 8-ring discs (applied field in kilogauss; (a) 0; (b) 1.4; (c) 2.4; (d) 3.4; (e) 5.2; field increased to 6.2, not shown; (f) 3.4; (g) 2.1; (h) 0; (i) −0.7; (j) −1.4; (k) −2.1; (l) −3.43).

penetration (b) a small high-field region appears (c), which expands as the applied field is increased until it penetrates into the center hole (e). Thereafter, flux penetrates nearly symmetrically from the outer edge in and from the inner edge out, thus forming a minimum in B as already seen in Figure 2. On decreasing H, flux leaves from the center hole through the same region it entered as shown by the darker region of the disc wall (h to l). There is no evidence of a multitude

of high-field "islands" in the film. Thus, it appears that the opposing currents in the 1-ring discs arise by the flux breaking through the superconducting ring at one or a few points rather than by the breakup of the film into many small areas of local circulating currents as visual-

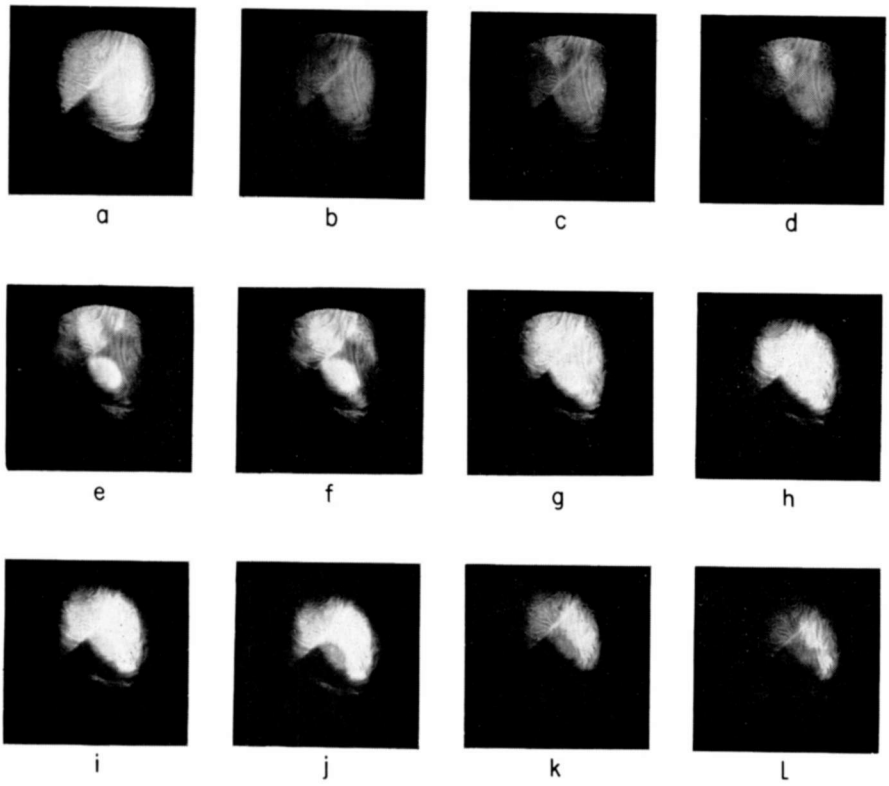

Fig. 7—Magnetic field penetration into four 1-ring discs ((a) 0; (b) 1.0; (c) 1.4; (d) 1.8; (e) 2.4; (f) 3.1; (g) 5.2; (h) 2.7; (i) 2.1; (j) 1.4; (k) 0.7; (l) 0 kilogauss).

ized in the original work.[1] The formation of opposing currents is shown schematically in Figure 8.

The anomalous behavior of the 1- and 4-ring discs appears to be due to the relatively large demagnetization coefficient of the wide films. Since the energy associated with field shielding or trapping is proportional to $H_s^2/(8\pi)$, the formation of opposing currents so as to lower H_s is favored in such films. In narrower films, such as the 8-ring discs,

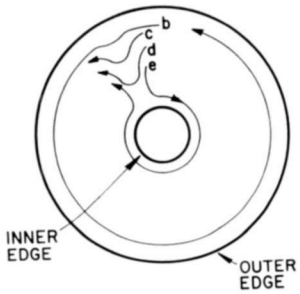

Fig. 8—Mechanism of formation of opposing currents in 1-ring discs (letters correspond to photographs in Figure 7).

transport currents are stabilized because the role of field shielding is divided among many rings. The decrease of H_s of the 20-ring discs may be due to instabilities introduced by considerable misalignment of the narrow rings on either side of the substrate and in a stack.

ACKNOWLEDGMENTS

The authors are grateful to A. Miller for the use of some of his optical equipment and valuable advice and to D. Leibowitz and C. Benyon for the construction of the bismuth magnetoresistance probe.

MAGNETIZATION OF NIOBIUM-STANNIDE FILMS IN TRANSVERSE FIELDS

By

J. J. Hanak

RCA Laboratories
Princeton, N. J.

Summary—*Magnetization measurements in fields transverse to the film plane have been made as a function of film geometry on 2.25-μ Nb_3Sn films vapor deposited on platinum foil. The specimens were in the shape of discs with the superconducting film subdivided into a varying number of concentric rings. Drastic differences in magnetic shielding and trapping have been observed as a function of subdivision, with a maximum occurring at intermediate ring widths.*

The occurrence of "flux jumps" was found to depend on the magnitude of magnetization, the rate of change of magnetic field, the insulation of the superconductor, and the specimen geometry. These results confirm that flux jumps are thermally activated. On the basis of these results a 60-kilogauss permanent magnet has been constructed by the use of the Nb_3Sn discs and copper foil discs in a laminar stacking. The resulting composite cylinder combines the high critical current density of Nb_3Sn with the high thermal and electrical conductivity of copper, which are the properties necessary to obtain stable high fields in a compact device (2.54-cm O.D., 0.508-cm I.D., and 2.1 cm long).

Introduction

THE DISCOVERY of superconducting materials having high transition temperature[1,2] and unusually high critical magnetic field[3] and current carrying capacity[4] signaled the advent of very high field solenoids.[5] At the same time, the possibility of permanent high field magnets in the form of hollow superconducting cylinders was

---

[1] G. F. Hardy and J. K. Hulm, "The Superconductivity of Some Transition Metal Compounds," *Phys. Rev.*, Vol. 93, p. 1004, 1 March 1954.

[2] B. T. Matthias, T. Geballe, S. Geller, and E. Corenzwit, Superconductivity of Nb_3Sn," *Phys. Rev.*, Vol. 95, p. 1435, 15 Sept. 1954.

[3] R. M. Bozorth, A. J. Williams, and D. D. Davis, "Critical Field for Superconductivity in Niobium-Tin," *Phys. Rev. Ltrs.*, Vol. 5, p. 148, 15 Aug. 1960.

[4] J. E. Kunzler, E. Buehler, F. J. L. Hsu, and J. H. Wernick, "Superconductivity in Nb_3Sn at High Current Density in a Magnetic Field of 88 KGauss," *Phys. Rev. Ltrs.*, Vol. 6, p. 89, 1 Feb. 1961.

[5] J. E. Kunzler, *High Magnetic Fields* (H. Kolm, B. Iax, T. Bitter, and R. Mills, editors), The MIT Press and John Wiley and Sons, New York, N. Y., 1962.

visualized.[6] Superconducting cylinders are of practical interest because they are simple to construct, are compact, possess extreme field stability, and are easy to operate. Their operation involves merely an initial inductive charging by means of an external magnet; thereafter the field remains trapped in the cylinder so long as it is maintained under liquid helium. A superconducting cylinder shields as well as traps magnetic fields, because the persistent currents induced in it always oppose changes in the external magnetic field. The behavior of hollow cylinders and the nature of the persistent current in type II superconductors such as Nb_3Sn has been described in detail by Kim et al.[7]

Although experimental results with small cylinders indicated the possibility of obtaining high-field magnets, these fields have not been realized because of magnetic flux instability known as the "flux jump," which marks a sudden loss of the persistent current.[6] This instability seemed to be associated with the magnitude of the cross-sectional area of the superconductor in the cylinder and of its shielded or trapped field. Thus, it appeared that the instability problem might be solved by constructing a composite cylinder consisting of a large number of thin superconducting rings insulated from each other by a highly conducting normal metal, since the presence of normal metal is known to enhance the stability of wire-wound superconducting solenoids.[8]

Experimental

Vapor-deposited films of Nb_3Sn were used in the construction of composite cylinders. The Nb_3Sn film was about 2.25×10^{-4} cm thick and was deposited on both sides of a 1.3×10^{-3}-cm-thick strip of platinum. The Nb_3Sn was deposited by a continuous process involving a simultaneous reduction of mixed niobium and tin chlorides with hydrogen as described in Reference (9), but modified to accommodate the wide strip. A specimen of this strip taken at random was a single-phase material with a β-tungsten structure. The critical temperature, T_c, ranged from 14° to 16°K, which is typical of vapor-deposited rib-

---

[6] F. Rothwarf, R. C. Thiel, S. H. Autler, and K. Gooen, "Persistent Currents in Hollow Cylinders of Niobium-Tin," *Bull. Amer. Phys. Soc.*, Vol. 7, p. 189, 1962.

[7] Y. B. Kim, C. F. Hempstead, and A. R. Strnad, "Magnetization and Critical Supercurrents," *Phys. Rev.*, Vol. 129, p. 528, 15 Jan. 1963.

[8] J. O. Betterton, Jr., G. D. Kneys, Jr., D. S. Easton, and J. O. Scarborough, p. 61 of *Superconductors*, M. Tanenbaum and W. V. Wright, editors, Interscience Publishers, Inc., New York, 1962.

[9] J. J. Hanak, in *Metallurgy of Advanced Electronic Materials*, G. E. Brock, editor, Interscience Publishers, Inc., New York, 1963, p. 161.

bons having a slight excess of niobium and some lattice disorder.[10] A 3-mm-wide specimen could carry a maximum current of 120 amperes at 4.2°K and a field of 12 kilogauss transverse to the film. The critical current density, J_c, was approximately 9×10^5 amperes/cm^2.

Disc patterns with a variable number of concentric rings were etched into the Nb_3Sn film, leaving the platinum substrate intact. The

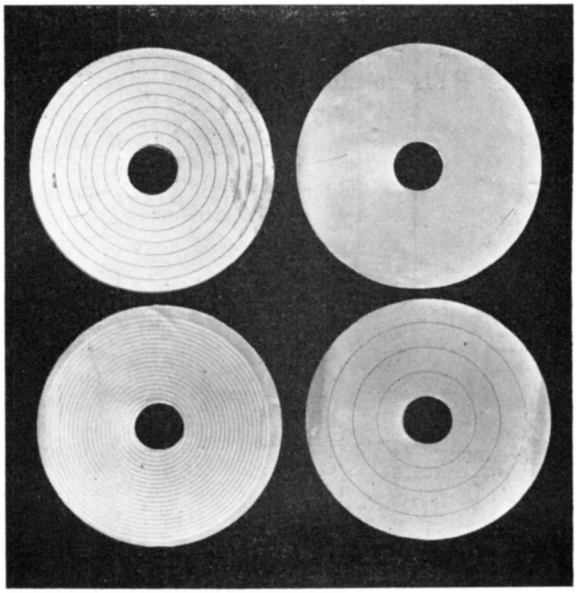

Fig. 1—Vapor-deposited Nb_3Sn discs on platinum foil (1-, 4-, 8-, and 20-ring discs).

discs, which had a 2.54-cm O.D. and a 0.254-cm I.D., were then punched out. Seven different kinds of discs were made, including full discs without a hole, 1-ring discs (hole only), and 4-, 6-, 7-, 8-, and 20-ring discs. A photograph of some of these discs appears in Figure 1, where the thin lines (0.005-0.008 cm) represent the etched lines, or platinum surfaces.

Measurements of the internal field (H') in an external field (H) were made as a function of the number and the kind of discs stacked, as shown in Figure 2. The applied field was always parallel to the cylinder axis and perpendicular to the film plane. Siemens Hall probes*

[10] J. J. Hanak, G. D. Cody, J. L. Cooper, and M. Rayl, *Eighth Int. Congress on Low Temperature Physics*, Butterworth and Co., Ltd., London, 1963.

* Flat, transverse-field Hall probe EA 218 was used with single discs or small stacks up to 30 discs. Cylindrical, axial-field Hall probe SBV 552 was used with larger stacks.

were used to measure H and H', although in most cases the external magnet current was used as the indication of the external field instead of the external Hall probe. Sample holders were made of cloth-base Bakelite for small stacks, and of brass for larger stacks. The stacked discs were insulated from each other either by 0.0013-cm thick Mylar discs or by OFHC copper discs of comparable thickness. At low and intermediate fields the external field was supplied by a 7.6-kilogauss conventional magnet or by an Nb_3Sn solenoid. At high fields, conventional air-core solenoids were used—an 80-kilogauss NASA* solenoid, and a 103-kilogauss BTL† solenoid.

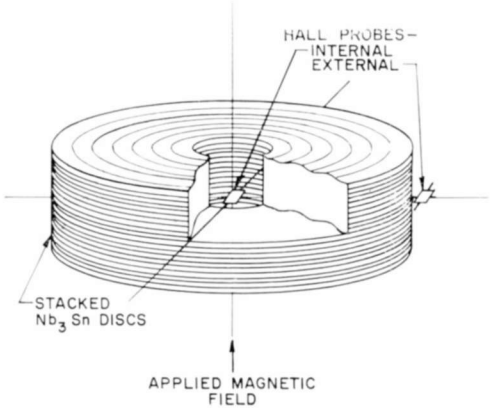

Fig. 2—Stacking of discs for magnetization measurements.

The magnetization measurements had a two-fold purpose. One of them was to determine the additivity of the shielded and trapped fields as a function of the number and the kind of discs in a stack. The other was to study the occurrence of flux jumps in various stacking arrangements as a function of the rate of change of magnetic field.

Additivity of Shielded and Trapped Fields

Measurements of H versus H' were made on five types of Nb_3Sn discs with each type arranged in stacks of 1 to 16 discs. Mylar discs were used as insulation with all but the 1-ring discs in which case copper discs were used to suppress the tendency to flux jumping. The magnitude of the shielded or trapped field was found to be unaffected by the copper discs. Typical curves obtained with the different kinds

* NASA Lewis Research Center, Cleveland, Ohio.
† Bell Telephone Laboratories, Murray Hill, N. J.

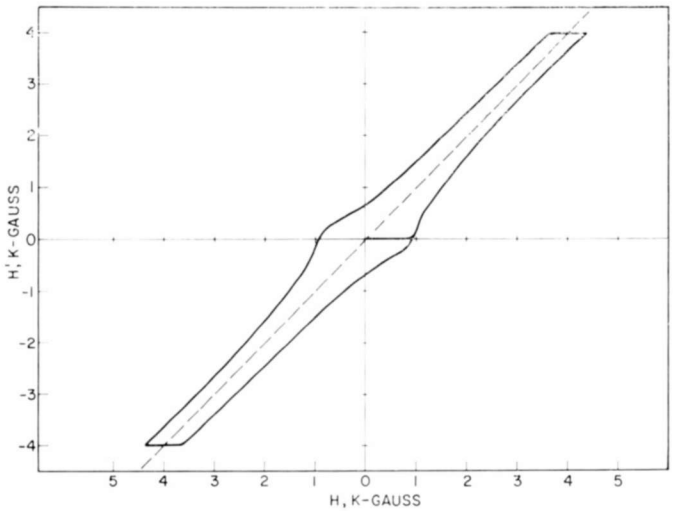

Fig. 3a—Typical magnetization curve of a stack of full discs.

of discs appear in Figures 3a and 3b. The shapes of these curves are discussed later. The shielded field H_s (the abcissa intercept) has been plotted in Figure 4 for the five series of discs as a function of the number of discs.‡ A striking variation in the additivity of the shielded field as a function of the disc geometry is evident, showing that at both low and high subdivision of discs into rings the shielded field tends to

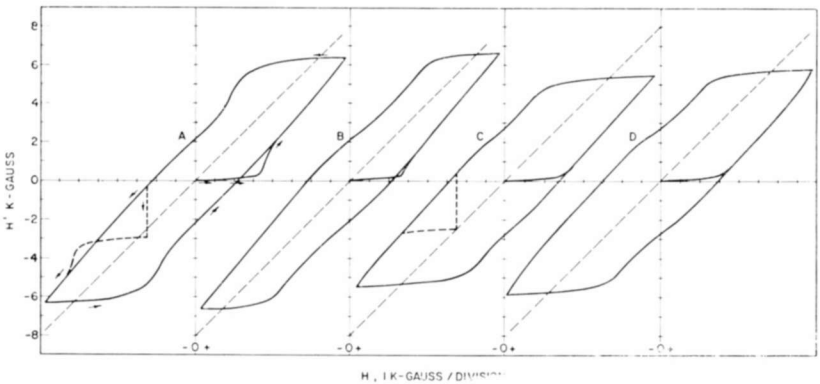

Fig. 3b—Typical magnetization curves of stacks of (a) 1-, (b) 4-, (c) 8-, and (d) 20-ring discs.

‡ Data for 1/2 disc were obtained with specimens on which the Nb_3Sn film was etched off on one side.

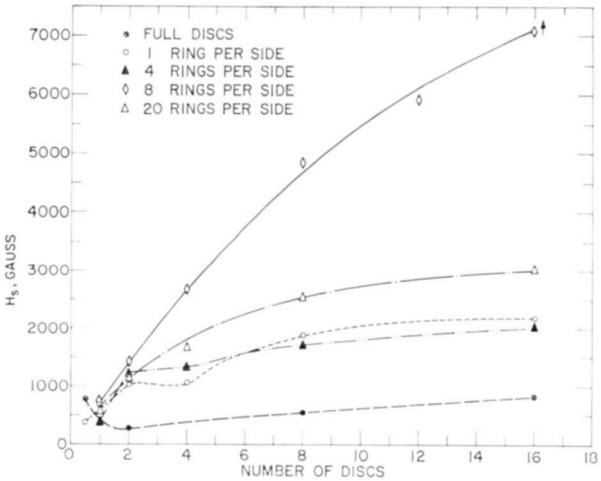

Fig. 4—Shielded field versus the number of discs for various kinds of discs.

saturate to a low, nearly constant value with added discs. A maximum in shielded field additivity is shown by the curve for the 8-ring discs, which also indicates that the shielded field would continue increasing with additional discs. The trapped field H_t (the ordinate intercept of the curves in Figure 3a,b) was usually about five per cent lower than the H_s for the 8- and 20-ring discs, but up to 20 per cent lower than the shielded field for the 1- and 4-ring discs. Only six of each of the 6- and 7-ring discs were available; hence, the H_s of these discs is compared with the H_s of equal number of discs of other geometries in Figure 5, which indicates that a maximum field shielding might be expected for disc geometries falling between the 8- and 20-ring discs.

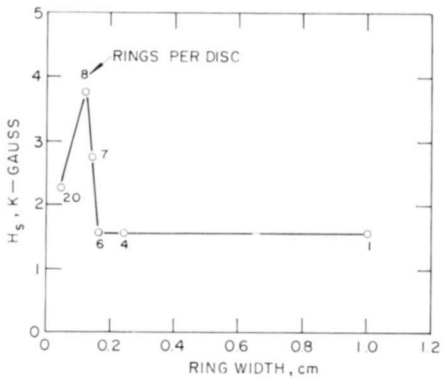

Fig. 5—Field shielding by stacks of six discs of various kinds versus ring width.

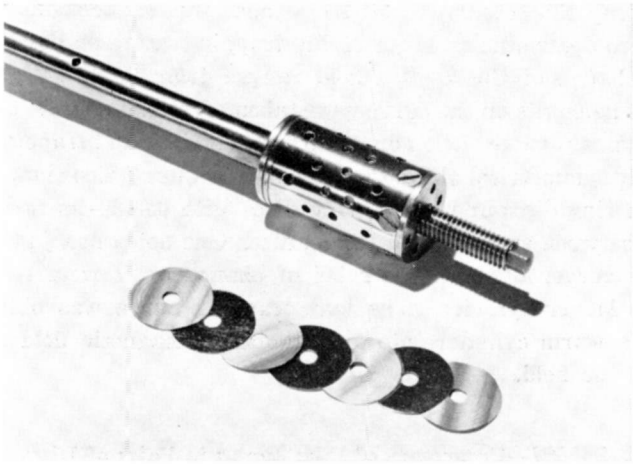

Fig. 6—Brass sample holder for the 60-kilogauss Nb_3Sn permanent magnet.

Additional discs were made with the 8- and 20-ring geometries to test the limits of H_s. Copper discs were used in between the Nb_3Sn discs for insulation. The trend observed in Figure 4 continued—for 176 20-ring discs the shielded or trapped field was only 9.1 kilogauss; however, 31 8-ring discs shielded 13 kilogauss. Furthermore, a 2.1-cm-long cylinder composed of 491 8-ring discs and 165 20-ring discs on the ends and an equal number of 0.0013-cm-thick copper discs (Figure 6) shielded and trapped a field of nearly 60 kilogauss. The magnetization curve for this cylinder up to H of 103 kilogauss appears in Figure 7.

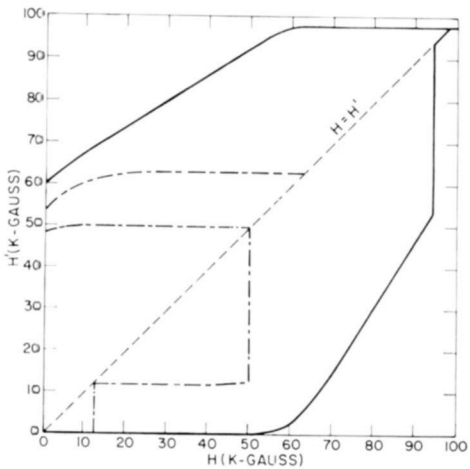

Fig. 7—Magnetization of 511 discs (dashed curve) and 656 discs (full curve).

A flux jump that occurred at 94 kilogauss was induced intentionally in order to determine as much of the trapping curve as possible. The rate of change of the applied field ranged from 25 to 50 gauss per second. The points on the curve were taken after allowing H' to assume nearly constant value. One notes that the shielding and trapping curves are nearly symmetrical about the diagonal. Figure 7 also shows a curve for 344 8-ring discs and 176 20-ring discs with 0.0025-cm-thick copper discs in between every second Nb_3Sn disc. One notes flux jumps in the shielding curve, although the rates of change of H were comparable with the larger cylinder. The lone trapping curve was obtained by dipping a warm cylinder into an established magnetic field and then reducing the field.

Table I—Occurrence of Flux Jumps in Pairs of Discs

No. of Rings per Side	Flux Jumps Per Cycle			H_s (gauss)
	$\frac{dH}{db} = 20$ gauss/sec	$\frac{dH}{db} = 187$ gauss/sec	$\frac{dH}{db} = 625$ gauss/sec	
1	3	22	—	1,025
4	0	6	—	1,225
8	0	4	—	1,370
20	0	0	8	1,105

Flux Jumping

The occurrence of flux jumps was studied as a function of variables that are controllable in the present composite cylinder design, namely, the disc geometry, the type of insulation used, the number of discs, and the magnitude of the external field.

Effect of Disc Geometry on Flux Jumps

The occurrence of flux jumps in pairs of discs was tested up to 7.6 kilogauss with variable rates of change of the magnetic field (dH/dt). The discs were separated from each other by a thin sheet of Bakelite and were completely enclosed in the Bakelite sample holder that was submerged in liquid helium. The data in Table I indicate that the number of flux jumps for a complete forward and reverse cycle of the external field is inversely proportional to the subdivision into rings, when the field shielding is of similar magnitude. The number of flux

jumps also increases with dH/dt. Full discs show no flux jumping up to 1500 gauss per second; however, they have very low H_s as shown in Figure 4. Data on single discs under the same conditions were similar.

Effect of Insulation on Flux Jumps

The preceding test was repeated with motor-driven dH/dt control for single discs with the specimen holder perforated to allow a direct contact of the specimen with liquid helium. There was a complete absence of flux jumps in all disc geometries up to dH/dt of 605 gauss per second and H of 12 kilogauss, except for the 1-ring disc where 2 flux jumps per cycle persisted down to dH/dt of 10 gauss per second. The contrasting result of this experiment with the one above clearly indicated the occurrence of thermal dissipation during the induction process and its effect on flux jumping when sufficient cooling is not provided.

Additional data on the effect of insulation on flux jumps were obtained by comparing the flux jump occurrence with stacks of discs using Mylar insulation and stacks using copper insulation between discs. For stacks of 1 to 8 discs of the 1-, 4-, 8-, and 20-ring geometry with Mylar insulation, flux jumps start at dH/dt of about 10 to 200 gauss per second. For similar stacks using copper insulation, flux jumps did not occur at dH/dt below 605 gauss per second (maximum rate available in this experiment). The improvement in stability is probably due to the high thermal conductivity of copper, which is helpful in preventing large local temperature increases, and also to its high electrical conductivity, which gradually attenuates local magnetic transients.

Effect of Stacking on Flux Jumps

Stacks of 8 discs with Mylar insulation and a perforated sample holder showed no flux jumping for dH/dt of up to 605 gauss/sec and an external field of 12 kilogauss for the 1-, 4-, and 20-ring discs. The 8-ring discs began flux jumping at 177 gauss per sec and continued the same with greater frequency at higher dH/dt. This experiment suggests that the magnitude of field shielding increases the tendency to flux jumping.

Effect of Magnetic Field on Flux Jumps

It is known that flux jumps occur more readily at lower fields, where field shielding is greater than at higher fields. In one experiment, with a single 8-ring disc enclosed in a bakelite sample holder (to permit flux jumps), the field at which repetitive flux jumping starts in the trapping

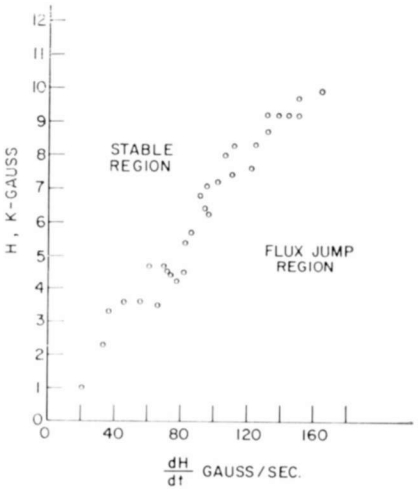

Fig. 8a—Stability boundary curve H versus dH/dt for an 8-ring disc.

portion of the curve (decreasing field) was measured as a function of dH/dt as shown in Figure 8(a). These data were also used to obtain M_+ (here $M_+ = H' - H$) as a function of H. M_+ was then plotted as a function of the value of dH/dt at which flux jumping starts. The resulting stability boundary curve appears in Figure 8(b). The curve is parabolic and fits the expression

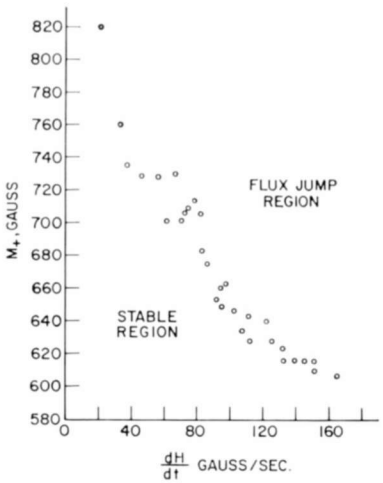

Fig. 8b—Stability boundary curve M_+ versus dH/dt for an 8-ring disc.

$$(M_+ - 56.4)\frac{dH}{dt} - 8{,}100 = 0, \tag{1}$$

where M_+ is in gauss and dH/dt is in gauss per second. A strong dependence of flux-jump occurrence on the magnitude of field trapping is again indicated. The occurrence of flux jumps in the shielding portion of the cycle are similar; however, the data are more scattered.

Discussion of Results

Magnetization of Tubular and Disc Specimens

The behavior of type II superconductors in long, thin-walled, tubular form has been described in detail by Kim and coworkers[7] following a theory proposed by Bean[11] which states that at high fields the diamagnetic behavior of these superconductors is due to persistent current induced within the superconductor. The state of magnetization of a tubular specimen is described by the expression

$$kw = \int_H^{H'} \frac{dB}{J(B)}, \tag{2}$$

where k is a geometric factor equal to 0.4π gauss-cm per ampere and w is the wall thickness of Nb_3Sn carrying the persistent current. The current density, J, is determined entirely by the local field, B; J has the distribution

$$J = \frac{\alpha}{B + B_0}, \tag{3}$$

where α and β_0 are constants characteristic of a given superconductor. Therefore, the knowledge of these constants alone enables one to describe the magnetization of a tubular specimen.

For a thin stack of discs, such as those used in this work, Equation (2) cannot be used with accuracy because the resulting cylinder is neither long nor thin walled. However, when the geometric factor k is allowed to vary with the dimensions of a stack, then a similar expression can be used with reasonable accuracy for the description of the present experimental results. This new variable geometric factor, g, can be approximated to a solenoid constant (in units of kilogauss per

[11] C. P. Bean, "Magnetization of Hard Superconductors," *Phys. Rev. Ltrs.*, Vol. 8, p. 250, 15 March 1962.

ampere), and its average value can be computed for a given stack of discs by established procedures.[12] With the assumption that B, and hence J, vary only radially and that only the axial field component, B_Z, is important, Equation (2) can be rewritten

$$2ngtw = \int_{H}^{H'} \frac{dB}{J(B)}, \tag{4}$$

where n is the number of discs and t is the average film thickness of Nb_3Sn. The quantity $2ngt$ increases with the number of discs from about 0.001 gauss-cm per ampere for 1 disc to a constant value of $0.4\pi\lambda$ gauss-cm per ampere for an infinitely long cylinder in which the packing factor is λ. Substituting Equation (3) into Equation (4) and performing the integration results in hyperbolas;

$$(H' + B_0)^2 - (H + B_0)^2 = \pm 4ngtw\alpha, \tag{5}$$

where the + sign is to be used with $H' > H > 0$ and the − sign for $H > H' > 0$. For $H > 0 > H'$ one obtains a circle;

$$(H + B_0)^2 + (H' + B_0)^2 = 4ngtw\alpha + 2B_0^2. \tag{6}$$

By letting H' or H equal zero in Equations (5) or (6), one obtains parabolas for the shielded and trapped field, which can be written in a linear form as

$$H_s = \frac{4ngtw}{H_s}\alpha - 2B_0 = 2\left(\frac{\alpha}{j} - B_0\right), \tag{7}$$

where j is the average current density of the superconductor in a given stack of discs. This expression can be used to determine the constants α and B_0 from experimental data by plotting H_s as a function of $2/j$. This has been done for the 8- and 20-ring discs (Figure 9) because the parabolic shape of H_s versus n curves in Figure 4 suggests that analytical treatment is possible. As one notes in Table II these constants for the 8-ring discs are well within the range of values reported in the literature, although B_0 tends to be on the high side. For the 20-ring

[12] R. W. Boom and R. S. Livingston, "Superconducting Solenoids," *Proc. I.R.E.*, Vol. 50, p. 274, March 1962.

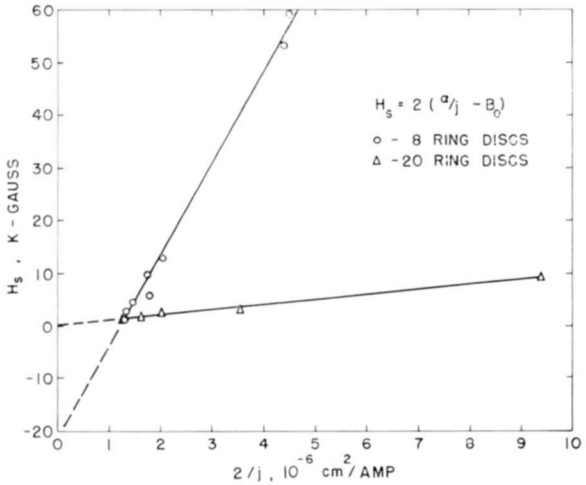

Fig. 9—Determination of α and B_0 from the shielded field as a function of stacking.

discs, α is smaller by a factor of 17 than for the 8-ring discs, although the superconducting material was the same. The very low value of B_0 compensates for the low value of α when a small number of discs is measured, in which case J_c is relatively high. The constants α and B_0 can be determined from an alternate form of Equation (5) as it is done for tubular specimens by Kim et al.[7] At low H the unusual flatness of the H versus H' curves obtained in the present work indicates that Equation (5) would yield very high values of B_0 (in some cases of the order of 40 kilogauss). A possible reason for this flatness is discussed later.

In Figure 4 one notes that the curves for the full discs, 1-ring discs and 4-ring discs depart from the parabolic shape predicted by Equation (7) after 1/2- and 2-disc stacking. It appears that at these points a mechanism sets in that prevents the attainment of the full value of the critical current throughout the stack. While the exact reason for this

Table II—α and B_0 for 8- and 20-Ring Discs

Disc Type	α kilogauss-amperes/cm²	B_0 kilogauss
8-ring	1.73×10^7	10.3
20-ring	9.66×10^5	—.013

breakdown is unknown, it is speculated that it is associated with the formation of a band of superconducting local currents within the disc walls in the wake of the current breakdown. This breakdown might arise because of the large width and, therefore, huge demagnetizing coefficient of the Nb_3Sn films. These local current ($I_{loc.}$) would flow at the expense of the transport currents ($I_{tr.}$) currents about the center hole as shown in Figure 10(a). The local currents result in two equal but opposite currents I_1 and I_2, Figure 10(b), hence these currents

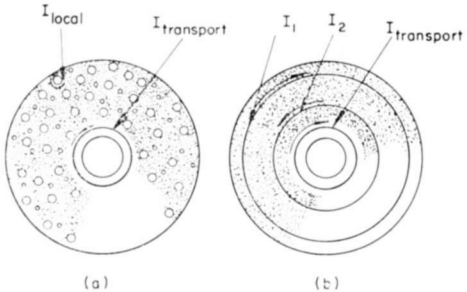

Fig. 10—Transport currents and local currents in 1-ring discs.

would be expected to contribute very little to field shielding or trapping as can be seen from the following approximate expression of H' for such a disc:

$$H' \approx H - 0.2\pi \left(\frac{I_1}{R_1} - \frac{I_2}{R_2} + \frac{I_t}{R_t} \right), \tag{8}$$

where R_1, R_2 and R_t are the mean radii of the regions of flow of the currents. Since $R_2 < R_1$, the quantity I_2/R_2 is slightly larger than I_1/R_1, hence the resulting contribution of these two currents to shielding is small but opposite in direction to I_t/R_t. This means that in the absence of the current I_t, the local currents would give rise to flux concentration. This situation might arise when a small sector of a disc suddenly becomes normal such as during a flux jump that destroys I_t but leaves local currents I_1 and I_2 essentially intact. Flux concentration suggestive of this mechanism was observed whenever a flux jump occurred with the 1- and 4-ring discs (see example of 1-ring disc in Figure 3(b)).

A breakdown in the transport current is also evident in the 1- and 4-ring discs whenever the area within the critical state envelope is crossed as indicated by the bulging in Figure 3(b). This breakdown

might be interpreted as the spreading of the local currents over large areas of the discs.

In the 8- and the 20-ring discs, such signs of the local currents as discussed above are missing; however, the existence of these currents might not be evident. A progressive subdivision of a disc into rings would tend to make the radii of I_1 and I_2 in each ring of similar magnitude and, hence, cancel out I_1/R_1 and I_2/R_2 from Equation (8). In the 8-ring discs the existence of appreciable local currents is doubtful because of the high value of α. However, with the 20-ring discs such currents might well exist in narrow bands near the numerous film edges, thereby making the effective cross-sectional area of Nb_3Sn much smaller than the actual area. Such bands of currents might arise either because of mechanical imperfections in the film or because of irregular magnetic gradients at the edges, possibly caused by the lack of alignment of these narrow rings into strata (see the 20-ring disc in Figure 1).

The drastic breakdown of the transport current observed with the 1-ring and 4-ring discs appears to be a function of the magnetization M. It is then of interest to consider whether there exists any disc geometry that is not susceptible to at least a partial breakdown. If not, then one would expect all disc geometries to show a greater breakdown in current at low fields where M is the greatest. The result of this effect would be a flat appearance of the H' versus H curves at low H, such as seen in the present experiments rather than the circular fat portion of the curves predicted by Equation (6) and evident with the tubular experiments.[7,13] An example of a pronounced and reproducible collapse in the low-field region of the critical-state envelope can be seen in Figure 11, which clearly shows the collapse occurring in the circular region $H > 0 > H'$ and $H' > 0 > H$. Therefore, the large value of B_0 obtained from the H versus H' curves from Equation (5) with the discs would be largely dependent on the specimen geometry and not so much on the material. It might be worth mentioning that even in the results on tubular specimens, Kim et al[7] show an increase in B_0 with wall thickness with similar materials. Thus, in order to keep α and B_0 as the critical constants of a given material, it would be necessary to change Equation (3) so as to include the specimen geometry effects. The new expression might have the form

$$J_c = \left(\frac{A_{\text{eff}}}{A}\right) \frac{\alpha}{B + B_0}, \tag{9}$$

[13] J. P. McEvoy, "Critical-State Phenomena and Flux-Jumping in Niobium Stannide," *RCA Review*, Vol. XXV, p. 533, Sept. 1964 (this issue).

where A is the total cross-sectional area and A_{eff} ($\leq A$) is the effective cross-sectional area of the superconductor. A_{eff}, in turn, could be a function of the demagnetizing coefficient (which is a function of specimen geometry), the magnetization, and the field.

The lack of symmetry of the critical state curves about the diagonal $H = H'$ (Figure 3b) can be accounted for, in part, by a partial breakdown of the critical current. Another factor contributing to the lack

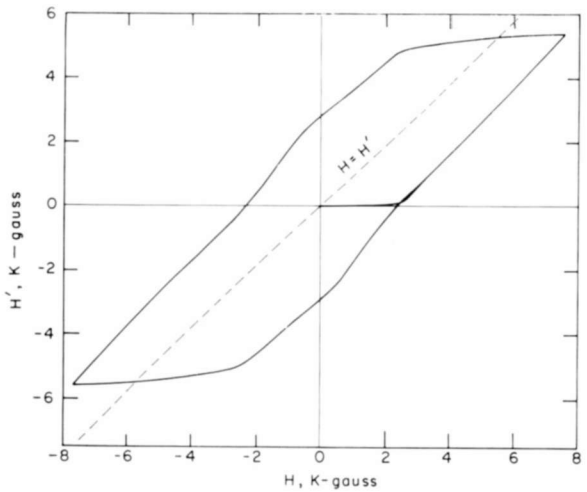

Fig. 11—Partial breakdown of the persistent current in a stack of 8-ring discs.

of symmetry, especially in short stacks, is that the geometric factor, g, of each individual ring in a given disc decreases appreciably with increasing radius. As the order of magnitudes of H and H' are inverted for the shielding and trapping cycles, it is reasonable to expect appreciable differences between the shielding and the trapping curves.

In the magnetization experiments, particularly with a thin stack of discs, H' changes slightly with H whenever the region within the critical state envelope is crossed (Figure 3b) although one might expect such cross-over lines to have zero slope on the basis of the flux conservation law.[14] It is possible for H' (the flux density) to change within this region, although the flux within the cylinder cavity remains constant for the same reason; this explains the field inhomogeneity in short solenoids.[12] The variation of H' within the critical-state region

[14] C. F. Hempstead, Y. B. Kim, and A. R. Strnad, "Inductive Behavior of Superconducting Magnets," *Jour. Appl. Phys.*, Vol. 34, p. 3226, 1963.

can be described approximately by the expression

$$H' = \frac{\frac{1}{2}(K-1)\,H + H_0}{1 + \frac{1}{2}(K-1)}, \tag{10}$$

which can be derived from the flux conservation law. In this expression K is the ratio of the maximum field of a solenoid at the inner winding and the field at its geometric center and H_0 is the average field in the cylinder when it enters the critical state envelope ($H_0 \approx H'$). It should be noted that when $K = 1$ (as with a long cylinder or a disc without a hole) $H' = H_0$ and the slope of the crossover line is zero, and when K becomes infinite (as with a ring of a large radius) $H' = H$ and the slope is unity. Because of the variation of J_c with H, K will change, thereby giving rise to nonlinearity of the crossover lines.

Flux Jumps

Recent theories and experiments indicate that when current flows through a type II superconductor in a transverse magnetic field thermal power dissipation takes place because of "flux creep".[15-17] Anderson and Kim[17] have shown that at a given temperature the power dissipation P is

$$P \propto J \exp\left\{\frac{\alpha}{\alpha_1}\right\}. \tag{11}$$

Here $\alpha \gg \alpha_1 \approx 10^{-2}\,\alpha_c$, where α_c is the critical value of α, as in Equation (3). Values of α significantly higher than α_c can be obtained when dH/dt is large. Therefore, Equation (11) also predicts a sharp rise in power dissipation in the superconductor with dH/dt. This power dissipation creates a rise in temperature that can cause parts or all of the superconductor to go normal. Anderson and Kim[17] derived an expression for the temperature rise, which can be rewritten to give explicitly the maximum allowable (critical) power density P_c as follows:

---

[15] Y. B. Kim, C. F. Hempstead, and A. R. Strnad, "Critical Persistent Currents in Hard Superconductors," *Phys. Rev. Ltrs.*, Vol. 9, p. 306, 1 Oct. 1962.

[16] P. W. Anderson, "Theory of Flux Creep in Hard Superconductors," *Phys. Rev. Ltrs.*, Vol. 9, p. 309, 1 Oct. 1962.

[17] P. W. Anderson and Y. B. Kim, "Hard Superconductivity: Theory of the Motion of Abrikasov Flux Lines," *Rev. Mod. Phys.*, Vol. 36, p. 39, Jan. 1964.

$$P_c \approx \frac{\kappa}{r^2} 10^{-3} T. \tag{12}$$

Here κ is the thermal conductivity and r is the size of the region of the specimen thermally affected. Thus, by taking r as the film thickness, McEvoy[13] estimates that for vapor-deposited Nb_3Sn tubular specimens with $r = 10^{-2}$ cm film thickness and with values of κ determined by Cody and Cohen,[18] $P_c \approx 0.1$ watt/cm^3. For the present discs, where $r = 2.25 \times 10^{-4}$ cm, one obtains $P_c \approx 40$ watts/cm^3. This drastic increase of P_c accounts for the vastly improved stability of the discs as compared to tubular specimens with respect to flux jumps. This prediction presupposes that the heat from each disc in a stack is removed by some efficient process.

Although Equation (12) also predicts an increase in stability with narrower rings, it is believed that the observed increase in stability is due to more etch lines, which diminish the ease of propagation of normal regions.

As predicted by Equation (11), P increases with J. This was borne out by the observed occurrence of flux jumping in a stack of 8 discs of the 8-ring geometry having a high J, and the absence of flux jumping at similar dH/dT with similar stacks of discs with other ring geometries having low J.

The experiment with a single disc showing progressively higher range of field in which flux jumps occur with increasing dH/dt (Figure 8(a,b)) qualitatively substantiates Equation (11). Although at higher H the quantity M_+ (and, hence, J) decreases, P can increase because α/α_1 increases with dH/dt, giving rise to flux jumps.

The result given by Equation (1), which represents the flux stability boundary, also strongly suggests that flux jumps are thermally activated because it is implied that

$$M \frac{dH}{dt} \propto JE = P_c.$$

Equation (1) also implies that at high fields, higher levels of power dissipation can be tolerated.

The increased tendency to flux jumping with thicker stacks can be understood by referring to Equation (12) where P_c decreases rapidly with increasing thickness. P_c would rapidly become too low were it

[18] G. D. Cody and R. W. Cohen, "Thermal Conductivity of Nb_3Sn," *Rev. Mod. Phys.*, Vol. 36, p. 121, Jan. 1964.

not for the high thermal conductivity of copper, which is greater by a factor of 10^4 than that of Nb_3Sn.

ACKNOWLEDGMENTS

The author wishes to acknowledge F. D. Rosi and G. D. Cody for their constructive suggestions in the discussion of the results, and G. Riddle, R. Filson, and S. Miszkowski for their technical assistance. The author is grateful to J. Fakan of NASA Lewis Research Center and to Y. B. Kim of Bell Telephone Laboratories for the use of their field magnets and their kind assistance with the high-field measurements.

ELECTROMAGNETIC PERFORMANCE OF NIOBIUM-STANNIDE RIBBON*

BY

H. C. SCHINDLER AND F. R. NYMAN

RCA Electronic Components and Devices,
Princeton, N. J.

Summary—*The degree of electromagnetic stability experienced with niobium-stannide ribbon is a function of the processing. Unstable or partially stable ribbon can be stabilized by electroplating the surface with copper at low plating-current densities. The current-carrying capacity, J, of copper-plated Nb_3Sn ribbon can be expressed as a function of the transverse magnetic field, H, by $J = \alpha/(B_0 + H)$, where $\alpha = 30 \times 10^6$ kilogauss-amperes per square centimeter and $B_0 = -7$ kilogauss. The performance of a magnet wound with niobium-stannide ribbon can be predicted from the critical data of the ribbon material. Solenoids wound with this ribbon have generated fields of 107 kilogauss in a one-inch bore.*

INTRODUCTION

A HIGH-TEMPERATURE gas-phase process for depositing single-phase superconducting niobium stannide, Nb_3Sn, continuously on platinum wire or ribbon has been developed at the RCA Laboratories.† The Nb_3Sn is formed in a gaseous-phase reduction atmosphere from the metal chlorides, according to the following basic reactions:

$$Nb + 2Cl_2 \xrightarrow{\Delta} NbCl_4 \tag{1}$$

$$Sn + Cl_2 \xrightarrow{\Delta} SnCl_2 \tag{2}$$

$$3\,NbCl_4 + SnCl_2 + 7H_2 \rightleftharpoons Nb_3Sn + 14HCl. \tag{3}$$

The apparatus used for this process and a detailed chemical description of the process are discussed in a paper by Hanak, Cullen, and Strater.[1]

In the original experimental vapor-deposition apparatus, niobium

---

* In addition to the RCA-supported effort, an evaluation study has been conducted by RCA Electronic Components and Devices for NASA under Contract NAS 3-2520 to determine the feasibility of designing high-field, large-bore magnets. Test data obtained under this contract provide extensive background for this paper.

† Sponsored in part under Contract No. AF33(616)-6405 Physics Lab., A.S.D. Wright-Patterson Air Force Base, (Report ASD-TDR-62-269), 1962.

[1] J. J. Hanak, K. Strater, and G. W. Cullen, "Preparation and Properties of Vapor-Deposited Niobium Stannide," *RCA Review*, Vol. XXV, p. 342, Sept. 1964 (this issue).

stannide was deposited on a platinum substrate approximately 18 mils wide and 2 mils thick. Physical properties of this material have been published;[2] current densities in the superconducting layer as high as 7×10^5 amperes per square centimeter at 90 kilogauss were attained. However, the prohibitive cost of platinum and its low strength and high ductility make its use impractical. After much experimentation, a relatively inexpensive stainless-steel alloy possessing high tensile strength and suitable thermal-expansion characteristics was selected for use as a substrate. In addition, the ribbon width was increased to

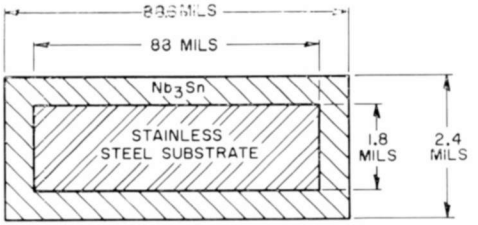

Fig. 1—Nb_3Sn ribbon cross section.

89 mils to improve equipment and process efficiencies and to increase the magnet packing factor. Niobium-tin-coated ribbon 89 mils wide and 2.4 mils thick was found to be most suitable in terms of both processing and winding flexibility for spiral-wound (module) and layer-wound coils. A cross section of this ribbon, which has been selected as a standard, is shown in Figure 1.

This paper discusses the physical and electromagnetic properties of vapor-deposited Nb_3Sn on a stainless-steel substrate. Included in the discussion are test methods used to measure the critical current as a function of transverse magnetic field, the concept of relative electromagnetic performance stability, techniques used to stabilize the electromagnetic performance, and physical properties of the Nb_3Sn ribbon.

Testing Techniques

Tests to evaluate the critical-field–critical-current (H_c-I_c) characteristics of Nb_3Sn ribbon are conducted on short samples approximately two centimeters long. To obtain the most critical evaluation, the ribbon is oriented with its width perpendicular to the magnetic field. Transition from the superconducting to the normal state is recorded when the

[2] J. J. Hanak, "Vapor Deposition of Nb_3Sn," *Metallurgy of Advanced Electronic Materials*, p. 161, Vol. 19, G. E. Brock, ed., Interscience, Inc., N. Y., 1961.

voltage drop across the sample exceeds five microvolts. The superconducting test sample is copper plated and soldered to the normal conducting copper power-supply busses with a 60/40 lead-tin solder to minimize the heat generated at the contact surfaces between the test sample and the test busses. Contact resistances of less than three millimicrohms have been observed. Because the current-carrying capacity of the ribbon exceeds several hundred amperes in transverse magnetic fields ranging from zero to 15 kilogauss, it is necessary to place shunts in parallel with the test samples to prevent destruction of the samples when the transition to normal conduction occurs.

Electromagnetic Performance of Nb_3Sn Deposits

According to Kim *et al*,[3] and as modified by Cody *et al*,[4] the performance of a type III superconductor can be described by the following expression for current-carrying capacity J_c:

$$J_c = \frac{\alpha}{B_0 + H \sin \theta} \text{ amperes/cm}^2, \tag{4}$$

where α is a material constant proportional to the density of pinning centers, B_0 is a measure of current density when the field and sample-current directions are parallel, θ is the angle between the sample-current and field directions, and H is the field (independent variable). The electromagnetic performance of certain types of vapor-deposited niobium-stannide ribbon is in agreement with the above expression; an example is shown in Figure 2. The value of α for this ribbon is 6.6 kilogauss-amperes per square centimeter; B_0 is 6.6 kilogauss. The superconducting-to-normal transition points were obtained in the order indicated by the lower-case letters in the figure. The arrows indicate the manner of testing. For example, in test (a) the current was first set to 60 amperes in a zero transverse magnetic field. With the current held constant at this value, the field was increased to 13 kilogauss. At 13 kilogauss, the transverse magnetic field was maintained constant and the current was increased until the sample "went normal." In test (b), the magnetic field was set to 12.5 kilogauss, and the current was increased until the sample went normal. The complete H_c-I_c characteristic of the sample was obtained in this manner. Niobium-stannide ribbon that satisfies Equation (4) will henceforth be identified as stable Nb_3Sn ribbon.

---

[3] Y. P. Kim, C. F. Hempstead, and A. R. Strnad, "Critical Persistent Current in Hard Superconductors," *Phys. Rev. Ltrs.*, Vol. 9, p. 306, Oct. 1962.

[4] G. D. Cody, G. W. Cullen, and J. P. McEvoy, Jr., "Field and Angular Dependence of Critical Currents in Nb_3Sn II," *Revs. Mod. Phys.*, Vol. 36, p. 65, Jan. 1964.

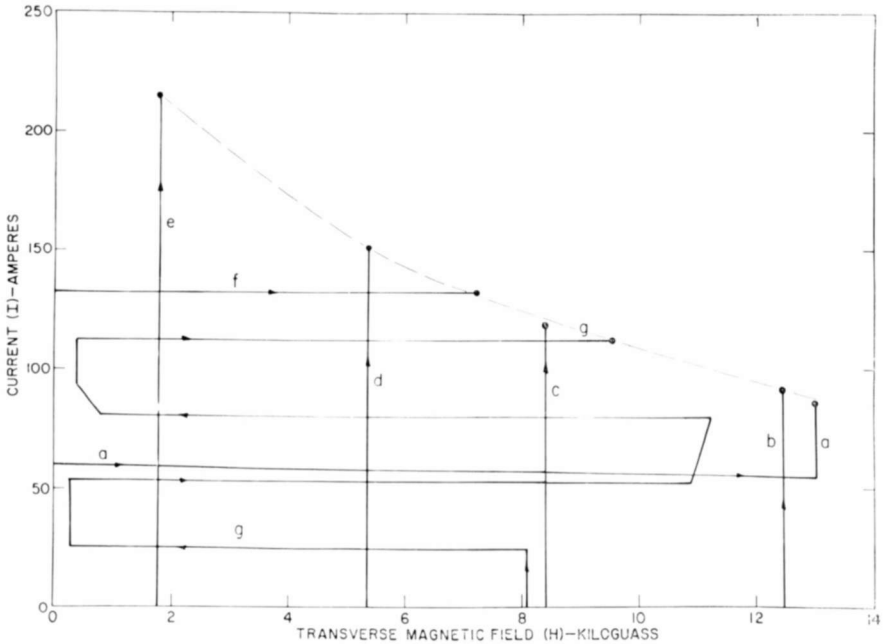

Fig. 2—Critical current versus magnetic field for stable Nb_3Sn ribbon.

If the deposition conditions of the ribbon are changed, an entirely different Nb_3Sn electromagnetic performance can be obtained, as shown in Figure 3. At magnetic-field values above 28 kilogauss, the H_c-I_c characteristic satisfies Equation (4) whether the current or the field is applied first. Below the 28-kilogauss value, however, the charac-

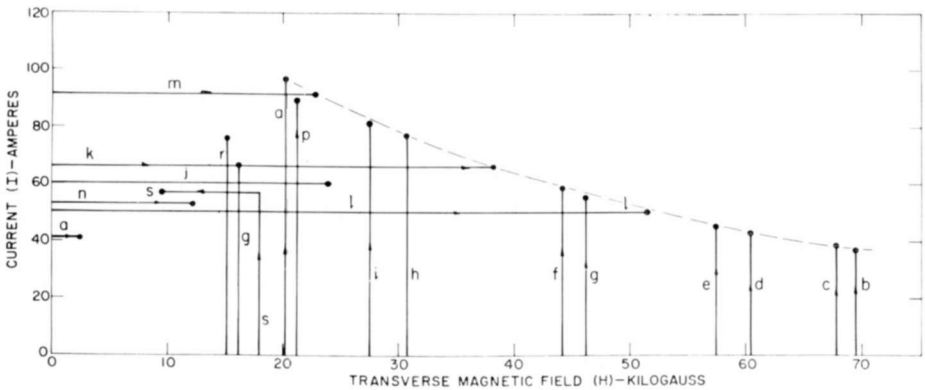

Fig. 3—Critical current versus magnetic field for partially stable Nb_3Sn ribbon.

teristic deviates from Equation (4) and the superconducting-to-normal transition occurs in a random manner as shown by the test runs s, j, n, r, and g. This behavior can be partially explained in terms of a recent theory of P. W. Anderson[5] which assumes that the flux lines are pinned to the crystal structure by lattice defects and stressed by the Lorentz force, $\mathbf{J} \times \mathbf{B}$. When this force exceeds a critical value, the flux lines

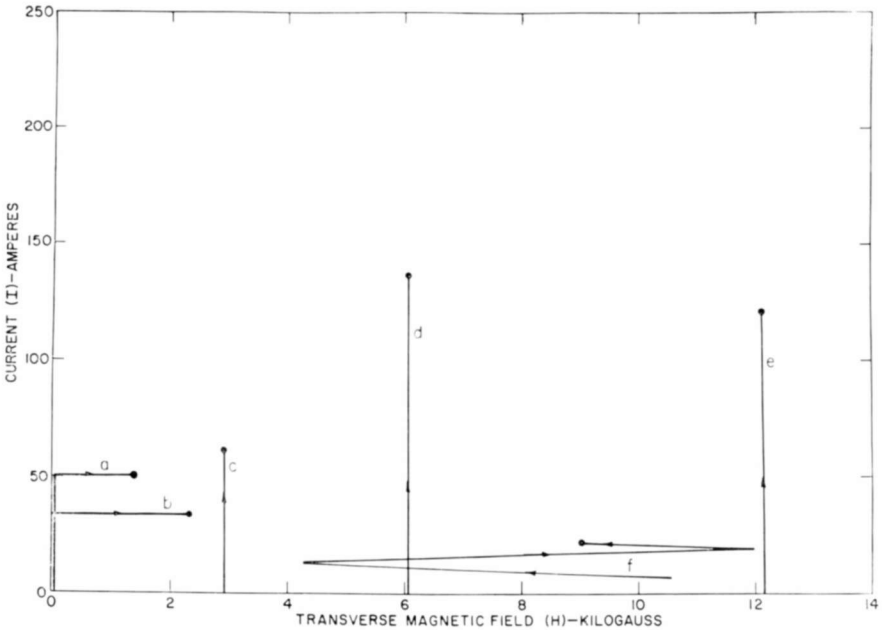

Fig. 4—Critical current versus magnetic field for unstable Nb_3Sn ribbon.

begin to creep; subsequently this creeping becomes a turbulent flow and the catastrophic breakdown of the flux structure that follows causes the sample to become normal. The power dissipated during the flux motion is inversely proportional to the applied transverse magnetic field.[6] Above a critical power level, catastrophic disintegration of the flux structure will occur. Consequently, increasing stability is anticipated for the same material as the field is increased. Material that is stable only above a certain transverse magnetic field is referred to as partially stable. This region of instability may be from zero to only a few kilogauss, or it may extend to 50 or 60 kilogauss.

---

[5] P. W. Anderson, "Theory of Flux Creep in Hard Superconductors," *Phys. Rev. Ltrs.*, Vol. 9, p. 309, 1 Oct. 1962.

[6] P. W. Anderson and Y. B. Kim, "Hard Superconductivity: Theory of the Motion of Abrikosov Flux Lines," *Rev. Mod. Phys.*, Vol. 36, p. 39, Jan. 1964.

An example of niobium-stannide ribbon that exhibits extreme instability up to 12 kilogauss transverse field is shown in Figure 4. Extensive testing in the regions of instability has shown that the points where the superconducting-to-normal transition occur are random in nature (i.e., they do not satisfy Equation (4)) and depend to some extent on the test conditions, such as rate of current and field application.

Table I is a compilation of the results of short-sample tests on several unstable samples. Numerous unstable samples were subjected

Table I

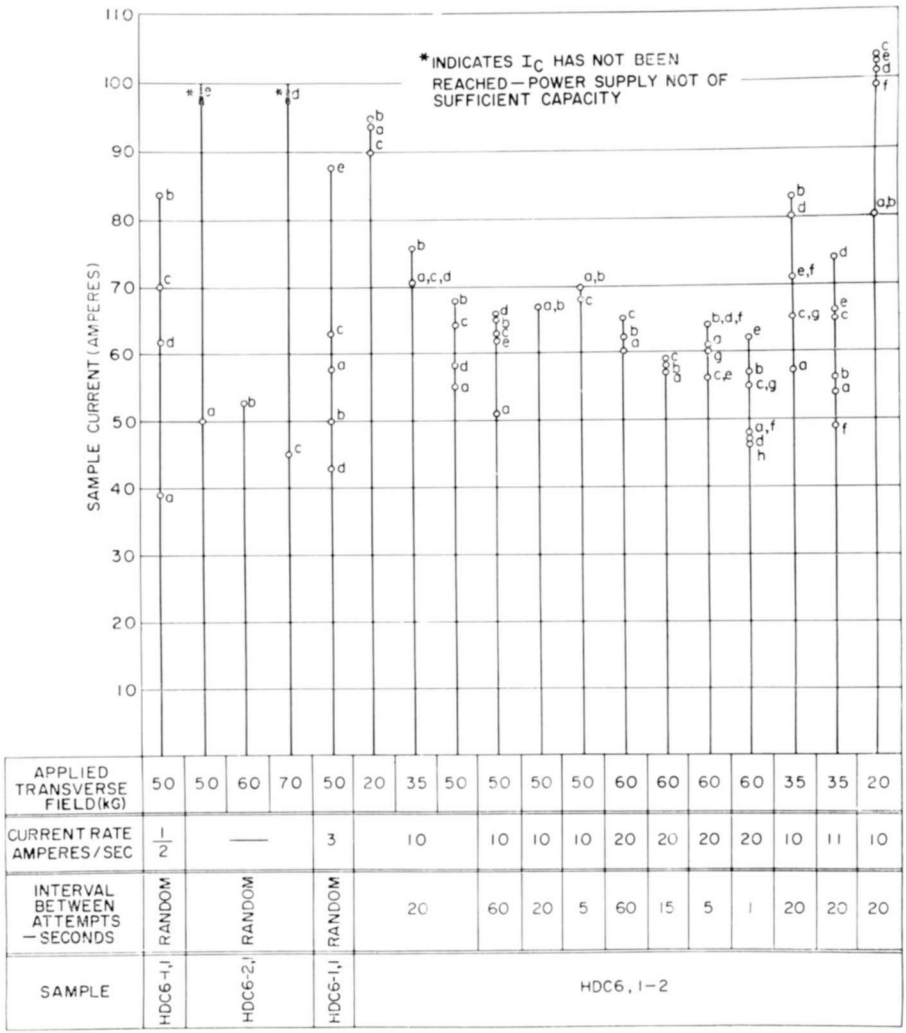

to different rates of current increase at constant field and different time intervals between tests. For example, a sample subjected to a 50-kilogauss background field with a current-rate increase of 1/2 ampere per second and random intervals between tests became normal at 38, 62, 70, and 82 amperes. Similarly, different background transverse magnetic fields with short and long time intervals between tests also showed this completely random behavior. From these tests, the following conclusions can be drawn:

1. At any one field, successive critical-current tests at a constant rate of current rise can yield a scatter in which the highest critical current is as much as twice the value of the lowest. There is no obvious hysteresis or dependence upon history. Several attempts to obtain consistent critical currents by raising the sample above the critical temperature between tests did not change the random behavior.
2. Variation of the rate of current application at any one field adds to the scatter effect.
3. The interval of time between successive critical-current tests is not significant on short samples for a time period as short as five seconds after the sample becomes normal.

The correlation between the performance of straight short samples and of coils is discussed in a paper by Schrader and Kolondra.[7]

Techniques for Stabilizing Bare Unstable Nb_3Sn Deposits

The stability of bare Nb_3Sn ribbon can be increased considerably by the use of copper plating. There are two possible explanations for this improvement:[8] (1) the copper may act as a sink for eddy currents, or (2) the plating may decrease the superconducting-to-normal transition velocity. The shunting effect and the fact that the plating acts as a transformer secondary also afford the added advantage of coil protection. The superconducting-to-normal transition velocity, V, in a superconductor has been treated both experimentally and theoretically.[9] A simplified expression for this velocity is given by[10]

---

[7] E. R. Schrader and F. Kolondra, "Analysis of Degradation Effects in Superconducting Niobium-Stannide Solenoids," *RCA Review*, Vol. XXV, p. 582, Sept. 1964 (this issue).

[8] Z. J. Stekly, "The Feasibility of Large Superconducting Coils," Avco Corp., Research Report 160, Sept. 1963.

[9] W. H. Cherry and J. I. Gittleman, "Thermal and Electrodynamic Aspects of Superconductive Transition Process," *Solid State Electronics*, Vol. 1, p. 287, Pergamon Press, 1960.

[10] Z. J. Stekly, "Theoretical and Experimental Study of an Unprotected Superconducting Coil Going Normal," *Advances in Cryogenic Engineering*, Vol. 8, K. D. Timmerhouse, ed., Plenum Press, 1963, p. 585.

$$V = \frac{j}{\gamma C_p} \left[\frac{k}{\sigma \, (T_c - T_0)} \right]^{1/2} \tag{5}$$

where C_p is the specific heat, k is the thermal conductivity, γ is the density, σ is the conductivity of the normal state, $T_c - T_0$ is the difference between the critical temperature and the ambient temperature, and j is the current density. These properties are all effective or averaged quantities. Equation (5) indicates that the transition velocity can readily be modified by changes in the resistivity of the metallic coating on the wire.

The resistivity of a normal metal containing impurity atoms and lattice defects is

$$\rho = \rho_i + \rho_l \tag{6}$$

where ρ_l is the resistivity caused by the thermal motion of the lattice and ρ_i is the resistivity caused by scattering waves, impurity atoms, and lattice imperfections. At low temperatures ρ_l approaches zero, and $\rho = \rho_i$. At room temperature ρ_l is the dominant term.

An indication of the impurity and imperfections of the plated metal can be obtained from the following ratio:

$$\frac{\rho_{\text{room}}}{\rho_{\text{liquid helium}}} \approx \frac{\rho_l}{\rho_i}. \tag{7}$$

Copper plating is used to stabilize both unstable and partially unstable Nb_3Sn ribbon. The resistivity ρ and the resistivity ratio ρ_l/ρ_i of copper-plated ribbon are strongly dependent upon the type of plating and the plating rate. The lowest resistivity of the plated metal and also the largest resistivity ratio is obtained from very pure plating solutions applied at very low plating-current densities. Use of the low current density helps in obtaining both a purer copper and a more regular crystal growth. Variation of the plating conditions imparts various degrees of stability to the bare Nb_3Sn.

Figure 5 shows the H_c-I_c characteristics of inherently unstable Nb_3Sn before plating. Figure 6 shows the partial stabilizing effect of high-current-density copper plating, and Figure 7 shows the complete stabilizing effect of low-current-density copper plating. When the short-sample Nb_3Sn ribbon was plated with copper at a low current density, it remained superconducting at fields from 0 to 13 kilogauss and at currents from 0 to 350 amperes when swept at a constant current in a changing transverse magnetic field or when the current was in-

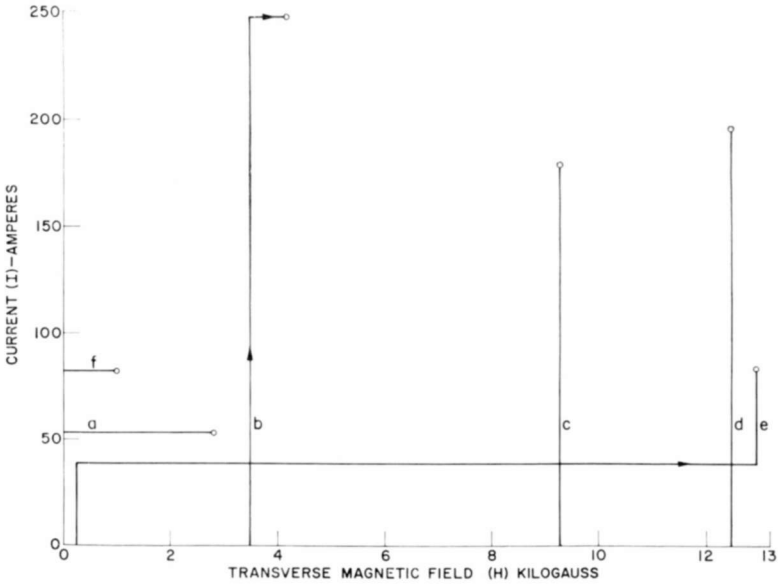

Fig. 5—Critical current versus magnetic field for unplated unstable Nb_3Sn Ribbon.

creased in a constant field. In contrast, when the ribbon plated at higher current densities was subjected to the same tests, it became normal considerably below the inherent H_c-I_c curve for the uncoated Nb_3Sn ribbon.

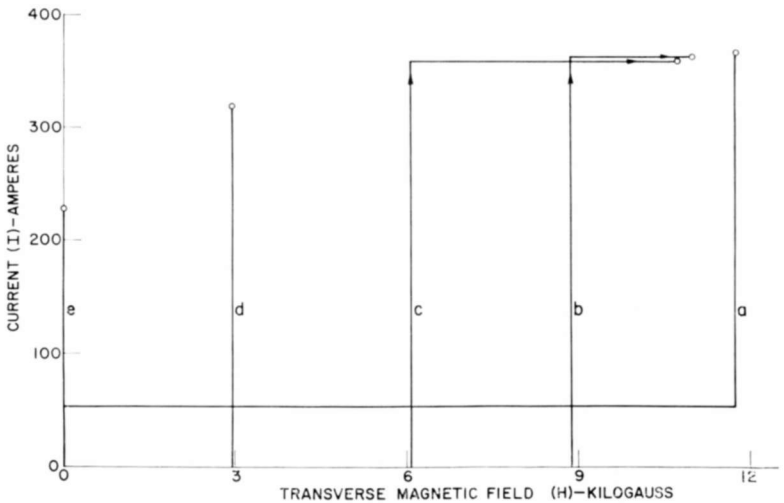

Fig. 6—Critical current versus magnetic field for high-current-density copper-plated unstable Nb_3Sn ribbon.

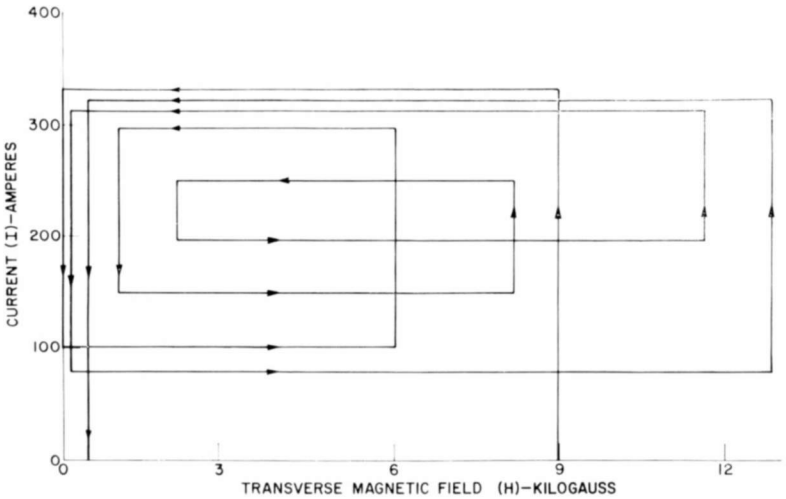

Fig. 7—Critical current versus magnetic field for low-current-density copper-plated unstable Nb_3Sn ribbon.

Extensive evaluation of numerous plating parameters indicates that the degree of stability achieved by plating is a function of the type and quality of the plating material. This dependence is most evident at low fields and for unstable Nb_3Sn, as shown by the spread of the curves in Figure 8. Areas B, C, and D represent the entire region (actually an

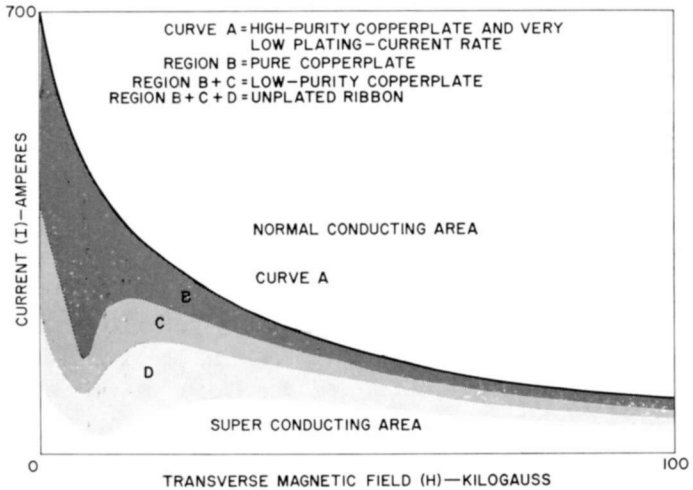

Fig. 8—Stabilizing effect of plating on inherently unstable Nb_3Sn ribbon.

infinite number of characteristic curves) in which the transition from super-to-normal conduction can occur. If the ribbon is copper plated, the region of instability becomes narrower and can be represented by regions B and C. If the purity of the plated metal is increased, the instability region is further decreased and is represented by region B. With very low plating rates and high-purity copper deposits, the instability region disappears completely and the thermodynamic H_c-I_c characteristic is represented by curve A.

Copper-plating has very little effect on the stability of inherently stable Nb_3Sn. The critical characteristic curves for this material lie in a much narrower, monotonic band approximately halfway between the boundaries of the shaded area in Figure 8.

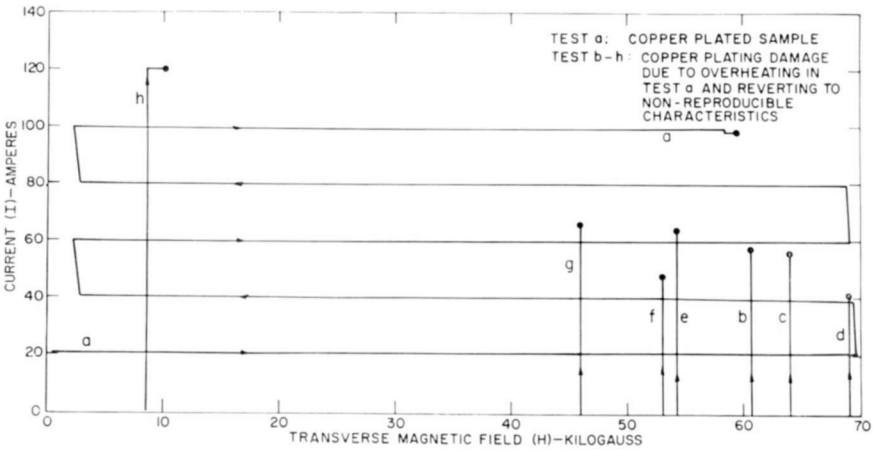

Fig. 9—Characteristics of copper-plated and unplated unstable Nb_3Sn ribbon.

Figure 9 shows the results of tests on unstable Nb_3Sn material with and without copper plating. The copper-plated sample showed no evidence of instability when swept by the changing magnetic fields and increasing currents shown by path "a". However, after the sample becomes normal at 100 amperes and 60 kilogauss, the plating was visibly melted off in a 1/32-inch ring around the sample. Further testing yielded the typically unstable pattern shown by paths "b" through "h".

By increasing the stability of the Nb_3Sn, the realized current-carrying capacity of the Nb_3Sn layer is increased. A typical sample of plated Nb_3Sn exhibits current densities two to three times greater than those of similar unplated ribbon. Data gathered from many tests and several laboratories have been combined to form the composite H_c-I_c curve for a straight short-sample of copper-plated Nb_3Sn ribbon shown

in Figure 10. When the expression for current density ($J = \alpha/(B_0 + H \sin \theta)$)$^{1.4}$ is applied to the H_c-I_c curve for this Nb_3Sn ribbon, the value of α is 30×10^6 kilogauss-amperes per square centimeter, and B_0 is —7 kilogauss.

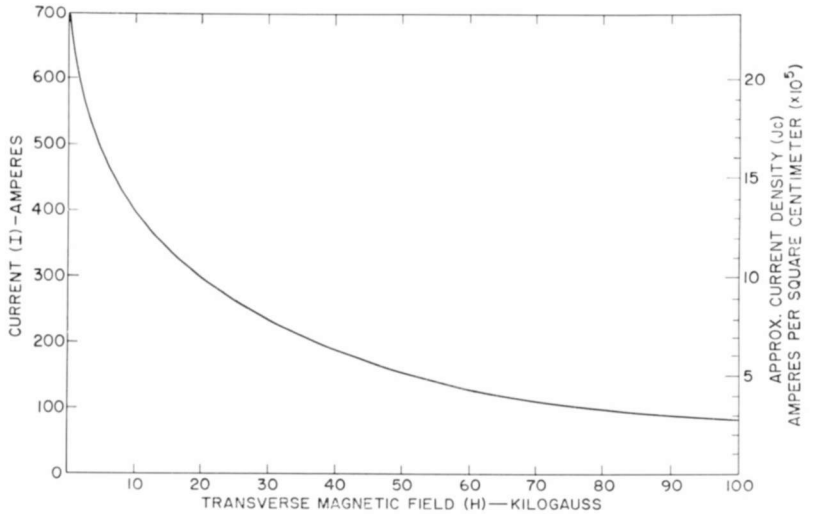

Fig. 10—Composite characteristic of short-sample copper-plated Nb_3Sn ribbon.

Physical Properties of Plated Ribbon

When Nb_3Sn ribbon is continuously electroplated with copper to enhance stability, the ribbon is flexible and can be wound over diameters as small as 3/8 inch with no deleterious effects on its superconductive properties. Nb_3Sn ribbon is sufficiently flexible that it can be readily wound, unwound, and rewound into different configurations. Tensile tests at liquid-helium temperatures have shown that the copper-plated Nb_3Sn ribbon remains superconductive up to a tensile stress of 115,000 psi.

Ribbon lengths in excess of 1,000 meters have been produced with negligible variation in electromagnetic performance from beginning to end. Solenoids wound with this ribbon have generated fields of 107 kilogauss in a one-inch bore.

Acknowledgment

The authors acknowledge the technical advice of a number of staff scientists in a group headed by F. D. Rosi at RCA Laboratories. They also wish to thank S. Husni for suggestions and technical assistance in plating the Nb_3Sn ribbon.

ANALYSIS OF DEGRADATION EFFECTS IN SUPERCONDUCTIVE NIOBIUM STANNIDE SOLENOIDS*

By

E. R. Schrader and F. Kolondra

RCA Special Electronic Components Division
Princeton, N. J.

Summary—*The results of extensive testing of superconductive coils wound with vapor-deposited Nb_3Sn ribbon have confirmed the theory that the low-field instabilities inherent in the superconductor are primarily responsible for the "degradation" phenomenon. Both short-sample and coil characteristics are discussed. Various means of minimizing and eliminating the degradation effect are suggested, with special emphasis on the use of magnetic fields for stabilization of the superconductor. These principles are illustrated by a description of a 107-kilogauss, 1-inch-bore all-Nb_3Sn magnet.*

Introduction

EARLY WORK WITH high-field solenoids in the last several years was described at the MIT Conference on High Magnetic Fields in December 1961.[1] Following this Conference, much data on coils wound with niobium–zirconium (Nb-Zr) was generated and eventually the testing of coils using various forms of niobium stannide (Nb_3Sn) was initiated. The development of the niobium-stannide vapor-deposition process[2] on a high-strength ribbon substrate[3] has resulted in a superconductive material that is particularly suitable for the winding of high-field (>100 kilogauss) solenoids. This paper describes studies of magnet coils in which the vapor-deposited Nb_3Sn material was wound and tested in a variety of configurations.

The Nb_3Sn ribbon, which is 0.090 inch wide and 0.003 inch thick, consists of a stainless-steel substrate, a 0.0002 to 0.0003-inch coating

---

* In addition to the RCA-supported effort, an evaluation study has been conducted by RCA Electronic Components and Devices for NASA under Contracts NAS 3-2520 and NAS 3-5240 to determine the feasibility of designing high-field large-bore magnets. Test data obtained under these contracts provide extensive background for this paper.

[1] *Proceedings of the International Conference on High Magnetic Fields*, MIT, John Wiley and Sons, Inc., New York, N. Y., 1961.

[2] J. J. Hanak, *Metallurgy of Advanced Electronic Materials*, G. E. Brock, Editor, Interscience. Inc., New York, N. Y., 1963, p. 161.

[3] H. C. Schindler and F. R. Nyman. "Electromagnetic Performance of Niobium Stannide," *RCA Review*, Vol. XXV, p. 570, Sept. 1964 (this issue).

of Nb_3Sn, and an equal thickness of copper or silver. Solenoid currents of approximately 85 amperes at fields of 100 kilogauss were achieved with this superconductive ribbon. This work has led to practical high-field (>100 kilogauss) magnets. Solenoids may be wound without special ribbon-handling or tension techniques. The Nb_3Sn ribbon is superconductive when cooled below its critical temperature and requires no heat treatment before or after coil winding.[3]

It was determined that coil "degradation" (defined as the difference between the critical current values for a short sample and for a coil-wound specimen divided by the short-sample value) is not a degradation of high-field performance but rather is caused in large part by instabilities apparently inherent to Nb_3Sn at low magnetic fields. Modification or control of these instabilities can be accomplished to different degrees by varying the Nb_3Sn deposition process or the plating and coil-winding techniques. The application of these principles was demonstrated on both a 92-kilogauss, 1/2-inch-bore solenoid[4] and a 107-kilogauss, 1-inch bore solenoid. The latter coil is described in this paper.

Superconductive Degradation—Coils and Short Samples

Ideally, a superconductor will revert to the normal state when the critical current (I_c), critical magnetic field (H_c), or critical temperature (T_c) is reached. With I_c, H_c and T_c known, it might be presumed that the performance characteristics of a superconductive coil would be predictable. During the early work on superconductive magnets, it had generally been assumed that the critical value of current and magnetic field for solenoids could be uniquely determined from measurements of I_c on short samples (2 to 3 centimeters long) mounted transverse to an externally applied magnetic field. Actually, critical currents for coils were found to be significantly lower than those expected from H_c-I_c measurements made on short samples. This apparent degradation (compared at the maximum magnetic field (H_{max}) at the solenoid windings) became more severe as coil size increased, and it appeared, therefore, that this degradation would pose a serious barrier to the development of large-volume, high-field superconductive magnets.

Early hopes that superconductive coils wound with Nb_3Sn would not exhibit the same degradation effects reported for Nb-Zr coils stemmed from the limited data then available on Nb_3Sn. Unplated Nb_3Sn ribbon, spirally wound into "pies" 0.150-inch wide (ribbon width 0.090-inch plus insulating discs) with an inner diameter of two inches

[4] E. R. Schrader, N. S. Freedman, J. C. Fakan, "High-Field Nb_3Sn Superconducting Magnets by Magnetic-Field Stabilization," *Appl. Phys. Ltrs.*, Vol. 4, p. 105, 1964.

and an outer diameter of three inches were tested. Instead of developing the predicted 25 kilogauss, they degraded to the point where it was even difficult to develop fields greater than eight kilogauss in a series-connected stack of six pies. Additional pies series-connected to the stack further reduced the critical current. Later experiments with pies of other geometries that were wound with copper-plated Nb_3Sn produced higher fields (19 kilogauss with eight pies 2-inch inside diameter, 5-inch outside diameter stacked together), but showed a trend in degradation similar to that for the unplated material. In such stacks of pies, coil critical currents were as low as 30 percent of those predicted from short-sample measurements. No simple relationship of coil degradation to coil geometry was found to correlate with test results; furthermore, it appeared unlikely that the observed solenoid limitations were related to H_{max} of the windings. Elsewhere, it had been reported that niobium–zirconium solenoids can go normal with the transition originating in a region within the coil that is not at the maximum field developed by the coil.[5,6]

Several models (Montgomery,[7] Chandrasekhar and Hulm[8], Gauster and Coffey[9]) have been proposed to explain the observed degradation of coils based upon diamagnetic currents that are induced in the turns of a superconductive coil as the magnetic field changes in the windings.

In most treatments of coil degradation to date, performance comparisons are made with respect to short-sample results, with the latter yielding the highest critical currents. Likewise, it was observed that the measured critical field and current characteristics of short samples of Nb-Zr also depend upon both rate and sequence of field and current application. A faster current rate resulted in a lower critical current. A preset current and swept magnetic field yielded a lower critical current than preset field with varying current. This variability of results on short samples was used by Rosner and Schadler[10] to predict

---

[5] H. Riemersma, J. K. Hulm, and B. S. Chandrasekhar, "Flux Jumping and Degradation in Superconducting Solenoids," Sci. Paper 63-128-280-P4, Westinghouse Research Labs., July 25, 1963.

[6] Z. J. J. Stekly, "The Feasibility of Large Superconducting Coils," Res. Report 160, Avco-Everett Res. Lab., Avco Corp., Sept. 1963.

[7] D. B. Montgomery, "Current-Carrying Capacity of Superconducting Nb-Zr Solenoids," *Appl. Phys. Ltrs.*, Vol. 1 (2), p. 41, 1 Oct. 1962.

[8] B. S. Chandrasekhar and J. K. Hulm, "Current-Carrying Capacity of High-Field Superconducting Solenoids," *Appl. Phys. Ltrs.*, Vol. 2, p. 43, Jan. 1963.

[9] W. F. Gauster and D. L. Coffey, "Current-Carrying Capacity and Transition State of Superconducting Solenoids," Semi-Annual Progress Report, Oak Ridge National Laboratory, Period Ending April 30, 1963, p. 84.

[10] C. H. Rosner and H. W. Schadler, "Relating Measurements on Short Superconducting Wires to Solenoid Performance," *Jour. Appl. Phys.*, Vol. 34, p. 2107, July 1963.

the critical current of Nb-Zr coils. There is a complicating factor due to the "training" effects of Nb-Zr coils; such effects have not been detected in coils wound with vapor-deposited Nb_3Sn. Although the training effect makes the analysis of degradation in Nb-Zr coils more difficult, there is no doubt that many of the effects described in this paper for vapor-deposited Nb_3Sn also apply to Nb-Zr.[11] If maximum critical current is the point of reference, then short samples also exhibit degradation when the measuring conditions are sufficiently severe.

The experimental results that led to the conclusion that short samples exhibit degradation are given in another paper.[3] It is pertinent to summarize some of these results, many of which were obtained from tests in the 4-inch-bore copper magnet at the NASA Lewis Research Center. Short samples of vapor-deposited Nb_3Sn ribbon, approximately four centimeters long and electroplated to permit contact to be made to current and voltage lead points, were mounted on probes for testing transverse to the applied background magnetic field. With varying sequence of background field and sample current application, a general set of patterns appeared in the critical-field–critical-current plots for each sample. Some samples showed good stability, so that the critical characteristics lay on a smooth monotonic curve and were substantially independent of the rate or sequence of testing. These samples were termed "reproducible" or "stable." When short samples of this ribbon were copper plated to a thickness equivalent to that of the Nb_3Sn layer (0.0002 to 0.0003 inch), most tests revealed a moderate (up to 50 percent) increase in the critical currents at all fields. Critical currents of small coils wound from this copper-plated stable Nb_3Sn ribbon were degraded, but to a lesser degree than coils wound with unstable Nb_3Sn.

Critical values for unstable material are very dependent upon rate and upon the sequence of testing. Varying magnetic field with preset current, particularly in the region where the applied magnetic field is low (0 to 10 kilogauss), is the most severe condition of testing and yields the lowest critical currents. A typical pattern shows severe instability with swept fields in the low-field region, with some approach to more stable behavior at the higher region approaching 70 kilogauss. On the other hand, in short-sample tests with preset fields and increasing current, observed critical current values are higher at all fields, with the greatest difference in the low-field region.

Using the most severe test conditions (preset current and varying applied fields), idealized H_c-I_c plots for the various types of stable to

[11] "Investigation of Current Degradation Phenomenon in Superconducting Solenoids," Monthly Technical Reports, Contract NAS 8-5356, June 1963—March 1964.

unstable Nb_3Sn are shown in Figure 1. Stable short samples show a monotonically decreasing dependence of critical current on magnetic field (curve "a"). The most unstable short samples (curve "d") attain higher currents at high fields, but the severe instabilities at the lower fields result in a dip in the H_c-I_c curves. Thus the expected currents are not attained at low magnetic fields. An evaluation of stability is as important as is the knowledge of the highest possible superconducting-to-normal transition of fields and currents.

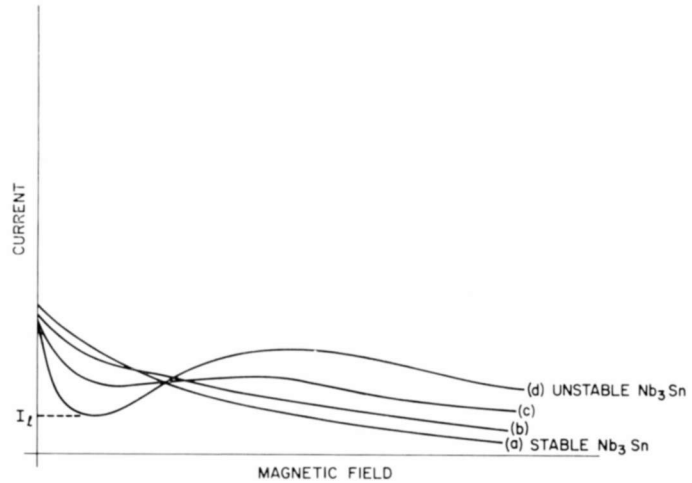

Fig. 1—General representation of critical characteristics (of the type measured with preset current-changing field) for short samples of unplated Nb_3Sn vapor-deposited ribbon showing different amounts of stability.

It was recognized that in a simple solenoid wound with unstable-type Nb_3Sn (Figure 1, curve d), some portion of the coil windings must have a low-field region within the unstable superconductor which would be the limiting factor.[12] It is this low-field region of the coil rather than the high-field region that limits the current to a value I_l (Figure 1d). Indications of this were also shown in Nb-Zr coils by Boom, Roberts, and Livingston.[13]

It was shown that coils wound with more stable Nb_3Sn (Figure 1, curves a and b) that had been subsequently copper plated resulted in only small (<50 percent) increases in critical current. It is reasoned

[12] J. C. Fakan and E. R. Schrader, "Experimental Evidence of Degradation Effects in Short Samples of Hard Superconductors," NASA Technical Note NASA TND-2345, June 1964.

[13] R. W. Boom, L. D. Roberts, and R. S. Livingston, "Developments in Superconducting Solenoids," *Nucl. Inst. Methods*, Vol. 20, p. 495, 1963.

that if the superconductor is inherently stable to begin with, the addition of energy sinks and electrical shunts by copper plating can add little to the initial stability. On the other hand, when the unstable-type Nb_3Sn (Figure 1c, d) is copper or silver plated, large increases (factor of 2 to 3) in critical currents at all fields are measured in short samples. This is discussed in detail by Schindler and Nyman.[3] Figure 2 shows typical changes in short-sample critical characteristics that are obtained when the Nb_3Sn ribbon depicted in Figure 1 is further stabil-

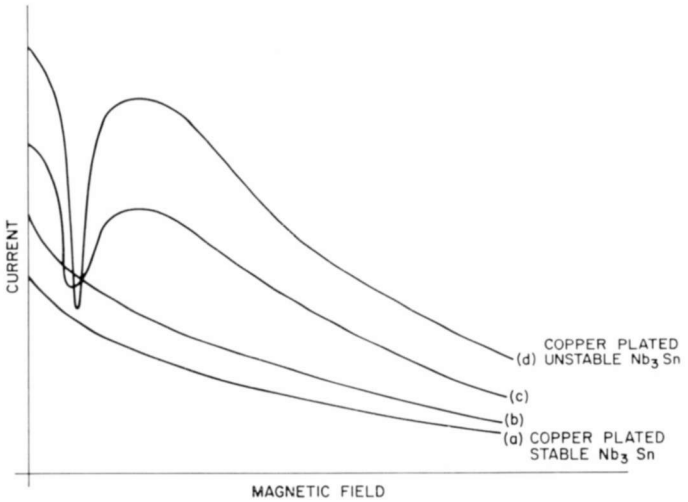

Fig. 2—General representation of critical characteristics (of the type measured with preset current-changing field) for short samples of copper-plated Nb_3Sn vapor-deposited ribbon showing different amounts of stability.

ized by copper plating. Maximum improvement from plating occurs for the Nb_3Sn that is inherently the least stable but that potentially has the highest critical current over the entire field range. The curves of Figures 1 and 2 are representative of measurements taken with swept field and preset current. Because of the instabilities and the many test variables involved, exact H_c-I_c curves for high-current Nb_3Sn cannot be accurately predicted.

Most of the discussion below concerns unstable Nb_3Sn ribbon (Figures 1d and 2d). With sufficient compensation for the instabilities of the unstable Nb_3Sn, higher coil currents are attained than could be achieved with the more stable material. A family of H_c-I_c curves for one type of high-current unstable material obtained under test conditions ranging from the least critical to the most severe is shown in

Figure 3. The upper solid curve represents averaged upper values of critical current of copper-plated short samples achieved under relatively stable test conditions. The lower solid curve represents the approximate locus (approximate due to the large scatter of measured data) of similar but unplated Nb_3Sn tested under the more severe swept-field conditions. The dashed curves between the two solid curves are a composite evaluation of many measured critical characteristics under various conditions of intermediate stability. While Figure 3 is a conceptual

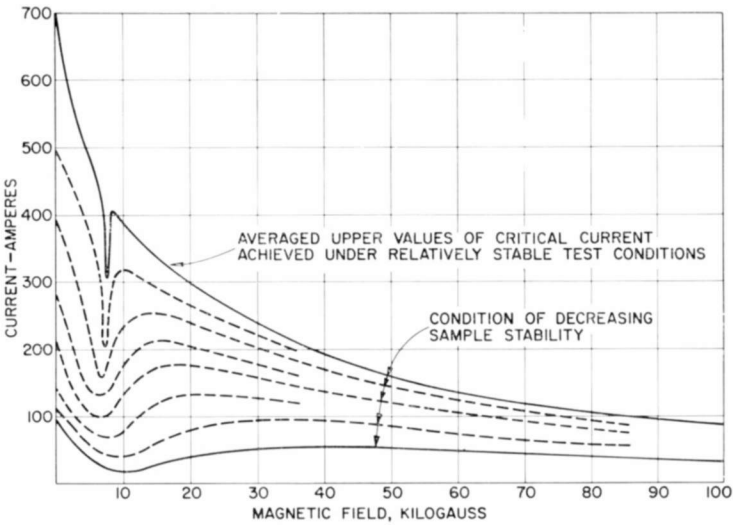

Fig. 3—Critical-field–critical-current plot of inherently unstable type Nb_3Sn ribbon with a general representation of the critical characteristics when the material has been stabilized to various degrees.

composite of observed data, it is an attempt to represent the critical characteristics of the Nb_3Sn with an as yet unspecified stability parameter and without reference to the source of the instability. Figure 3 therefore is a degradation diagram, not of any particular coil, but of unstable Nb_3Sn under a wide range of conditions and material preparation.

Low-Field Instabilities

Difficulties in controlling experiments with coils are due to the number of variables involved in geometry (over-all dimensions, winding pitch, interlayer dimensions, packing factor), winding techniques (position and resistance of contacts, winding tension, interlayer insulation), and test techniques (coil shunts, power supply noise, rate of application of coil current). Using a 0.090-inch-wide ribbon and winding

spirally to exact dimensions, turns, etc., reliable coil data for many different geometries were obtained. These superconductive test coils were immersed in the background magnetic field of an outer coil and the critical characteristics of the test coils were determined.

Figures 4a and b illustrate a test on a stack of 12 series-connected spirally wound pies each having an inner diameter of 9/16 inch, and an outer diameter of 1¼ inches, with a width equal to that of one

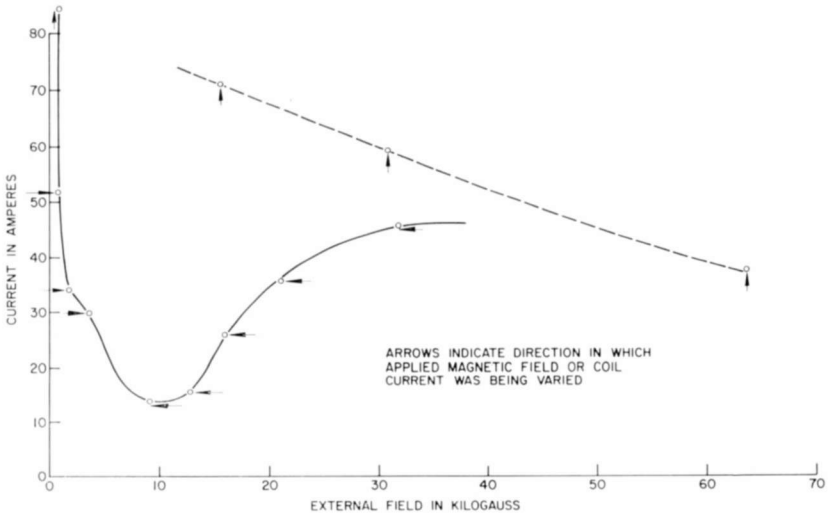

Fig. 4—(a) Critical-field–critical-current characteristics of a series-connected stack of 12 "pies", each 9/16-inch inner diameter, 1¼-inch outer diameter with a width of 0.120-inch (0.090 ribbon width plus 1/32-inch insulator). Points show the greater low-field instability when current is preset and external field is varied.

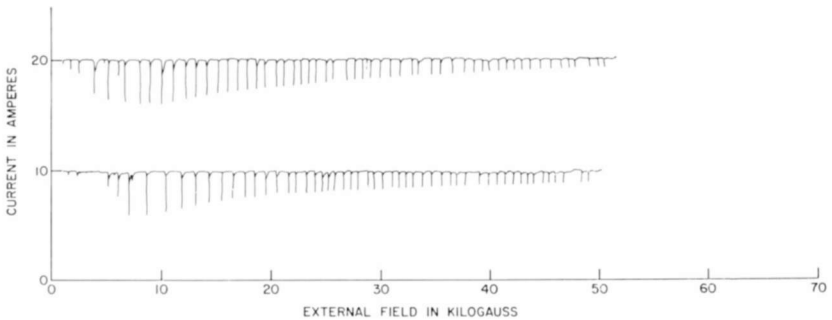

Fig. 4—(b) Changes in coil current as the external magnetic field is increased, showing largest coil instability in low-field region. The test coil did not go normal during the traces indicated here.

ribbon and a 1/32-inch thick Bakelite insulating washer between adjacent pies. Mylar ribbon (0.090 × 0.0005 inch) was bifilarly wound with the ribbon to provide insulation. As mylar does not add to the stability of the coil, the 12-pie stack is stabilized only by the copper plating on the ribbon. The coil was not otherwise shunted in these tests. During the test, the 12-pie stack was aligned axially in the central field of the background magnet. As with short-sample testing, the test coil was made to go normal under conditions of preset field (varying current) and preset current (varying field). The critical currents and fields are shown in Figure 4a. The much greater effect on coil degradation of the changing background field at constant current as compared with changing current at constant background field is evident. This relatively unstabilized coil, when tested under the severe condition of a varying background field with a preset current, corresponds to about the lowest pattern of critical current in the H_c-I_c curve shown in Figure 3. If this coil were wound for more stable performance (i.e., metallic insulation between layers, shunts, etc.) both curves of Figure 4a would be higher. The abscissa represents the background field only and does not include the contribution of the total central field of the test coil itself (H/I of the test coil $\approx$ 380 gauss/ampere).

Figure 4a shows the background fields and coil currents at which the coil became normal. Many other field and current ranges were used to find these normal points, including several field sweeps that actually went through the dip of Figure 4a without causing the coil to go normal. Two such field sweeps with preset coil currents of 10 and 20 amperes are shown in Figure 4b. Severe coil instabilities are manifested as sharp drops in coil current, reflecting sudden flux movements within the coil that temporarily induce opposing currents. Maximum amplitude coil current fluctuations occur at approximately the same background field value as the maximum degradation of the coil under unstable test conditions as shown in the lower curve of Figure 4a. Plots analogous to those of Figure 4b were obtained (not shown) in which current spikes of the opposite polarity resulted when the background field was reduced at the same preset current; whenever the coil did go normal, it occurred at one of these points. Such performance was obtained repeatedly on many other unstable coils, and similar effects have been reported[14] for Nb-Zr coils. It is evident that coil degradation results from the coil instabilities that cause these severe current

[14] M. S. Lubell, B. S. Chandrasekhar, and B. S. Mallick, "Degradation and Flux Jumping in Solenoids of Heat Treated Nb-25% Zr Wire," *Appl. Phys. Ltrs.*, Vol. 3, p. 79, 1 Sept. 1963.

changes, and that the most severe current changes are due to larger flux movements that occur at the lower fields.

It follows then that the removal of low-field areas from superconductive coil windings will provide for increased coil stabilization. We have found that providing a minimum ambient magnetic field above the low-field instability region for the Nb_3Sn windings enhances stability, and results in coil performance free of degradation effects.[4,12]

Coil Stabilization

From the results of many tests on coils such as the 12-pie stack (Figure 4) in which Mylar insulation was used between the Nb_3Sn winding layers, it was evident that additional stabilization was required if the full capabilities of the Nb_3Sn ribbon were to be realized. A significant increase in stability at both low and high fields was obtained when anodized aluminum sheet was substituted for the Mylar between each Nb_3Sn layer. The anodized aluminum surface provides the electrical insulation. The improved stability is believed due to the increase by orders of magnitude in thermal and electrical conductivity of the aluminum over the Mylar. The use of anodized aluminum interlayer insulation, the use of copper or silver plated ribbon, and the use of magnetic-field stabilization increases the over-all stabilization sufficiently to achieve the same high critical current values in coils as are achieved by short-sample tests. It is now possible, therefore, to make superconductive coils having no degradation.

Figure 5, previously published in part,[4] is a set of composite H_c-I_c curves showing the reduction and effective elimination of degradation in small coils (200 gauss per ampere, 1¼-inch inner diameter, 1¾-inch outer diameter, and 2 inches long) as tested in the background field of the Lewis Research Center's 4-inch-inner-diameter copper magnet. The highest stable H_c-I_c Nb_3Sn data from Figure 3 is superimposed to show the agreement at higher fields. Coils A and B were wound from slightly different Nb_3Sn ribbon. The unstable, relatively flat current portion of each curve below 25-30 kilogauss shows again the limitation due to the existence of a low-field region in the windings. Unlike Figure 4, the abscissa in Figure 5 is the total central field of the test coil including the background field. Coil A contributes approximately 30 kilogauss to give a total field of 60 kilogauss. Thus, a background field of 30 kilogauss was necessary to stabilize this coil.

Included in Figure 5 are points labeled "coil C" from a test on a 390-gauss-per-ampere coil immersed in the background field of a copper magnet* that could be varied to yield up to 100 kilogauss. These data

extend the measured high-field performance of coils using vapor-deposited Nb_3Sn to 122 kilogauss.

Figure 5 also shows two critical currents of the inner coil of an Nb_3Sn ribbon, three-coil compound solenoid with a 1/2-inch-inside-diameter winding that developed a 92-kilogauss central field. Data obtained with this solenoid[4] are presented to show that the critical currents coincide with short-sample data (i.e., zero degradation).

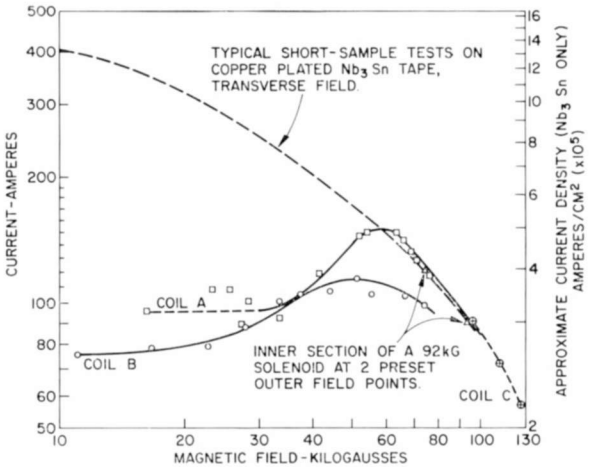

Fig. 5—Critical-field–critical-current plots of short samples and coils showing the removal of low-field instabilities in coils at increased background fields.

107-Kilogauss, 1-Inch-Bore Superconductive Solenoid

To ascertain whether degradation can be eliminated from larger-size superconductive coils, a magnet was designed to produce a minimum of 100 kilogauss in a 1-inch working bore. Although wound on two concentric cylindrical forms, this compound solenoid consists of three separate coils, each independently energized. The coils were wound from 12 separate lengths of experimental Nb_3Sn ribbon totaling 4,440 meters; the characteristics are shown in Table I. The critical characteristics of each length of Nb_3Sn ribbon were determined by measurements using a 50-meter sample from each length wound into a small solenoid and tested in the background field of another Nb_3Sn solenoid. Critical characteristics determined in this way are more reliable and repeatable than those of short samples, and are preferred

[4] These measurements were made at the Bell Telephone Laboratories, Murray Hill, N. J.

Table I—Parameters of 1-Inch Bore Compound High-Field Magnet

	Dimensions of Magnet Sections — Inches				Ribbon Length Meters	No. of Turns	Induc. (Calc.) Henrys	H/I (Ca.c.) Gauss Per Ampere	Coil Currents, Amp. (N)—Normal Current (S)—Set Current			Current Density per turn for 107kG Test Amp/Cm^2(x10^4)	Shunt Resistance Milliohms
	I.D.	O.D.	Axial Length	Bore					Self Field	56 kG 3.4″ Bore	107 kG 1″ Bore		
Inner Section													
	1.25	2.80	3.5	1.0	1000	6240	0.66	770	63(N)	—	60(N)	2.13	4.8
Outer Section													
1st Winding	3.5	4.3	5.44	3.4	1090	3150	0.48	250	—	117(N)	95(S)	2.13	11.0
2nd Winding	4.3	5.6	5.44	—	2360	5980	2.51	413	84(N)	76(S)	73(S)	1.90	32.0

Totals—Complete Magnet: Field in 1″ bore, 103-107 kilogauss; Total energy, 20,725 joules; Total Inductance, 6.8 henrys.

for predicting large-coil performance. The joints between the separate lengths of the vapor-deposited Nb_3Sn were soldered (60-40 Pb-Sn) with 1/2 inch overlap joints directly within the layers; it was previously established that the resistance ($\approx 10^{-8}$ ohm) of the nonsuperconductive joints have no effect on the critical current of the ribbon. The inner coil contained ten interleaved thin (0.001 inch thick) sheets of copper uniformly distributed throughout the layer windings and overlapped to form shorted secondary turns. After preliminary experimentation, optimized test conditions for combining the fields of the three coils were established; the complete coil was then brought up to the field at which the inner coil went normal with the outer two coils preset at currents 8 percent lower than their critical value. This field was measured as 107 kilogauss with a Hall probe calibrated at the Lewis Research Center, and 103 kilogauss with a magnetoresistive probe calibrated at Bell Telephone Laboratories. During this first test, the full field was achieved twice, with no mechanical damage to the ribbon caused by the strong magnetic forces experienced.

Prior to the next test series, the magnet was warmed to room temperature and the outside copper secondary turn was replaced.* The magnet was then brought up to the same critical currents and fields as in previous high-field tests.

Figure 6 shows the composite *H-I* diagram for the three coils. The shaded portions cover the range of critical values measured in the twelve 50-meter sample test coils. Degradation in the outer magnetic field stabilizing coil is clearly shown. As expected, the inner two coils both attain short-sample performance with no degradation.

Conclusions

The work on superconductive coils wound with vapor-deposited Nb_3Sn ribbon described in this paper stresses the importance of instabilities within the coil as a major reason for degradation. This is discussed in terms of stability variations relating to the process variables in depositing the Nb_3Sn as well as the influence of copper or silver plating of the ribbon. Techniques of metal interleaving between layers and magnetic field stabilization using compound coils were additionally effective in minimizing these instabilities. No further specification of the nature of the instabilities are treated in this paper, but the data are consistent with present theories relating this instability to flux

* The effect of the collapsing field each time the coil went normal acting on the large induced currents in the single unsupported outer shorted copper turn compressed the copper turn from a 5.4-inch long cylinder to a 2½-inch long bellows-like shape.

movements in the superconductor as a result of the sudden relaxation of localized concentrations of magnetic pressure.[5,15,16]

To demonstrate the ability to minimize or overcome the described degradation effects, a superconducting solenoid with a 1-inch bore and 5 inches long was constructed; it developed a field of 107 kilogauss. This is the highest field ever achieved for any all-superconducting magnet yet reported.

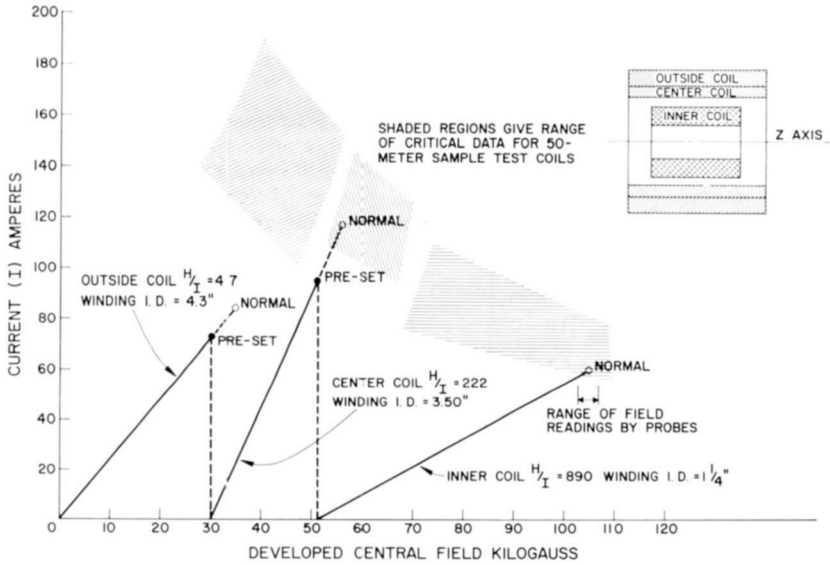

Fig. 6—Critical (and preset) fields and currents for each of three axially aligned coils yielding 103-107 kilogauss central field in 1-inch bore.

Acknowledgments

The authors acknowledge the technical advice of a number of staff scientists in a group headed by F. D. Rosi at the RCA Laboratories. They also wish to note the significant contributions made by the staff of the Lewis Research Center serving under J. C. Laurence, in particular J. C. Fakan for his suggestion on some of the underlying concepts, and in addition, for his help with the high-field magnet facilities at Lewis Research Center. In addition, Y. Kim and his associates at the Bell Telephone Laboratories are thanked for their aid in securing data on coils at high magnetic fields.

---

[15] C. P. Bean and R. W. Schmitt, "The Physics of High-Field Superconductors," *Science*, Vol. 140, p. 26, April 1963.

[16] P. W. Anderson and Y. B. Kim, "Hard Superconductivity: Theory of the Motion of Abvikosov Flux Lines," *Rev. Mod. Phys.*, Vol. 36, p. 39, Jan. 1964.

SUPERCONDUCTING ENERGY GAP AND NET ELECTRON DRIFT VELOCITY AS FUNCTIONS OF TEMPERATURE AND COOPER-PAIR DRIFT VELOCITY

By

R. H. Parmenter and L. J. Berton

RCA Laboratories
Princeton, N. J.

Summary—*A tabulation is given of the superconducting energy gap and the net electron drift velocity as functions of temperature and Cooper-pair drift velocity. Reduced variables are used to make the tables applicable to an arbitrary weak-coupling superconductor. A brief discussion is given of the method of calculating the quantities. Several uses of the tables are pointed out.*

IN THE FOLLOWING pages the superconducting energy gap, ϵ_0, and the net electronic drift velocity, v, are tabulated as functions of temperature, T, and Cooper-pair drift velocity, v_0. We restrict ourselves to the case of weak coupling, where the Debye temperature is much greater than the superconducting transition temperature, T_c. Subject to such a restriction, it is possible to tabulate a set of reduced variables appropriate to any superconductor. Specifically, we tabulate ϵ_0/ϵ_{00} and v/v_{00} as functions of T/T_c and v_0/v_{00}. Here ϵ_{00} is the value of the energy gap at $T=0$, $v=0$; while $v_{00} \equiv \epsilon_{00}/p_F$, p_F being the Fermi momentum.

By definition, v is such that $J = n_0 e v$ is the superconducting current density, where n_0 is the conduction-electron density and e the electronic charge. It should be emphasized that J is not necessarily equal to $J_0 = n_0 e v_0$, the current density due to the Cooper pairs alone. There may be an additional (negative) contribution to J from the quasi-particle excitations (normal carriers) when in the distribution that minimizes the free energy of the superconductor (for a given T and v_0). Thus v may be smaller than v_0.

The detailed derivation of the equations relating ϵ_0 and v to T and v_0 was given in a previous work[1] by one of the authors. For computational purposes, they can be cast in the following form: Let $\epsilon = \epsilon_0/\epsilon_{00}$, $v_0 = v_0/v_{00}$, $v = v/v_{00}$, $t = T/T_c$, and $K = \pi e^{-\gamma} = 1.7638588$, $a = (K/t)\epsilon$, $b = (K/t)v_0$, $g(x) = \sqrt{x^2 + a^2}$.

---

[1] R. H. Parmenter, "Nonlinear Electrodynamics of Superconductors with a Very Small Coherence Distance," *RCA Review*, Vol. 23, p. 323, September, 1962.

Here $\gamma = 0.5772157$ is Euler's constant. For given v_0 and t, ϵ can be found by solving the integral equation,

$$\frac{1}{b}\ln\left[\frac{\cosh(1/2)(a+b)}{\cosh(1/2)(a-b)}\right]\ln a - \ln\frac{K}{t}$$

$$+\frac{\sinh b}{b}\int_0^\infty \frac{x\ln[x+g(x)]\,dx}{g(x)[\cosh g(x)+\cosh b]} = 0. \qquad (1)$$

The integral appearing in Equation (1) was first evaluated for arbitrary values of ϵ, v_0, and t. For given v_0 and t, the value of ϵ satisfying Equation (1) was then found by an iterative root-bracketing technique. The resulting triplet of numbers ϵ, v_0, t was substituted into the equation

$$v = v_0 + \frac{3}{2}\frac{t}{K}\int_0^\infty dx \int_{-1}^{+1} \mu d\mu \left\{1 - \tanh\frac{1}{2}[g(x)+b\mu]\right\} \qquad (2)$$

in order to find v. The integrals appearing in Equations (1) and (2) were evaluated by numerical integration of appropriate differential equations. Finally $dv/dv_0 = dv/dv_0$ was obtained by numerical differentiation. The RCA 601/301 computer installation at RCA Laboratories was utilized in carrying out these calculations.

Plots of ϵ_0/ϵ_{00} and v/v_{00} versus v_0/v_{00} are shown in Figures 1 and 2, respectively. There is a curve for each value, T/T_c from zero to 0.98 in intervals of 0.02 (the lower the curve, the higher the temperature). At a given temperature, ϵ_0 and v vanish at the same value of v_0. The maximum value of v is proportional to the critical current density at the given temperature. In the tables, ϵ_0/ϵ_{00}, v/v_{00}, and dv/dv_0 are listed as functions of T/T_c and v_0/v_{00}, the latter running from zero to a maximum possible value in intervals of 0.02. At $T = 0$, this maximum value is $e/2 = 1.359$. As T increases toward T_c, the maximum possible value of v_0 decreases to zero.

Knowledge of v versus v_0 is essential in solving the nonlinear generalization of London's equation,[1]

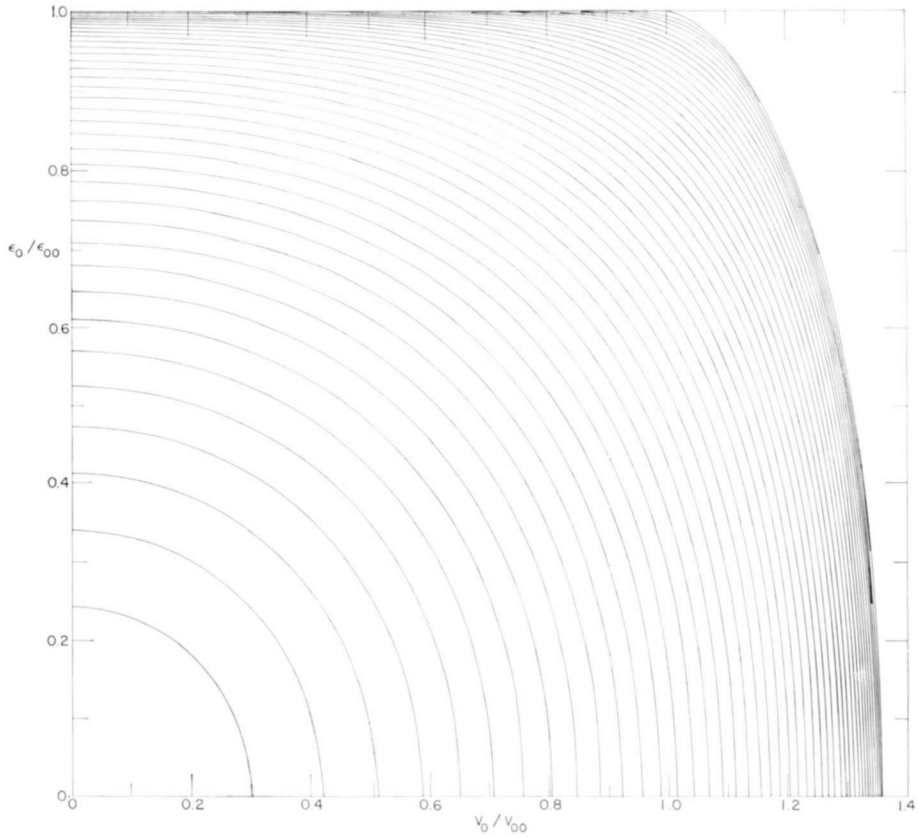

Fig. 1—Plot of ϵ_0/ϵ_{00} versus v_0/v_{00} for various values of T/T_c. T/T_c runs from zero to 0.98 in intervals of 0.02, the lower the curve the larger is T/T_c.

$$\lambda^2 \nabla^2 v_0 = v(v_0) \tag{3}$$

where λ is the London penetration depth. This equation is applicable to situations* where the effective size of a Cooper pair is small compared with λ. The slope dv/dv_0 can be related to the microwave conductivity in the presence of a d-c current density.[2] In particular, the

* In Reference (1), Equation (3) was applied to the problem of the mixed state of a superconductor with a very small coherence distance. Incorrect results were obtained because of the incorrect assumption of continuity of ϵ_0 at a normal–superconducting interface. Since ϵ_0 may change appreciably over distances comparable with the coherence distance, one must be prepared to allow for discontinuous changes in ϵ_0 at such an interface in the limit of a vanishingly small coherence distance.

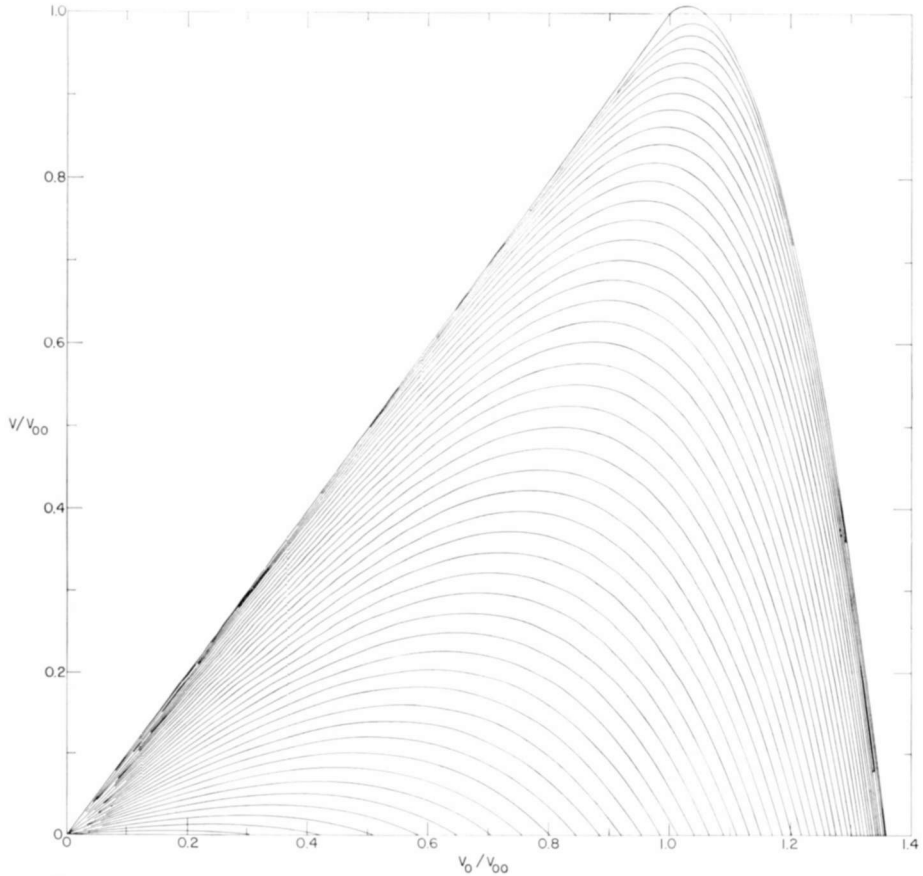

Fig. 2—Plot of v/v_∞ versus v_0/v_∞ for various values of T/T_c. T/T_c runs from zero to 0.98 in intervals of 0.02, the lower the curve the larger is T/T_c.

slope at vanishing v_0 determines the temperature-dependent effective penetration depth

$$\lambda_{\text{eff}} = \lambda \left[\left(\frac{dv}{dv_0} \right)_{v_0=0} \right]^{-1/2}. \tag{4}$$

In London's notation, $(dv/dv_0)_{v_0=0}$ is (Λ_0/Λ_T), a quantity previously tabulated by Mühlschlegel.[3]

---

[2] J. Gittleman, B. Rosenblum, T. Seidel, and A. Wicklund, "The Dependence of the Microwave Impedance of a Superconductor on Direct Current," *Proc. 8th International Conf. on Low-Temperature Physics*, Butterworth Scientific Publications, Ltd., London, 1963, p. 336.

[3] B. Mühlschlegel, "Die thermodynamischen Funktionen des Supraleiters," *Zeitschrift für Physik*, Vol. 155, p. 313, 1959.

T/T_s	v_0/v_∞	$\epsilon_0/\epsilon_\infty$	v/v_∞	dv/dv_0	T/T_s	v_0/v_∞	$\epsilon_0/\epsilon_\infty$	v/v_∞	dv/dv_0	T/T_s	v_0/v_∞	$\epsilon_0/\epsilon_\infty$	v/v_∞	dv/dv_0	T/T_s	v_0/v_∞	$\epsilon_0/\epsilon_\infty$	v/v_∞	dv/dv_0
0.0000	0.0000	1.0000	0.0000	1.0000	0.0000	1.1800	0.8536	0.7916	-2.8313	0.0200	0.9600	0.9996	0.9589	0.9540	0.0400	0.7400	1.0000	0.7400	1.0000
0.0000	0.0200	1.0000	0.0200	1.0000	0.0000	1.2000	0.8189	0.7314	-3.1898	0.0200	0.9800	0.9992	0.9775	0.9187	0.0400	0.7600	1.0000	0.7600	1.0000
0.0000	0.0400	1.0000	0.0400	1.0000	0.0000	1.2200	0.7791	0.6640	-3.5397	0.0200	1.0000	0.9982	0.9945	0.6941	0.0400	0.7800	1.0000	0.7800	1.0000
0.0000	0.0600	1.0000	0.0600	1.0000	0.0000	1.2400	0.7333	0.5898	-3.8936	0.0200	1.0200	0.9946	1.0040	0.2548	0.0400	0.8000	1.0000	0.8000	1.0000
0.0000	0.0800	1.0000	0.0800	1.0000	0.0000	1.2600	0.6801	0.5083	-4.2516	0.0200	1.0400	0.9880	1.0046	-0.1851	0.0400	0.8200	1.0000	0.8200	1.0000
0.0000	0.1000	1.0000	0.1000	1.0000	0.0000	1.2800	0.6175	0.4197	-4.5991	0.0200	1.0600	0.9783	0.9968	-0.5973	0.0400	0.8400	1.0000	0.8400	1.0003
0.0000	0.1200	1.0000	0.1200	1.0000	0.0000	1.3000	0.5425	0.3243	-4.9525	0.0200	1.0800	0.9657	0.9808	-0.9932	0.0400	0.8600	1.0000	0.8600	0.9983
0.0000	0.1400	1.0000	0.1400	1.0000	0.0000	1.3200	0.4482	0.2216	-5.3102	0.0200	1.1000	0.9499	0.9572	-1.3704	0.0400	0.8800	1.0000	0.8799	0.9960
0.0000	0.1600	1.0000	0.1600	1.0000	0.0000	1.3400	0.3184	0.1119	-5.6680	0.0200	1.1200	0.9309	0.9261	-1.7411	0.0400	0.9000	0.9999	0.8998	0.9930
0.0000	0.1800	1.0000	0.1800	1.0000						0.0200	1.1400	0.9085	0.8876	-2.1062	0.0400	0.9200	0.9999	0.9196	0.9830
0.0000	0.2000	1.0000	0.2000	1.0000						0.0200	1.1600	0.8825	0.8418	-2.4662	0.0400	0.9400	0.9997	0.9391	0.9602
0.0000	0.2200	1.0000	0.2200	1.0000	0.0200	0.0000	1.0000	0.0000	1.0000	0.0200	1.1800	0.8524	0.7889	-2.8248	0.0400	0.9600	0.9992	0.9578	0.9079
0.0000	0.2400	1.0000	0.2400	1.0000	0.0200	0.0200	1.0000	0.0200	1.0000	0.0200	1.2000	0.8177	0.7289	-3.1810	0.0400	0.9800	0.9983	0.9750	0.7969
0.0000	0.2600	1.0000	0.2600	1.0000	0.0200	0.0400	1.0000	0.0400	1.0000	0.0200	1.2200	0.7779	0.6617	-3.5382	0.0400	1.0000	0.9963	0.9890	0.5873
0.0000	0.2800	1.0000	0.2800	1.0000	0.0200	0.0600	1.0000	0.0600	1.0000	0.0200	1.2400	0.7319	0.5874	-3.8928	0.0400	1.0200	0.9924	0.9977	0.2633
0.0000	0.3000	1.0000	0.3000	1.0000	0.0200	0.0800	1.0000	0.0800	1.0000	0.0200	1.2600	0.6786	0.5060	-4.2467	0.0400	1.0400	0.9860	0.9991	-0.1361
0.0000	0.3200	1.0000	0.3200	1.0000	0.0200	0.1000	1.0000	0.1000	1.0000	0.0200	1.2800	0.6159	0.4175	-4.5886	0.0400	1.0600	0.9766	0.9921	-0.5595
0.0000	0.3400	1.0000	0.3400	1.0000	0.0200	0.1200	1.0000	0.1200	1.0000	0.0200	1.3000	0.5409	0.3224	-4.9493	0.0400	1.0800	0.9641	0.9768	-0.9672
0.0000	0.3600	1.0000	0.3600	1.0000	0.0200	0.1400	1.0000	0.1400	1.0000	0.0200	1.3200	0.4461	0.2195	-5.3143	0.0400	1.1000	0.9485	0.9536	-1.3519
0.0000	0.3800	1.0000	0.3800	1.0000	0.0200	0.1600	1.0000	0.1600	1.0000	0.0200	1.3400	0.3153	0.1098	-5.6793	0.0400	1.1200	0.9296	0.9228	-1.7267
0.0000	0.4000	1.0000	0.4000	1.0000	0.0200	0.1800	1.0000	0.1800	1.0000						0.0400	1.1400	0.9072	0.8846	-2.0943
0.0000	0.4200	1.0000	0.4200	1.0000	0.0200	0.2000	1.0000	0.2000	1.0000						0.0400	1.1600	0.8812	0.8390	-2.4600
0.0000	0.4400	1.0000	0.4400	1.0000	0.0200	0.2200	1.0000	0.2200	1.0000	0.0400	0.0000	1.0000	0.0000	1.0000	0.0400	1.1800	0.8511	0.7862	-2.8183
0.0000	0.4600	1.0000	0.4600	1.0000	0.0200	0.2400	1.0000	0.2400	1.0000	0.0400	0.0200	1.0000	0.0200	1.0000	0.0400	1.2000	0.8164	0.7263	-3.1722
0.0000	0.4800	1.0000	0.4800	1.0000	0.0200	0.2600	1.0000	0.2600	1.0000	0.0400	0.0400	1.0000	0.0400	1.0000	0.0400	1.2200	0.7766	0.6593	-3.5367
0.0000	0.5000	1.0000	0.5000	1.0000	0.0200	0.2800	1.0000	0.2800	1.0000	0.0400	0.0600	1.0000	0.0600	1.0000	0.0400	1.2400	0.7305	0.5849	-3.8919
0.0000	0.5200	1.0000	0.5200	1.0000	0.0200	0.3000	1.0000	0.3000	1.0000	0.0400	0.0800	1.0000	0.0800	1.0000	0.0400	1.2600	0.6771	0.5036	-4.2417
0.0000	0.5400	1.0000	0.5400	1.0000	0.0200	0.3200	1.0000	0.3200	1.0000	0.0400	0.1000	1.0000	0.1000	1.0000	0.0400	1.2800	0.6143	0.4153	-4.5781
0.0000	0.5600	1.0000	0.5600	1.0000	0.0200	0.3400	1.0000	0.3400	1.0000	0.0400	0.1200	1.0000	0.1200	1.0000	0.0400	1.3000	0.5392	0.3204	-4.9461
0.0000	0.5800	1.0000	0.5800	1.0000	0.0200	0.3600	1.0000	0.3600	1.0000	0.0400	0.1400	1.0000	0.1400	1.0000	0.0400	1.3200	0.4440	0.2174	-5.3183
0.0000	0.6000	1.0000	0.6000	1.0000	0.0200	0.3800	1.0000	0.3800	1.0000	0.0400	0.1600	1.0000	0.1600	1.0000	0.0400	1.3400	0.3122	0.1076	-5.6905
0.0000	0.6200	1.0000	0.6200	1.0000	0.0200	0.4000	1.0000	0.4000	1.0000	0.0400	0.1800	1.0000	0.1800	1.0000					
0.0000	0.6400	1.0000	0.6400	1.0000	0.0200	0.4200	1.0000	0.4200	1.0000	0.0400	0.2000	1.0000	0.2000	1.0000					
0.0000	0.6600	1.0000	0.6600	1.0000	0.0200	0.4400	1.0000	0.4400	1.0000	0.0400	0.2200	1.0000	0.2200	1.0000	0.0600	0.0000	1.0000	0.0000	1.0000
0.0000	0.6800	1.0000	0.6800	1.0000	0.0200	0.4600	1.0000	0.4600	1.0000	0.0400	0.2400	1.0000	0.2400	1.0000	0.0600	0.0200	1.0000	0.0200	1.0000
0.0000	0.7000	1.0000	0.7000	1.0000	0.0200	0.4800	1.0000	0.4800	1.0000	0.0400	0.2600	1.0000	0.2600	1.0000	0.0600	0.0400	1.0000	0.0400	1.0000
0.0000	0.7200	1.0000	0.7200	1.0000	0.0200	0.5000	1.0000	0.5000	1.0000	0.0400	0.2800	1.0000	0.2800	1.0000	0.0600	0.0600	1.0000	0.0600	1.0000
0.0000	0.7400	1.0000	0.7400	1.0000	0.0200	0.5200	1.0000	0.5200	1.0000	0.0400	0.3000	1.0000	0.3000	1.0000	0.0600	0.0800	1.0000	0.0800	1.0000
0.0000	0.7600	1.0000	0.7600	1.0000	0.0200	0.5400	1.0000	0.5400	1.0000	0.0400	0.3200	1.0000	0.3200	1.0000	0.0600	0.1000	1.0000	0.1000	1.0000
0.0000	0.7800	1.0000	0.7800	1.0000	0.0200	0.5600	1.0000	0.5600	1.0000	0.0400	0.3400	1.0000	0.3400	1.0000	0.0600	0.1200	1.0000	0.1200	1.0000
0.0000	0.8000	1.0000	0.8000	1.0000	0.0200	0.5800	1.0000	0.5800	1.0000	0.0400	0.3600	1.0000	0.3600	1.0000	0.0600	0.1400	1.0000	0.1400	1.0000
0.0000	0.8200	1.0000	0.8200	1.0000	0.0200	0.6000	1.0000	0.6000	1.0000	0.0400	0.3800	1.0000	0.3800	1.0000	0.0600	0.1600	1.0000	0.1600	1.0000
0.0000	0.8400	1.0000	0.8400	1.0000	0.0200	0.6200	1.0000	0.6200	1.0000	0.0400	0.4000	1.0000	0.4000	1.0000	0.0600	0.1800	1.0000	0.1800	1.0000
0.0000	0.8600	1.0000	0.8600	1.0000	0.0200	0.6400	1.0000	0.6400	1.0000	0.0400	0.4200	1.0000	0.4200	1.0000	0.0600	0.2000	1.0000	0.2000	1.0000
0.0000	0.8800	1.0000	0.8800	1.0000	0.0200	0.6600	1.0000	0.6600	1.0000	0.0400	0.4400	1.0000	0.4400	1.0000	0.0600	0.2200	1.0000	0.2200	1.0000
0.0000	0.9000	1.0000	0.9000	1.0000	0.0200	0.6800	1.0000	0.6800	1.0000	0.0400	0.4600	1.0000	0.4600	1.0000	0.0600	0.2400	1.0000	0.2400	1.0000
0.0000	0.9200	1.0000	0.9200	1.0000	0.0200	0.7000	1.0000	0.7000	1.0000	0.0400	0.4800	1.0000	0.4800	1.0000	0.0600	0.2600	1.0000	0.2600	1.0000
0.0000	0.9400	1.0000	0.9400	1.0000	0.0200	0.7200	1.0000	0.7200	1.0000	0.0400	0.5000	1.0000	0.5000	1.0000	0.0600	0.2800	1.0000	0.2800	1.0000
0.0000	0.9600	1.0000	0.9600	1.0000	0.0200	0.7400	1.0000	0.7400	1.0000	0.0400	0.5200	1.0000	0.5200	1.0000	0.0600	0.3000	1.0000	0.3000	1.0000
0.0000	0.9800	1.0000	0.9800	1.0000	0.0200	0.7600	1.0000	0.7600	1.0000	0.0400	0.5400	1.0000	0.5400	1.0000	0.0600	0.3200	1.0000	0.3200	1.0000
0.0000	1.0000	1.0000	1.0000	1.0000	0.0200	0.7800	1.0000	0.7800	1.0000	0.0400	0.5600	1.0000	0.5600	1.0000	0.0600	0.3400	1.0000	0.3400	1.0000
0.0000	1.0200	0.9968	1.0103	0.2462	0.0200	0.8000	1.0000	0.8000	1.0000	0.0400	0.5800	1.0000	0.5800	1.0000	0.0600	0.3600	1.0000	0.3600	1.0000
0.0000	1.0400	0.9899	1.0101	-0.2340	0.0200	0.8200	1.0000	0.8200	1.0000	0.0400	0.6000	1.0000	0.6000	1.0000	0.0600	0.3800	1.0000	0.3800	1.0000
0.0000	1.0600	0.9800	1.0014	-0.6350	0.0200	0.8400	1.0000	0.8400	1.0002	0.0400	0.6200	1.0000	0.6200	1.0000	0.0600	0.4000	1.0000	0.4000	1.0000
0.0000	1.0800	0.9672	0.9848	-1.0192	0.0200	0.8600	1.0000	0.8600	0.9992	0.0400	0.6400	1.0000	0.6400	1.0000	0.0600	0.4200	1.0000	0.4200	1.0000
0.0000	1.1000	0.9512	0.9607	-1.3888	0.0200	0.8800	1.0000	0.8800	0.9980	0.0400	0.6600	1.0000	0.6600	1.0000	0.0600	0.4400	1.0000	0.4400	1.0000
0.0000	1.1200	0.9322	0.9293	-1.7555	0.0200	0.9000	1.0000	0.8999	0.9965	0.0400	0.6800	1.0000	0.6800	1.0000	0.0600	0.4600	1.0000	0.4600	1.0000
0.0000	1.1400	0.9097	0.8905	-2.1181	0.0200	0.9200	1.0000	0.9198	0.9915	0.0400	0.7000	1.0000	0.7000	1.0000	0.0600	0.4800	1.0000	0.4800	1.0000
0.0000	1.1600	0.8837	0.8446	-2.4723	0.0200	0.9400	0.9999	0.9396	0.9801	0.0400	0.7200	1.0000	0.7200	1.0000	0.0600	0.5000	1.0000	0.5000	1.0000

T/T_e	v_0/v_{00}	ϵ_0/ϵ_{00}	v/v_{00}	dv/dv_0	T/T_e	v_0/v_{00}	ϵ_0/ϵ_{00}	v/v_{00}	dv/dv_0	T/T_e	v_0/v_{00}	ϵ_0/ϵ_{00}	v/v_{00}	dv/dv_0	T/T_e	v_0/v_{00}	ϵ_0/ϵ_{00}	v/v_{00}	dv/dv_0
0.0600	0.5200	1.0000	0.5200	1.0000	0.0800	0.3000	1.0000	0.3000	1.0000	0.1000	0.0800	1.0000	0.0800	1.0000	0.1000	1.2600	0.6626	0.4805	-4.1798
0.0600	0.5400	1.0000	0.5400	1.0000	0.0800	0.3200	1.0000	0.3200	1.0000	0.1000	0.1000	1.0000	0.1000	1.0000	0.1000	1.2800	0.5989	0.3933	-4.5661
0.0600	0.5600	1.0000	0.5600	1.0000	0.0800	0.3400	1.0000	0.3400	1.0000	0.1000	0.1200	1.0000	0.1200	1.0000	0.1000	1.3000	0.5209	0.2980	-4.9132
0.0600	0.5800	1.0000	0.5800	1.0000	0.0800	0.3600	1.0000	0.3600	1.0000	0.1000	0.1400	1.0000	0.1400	1.0000	0.1000	1.3200	0.4231	0.1968	-5.2596
0.0600	0.6000	1.0000	0.6000	1.0000	0.0800	0.3800	1.0000	0.3800	1.0000	0.1000	0.1600	1.0000	0.1600	1.0000	0.1000	1.3400	0.2822	0.0876	-5.6059
0.0600	0.6200	1.0000	0.6200	1.0000	0.0800	0.4000	1.0000	0.4000	1.0000	0.1000	0.1800	1.0000	0.1800	1.0000					
0.0600	0.6400	1.0000	0.6400	1.0000	0.0800	0.4200	1.0000	0.4200	1.0000	0.1000	0.2000	1.0000	0.2000	1.0000					
0.0600	0.6600	1.0000	0.6600	1.0000	0.0800	0.4400	1.0000	0.4400	1.0000	0.1000	0.2200	1.0000	0.2200	1.0000	0.1200	0.0000	1.0000	0.0000	1.0000
0.0600	0.6800	1.0000	0.6800	1.0000	0.0800	0.4600	1.0000	0.4600	1.0000	0.1000	0.2400	1.0000	0.2400	1.0000	0.1200	0.0200	1.0000	0.0200	1.0000
0.0600	0.7000	1.0000	0.7000	1.0000	0.0800	0.4800	1.0000	0.4800	1.0000	0.1000	0.2600	1.0000	0.2600	1.0000	0.1200	0.0400	1.0000	0.0400	1.0000
0.0600	0.7200	1.0000	0.7200	1.0000	0.0800	0.5000	1.0000	0.5000	1.0000	0.1000	0.2800	1.0000	0.2800	1.0000	0.1200	0.0600	1.0000	0.0600	1.0000
0.0600	0.7400	1.0000	0.7400	1.0000	0.0800	0.5200	1.0000	0.5200	1.0000	0.1000	0.3000	1.0000	0.3000	1.0000	0.1200	0.0800	1.0000	0.0800	1.0000
0.0600	0.7600	1.0000	0.7600	1.0003	0.0800	0.5400	1.0000	0.5400	1.0000	0.1000	0.3200	1.0000	0.3200	1.0000	0.1200	0.1000	1.0000	0.1000	1.0000
0.0600	0.7800	1.0000	0.7800	0.9979	0.0800	0.5600	1.0000	0.5600	1.0000	0.1000	0.3400	1.0000	0.3400	1.0000	0.1200	0.1200	1.0000	0.1200	1.0000
0.0600	0.8000	1.0000	0.7999	0.9963	0.0800	0.5800	1.0000	0.5800	1.0000	0.1000	0.3600	1.0000	0.3600	1.0000	0.1200	0.1400	1.0000	0.1400	1.0000
0.0600	0.8200	1.0000	0.8199	0.9962	0.0800	0.6000	1.0000	0.6000	1.0000	0.1000	0.3800	1.0000	0.3800	1.0000	0.1200	0.1600	1.0000	0.1600	1.0000
0.0600	0.8400	0.9999	0.8398	0.9990	0.0800	0.6200	1.0000	0.6200	1.0000	0.1000	0.4000	1.0000	0.4000	1.0000	0.1200	0.1800	1.0000	0.1800	1.0000
0.0600	0.8600	0.9999	0.8596	0.9877	0.0800	0.6400	1.0000	0.6400	1.0000	0.1000	0.4200	1.0000	0.4200	1.0000	0.1200	0.2000	1.0000	0.2000	1.0000
0.0600	0.8800	0.9997	0.8792	0.9785	0.0800	0.6600	1.0000	0.6600	1.0003	0.1000	0.4400	1.0000	0.4400	1.0000	0.1200	0.2200	1.0000	0.2200	1.0000
0.0600	0.9000	0.9995	0.8987	0.9623	0.0800	0.6800	1.0000	0.6800	0.9982	0.1000	0.4600	1.0000	0.4600	1.0000	0.1200	0.2400	1.0000	0.2400	1.0000
0.0600	0.9200	0.9992	0.9176	0.9341	0.0800	0.7000	1.0000	0.6999	0.9973	0.1000	0.4800	1.0000	0.4800	1.0000	0.1200	0.2600	1.0000	0.2600	1.0000
0.0600	0.9400	0.9986	0.9359	0.8857	0.0800	0.7200	1.0000	0.7199	0.9981	0.1000	0.5000	1.0000	0.5000	1.0000	0.1200	0.2800	1.0000	0.2800	1.0000
0.0600	0.9600	0.9975	0.9528	0.8041	0.0800	0.7400	0.9999	0.7398	0.9968	0.1000	0.5200	1.0000	0.5200	1.0000	0.1200	0.3000	1.0000	0.3000	1.0000
0.0600	0.9800	0.9957	0.9677	0.6747	0.0800	0.7600	0.9999	0.7598	0.9952	0.1000	0.5400	1.0000	0.5400	1.0000	0.1200	0.3200	1.0000	0.3200	1.0000
0.0600	1.0000	0.9930	0.9794	0.4792	0.0800	0.7800	0.9999	0.7797	0.9927	0.1000	0.5600	1.0000	0.5600	1.0000	0.1200	0.3400	1.0000	0.3400	1.0000
0.0600	1.0200	0.9885	0.9864	0.2066	0.0800	0.8000	0.9998	0.7995	0.9890	0.1000	0.5800	1.0000	0.5800	1.0004	0.1200	0.3600	1.0000	0.3600	1.0000
0.0600	1.0400	0.9818	0.9872	-0.1317	0.0800	0.8200	0.9997	0.8192	0.9832	0.1000	0.6000	1.0000	0.6000	0.9974	0.1200	0.3800	1.0000	0.3800	1.0000
0.0600	1.0600	0.9725	0.9808	-0.5128	0.0800	0.8400	0.9996	0.8388	0.9745	0.1000	0.6200	1.0000	0.6199	0.9964	0.1200	0.4000	1.0000	0.4000	1.0000
0.0600	1.0800	0.9603	0.9666	-0.9102	0.0800	0.8600	0.9994	0.8581	0.9614	0.1000	0.6400	1.0000	0.6399	0.9982	0.1200	0.4200	1.0000	0.4200	1.0000
0.0600	1.1000	0.9449	0.9444	-1.3048	0.0800	0.8800	0.9990	0.8772	0.9415	0.1000	0.6600	0.9999	0.6598	0.9971	0.1200	0.4400	1.0000	0.4400	1.0000
0.0600	1.1200	0.9262	0.9145	-1.6902	0.0800	0.9000	0.9985	0.8957	0.9114	0.1000	0.6800	0.9999	0.6798	0.9960	0.1200	0.4600	1.0000	0.4600	1.0000
0.0600	1.1400	0.9040	0.8769	-2.0666	0.0800	0.9200	0.9978	0.9135	0.8665	0.1000	0.7000	0.9999	0.6997	0.9944	0.1200	0.4800	1.0000	0.4800	1.0004
0.0600	1.1600	0.8780	0.8319	-2.4342	0.0800	0.9400	0.9966	0.9302	0.7998	0.1000	0.7200	0.9998	0.7195	0.9922	0.1200	0.5000	1.0000	0.5000	0.9972
0.0600	1.1800	0.8480	0.7796	-2.7988	0.0800	0.9600	0.9949	0.9453	0.7024	0.1000	0.7400	0.9998	0.7393	0.9892	0.1200	0.5200	1.0000	0.5199	0.9964
0.0600	1.2000	0.8133	0.7200	-3.1557	0.0800	0.9800	0.9924	0.9581	0.5678	0.1000	0.7600	0.9997	0.7591	0.9850	0.1200	0.5400	1.0000	0.5399	0.9986
0.0600	1.2200	0.7734	0.6533	-3.5215	0.0800	1.0000	0.9889	0.9677	0.3827	0.1000	0.7800	0.9996	0.7787	0.9791	0.1200	0.5600	0.9999	0.5598	0.9978
0.0600	1.2400	0.7272	0.5791	-3.8805	0.0800	1.0200	0.9838	0.9730	0.1399	0.1000	0.8000	0.9994	0.7982	0.9709	0.1200	0.5800	0.9999	0.5798	0.9971
0.0600	1.2600	0.6738	0.4982	-4.2126	0.0800	1.0400	0.9767	0.9730	-0.1561	0.1000	0.8200	0.9991	0.8175	0.9595	0.1200	0.6000	0.9999	0.5997	0.9963
0.0600	1.2800	0.6111	0.4105	-4.5729	0.0800	1.0600	0.9673	0.9665	-0.4974	0.1000	0.8400	0.9988	0.8366	0.9436	0.1200	0.6200	0.9999	0.6196	0.9951
0.0600	1.3000	0.5351	0.3152	-4.9608	0.0800	1.0800	0.9551	0.9529	-0.8691	0.1000	0.8600	0.9984	0.8552	0.9216	0.1200	0.6400	0.9998	0.6395	0.9936
0.0600	1.3200	0.4390	0.2123	-5.2950	0.0800	1.1000	0.9399	0.9316	-1.2527	0.1000	0.8800	0.9977	0.8734	0.8910	0.1200	0.6600	0.9998	0.6594	0.9916
0.0600	1.3400	0.3062	0.1034	-5.6291	0.0800	1.1200	0.9215	0.9027	-1.6387	0.1000	0.9000	0.9968	0.8908	0.8489	0.1200	0.6800	0.9997	0.6792	0.9890
					0.0800	1.1400	0.8995	0.8661	-2.0230	0.1000	0.9200	0.9956	0.9072	0.7913	0.1200	0.7000	0.9996	0.6989	0.9856
					0.0800	1.1600	0.8736	0.8219	-2.3995	0.1000	0.9400	0.9938	0.9223	0.7130	0.1200	0.7200	0.9995	0.7186	0.9811
0.0800	0.0000	1.0000	0.0000	1.0000	0.0800	1.1800	0.8436	0.7702	-2.7676	0.1000	0.9600	0.9915	0.9356	0.6075	0.1200	0.7400	0.9993	0.7382	0.9752
0.0800	0.0200	1.0000	0.0200	1.0000	0.0800	1.2000	0.8089	0.7111	-3.1512	0.1000	0.9800	0.9882	0.9464	0.4714	0.1200	0.7600	0.9991	0.7576	0.9674
0.0800	0.0400	1.0000	0.0400	1.0000	0.0800	1.2200	0.7686	0.6443	-3.5036	0.1000	1.0000	0.9840	0.9542	0.2947	0.1200	0.7800	0.9989	0.7768	0.9571
0.0800	0.0600	1.0000	0.0600	1.0000	0.0800	1.2400	0.7226	0.5710	-3.8463	0.1000	1.0200	0.9783	0.9579	0.0710	0.1200	0.8000	0.9985	0.7959	0.9437
0.0800	0.0800	1.0000	0.0800	1.0000	0.0800	1.2600	0.6688	0.4903	-4.2038	0.1000	1.0400	0.9708	0.9567	-0.1957	0.1200	0.8200	0.9981	0.8146	0.9262
0.0800	0.1000	1.0000	0.1000	1.0000	0.0800	1.2800	0.6056	0.4028	-4.5625	0.1000	1.0600	0.9611	0.9498	-0.5047	0.1200	0.8400	0.9975	0.8329	0.9031
0.0800	0.1200	1.0000	0.1200	1.0000	0.0800	1.3000	0.5290	0.3078	-4.9346	0.1000	1.0800	0.9488	0.9363	-0.8476	0.1200	0.8600	0.9967	0.8506	0.8728
0.0800	0.1400	1.0000	0.1400	1.0000	0.0800	1.3200	0.4320	0.2055	-5.2923	0.1000	1.1000	0.9337	0.9157	-1.2134	0.1200	0.8800	0.9957	0.8677	0.8332
0.0800	0.1600	1.0000	0.1600	1.0000	0.0800	1.3400	0.2953	0.0961	-5.6500	0.1000	1.1200	0.9153	0.8877	-1.5914	0.1200	0.9000	0.9943	0.8839	0.7816
0.0800	0.1800	1.0000	0.1800	1.0000						0.1000	1.1400	0.8935	0.8521	-1.9725	0.1200	0.9200	0.9926	0.8989	0.7147
0.0800	0.2000	1.0000	0.2000	1.0000						0.1000	1.1600	0.8678	0.8088	-2.3555	0.1200	0.9400	0.9903	0.9123	0.6284
0.0800	0.2200	1.0000	0.2200	1.0000	0.1000	0.0000	1.0000	0.0000	1.0000	0.1000	1.1800	0.8378	0.7579	-2.7319	0.1200	0.9600	0.9873	0.9239	0.5202
0.0800	0.2400	1.0000	0.2400	1.0000	0.1000	0.0200	1.0000	0.0200	1.0000	0.1000	1.2000	0.8032	0.6996	-3.0974	0.1200	0.9800	0.9835	0.9330	0.3826
0.0800	0.2600	1.0000	0.2600	1.0000	0.1000	0.0400	1.0000	0.0400	1.0000	0.1000	1.2200	0.7631	0.6339	-3.4727	0.1200	1.0000	0.9785	0.9389	0.2104
0.0800	0.2800	1.0000	0.2800	1.0000	0.1000	0.0600	1.0000	0.0600	1.0000	0.1000	1.2400	0.7166	0.5607	-3.8387	0.1200	1.0200	0.9721	0.9411	0.0031

T/T_c	v_0/v_{00}	ϵ_0/ϵ_{00}	v/v_{00}	dv/dv_0	T/T_c	v_0/v_{00}	ϵ_0/ϵ_{00}	v/v_{00}	dv/dv_0	T/T_c	v_0/v_{00}	ϵ_0/ϵ_{00}	v/v_{00}	dv/dv_0	T/T_c	v_0/v_{00}	ϵ_0/ϵ_{00}	v/v_{00}	dv/dv_0
0.1200	1.0400	0.9641	0.9388	-0.2430	0.1400	0.8200	0.9965	0.8101	0.8858	0.1600	0.6000	0.9993	0.5982	0.9822	0.1800	0.3800	0.9998	0.3794	0.9954
0.1200	1.0600	0.9540	0.9312	-0.5267	0.1400	0.8400	0.9956	0.8275	0.8560	0.1600	0.6200	0.9992	0.6178	0.9784	0.1800	0.4000	0.9997	0.3993	0.9946
0.1200	1.0800	0.9415	0.9175	-0.8436	0.1400	0.8600	0.9944	0.8443	0.8186	0.1600	0.6400	0.9990	0.6373	0.9737	0.1800	0.4200	0.9997	0.4192	0.9936
0.1200	1.1000	0.9263	0.8972	-1.1884	0.1400	0.8800	0.9930	0.8602	0.7715	0.1600	0.6600	0.9988	0.6567	0.9679	0.1800	0.4400	0.9996	0.4391	0.9925
0.1200	1.1200	0.9080	0.8699	-1.5528	0.1400	0.9000	0.9911	0.8751	0.7125	0.1600	0.6800	0.9985	0.6760	0.9609	0.1800	0.4600	0.9996	0.4589	0.9910
0.1200	1.1400	0.8862	0.8351	-1.9265	0.1400	0.9200	0.9889	0.8886	0.6388	0.1600	0.7000	0.9982	0.6951	0.9522	0.1800	0.4800	0.9995	0.4787	0.9893
0.1200	1.1600	0.8606	0.7928	-2.3042	0.1400	0.9400	0.9860	0.9005	0.5470	0.1600	0.7200	0.9978	0.7141	0.9416	0.1800	0.5000	0.9994	0.4985	0.9874
0.1200	1.1800	0.8307	0.7429	-2.6822	0.1400	0.9600	0.9823	0.9103	0.4364	0.1600	0.7400	0.9974	0.7328	0.9287	0.1800	0.5200	0.9993	0.5182	0.9851
0.1200	1.2000	0.7960	0.6854	-3.0755	0.1400	0.9800	0.9779	0.9178	0.2998	0.1600	0.7600	0.9968	0.7512	0.9128	0.1800	0.5400	0.9992	0.5379	0.9823
0.1200	1.2200	0.7556	0.6200	-3.4378	0.1400	1.0000	0.9723	0.9221	0.1329	0.1600	0.7800	0.9961	0.7693	0.8934	0.1800	0.5600	0.9990	0.5575	0.9789
0.1200	1.2400	0.7092	0.5480	-3.7897	0.1400	1.0200	0.9653	0.9229	-0.0638	0.1600	0.8000	0.9953	0.7869	0.8696	0.1800	0.5800	0.9989	0.5770	0.9749
0.1200	1.2600	0.6547	0.4683	-4.1811	0.1400	1.0400	0.9567	0.9194	-0.2936	0.1600	0.8200	0.9942	0.8040	0.8404	0.1800	0.6000	0.9987	0.5965	0.9702
0.1200	1.2800	0.5898	0.3809	-4.5445	0.1400	1.0600	0.9462	0.9109	-0.5577	0.1600	0.8400	0.9930	0.8205	0.8047	0.1800	0.6200	0.9984	0.6158	0.9645
0.1200	1.3000	0.5113	0.2866	-4.8752	0.1400	1.0800	0.9333	0.8969	-0.8535	0.1600	0.8600	0.9914	0.8362	0.7612	0.1800	0.6400	0.9981	0.6351	0.9577
0.1200	1.3200	0.4113	0.1857	-5.2373	0.1400	1.1000	0.9179	0.8766	-1.1771	0.1600	0.8800	0.9895	0.8509	0.7080	0.1800	0.6600	0.9978	0.6541	0.9496
0.1200	1.3400	0.2649	0.0772	-5.5994	0.1400	1.1200	0.8995	0.8496	-1.5232	0.1600	0.9000	0.9872	0.8644	0.6432	0.1800	0.6800	0.9974	0.6730	0.9399
					0.1400	1.1400	0.8777	0.8156	-1.8862	0.1600	0.9200	0.9844	0.8765	0.5661	0.1800	0.7000	0.9969	0.6917	0.9283
					0.1400	1.1600	0.8521	0.7741	-2.2589	0.1600	0.9400	0.9809	0.8869	0.4691	0.1800	0.7200	0.9964	0.7102	0.9145
0.1400	0.0000	1.0000	0.0000	1.0000	0.1400	1.1800	0.8222	0.7252	-2.6340	0.1600	0.9600	0.9767	0.8952	0.3574	0.1800	0.7400	0.9957	0.7283	0.8979
0.1400	0.0200	1.0000	0.0200	1.0000	0.1400	1.2000	0.7875	0.6687	-3.0292	0.1600	0.9800	0.9716	0.9010	0.2221	0.1800	0.7600	0.9949	0.7461	0.8780
0.1400	0.0400	1.0000	0.0400	1.0000	0.1400	1.2200	0.7469	0.6041	-3.3951	0.1600	1.0000	0.9654	0.9039	0.0596	0.1800	0.7800	0.9939	0.7634	0.8542
0.1400	0.0600	1.0000	0.0600	1.0000	0.1400	1.2400	0.7002	0.5329	-3.7551	0.1600	1.0200	0.9578	0.9032	-0.1285	0.1800	0.8000	0.9928	0.7802	0.8258
0.1400	0.0800	1.0000	0.0800	1.0000	0.1400	1.2600	0.6453	0.4538	-4.1513	0.1600	1.0400	0.9486	0.8985	-0.3462	0.1800	0.8200	0.9916	0.7964	0.7918
0.1400	0.1000	1.0000	0.1000	1.0000	0.1400	1.2800	0.5797	0.3671	-4.4899	0.1600	1.0600	0.9376	0.8892	-0.5939	0.1800	0.8400	0.9897	0.8118	0.7510
0.1400	0.1200	1.0000	0.1200	1.0000	0.1400	1.3000	0.5005	0.2741	-4.8487	0.1600	1.0800	0.9243	0.8746	-0.8714	0.1800	0.8600	0.9878	0.8264	0.7023
0.1400	0.1400	1.0000	0.1400	1.0000	0.1400	1.3200	0.3973	0.1730	-5.2306	0.1600	1.1000	0.9086	0.8541	-1.1762	0.1800	0.8800	0.9854	0.8398	0.6441
0.1400	0.1600	1.0000	0.1600	1.0000	0.1400	1.3400	0.2431	0.0649	-5.6125	0.1600	1.1200	0.8900	0.8274	-1.5058	0.1800	0.9000	0.9826	0.8521	0.5748
0.1400	0.1800	1.0000	0.1800	1.0000						0.1600	1.1400	0.8680	0.7938	-1.8551	0.1800	0.9200	0.9792	0.8627	0.4925
0.1400	0.2000	1.0000	0.2000	1.0000						0.1600	1.1600	0.8423	0.7531	-2.2191	0.1800	0.9400	0.9751	0.8717	0.3944
0.1400	0.2200	1.0000	0.2200	1.0000	0.1600	0.0000	1.0000	0.0000	0.9999	0.1600	1.1800	0.8124	0.7050	-2.5891	0.1800	0.9600	0.9703	0.8784	0.2824
0.1400	0.2400	1.0000	0.2400	1.0000	0.1600	0.0200	1.0000	0.0200	1.0000	0.1600	1.2000	0.7776	0.6495	-2.9633	0.1800	0.9800	0.9646	0.8828	0.1487
0.1400	0.2600	1.0000	0.2600	1.0000	0.1600	0.0400	1.0000	0.0400	1.0000	0.1600	1.2200	0.7371	0.5864	-3.3491	0.1800	1.0000	0.9578	0.8842	-0.0103
0.1400	0.2800	1.0000	0.2800	1.0000	0.1600	0.0600	1.0000	0.0600	1.0000	0.1600	1.2400	0.6898	0.5155	-3.7323	0.1800	1.0200	0.9496	0.8822	-0.1911
0.1400	0.3000	1.0000	0.3000	1.0000	0.1600	0.0800	1.0000	0.0800	1.0000	0.1600	1.2600	0.6342	0.4372	-4.0888	0.1800	1.0400	0.9398	0.8764	-0.3994
0.1400	0.3200	1.0000	0.3200	1.0000	0.1600	0.1000	1.0000	0.1000	1.0000	0.1600	1.2800	0.5682	0.3518	-4.4779	0.1800	1.0600	0.9282	0.8661	-0.6335
0.1400	0.3400	1.0000	0.3400	1.0000	0.1600	0.1200	1.0000	0.1200	1.0000	0.1600	1.3000	0.4862	0.2582	-4.8412	0.1800	1.0800	0.9145	0.8509	-0.8951
0.1400	0.3600	1.0000	0.3600	1.0004	0.1600	0.1400	1.0000	0.1400	1.0000	0.1600	1.3200	0.3804	0.1582	-5.1966	0.1800	1.1000	0.8984	0.8301	-1.1848
0.1400	0.3800	1.0000	0.3800	0.9974	0.1600	0.1600	1.0000	0.1600	1.0000	0.1600	1.3400	0.2143	0.0503	-5.5521	0.1800	1.1200	0.8794	0.8033	-1.4975
0.1400	0.4000	1.0000	0.3999	0.9968	0.1600	0.1800	1.0000	0.1800	1.0000						0.1800	1.1400	0.8573	0.7701	-1.8319
0.1400	0.4200	1.0000	0.4199	0.9991	0.1600	0.2000	1.0000	0.2000	1.0000						0.1800	1.1600	0.8314	0.7299	-2.1850
0.1400	0.4400	0.9999	0.4399	0.9985	0.1600	0.2200	1.0000	0.2200	1.0000	0.1800	0.0000	1.0000	0.0000	0.9995	0.1800	1.1800	0.8012	0.6826	-2.5475
0.1400	0.4600	0.9999	0.4598	0.9981	0.1600	0.2400	1.0000	0.2400	1.0004	0.1800	0.0200	1.0000	0.0200	0.9998	0.1800	1.2000	0.7662	0.6279	-2.9358
0.1400	0.4800	0.9999	0.4798	0.9976	0.1600	0.2600	1.0000	0.2600	0.9974	0.1800	0.0400	1.0000	0.0400	1.0000	0.1800	1.2200	0.7251	0.5653	-3.2993
0.1400	0.5000	0.9999	0.4997	0.9971	0.1600	0.2800	1.0000	0.2799	0.9969	0.1800	0.0600	1.0000	0.0600	1.0000	0.1800	1.2400	0.6777	0.4959	-3.6705
0.1400	0.5200	0.9999	0.5197	0.9963	0.1600	0.3000	1.0000	0.2999	0.9993	0.1800	0.0800	1.0000	0.0800	1.0000	0.1800	1.2600	0.6214	0.4184	-4.0517
0.1400	0.5400	0.9998	0.5396	0.9954	0.1600	0.3200	0.9999	0.3199	0.9988	0.1800	0.1000	0.9999	0.1000	1.0000	0.1800	1.2800	0.5543	0.3339	-4.4160
0.1400	0.5600	0.9998	0.5595	0.9942	0.1600	0.3400	0.9999	0.3398	0.9986	0.1800	0.1200	0.9999	0.1200	1.0004	0.1800	1.3000	0.4710	0.2416	-4.8174
0.1400	0.5800	0.9998	0.5794	0.9928	0.1600	0.3600	0.9999	0.3598	0.9983	0.1800	0.1400	0.9999	0.1400	0.9974	0.1800	1.3200	0.3599	0.1414	-5.1809
0.1400	0.6000	0.9997	0.5992	0.9909	0.1600	0.3800	0.9999	0.3798	0.9979	0.1800	0.1600	0.9999	0.1599	0.9969	0.1800	1.3400	0.1772	0.0344	-5.5444
0.1400	0.6200	0.9996	0.6190	0.9886	0.1600	0.4000	0.9999	0.3997	0.9975	0.1800	0.1800	0.9999	0.1799	0.9994					
0.1400	0.6400	0.9995	0.6387	0.9857	0.1600	0.4200	0.9999	0.4197	0.9969	0.1800	0.2000	0.9999	0.1999	0.9989					
0.1400	0.6600	0.9994	0.6584	0.9820	0.1600	0.4400	0.9998	0.4396	0.9963	0.1800	0.2200	0.9999	0.2198	0.9987	0.2000	0.0000	0.9999	0.0000	0.9989
0.1400	0.6800	0.9993	0.6780	0.9773	0.1600	0.4600	0.9998	0.4595	0.9955	0.1800	0.2400	0.9999	0.2398	0.9985	0.2000	0.0200	0.9999	0.0200	0.9995
0.1400	0.7000	0.9991	0.6975	0.9714	0.1600	0.4800	0.9998	0.4794	0.9945	0.1800	0.2600	0.9999	0.2598	0.9983	0.2000	0.0400	0.9999	0.0400	1.0000
0.1400	0.7200	0.9989	0.7168	0.9641	0.1600	0.5000	0.9997	0.4993	0.9933	0.1800	0.2800	0.9999	0.2797	0.9980	0.2000	0.0600	0.9999	0.0600	0.9973
0.1400	0.7400	0.9986	0.7360	0.9548	0.1600	0.5200	0.9997	0.5192	0.9919	0.1800	0.3000	0.9999	0.2997	0.9976	0.2000	0.0800	0.9999	0.0799	0.9965
0.1400	0.7600	0.9982	0.7550	0.9430	0.1600	0.5400	0.9996	0.5390	0.9902	0.1800	0.3200	0.9998	0.3197	0.9972	0.2000	0.1000	0.9999	0.0999	0.9989
0.1400	0.7800	0.9978	0.7737	0.9282	0.1600	0.5600	0.9995	0.5588	0.9881	0.1800	0.3400	0.9998	0.3396	0.9967	0.2000	0.1200	0.9999	0.1198	0.9984
0.1400	0.8000	0.9972	0.7921	0.9094	0.1600	0.5800	0.9994	0.5785	0.9854	0.1800	0.3600	0.9998	0.3595	0.9961	0.2000	0.1400	0.9998	0.1398	0.9983

T/T_e	v_0/v_∞	$\epsilon_0/\epsilon_\infty$	v/v_∞	dv/dv_0
0.2000	0.1600	0.9998	0.1598	0.9981
0.2000	0.1800	0.9998	0.1797	0.9978
0.2000	0.2000	0.9998	0.1997	0.9976
0.2000	0.2200	0.9998	0.2196	0.9972
0.2000	0.2400	0.9998	0.2396	0.9968
0.2000	0.2600	0.9997	0.2595	0.9964
0.2000	0.2800	0.9997	0.2794	0.9958
0.2000	0.3000	0.9997	0.2993	0.9952
0.2000	0.3200	0.9996	0.3192	0.9945
0.2000	0.3400	0.9996	0.3391	0.9936
0.2000	0.3600	0.9995	0.3590	0.9926
0.2000	0.3800	0.9995	0.3788	0.9915
0.2000	0.4000	0.9994	0.3986	0.9901
0.2000	0.4200	0.9993	0.4184	0.9885
0.2000	0.4400	0.9992	0.4382	0.9867
0.2000	0.4600	0.9991	0.4579	0.9845
0.2000	0.4800	0.9990	0.4776	0.9820
0.2000	0.5000	0.9988	0.4972	0.9790
0.2000	0.5200	0.9987	0.5167	0.9755
0.2000	0.5400	0.9985	0.5362	0.9715
0.2000	0.5600	0.9983	0.5556	0.9667
0.2000	0.5800	0.9980	0.5749	0.9612
0.2000	0.6000	0.9977	0.5940	0.9546
0.2000	0.6200	0.9973	0.6130	0.9470
0.2000	0.6400	0.9969	0.6319	0.9381
0.2000	0.6600	0.9964	0.6505	0.9275
0.2000	0.6800	0.9958	0.6690	0.9151
0.2000	0.7000	0.9951	0.6871	0.9006
0.2000	0.7200	0.9944	0.7050	0.8835
0.2000	0.7400	0.9934	0.7225	0.8634
0.2000	0.7600	0.9923	0.7395	0.8398
0.2000	0.7800	0.9911	0.7560	0.8120
0.2000	0.8000	0.9896	0.7719	0.7794
0.2000	0.8200	0.9878	0.7872	0.7410
0.2000	0.8400	0.9858	0.8015	0.6958
0.2000	0.8600	0.9834	0.8149	0.6428
0.2000	0.8800	0.9805	0.8272	0.5807
0.2000	0.9000	0.9772	0.8381	0.5078
0.2000	0.9200	0.9733	0.8474	0.4225
0.2000	0.9400	0.9686	0.8549	0.3229
0.2000	0.9600	0.9632	0.8602	0.2109
0.2000	0.9800	0.9569	0.8632	0.0784
0.2000	1.0000	0.9494	0.8632	-0.0773
0.2000	1.0200	0.9406	0.8600	-0.2521
0.2000	1.0400	0.9303	0.8530	-0.4512
0.2000	1.0600	0.9181	0.8418	-0.6756
0.2000	1.0800	0.9039	0.8258	-0.9247
0.2000	1.1000	0.8873	0.8046	-1.1990
0.2000	1.1200	0.8680	0.7777	-1.4979
0.2000	1.1400	0.8454	0.7445	-1.8180
0.2000	1.1600	0.8192	0.7048	-2.1591
0.2000	1.1800	0.7887	0.6581	-2.5099
0.2000	1.2000	0.7534	0.6043	-2.8804
0.2000	1.2200	0.7119	0.5425	-3.2552
0.2000	1.2400	0.6639	0.4740	-3.6273
0.2000	1.2600	0.6067	0.3973	-4.0244
0.2000	1.2800	0.5377	0.3132	-4.3840
0.2000	1.3000	0.4520	0.2219	-4.7613
0.2000	1.3200	0.3357	0.1228	-5.1332
0.2000	1.3400	0.1224	0.0166	-5.5051
0.2200	0.0000	0.9997	0.0000	0.9976
0.2200	0.0200	0.9997	0.0200	0.9969
0.2200	0.0400	0.9997	0.0399	0.9962
0.2200	0.0600	0.9997	0.0598	0.9976
0.2200	0.0800	0.9997	0.0798	0.9972
0.2200	0.1000	0.9997	0.0997	0.9971
0.2200	0.1200	0.9997	0.1197	0.9968
0.2200	0.1400	0.9996	0.1396	0.9965
0.2200	0.1600	0.9996	0.1595	0.9962
0.2200	0.1800	0.9996	0.1795	0.9958
0.2200	0.2000	0.9996	0.1994	0.9953
0.2200	0.2200	0.9995	0.2193	0.9948
0.2200	0.2400	0.9995	0.2392	0.9942
0.2200	0.2600	0.9995	0.2590	0.9934
0.2200	0.2800	0.9994	0.2789	0.9926
0.2200	0.3000	0.9993	0.2987	0.9916
0.2200	0.3200	0.9993	0.3186	0.9904
0.2200	0.3400	0.9992	0.3384	0.9891
0.2200	0.3600	0.9991	0.3581	0.9876
0.2200	0.3800	0.9990	0.3779	0.9858
0.2200	0.4000	0.9989	0.3976	0.9838
0.2200	0.4200	0.9988	0.4172	0.9815
0.2200	0.4400	0.9986	0.4368	0.9788
0.2200	0.4600	0.9984	0.4564	0.9757
0.2200	0.4800	0.9982	0.4758	0.9722
0.2200	0.5000	0.9980	0.4952	0.9681
0.2200	0.5200	0.9978	0.5146	0.9634
0.2200	0.5400	0.9976	0.5338	0.9580
0.2200	0.5600	0.9971	0.5529	0.9517
0.2200	0.5800	0.9967	0.5718	0.9444
0.2200	0.6000	0.9963	0.5906	0.9360
0.2200	0.6200	0.9958	0.6093	0.9262
0.2200	0.6400	0.9952	0.6277	0.9150
0.2200	0.6600	0.9945	0.6458	0.9021
0.2200	0.6800	0.9937	0.6637	0.8870
0.2200	0.7000	0.9928	0.6813	0.8696
0.2200	0.7200	0.9918	0.6985	0.8494
0.2200	0.7400	0.9906	0.7153	0.8261
0.2200	0.7600	0.9892	0.7315	0.7990
0.2200	0.7800	0.9876	0.7472	0.7676
0.2200	0.8000	0.9858	0.7622	0.7312
0.2200	0.8200	0.9836	0.7764	0.6890
0.2200	0.8400	0.9812	0.7897	0.6401
0.2200	0.8600	0.9783	0.8020	0.5836
0.2200	0.8800	0.9748	0.8130	0.5180
0.2200	0.9000	0.9711	0.8226	0.4423
0.2200	0.9200	0.9666	0.8306	0.3550
0.2200	0.9400	0.9614	0.8367	0.2539
0.2200	0.9600	0.9554	0.8407	0.1423
0.2200	0.9800	0.9485	0.8423	0.0113
0.2200	1.0000	0.9404	0.8410	-0.1418
0.2200	1.0200	0.9310	0.8365	-0.3114
0.2200	1.0400	0.9200	0.8284	-0.5034
0.2200	1.0600	0.9073	0.8162	-0.7181
0.2200	1.0800	0.8925	0.7995	-0.9565
0.2200	1.1000	0.8754	0.7778	-1.2193
0.2200	1.1200	0.8555	0.7506	-1.5043
0.2200	1.1400	0.8325	0.7175	-1.8110
0.2200	1.1600	0.8059	0.6780	-2.1383
0.2200	1.1800	0.7750	0.6318	-2.4816
0.2200	1.2000	0.7392	0.5786	-2.8547
0.2200	1.2200	0.6971	0.5177	-3.2087
0.2200	1.2400	0.6485	0.4502	-3.5827
0.2200	1.2600	0.5901	0.3744	-3.9548
0.2200	1.2800	0.5200	0.2919	-4.3457
0.2200	1.3000	0.4305	0.2006	-4.7223
0.2200	1.3200	0.3079	0.1030	-5.0988
0.2400	0.0000	0.9994	0.0000	0.9954
0.2400	0.0200	0.9994	0.0199	0.9954
0.2400	0.0400	0.9994	0.0398	0.9953
0.2400	0.0600	0.9994	0.0597	0.9951
0.2400	0.0800	0.9994	0.0796	0.9949
0.2400	0.1000	0.9994	0.0995	0.9946
0.2400	0.1200	0.9993	0.1194	0.9943
0.2400	0.1400	0.9993	0.1393	0.9938
0.2400	0.1600	0.9993	0.1592	0.9933
0.2400	0.1800	0.9992	0.1790	0.9927
0.2400	0.2000	0.9992	0.1989	0.9920
0.2400	0.2200	0.9991	0.2187	0.9912
0.2400	0.2400	0.9991	0.2385	0.9902
0.2400	0.2600	0.9990	0.2583	0.9891
0.2400	0.2800	0.9989	0.2781	0.9879
0.2400	0.3000	0.9988	0.2978	0.9864
0.2400	0.3200	0.9987	0.3175	0.9848
0.2400	0.3400	0.9986	0.3372	0.9829
0.2400	0.3600	0.9984	0.3568	0.9808
0.2400	0.3800	0.9983	0.3764	0.9783
0.2400	0.4000	0.9981	0.3960	0.9756
0.2400	0.4200	0.9979	0.4155	0.9724
0.2400	0.4400	0.9977	0.4349	0.9688
0.2400	0.4600	0.9974	0.4542	0.9647
0.2400	0.4800	0.9971	0.4735	0.9600
0.2400	0.5000	0.9968	0.4926	0.9547
0.2400	0.5200	0.9965	0.5116	0.9486
0.2400	0.5400	0.9960	0.5305	0.9417
0.2400	0.5600	0.9956	0.5493	0.9338
0.2400	0.5800	0.9950	0.5679	0.9247
0.2400	0.6000	0.9944	0.5863	0.9144
0.2400	0.6200	0.9937	0.6044	0.9026
0.2400	0.6400	0.9930	0.6224	0.8892
0.2400	0.6600	0.9921	0.6400	0.8738
0.2400	0.6800	0.9911	0.6573	0.8561
0.2400	0.7000	0.9899	0.6742	0.8360
0.2400	0.7200	0.9886	0.6907	0.8129
0.2400	0.7400	0.9871	0.7067	0.7865
0.2400	0.7600	0.9854	0.7222	0.7562
0.2400	0.7800	0.9835	0.7369	0.7216
0.2400	0.8000	0.9813	0.7510	0.6819
0.2400	0.8200	0.9787	0.7642	0.6364
0.2400	0.8400	0.9758	0.7764	0.5844
0.2400	0.8600	0.9725	0.7875	0.5248
0.2400	0.8800	0.9687	0.7973	0.4565
0.2400	0.9000	0.9643	0.8057	0.3786
0.2400	0.9200	0.9593	0.8124	0.2889
0.2400	0.9400	0.9535	0.8172	0.1873
0.2400	0.9600	0.9468	0.8198	0.0769
0.2400	0.9800	0.9394	0.8201	-0.0538
0.2400	1.0000	0.9306	0.8176	-0.2034
0.2400	1.0200	0.9206	0.8119	-0.3693
0.2400	1.0400	0.9090	0.8026	-0.5560
0.2400	1.0600	0.8956	0.7895	-0.7613
0.2400	1.0800	0.8802	0.7720	-0.9908
0.2400	1.1000	0.8625	0.7497	-1.2418
0.2400	1.1200	0.8421	0.7222	-1.5143
0.2400	1.1400	0.8185	0.6890	-1.8110
0.2400	1.1600	0.7913	0.6497	-2.1263
0.2400	1.1800	0.7599	0.6038	-2.4576
0.2400	1.2000	0.7235	0.5512	-2.8171
0.2400	1.2200	0.6808	0.4911	-3.1827
0.2400	1.2400	0.6308	0.4239	-3.5371
0.2400	1.2600	0.5714	0.3496	-3.8969
0.2400	1.2800	0.4992	0.2679	-4.2931
0.2400	1.3000	0.4059	0.1778	-4.6916
0.2400	1.3200	0.2721	0.0802	-5.0902
0.2600	0.0000	0.9989	0.0000	0.9922
0.2600	0.0200	0.9989	0.0198	0.9921
0.2600	0.0400	0.9989	0.0397	0.9920
0.2600	0.0600	0.9989	0.0595	0.9918
0.2600	0.0800	0.9989	0.0794	0.9915
0.2600	0.1000	0.9988	0.0992	0.9911
0.2600	0.1200	0.9988	0.1190	0.9905
0.2600	0.1400	0.9988	0.1388	0.9899
0.2600	0.1600	0.9987	0.1586	0.9892
0.2600	0.1800	0.9986	0.1784	0.9883
0.2600	0.2000	0.9986	0.1981	0.9873
0.2600	0.2200	0.9985	0.2179	0.9862
0.2600	0.2400	0.9984	0.2376	0.9848
0.2600	0.2600	0.9983	0.2573	0.9833
0.2600	0.2800	0.9981	0.2769	0.9816
0.2600	0.3000	0.9980	0.2965	0.9796
0.2600	0.3200	0.9978	0.3161	0.9774
0.2600	0.3400	0.9977	0.3356	0.9749
0.2600	0.3600	0.9975	0.3551	0.9721
0.2600	0.3800	0.9973	0.3745	0.9689
0.2600	0.4000	0.9970	0.3938	0.9653
0.2600	0.4200	0.9967	0.4131	0.9612
0.2600	0.4400	0.9964	0.4323	0.9566
0.2600	0.4600	0.9961	0.4514	0.9514
0.2600	0.4800	0.9957	0.4703	0.9455
0.2600	0.5000	0.9952	0.4892	0.9389
0.2600	0.5200	0.9947	0.5079	0.9314
0.2600	0.5400	0.9942	0.5264	0.9230
0.2600	0.5600	0.9936	0.5448	0.9134
0.2600	0.5800	0.9929	0.5630	0.9026
0.2600	0.6000	0.9921	0.5809	0.8904
0.2600	0.6200	0.9912	0.5986	0.8766
0.2600	0.6400	0.9902	0.6159	0.8609
0.2600	0.6600	0.9891	0.6330	0.8432
0.2600	0.6800	0.9878	0.6497	0.8231
0.2600	0.7000	0.9864	0.6659	0.8004

T/T_e	v_0/v_∞	$\epsilon_0/\epsilon_\infty$	v/v_∞	dv/dv_0	T/T_e	v_0/v_∞	$\epsilon_0/\epsilon_\infty$	v/v_∞	dv/dv_0	T/T_e	v_0/v_∞	$\epsilon_0/\epsilon_\infty$	v/v_∞	dv/dv_0	T/T_e	v_0/v_∞	$\epsilon_0/\epsilon_\infty$	v/v_∞	dv/dv_0
0.2600	0.7200	0.9848	0.6816	0.7746	0.2800	0.5200	0.9925	0.5033	0.9120	0.3000	0.3200	0.9951	0.3118	0.9574	0.3200	0.1200	0.9954	0.1168	0.9708
0.2600	0.7400	0.9830	0.6969	0.7454	0.2800	0.5400	0.9918	0.5214	0.9020	0.3000	0.3400	0.9948	0.3309	0.9534	0.3200	0.1400	0.9952	0.1362	0.9694
0.2600	0.7600	0.9810	0.7114	0.7123	0.2800	0.5600	0.9910	0.5393	0.8908	0.3000	0.3600	0.9944	0.3499	0.9491	0.3200	0.1600	0.9951	0.1556	0.9679
0.2600	0.7800	0.9787	0.7254	0.6743	0.2800	0.5800	0.9902	0.5570	0.8783	0.3000	0.3800	0.9940	0.3688	0.9442	0.3200	0.1800	0.9949	0.1749	0.9661
0.2600	0.8000	0.9761	0.7384	0.6316	0.2800	0.6000	0.9892	0.5744	0.8642	0.3000	0.4000	0.9936	0.3877	0.9388	0.3200	0.2000	0.9947	0.1942	0.9640
0.2600	0.8200	0.9731	0.7505	0.5837	0.2800	0.6200	0.9881	0.5916	0.8484	0.3000	0.4200	0.9931	0.4064	0.9327	0.3200	0.2200	0.9945	0.2134	0.9616
0.2600	0.8400	0.9698	0.7617	0.5288	0.2800	0.6400	0.9869	0.6084	0.8304	0.3000	0.4400	0.9926	0.4250	0.9260	0.3200	0.2400	0.9943	0.2327	0.9589
0.2600	0.8600	0.9660	0.7716	0.4666	0.2800	0.6600	0.9855	0.6248	0.8105	0.3000	0.4600	0.9920	0.4434	0.9185	0.3200	0.2600	0.9940	0.2518	0.9559
0.2600	0.8800	0.9616	0.7803	0.3960	0.2800	0.6800	0.9840	0.6408	0.7883	0.3000	0.4800	0.9913	0.4617	0.9102	0.3200	0.2800	0.9937	0.2709	0.9526
0.2600	0.9000	0.9567	0.7874	0.3169	0.2800	0.7000	0.9823	0.6563	0.7632	0.3000	0.5000	0.9906	0.4798	0.9007	0.3200	0.3000	0.9934	0.2899	0.9488
0.2600	0.9200	0.9511	0.7929	0.2257	0.2800	0.7200	0.9804	0.6713	0.7349	0.3000	0.5200	0.9898	0.4977	0.8903	0.3200	0.3200	0.9930	0.3088	0.9446
0.2600	0.9400	0.9448	0.7964	0.1226	0.2800	0.7400	0.9782	0.6857	0.7031	0.3000	0.5400	0.9889	0.5154	0.8790	0.3200	0.3400	0.9926	0.3277	0.9399
0.2600	0.9600	0.9375	0.7977	0.0130	0.2800	0.7600	0.9758	0.6994	0.6674	0.3000	0.5600	0.9879	0.5329	0.8662	0.3200	0.3600	0.9922	0.3464	0.9348
0.2600	0.9800	0.9295	0.7968	-0.1153	0.2800	0.7800	0.9732	0.7123	0.6271	0.3000	0.5800	0.9869	0.5501	0.8519	0.3200	0.3800	0.9917	0.3651	0.9290
0.2600	1.0000	0.9201	0.7930	-0.2630	0.2800	0.8000	0.9702	0.7244	0.5819	0.3000	0.6000	0.9857	0.5669	0.8361	0.3200	0.4000	0.9911	0.3836	0.9227
0.2600	1.0200	0.9094	0.7861	-0.4254	0.2800	0.8200	0.9668	0.7356	0.5309	0.3000	0.6200	0.9844	0.5835	0.8183	0.3200	0.4200	0.9905	0.4020	0.9154
0.2600	1.0400	0.8971	0.7759	-0.6061	0.2800	0.8400	0.9630	0.7456	0.4736	0.3000	0.6400	0.9829	0.5997	0.7986	0.3200	0.4400	0.9899	0.4202	0.9076
0.2600	1.0600	0.8831	0.7618	-0.8055	0.2800	0.8600	0.9587	0.7545	0.4093	0.3000	0.6600	0.9813	0.6154	0.7766	0.3200	0.4600	0.9891	0.4383	0.8991
0.2600	1.0800	0.8671	0.7435	-1.0263	0.2800	0.8800	0.9538	0.7619	0.3369	0.3000	0.6800	0.9795	0.6307	0.7520	0.3200	0.4800	0.9883	0.4562	0.8895
0.2600	1.1000	0.8487	0.7206	-1.2671	0.2800	0.9000	0.9484	0.7679	0.2656	0.3000	0.7000	0.9775	0.6445	0.7247	0.3200	0.5000	0.9875	0.4738	0.8780
0.2600	1.1200	0.8277	0.6927	-1.5310	0.2800	0.9200	0.9423	0.7721	0.1638	0.3000	0.7200	0.9742	0.6557	0.6941	0.3200	0.5200	0.9865	0.4913	0.8672
0.2600	1.1400	0.8035	0.6592	-1.8146	0.2800	0.9400	0.9353	0.7744	0.0651	0.3000	0.7400	0.9727	0.6632	0.6600	0.3200	0.5400	0.9854	0.5085	0.8542
0.2600	1.1600	0.7756	0.6200	-2.1176	0.2800	0.9600	0.9276	0.7746	-0.0486	0.3000	0.7600	0.9700	0.6681	0.6218	0.3200	0.5600	0.9843	0.5255	0.8398
0.2600	1.1800	0.7435	0.5744	-2.4388	0.2800	0.9800	0.9188	0.7727	-0.1794	0.3000	0.7800	0.9669	0.6981	0.5793	0.3200	0.5800	0.9830	0.5421	0.8240
0.2600	1.2000	0.7064	0.5222	-2.7902	0.2800	1.0000	0.9087	0.7673	-0.3213	0.3000	0.8000	0.9635	0.7092	0.5317	0.3200	0.6000	0.9815	0.5584	0.8064
0.2600	1.2200	0.6628	0.4628	-3.1291	0.2800	1.0200	0.8974	0.7594	-0.4798	0.3000	0.8200	0.9597	0.7193	0.4786	0.3200	0.6200	0.9800	0.5743	0.7868
0.2600	1.2400	0.6119	0.3969	-3.4994	0.2800	1.0400	0.8844	0.7480	-0.6553	0.3000	0.8400	0.9554	0.7283	0.4192	0.3200	0.6400	0.9783	0.5899	0.7652
0.2600	1.2600	0.5504	0.3228	-3.8725	0.2800	1.0600	0.8698	0.7330	-0.8492	0.3000	0.8600	0.9506	0.7360	0.3529	0.3200	0.6600	0.9763	0.6049	0.7413
0.2600	1.2800	0.4756	0.2420	-4.2368	0.2800	1.0800	0.8530	0.7140	-1.0616	0.3000	0.8800	0.9453	0.7424	0.2790	0.3200	0.6800	0.9742	0.6195	0.7147
0.2600	1.3000	0.3775	0.1532	-4.6315	0.2800	1.1000	0.8340	0.6904	-1.2949	0.3000	0.9000	0.9393	0.7471	0.1963	0.3200	0.7000	0.9719	0.6335	0.6851
0.2600	1.3200	0.2293	0.0568	-5.0261	0.2800	1.1200	0.8122	0.6620	-1.5490	0.3000	0.9200	0.9326	0.7501	0.1038	0.3200	0.7200	0.9694	0.6449	0.6525
					0.2800	1.1400	0.7873	0.6283	-1.8216	0.3000	0.9400	0.9251	0.7512	0.0053	0.3200	0.7400	0.9665	0.6536	0.6163
					0.2800	1.1600	0.7587	0.5890	-2.1160	0.3000	0.9600	0.9167	0.7503	-0.1079	0.3200	0.7600	0.9634	0.6715	0.5760
0.2800	0.0000	0.9982	0.0000	0.9877	0.2800	1.1800	0.7258	0.5436	-2.4236	0.3000	0.9800	0.9073	0.7468	-0.2378	0.3200	0.7800	0.9599	0.6826	0.5313
0.2800	0.0200	0.9982	0.0198	0.9876	0.2800	1.2000	0.6877	0.4919	-2.7648	0.3000	1.0000	0.8966	0.7407	-0.3777	0.3200	0.8000	0.9561	0.6927	0.4817
0.2800	0.0400	0.9982	0.0395	0.9874	0.2800	1.2200	0.6430	0.4330	-3.1062	0.3000	1.0200	0.8845	0.7316	-0.5329	0.3200	0.8200	0.9518	0.7018	0.4266
0.2800	0.0600	0.9981	0.0593	0.9871	0.2800	1.2400	0.5906	0.3676	-3.4472	0.3000	1.0400	0.8709	0.7199	-0.7035	0.3200	0.8400	0.9471	0.7098	0.3656
0.2800	0.0800	0.9981	0.0790	0.9867	0.2800	1.2600	0.5275	0.2949	-3.8259	0.3000	1.0600	0.8555	0.7033	-0.8919	0.3200	0.8600	0.9418	0.7164	0.2977
0.2800	0.1000	0.9981	0.0987	0.9862	0.2800	1.2800	0.4489	0.2145	-4.2129	0.3000	1.0800	0.8380	0.6835	-1.0995	0.3200	0.8800	0.9359	0.7216	0.2222
0.2800	0.1200	0.9980	0.1184	0.9855	0.2800	1.3000	0.3438	0.1264	-4.5978	0.3000	1.1000	0.8182	0.6593	-1.3242	0.3200	0.9000	0.9294	0.7252	0.1386
0.2800	0.1400	0.9979	0.1381	0.9846	0.2800	1.3200	0.1684	0.0306	-4.9846	0.3000	1.1200	0.7957	0.6304	-1.5694	0.3200	0.9200	0.9221	0.7271	0.0452
0.2800	0.1600	0.9979	0.1578	0.9837						0.3000	1.1400	0.7699	0.5963	-1.8338	0.3200	0.9400	0.9140	0.7270	-0.0530
0.2800	0.1800	0.9978	0.1775	0.9825						0.3000	1.1600	0.7405	0.5569	-2.1158	0.3200	0.9600	0.9040	0.7249	-0.1654
0.2800	0.2000	0.9977	0.1971	0.9812	0.3000	0.0000	0.9971	0.0000	0.9818	0.3000	1.1800	0.7066	0.5116	-2.4184	0.3200	0.9800	0.8949	0.7209	-0.2945
0.2800	0.2200	0.9975	0.2167	0.9796	0.3000	0.0200	0.9971	0.0196	0.9816	0.3000	1.2000	0.6674	0.4600	-2.7422	0.3200	1.0000	0.8835	0.7130	-0.4320
0.2800	0.2400	0.9974	0.2363	0.9779	0.3000	0.0400	0.9971	0.0393	0.9814	0.3000	1.2200	0.6214	0.4018	-3.0701	0.3200	1.0200	0.8708	0.7029	-0.5839
0.2800	0.2600	0.9972	0.2558	0.9759	0.3000	0.0600	0.9971	0.0589	0.9811	0.3000	1.2400	0.5671	0.3368	-3.4177	0.3200	1.0400	0.8564	0.6896	-0.7524
0.2800	0.2800	0.9971	0.2753	0.9737	0.3000	0.0800	0.9970	0.0785	0.9805	0.3000	1.2600	0.5014	0.2650	-3.7807	0.3200	1.0600	0.8402	0.6727	-0.9359
0.2800	0.3000	0.9969	0.2948	0.9711	0.3000	0.1000	0.9970	0.0981	0.9798	0.3000	1.2800	0.4184	0.1854	-4.1176	0.3200	1.0800	0.8220	0.6520	-1.1362
0.2800	0.3200	0.9967	0.3142	0.9683	0.3000	0.1200	0.9969	0.1177	0.9789	0.3000	1.3000	0.3034	0.0980	-4.5399	0.3200	1.1000	0.8014	0.6271	-1.3551
0.2800	0.3400	0.9964	0.3335	0.9651	0.3000	0.1400	0.9968	0.1373	0.9778	0.3000	1.3200	0.0585	0.0038	-4.9022	0.3200	1.1200	0.7780	0.5977	-1.5911
0.2800	0.3600	0.9961	0.3528	0.9615	0.3000	0.1600	0.9967	0.1568	0.9766						0.3200	1.1400	0.7513	0.5634	-1.8463
0.2800	0.3800	0.9958	0.3720	0.9575	0.3000	0.1800	0.9966	0.1763	0.9751						0.3200	1.1600	0.7209	0.5237	-2.1198
0.2800	0.4000	0.9955	0.3911	0.9530	0.3000	0.2000	0.9964	0.1958	0.9734	0.3200	0.0000	0.9957	0.0000	0.9743	0.3200	1.1800	0.6869	0.4784	-2.4279
0.2800	0.4200	0.9951	0.4101	0.9479	0.3000	0.2200	0.9962	0.2153	0.9715	0.3200	0.0200	0.9957	0.0195	0.9741	0.3200	1.2000	0.6440	0.4266	-2.7247
0.2800	0.4400	0.9947	0.4290	0.9423	0.3000	0.2400	0.9961	0.2347	0.9693	0.3200	0.0400	0.9957	0.0390	0.9739	0.3200	1.2200	0.5977	0.3693	-3.0451
0.2800	0.4600	0.9943	0.4478	0.9360	0.3000	0.2600	0.9959	0.2540	0.9668	0.3200	0.0600	0.9956	0.0584	0.9734	0.3200	1.2400	0.5410	0.3047	-3.3017
0.2800	0.4800	0.9937	0.4664	0.9289	0.3000	0.2800	0.9956	0.2733	0.9640	0.3200	0.0800	0.9955	0.0779	0.9727	0.3200	1.2600	0.4722	0.2335	-3.7653
0.2800	0.5000	0.9932	0.4849	0.9209	0.3000	0.3000	0.9954	0.2926	0.9609	0.3200	0.1000	0.9955	0.0973	0.9719	0.3200	1.2800	0.3829	0.1545	-4.1157

T/T_e	τ_0/v_{00}	ϵ_0/ϵ_{00}	v/v_{00}	dv/dv_0
0.3200	1.3000	0.2549	0.0689	-4.4761
0.3400	0.0000	0.9938	0.0000	0.9652
0.3400	0.0200	0.9938	0.0193	0.9650
0.3400	0.0400	0.9938	0.0386	0.9647
0.3400	0.0600	0.9937	0.0579	0.9642
0.3400	0.0800	0.9936	0.0772	0.9634
0.3400	0.1000	0.9935	0.0964	0.9623
0.3400	0.1200	0.9934	0.1157	0.9610
0.3400	0.1400	0.9933	0.1349	0.9594
0.3400	0.1600	0.9931	0.1540	0.9575
0.3400	0.1800	0.9929	0.1732	0.9553
0.3400	0.2000	0.9926	0.1922	0.9529
0.3400	0.2200	0.9924	0.2113	0.9500
0.3400	0.2400	0.9921	0.2302	0.9468
0.3400	0.2600	0.9917	0.2491	0.9433
0.3400	0.2800	0.9913	0.2680	0.9394
0.3400	0.3000	0.9909	0.2867	0.9350
0.3400	0.3200	0.9905	0.3054	0.9301
0.3400	0.3400	0.9900	0.3239	0.9246
0.3400	0.3600	0.9894	0.3423	0.9186
0.3400	0.3800	0.9888	0.3607	0.9120
0.3400	0.4000	0.9881	0.3788	0.9047
0.3400	0.4200	0.9874	0.3968	0.8966
0.3400	0.4400	0.9866	0.4147	0.8877
0.3400	0.4600	0.9857	0.4323	0.8779
0.3400	0.4800	0.9848	0.4498	0.8672
0.3400	0.5000	0.9837	0.4670	0.8553
0.3400	0.5200	0.9826	0.4840	0.8422
0.3400	0.5400	0.9813	0.5007	0.8278
0.3400	0.5600	0.9799	0.5171	0.8119
0.3400	0.5800	0.9784	0.5332	0.7945
0.3400	0.6000	0.9767	0.5489	0.7752
0.3400	0.6200	0.9749	0.5642	0.7540
0.3400	0.6400	0.9729	0.5790	0.7306
0.3400	0.6600	0.9707	0.5934	0.7047
0.3400	0.6800	0.9683	0.6072	0.6763
0.3400	0.7000	0.9657	0.6204	0.6450
0.3400	0.7200	0.9628	0.6330	0.6103
0.3400	0.7400	0.9596	0.6448	0.5720
0.3400	0.7600	0.9560	0.6558	0.5300
0.3400	0.7800	0.9522	0.6660	0.4835
0.3400	0.8000	0.9479	0.6751	0.4319
0.3400	0.8200	0.9431	0.6832	0.3751
0.3400	0.8400	0.9379	0.6901	0.3124
0.3400	0.8600	0.9321	0.6958	0.2432
0.3400	0.8800	0.9257	0.6998	0.1668
0.3400	0.9000	0.9186	0.7023	0.0822
0.3400	0.9200	0.9108	0.7030	-0.0117
0.3400	0.9400	0.9020	0.7018	-0.1090
0.3400	0.9600	0.8924	0.6985	-0.2210
0.3400	0.9800	0.8816	0.6928	-0.3498
0.3400	1.0000	0.8696	0.6845	-0.4854
0.3400	1.0200	0.8561	0.6733	-0.6349
0.3400	1.0400	0.8409	0.6590	-0.7994
0.3400	1.0600	0.8240	0.6412	-0.9787
0.3400	1.0800	0.8049	0.6197	-1.1738
0.3400	1.1000	0.7834	0.5942	-1.3854

T/T_e	v_0/v_{00}	ϵ_0/ϵ_{00}	v/v_{00}	dv/dv_0
0.3400	1.1200	0.7590	0.5642	-1.6147
0.3400	1.1400	0.7314	0.5295	-1.8633
0.3400	1.1600	0.6998	0.4896	-2.1284
0.3400	1.1800	0.6635	0.4442	-2.4203
0.3400	1.2000	0.6211	0.3927	-2.7120
0.3400	1.2200	0.5719	0.3355	-3.0373
0.3400	1.2400	0.5122	0.2712	-3.3653
0.3400	1.2600	0.4393	0.2008	-3.7038
0.3400	1.2800	0.3424	0.1238	-4.0802
0.3400	1.3000	0.1886	0.0376	-4.4566
0.3600	0.0000	0.9915	0.0000	0.9544
0.3600	0.0200	0.9914	0.0191	0.9541
0.3600	0.0400	0.9914	0.0382	0.9538
0.3600	0.0600	0.9913	0.0572	0.9532
0.3600	0.0800	0.9912	0.0763	0.9522
0.3600	0.1000	0.9911	0.0953	0.9510
0.3600	0.1200	0.9909	0.1143	0.9494
0.3600	0.1400	0.9908	0.1333	0.9476
0.3600	0.1600	0.9905	0.1522	0.9454
0.3600	0.1800	0.9903	0.1711	0.9429
0.3600	0.2000	0.9900	0.1899	0.9400
0.3600	0.2200	0.9897	0.2087	0.9368
0.3600	0.2400	0.9893	0.2274	0.9331
0.3600	0.2600	0.9889	0.2460	0.9290
0.3600	0.2800	0.9884	0.2646	0.9244
0.3600	0.3000	0.9879	0.2830	0.9194
0.3600	0.3200	0.9874	0.3013	0.9138
0.3600	0.3400	0.9868	0.3196	0.9076
0.3600	0.3600	0.9861	0.3376	0.9008
0.3600	0.3800	0.9854	0.3556	0.8933
0.3600	0.4000	0.9846	0.3734	0.8851
0.3600	0.4200	0.9837	0.3910	0.8760
0.3600	0.4400	0.9827	0.4084	0.8661
0.3600	0.4600	0.9817	0.4256	0.8552
0.3600	0.4800	0.9806	0.4426	0.8432
0.3600	0.5000	0.9793	0.4593	0.8301
0.3600	0.5200	0.9780	0.4758	0.8157
0.3600	0.5400	0.9765	0.4920	0.7999
0.3600	0.5600	0.9749	0.5078	0.7826
0.3600	0.5800	0.9731	0.5233	0.7636
0.3600	0.6000	0.9712	0.5383	0.7428
0.3600	0.6200	0.9691	0.5529	0.7200
0.3600	0.6400	0.9669	0.5671	0.6949
0.3600	0.6600	0.9644	0.5807	0.6674
0.3600	0.6800	0.9616	0.5938	0.6372
0.3600	0.7000	0.9587	0.6062	0.6041
0.3600	0.7200	0.9554	0.6179	0.5678
0.3600	0.7400	0.9518	0.6289	0.5278
0.3600	0.7600	0.9479	0.6390	0.4839
0.3600	0.7800	0.9436	0.6482	0.4356
0.3600	0.8000	0.9389	0.6564	0.3825
0.3600	0.8200	0.9337	0.6635	0.3243
0.3600	0.8400	0.9279	0.6693	0.2599
0.3600	0.8600	0.9216	0.6738	0.1893
0.3600	0.8800	0.9147	0.6769	0.1120
0.3600	0.9000	0.9070	0.6783	0.0270
0.3600	0.9200	0.8985	0.6779	-0.0625

T/T_e	v_0/v_{00}	ϵ_0/ϵ_{00}	v/v_{00}	dv/dv_0
0.3600	0.9400	0.8893	0.6757	-0.1643
0.3600	0.9600	0.8789	0.6712	-0.2799
0.3600	0.9800	0.8674	0.6644	-0.4027
0.3600	1.0000	0.8546	0.6551	-0.5377
0.3600	1.0200	0.8404	0.6428	-0.6849
0.3600	1.0400	0.8244	0.6276	-0.8457
0.3600	1.0600	0.8066	0.6089	-1.0209
0.3600	1.0800	0.7867	0.5866	-1.2109
0.3600	1.1000	0.7642	0.5604	-1.4169
0.3600	1.1200	0.7388	0.5298	-1.6401
0.3600	1.1400	0.7100	0.4947	-1.8815
0.3600	1.1600	0.6771	0.4545	-2.1388
0.3600	1.1800	0.6392	0.4090	-2.4201
0.3600	1.2000	0.5950	0.3576	-2.7052
0.3600	1.2200	0.5433	0.3006	-3.0252
0.3600	1.2400	0.4801	0.2366	-3.3386
0.3600	1.2600	0.4018	0.1669	-3.6788
0.3600	1.2800	0.2929	0.0893	-4.0408
0.3600	1.3000	0.0696	0.0052	-4.4028
0.3800	0.0000	0.9885	0.0000	0.9420
0.3800	0.0200	0.9885	0.0188	0.9417
0.3800	0.0400	0.9885	0.0377	0.9413
0.3800	0.0600	0.9884	0.0565	0.9406
0.3800	0.0800	0.9883	0.0753	0.9395
0.3800	0.1000	0.9881	0.0941	0.9380
0.3800	0.1200	0.9879	0.1128	0.9363
0.3800	0.1400	0.9877	0.1315	0.9341
0.3800	0.1600	0.9874	0.1502	0.9316
0.3800	0.1800	0.9871	0.1688	0.9288
0.3800	0.2000	0.9868	0.1873	0.9255
0.3800	0.2200	0.9864	0.2058	0.9218
0.3800	0.2400	0.9859	0.2242	0.9176
0.3800	0.2600	0.9854	0.2425	0.9130
0.3800	0.2800	0.9849	0.2607	0.9078
0.3800	0.3000	0.9843	0.2788	0.9022
0.3800	0.3200	0.9836	0.2968	0.8959
0.3800	0.3400	0.9829	0.3146	0.8889
0.3800	0.3600	0.9821	0.3323	0.8813
0.3800	0.3800	0.9813	0.3499	0.8730
0.3800	0.4000	0.9803	0.3673	0.8638
0.3800	0.4200	0.9793	0.3844	0.8538
0.3800	0.4400	0.9782	0.4014	0.8428
0.3800	0.4600	0.9770	0.4181	0.8309
0.3800	0.4800	0.9757	0.4346	0.8177
0.3800	0.5000	0.9742	0.4508	0.8034
0.3800	0.5200	0.9727	0.4668	0.7878
0.3800	0.5400	0.9710	0.4823	0.7707
0.3800	0.5600	0.9691	0.4976	0.7520
0.3800	0.5800	0.9671	0.5124	0.7316
0.3800	0.6000	0.9650	0.5268	0.7094
0.3800	0.6200	0.9626	0.5408	0.6850
0.3800	0.6400	0.9600	0.5542	0.6584
0.3800	0.6600	0.9572	0.5671	0.6293
0.3800	0.6800	0.9542	0.5794	0.5976
0.3800	0.7000	0.9508	0.5910	0.5628
0.3800	0.7200	0.9472	0.6019	0.5248
0.3800	0.7400	0.9432	0.6119	0.4833

T/T_e	v_0/v_{00}	ϵ_0/ϵ_{00}	v/v_{00}	dv/dv_0
0.3800	0.7600	0.9389	0.6212	0.4378
0.3800	0.7800	0.9342	0.6294	0.3879
0.3800	0.8000	0.9290	0.6366	0.3333
0.3800	0.8200	0.9233	0.6427	0.2737
0.3800	0.8400	0.9171	0.6476	0.2086
0.3800	0.8600	0.9102	0.6510	0.1367
0.3800	0.8800	0.9027	0.6530	0.0586
0.3800	0.9000	0.8944	0.6533	-0.0273
0.3800	0.9200	0.8854	0.6519	-0.1168
0.3800	0.9400	0.8755	0.6486	-0.2179
0.3800	0.9600	0.8644	0.6431	-0.3334
0.3800	0.9800	0.8522	0.6352	-0.4551
0.3800	1.0000	0.8386	0.6248	-0.5885
0.3800	1.0200	0.8236	0.6116	-0.7334
0.3800	1.0400	0.8068	0.5954	-0.8910
0.3800	1.0600	0.7881	0.5758	-1.0621
0.3800	1.0800	0.7672	0.5528	-1.2477
0.3800	1.1000	0.7436	0.5258	-1.4498
0.3800	1.1200	0.7171	0.4947	-1.6672
0.3800	1.1400	0.6870	0.4590	-1.9008
0.3800	1.1600	0.6526	0.4186	-2.1476
0.3800	1.1800	0.6129	0.3730	-2.4190
0.3800	1.2000	0.5666	0.3217	-2.7088
0.3800	1.2200	0.5117	0.2646	-2.9989
0.3800	1.2400	0.4448	0.2015	-3.3339
0.3800	1.2600	0.3576	0.1312	-3.6682
0.3800	1.2800	0.2308	0.0552	-3.9825
0.4000	0.0000	0.9850	0.0000	0.9279
0.4000	0.0200	0.9850	0.0186	0.9275
0.4000	0.0400	0.9850	0.0371	0.9271
0.4000	0.0600	0.9849	0.0556	0.9263
0.4000	0.0800	0.9847	0.0742	0.9251
0.4000	0.1000	0.9845	0.0926	0.9234
0.4000	0.1200	0.9843	0.1111	0.9214
0.4000	0.1400	0.9840	0.1295	0.9190
0.4000	0.1600	0.9837	0.1479	0.9162
0.4000	0.1800	0.9833	0.1661	0.9130
0.4000	0.2000	0.9829	0.1844	0.9093
0.4000	0.2200	0.9825	0.2025	0.9052
0.4000	0.2400	0.9819	0.2206	0.9005
0.4000	0.2600	0.9814	0.2385	0.8954
0.4000	0.2800	0.9807	0.2564	0.8896
0.4000	0.3000	0.9800	0.2741	0.8833
0.4000	0.3200	0.9793	0.2917	0.8763
0.4000	0.3400	0.9784	0.3092	0.8687
0.4000	0.3600	0.9775	0.3265	0.8603
0.4000	0.3800	0.9765	0.3436	0.8511
0.4000	0.4000	0.9754	0.3605	0.8411
0.4000	0.4200	0.9742	0.3772	0.8301
0.4000	0.4400	0.9730	0.3937	0.8182
0.4000	0.4600	0.9716	0.4099	0.8051
0.4000	0.4800	0.9701	0.4259	0.7909
0.4000	0.5000	0.9684	0.4416	0.7755
0.4000	0.5200	0.9667	0.4569	0.7587
0.4000	0.5400	0.9647	0.4719	0.7404
0.4000	0.5600	0.9626	0.4865	0.7204
0.4000	0.5800	0.9604	0.5007	0.6986

T/T_e	v_0/v_∞	$\epsilon_0/\epsilon_\infty$	v/v_∞	dv/dv_0	T/T_e	v_0/v_∞	$\epsilon_0/\epsilon_\infty$	v/v_∞	dv/dv_0	T/T_e	v_0/v_∞	$\epsilon_0/\epsilon_\infty$	v/v_∞	dv/dv_0	T/T_e	v_0/v_∞	$\epsilon_0/\epsilon_\infty$	v/v_∞	dv/dv_0
0.4000	0.6000	0.9579	0.5144	0.6750	0.4200	0.4400	0.9670	0.3853	0.7921	0.4400	0.3000	0.9694	0.2633	0.8410	0.4600	0.1600	0.9684	0.1393	0.8605
0.4000	0.6200	0.9553	0.5277	0.6492	0.4200	0.4600	0.9654	0.4010	0.7781	0.4400	0.3200	0.9684	0.2800	0.8328	0.4600	0.1800	0.9679	0.1565	0.8563
0.4000	0.6400	0.9524	0.5404	0.6212	0.4200	0.4800	0.9637	0.4164	0.7629	0.4400	0.3400	0.9673	0.2966	0.8237	0.4600	0.2000	0.9672	0.1736	0.8515
0.4000	0.6600	0.9493	0.5525	0.5907	0.4200	0.5000	0.9618	0.4315	0.7463	0.4400	0.3600	0.9661	0.3130	0.8139	0.4600	0.2200	0.9665	0.1906	0.8460
0.4000	0.6800	0.9459	0.5640	0.5574	0.4200	0.5200	0.9598	0.4462	0.7284	0.4400	0.3800	0.9648	0.3291	0.8031	0.4600	0.2400	0.9658	0.2074	0.8400
0.4000	0.7000	0.9422	0.5748	0.5210	0.4200	0.5400	0.9577	0.4606	0.7089	0.4400	0.4000	0.9634	0.3451	0.7914	0.4600	0.2600	0.9649	0.2242	0.8333
0.4000	0.7200	0.9382	0.5848	0.4815	0.4200	0.5600	0.9553	0.4746	0.6878	0.4400	0.4200	0.9619	0.3608	0.7787	0.4600	0.2800	0.9639	0.2408	0.8259
0.4000	0.7400	0.9338	0.5940	0.4386	0.4200	0.5800	0.9528	0.4881	0.6647	0.4400	0.4400	0.9602	0.3762	0.7649	0.4600	0.3000	0.9629	0.2572	0.8178
0.4000	0.7600	0.9290	0.6023	0.3919	0.4200	0.6000	0.9501	0.5012	0.6397	0.4400	0.4600	0.9584	0.3914	0.7499	0.4600	0.3200	0.9618	0.2735	0.8089
0.4000	0.7800	0.9239	0.6097	0.3407	0.4200	0.6200	0.9471	0.5137	0.6127	0.4400	0.4800	0.9565	0.4062	0.7337	0.4600	0.3400	0.9605	0.2896	0.7992
0.4000	0.8000	0.9182	0.6159	0.2845	0.4200	0.6400	0.9439	0.5257	0.5833	0.4400	0.5000	0.9545	0.4207	0.7161	0.4600	0.3600	0.9592	0.3054	0.7886
0.4000	0.8200	0.9120	0.6210	0.2237	0.4200	0.6600	0.9405	0.5370	0.5514	0.4400	0.5200	0.9522	0.4349	0.6970	0.4600	0.3800	0.9577	0.3211	0.7771
0.4000	0.8400	0.9053	0.6248	0.1574	0.4200	0.6800	0.9367	0.5477	0.5167	0.4400	0.5400	0.9498	0.4486	0.6764	0.4600	0.4000	0.9562	0.3365	0.7646
0.4000	0.8600	0.8979	0.6273	0.0851	0.4200	0.7000	0.9327	0.5577	0.4790	0.4400	0.5600	0.9472	0.4619	0.6542	0.4600	0.4200	0.9545	0.3517	0.7511
0.4000	0.8800	0.8898	0.6282	0.0056	0.4200	0.7200	0.9283	0.5668	0.4385	0.4400	0.5800	0.9444	0.4747	0.6300	0.4600	0.4400	0.9526	0.3665	0.7364
0.4000	0.9000	0.8809	0.6275	-0.0806	0.4200	0.7400	0.9235	0.5752	0.3938	0.4400	0.6000	0.9414	0.4871	0.6039	0.4600	0.4600	0.9507	0.3811	0.7205
0.4000	0.9200	0.8712	0.6249	-0.1688	0.4200	0.7600	0.9183	0.5826	0.3452	0.4400	0.6200	0.9381	0.4989	0.5756	0.4600	0.4800	0.9485	0.3954	0.7034
0.4000	0.9400	0.8607	0.6206	-0.2710	0.4200	0.7800	0.9126	0.5890	0.2935	0.4400	0.6400	0.9346	0.5101	0.5447	0.4600	0.5000	0.9462	0.4092	0.6848
0.4000	0.9600	0.8489	0.6140	-0.3865	0.4200	0.8000	0.9065	0.5943	0.2366	0.4400	0.6600	0.9308	0.5207	0.5116	0.4600	0.5200	0.9438	0.4227	0.6647
0.4000	0.9800	0.8359	0.6051	-0.5061	0.4200	0.8200	0.8998	0.5984	0.1743	0.4400	0.6800	0.9267	0.5305	0.4758	0.4600	0.5400	0.9411	0.4358	0.6431
0.4000	1.0000	0.8216	0.5937	-0.6380	0.4200	0.8400	0.8925	0.6012	0.1068	0.4400	0.7000	0.9222	0.5397	0.4370	0.4600	0.5600	0.9382	0.4485	0.6197
0.4000	1.0200	0.8057	0.5795	-0.7810	0.4200	0.8600	0.8846	0.6026	0.0340	0.4400	0.7200	0.9174	0.5480	0.3947	0.4600	0.5800	0.9351	0.4606	0.5944
0.4000	1.0400	0.7880	0.5624	-0.9358	0.4200	0.8800	0.8759	0.6025	-0.0457	0.4400	0.7400	0.9122	0.5554	0.3691	0.4600	0.6000	0.9318	0.4722	0.5670
0.4000	1.0600	0.7683	0.5420	-1.1033	0.4200	0.9000	0.8664	0.6008	-0.1279	0.4400	0.7600	0.9066	0.5619	0.2996	0.4600	0.6200	0.9282	0.4833	0.5380
0.4000	1.0800	0.7463	0.5182	-1.2851	0.4200	0.9200	0.8562	0.5973	-0.2210	0.4400	0.7800	0.9004	0.5674	0.2461	0.4600	0.6400	0.9243	0.4937	0.5061
0.4000	1.1000	0.7216	0.4905	-1.4820	0.4200	0.9400	0.8448	0.5919	-0.3266	0.4400	0.8000	0.8938	0.5717	0.1882	0.4600	0.6600	0.9202	0.5035	0.4716
0.4000	1.1200	0.6938	0.4588	-1.6941	0.4200	0.9600	0.8323	0.5842	-0.4375	0.4400	0.8200	0.8866	0.5749	0.1252	0.4600	0.6800	0.9157	0.5126	0.4346
0.4000	1.1400	0.6622	0.4224	-1.9203	0.4200	0.9800	0.8185	0.5743	-0.5574	0.4400	0.8400	0.8788	0.5767	0.0577	0.4600	0.7000	0.9108	0.5209	0.3944
0.4000	1.1600	0.6260	0.3818	-2.1749	0.4200	1.0000	0.8033	0.5619	-0.6860	0.4400	0.8600	0.8702	0.5772	-0.0169	0.4600	0.7200	0.9056	0.5283	0.3512
0.4000	1.1800	0.5840	0.3356	-2.4214	0.4200	1.0200	0.7865	0.5468	-0.8268	0.4400	0.8800	0.8609	0.5760	-0.0929	0.4600	0.7400	0.9000	0.5349	0.3043
0.4000	1.2000	0.5354	0.2848	-2.7000	0.4200	1.0400	0.7678	0.5287	-0.9798	0.4400	0.9000	0.8509	0.5734	-0.1784	0.4600	0.7600	0.8939	0.5405	0.2538
0.4000	1.2200	0.4764	0.2275	-2.9948	0.4200	1.0600	0.7471	0.5075	-1.1445	0.4400	0.9200	0.8399	0.5688	-0.2763	0.4600	0.7800	0.8872	0.5450	0.1994
0.4000	1.2400	0.4039	0.1649	-3.2960	0.4200	1.0800	0.7239	0.4829	-1.3230	0.4400	0.9400	0.8277	0.5623	-0.3770	0.4600	0.8000	0.8801	0.5484	0.1405
0.4000	1.2600	0.3161	0.0955	-3.6332	0.4200	1.1000	0.6980	0.4545	-1.5156	0.4400	0.9600	0.8145	0.5537	-0.4864	0.4600	0.8200	0.8723	0.5506	0.0770
0.4000	1.2800	0.1374	0.0196	-3.9704	0.4200	1.1200	0.6687	0.4222	-1.7191	0.4400	0.9800	0.7999	0.5428	-0.6057	0.4600	0.8400	0.8639	0.5515	0.0082
					0.4200	1.1400	0.6365	0.3856	-1.9358	0.4400	1.0000	0.7838	0.5294	-0.7342	0.4600	0.8600	0.8548	0.5509	-0.0663
					0.4200	1.1600	0.5973	0.3445	-2.1825	0.4400	1.0200	0.7660	0.5133	-0.8723	0.4600	0.8800	0.8448	0.5488	-0.1473
0.4200	0.0000	0.9809	0.0000	0.9122	0.4200	1.1800	0.5529	0.2982	-2.4430	0.4400	1.0400	0.7463	0.4944	-1.0225	0.4600	0.9000	0.8340	0.5450	-0.2287
0.4200	0.0200	0.9809	0.0182	0.9118	0.4200	1.2000	0.5007	0.2468	-2.6984	0.4400	1.0600	0.7244	0.4724	-1.1847	0.4600	0.9200	0.8224	0.5395	-0.3212
0.4200	0.0400	0.9808	0.0365	0.9113	0.4200	1.2200	0.4374	0.1901	-2.9830	0.4400	1.0800	0.7000	0.4469	-1.3596	0.4600	0.9400	0.8095	0.5320	-0.4278
0.4200	0.0600	0.9807	0.0547	0.9104	0.4200	1.2400	0.3564	0.1274	-3.2938	0.4400	1.1000	0.6726	0.4179	-1.5477	0.4600	0.9600	0.7954	0.5224	-0.5367
0.4200	0.0800	0.9805	0.0729	0.9090	0.4200	1.2600	0.2401	0.0584	-3.6046	0.4400	1.1200	0.6416	0.3850	-1.7476	0.4600	0.9800	0.7799	0.5105	-0.6530
0.4200	0.1000	0.9803	0.0911	0.9072						0.4400	1.1400	0.6064	0.3479	-1.9721	0.4600	1.0000	0.7628	0.4962	-0.7804
0.4200	0.1200	0.9800	0.1092	0.9050						0.4400	1.1600	0.5656	0.3060	-2.1977	0.4600	1.0200	0.7440	0.4792	-0.9176
0.4200	0.1400	0.9797	0.1273	0.9023	0.4400	0.0000	0.9760	0.0000	0.8945	0.4400	1.1800	0.5184	0.2598	-2.4428	0.4600	1.0400	0.7232	0.4594	-1.0666
0.4200	0.1600	0.9793	0.1453	0.8992	0.4400	0.0200	0.9760	0.0179	0.8942	0.4400	1.2000	0.4618	0.2082	-2.7019	0.4600	1.0600	0.7000	0.4365	-1.2250
0.4200	0.1800	0.9789	0.1632	0.8956	0.4400	0.0400	0.9759	0.0358	0.8939	0.4400	1.2200	0.3921	0.1516	-2.9834	0.4600	1.0800	0.6742	0.4104	-1.3950
0.4200	0.2000	0.9784	0.1811	0.8916	0.4400	0.0600	0.9758	0.0537	0.8929	0.4400	1.2400	0.2986	0.0887	-3.2892	0.4600	1.1000	0.6451	0.3806	-1.5822
0.4200	0.2200	0.9779	0.1989	0.8870	0.4400	0.0800	0.9756	0.0715	0.8914	0.4400	1.2600	0.1406	0.0200	-3.5950	0.4600	1.1200	0.6122	0.3470	-1.7761
0.4200	0.2400	0.9773	0.2166	0.8819	0.4400	0.1000	0.9753	0.0893	0.8894						0.4600	1.1400	0.5748	0.3094	-1.9948
0.4200	0.2600	0.9766	0.2341	0.8762	0.4400	0.1200	0.9750	0.1071	0.8870						0.4600	1.1600	0.5311	0.2672	-2.2146
0.4200	0.2800	0.9759	0.2516	0.8699	0.4400	0.1400	0.9747	0.1248	0.8840	0.4600	0.0000	0.9704	0.0000	0.8761	0.4600	1.1800	0.4801	0.2208	-2.4451
0.4200	0.3000	0.9751	0.2689	0.8629	0.4400	0.1600	0.9743	0.1424	0.8806	0.4600	0.0200	0.9704	0.0175	0.8756	0.4600	1.2000	0.4182	0.1692	-2.7108
0.4200	0.3200	0.9742	0.2861	0.8553	0.4400	0.1800	0.9738	0.1600	0.8767	0.4600	0.0400	0.9703	0.0350	0.8750	0.4600	1.2200	0.3389	0.1123	-2.9851
0.4200	0.3400	0.9732	0.3031	0.8469	0.4400	0.2000	0.9732	0.1775	0.8722	0.4600	0.0600	0.9702	0.0525	0.8739	0.4600	1.2400	0.2244	0.0498	-3.2594
0.4200	0.3600	0.9722	0.3200	0.8378	0.4400	0.2200	0.9726	0.1949	0.8672	0.4600	0.0800	0.9699	0.0700	0.8723					
0.4200	0.3800	0.9710	0.3366	0.8278	0.4400	0.2400	0.9719	0.2122	0.8617	0.4600	0.1000	0.9697	0.0874	0.8701					
0.4200	0.4000	0.9698	0.3531	0.8169	0.4400	0.2600	0.9711	0.2294	0.8554	0.4600	0.1200	0.9693	0.1048	0.8674	0.4800	0.0000	0.9641	0.0000	0.8558
0.4200	0.4200	0.9684	0.3693	0.8050	0.4400	0.2800	0.9703	0.2464	0.8486	0.4600	0.1400	0.9689	0.1221	0.8643	0.4800	0.0200	0.9640	0.0171	0.8552

T/T_e	v_0/v_{00}	ϵ_0/ϵ_{00}	v/v_{00}	dv/dv_0	T/T_e	v_0/v_{00}	ϵ_0/ϵ_{00}	v/v_{00}	dv/dv_0	T/T_e	v_0/v_{00}	ϵ_0/ϵ_{00}	v/v_{00}	dv/dv_0	T/T_e	v_0/v_{00}	ϵ_0/ϵ_{00}	v/v_{00}	dv/dv_0
0.4800	0.0400	0.9639	0.0342	0.8546	0.4800	1.2200	0.2726	0.0720	-2.9853	0.5000	1.1000	0.5828	0.3043	-1.6460	0.5200	1.0000	0.6900	0.3930	-0.9174
0.4800	0.0600	0.9638	0.0513	0.8535	0.4800	1.2400	0.0992	0.0098	-3.2503	0.5000	1.1200	0.5451	0.2697	-1.8383	0.5200	1.0200	0.6674	0.3734	-1.0496
0.4800	0.0800	0.9635	0.0684	0.8517						0.5000	1.1400	0.5011	0.2307	-2.0408	0.5200	1.0400	0.6423	0.3510	-1.1920
0.4800	0.1000	0.9632	0.0854	0.8493						0.5000	1.1600	0.4497	0.1880	-2.2448	0.5200	1.0600	0.6143	0.3256	-1.3431
0.4800	0.1200	0.9628	0.1023	0.8465	0.5000	0.0000	0.9569	0.0000	0.8340	0.5000	1.1800	0.3869	0.1407	-2.4817	0.5200	1.0800	0.5828	0.2972	-1.5048
0.4800	0.1400	0.9623	0.1192	0.8430	0.5000	0.0200	0.9568	0.0167	0.8335	0.5000	1.2000	0.3054	0.0886	-2.7276	0.5200	1.1000	0.5471	0.2653	-1.6849
0.4800	0.1600	0.9618	0.1360	0.8390	0.5000	0.0400	0.9567	0.0333	0.8329	0.5000	1.2200	0.1810	0.0316	-2.9735	0.5200	1.1200	0.5057	0.2298	-1.8604
0.4800	0.1800	0.9612	0.1528	0.8345	0.5000	0.0600	0.9565	0.0500	0.8316						0.5200	1.1400	0.4580	0.1908	-2.0645
0.4800	0.2000	0.9605	0.1694	0.8293	0.5000	0.0800	0.9563	0.0666	0.8297						0.5200	1.1600	0.3999	0.1472	-2.2718
0.4800	0.2200	0.9597	0.1859	0.8235	0.5000	0.1000	0.9559	0.0832	0.8272	0.5200	0.0000	0.9488	0.0000	0.8110	0.5200	1.1800	0.3274	0.0998	-2.4934
0.4800	0.2400	0.9588	0.2023	0.8170	0.5000	0.1200	0.9555	0.0997	0.8241	0.5200	0.0200	0.9488	0.0162	0.8104	0.5200	1.2000	0.2243	0.0474	-2.7150
0.4800	0.2600	0.9578	0.2186	0.8098	0.5000	0.1400	0.9549	0.1161	0.8204	0.5200	0.0400	0.9487	0.0324	0.8097					
0.4800	0.2800	0.9568	0.2347	0.8019	0.5000	0.1600	0.9543	0.1325	0.8162	0.5200	0.0600	0.9484	0.0486	0.8084					
0.4800	0.3000	0.9556	0.2507	0.7932	0.5000	0.1800	0.9536	0.1488	0.8113	0.5200	0.0800	0.9481	0.0648	0.8063	0.5400	0.0000	0.9399	0.0000	0.7867
0.4800	0.3200	0.9544	0.2665	0.7837	0.5000	0.2000	0.9529	0.1649	0.8057	0.5200	0.1000	0.9477	0.0809	0.8037	0.5400	0.0200	0.9398	0.0157	0.7860
0.4800	0.3400	0.9530	0.2820	0.7734	0.5000	0.2200	0.9520	0.1810	0.7996	0.5200	0.1200	0.9473	0.0969	0.8004	0.5400	0.0400	0.9397	0.0314	0.7853
0.4800	0.3600	0.9515	0.2974	0.7621	0.5000	0.2400	0.9510	0.1969	0.7927	0.5200	0.1400	0.9467	0.1129	0.7965	0.5400	0.0600	0.9394	0.0471	0.7839
0.4800	0.3800	0.9499	0.3125	0.7500	0.5000	0.2600	0.9499	0.2127	0.7850	0.5200	0.1600	0.9460	0.1288	0.7920	0.5400	0.0800	0.9391	0.0628	0.7817
0.4800	0.4000	0.9481	0.3274	0.7368	0.5000	0.2800	0.9488	0.2283	0.7766	0.5200	0.1800	0.9452	0.1445	0.7868	0.5400	0.1000	0.9387	0.0784	0.7789
0.4800	0.4200	0.9462	0.3420	0.7224	0.5000	0.3000	0.9475	0.2438	0.7674	0.5200	0.2000	0.9444	0.1602	0.7809	0.5400	0.1200	0.9381	0.0940	0.7755
0.4800	0.4400	0.9442	0.3563	0.7069	0.5000	0.3200	0.9461	0.2590	0.7574	0.5200	0.2200	0.9434	0.1758	0.7744	0.5400	0.1400	0.9375	0.1094	0.7714
0.4800	0.4600	0.9420	0.3702	0.6902	0.5000	0.3400	0.9445	0.2741	0.7464	0.5200	0.2400	0.9423	0.1912	0.7671	0.5400	0.1600	0.9367	0.1248	0.7666
0.4800	0.4800	0.9396	0.3839	0.6722	0.5000	0.3600	0.9429	0.2889	0.7345	0.5200	0.2600	0.9411	0.2065	0.7590	0.5400	0.1800	0.9359	0.1401	0.7611
0.4800	0.5000	0.9371	0.3971	0.6527	0.5000	0.3800	0.9411	0.3034	0.7216	0.5200	0.2800	0.9398	0.2215	0.7501	0.5400	0.2000	0.9349	0.1552	0.7550
0.4800	0.5200	0.9344	0.4100	0.6316	0.5000	0.4000	0.9392	0.3177	0.7078	0.5200	0.3000	0.9384	0.2365	0.7404	0.5400	0.2200	0.9339	0.1703	0.7480
0.4800	0.5400	0.9314	0.4224	0.6090	0.5000	0.4200	0.9371	0.3317	0.6927	0.5200	0.3200	0.9369	0.2512	0.7299	0.5400	0.2400	0.9327	0.1852	0.7404
0.4800	0.5600	0.9283	0.4343	0.5846	0.5000	0.4400	0.9348	0.3454	0.6764	0.5200	0.3400	0.9352	0.2656	0.7184	0.5400	0.2600	0.9314	0.1999	0.7319
0.4800	0.5800	0.9249	0.4457	0.5582	0.5000	0.4600	0.9324	0.3588	0.6588	0.5200	0.3600	0.9334	0.2799	0.7058	0.5400	0.2800	0.9300	0.2144	0.7225
0.4800	0.6000	0.9213	0.4566	0.5299	0.5000	0.4800	0.9298	0.3718	0.6399	0.5200	0.3800	0.9314	0.2939	0.6923	0.5400	0.3000	0.9284	0.2288	0.7123
0.4800	0.6200	0.9173	0.4669	0.4994	0.5000	0.5000	0.9270	0.3844	0.6196	0.5200	0.4000	0.9293	0.3076	0.6777	0.5400	0.3200	0.9267	0.2429	0.7012
0.4800	0.6400	0.9131	0.4766	0.4664	0.5000	0.5200	0.9241	0.3965	0.5976	0.5200	0.4200	0.9270	0.3210	0.6619	0.5400	0.3400	0.9248	0.2568	0.6892
0.4800	0.6600	0.9086	0.4856	0.4311	0.5000	0.5400	0.9208	0.4083	0.5741	0.5200	0.4400	0.9245	0.3340	0.6449	0.5400	0.3600	0.9229	0.2705	0.6761
0.4800	0.6800	0.9037	0.4938	0.3929	0.5000	0.5600	0.9174	0.4195	0.5486	0.5200	0.4600	0.9219	0.3468	0.6266	0.5400	0.3800	0.9207	0.2839	0.6620
0.4800	0.7000	0.8985	0.5013	0.3518	0.5000	0.5800	0.9137	0.4302	0.5213	0.5200	0.4800	0.9190	0.3591	0.6069	0.5400	0.4000	0.9184	0.2969	0.6467
0.4800	0.7200	0.8928	0.5079	0.3074	0.5000	0.6000	0.9097	0.4403	0.4921	0.5200	0.5000	0.9160	0.3710	0.5857	0.5400	0.4200	0.9159	0.3097	0.6302
0.4800	0.7400	0.8867	0.5135	0.2600	0.5000	0.6200	0.9055	0.4499	0.4606	0.5200	0.5200	0.9127	0.3825	0.5629	0.5400	0.4400	0.9132	0.3221	0.6125
0.4800	0.7600	0.8801	0.5182	0.2085	0.5000	0.6400	0.9009	0.4587	0.4267	0.5200	0.5400	0.9092	0.3935	0.5384	0.5400	0.4600	0.9103	0.3342	0.5934
0.4800	0.7800	0.8730	0.5218	0.1529	0.5000	0.6600	0.8960	0.4669	0.3903	0.5200	0.5600	0.9055	0.4040	0.5122	0.5400	0.4800	0.9072	0.3459	0.5730
0.4800	0.8000	0.8653	0.5243	0.0932	0.5000	0.6800	0.8907	0.4743	0.3511	0.5200	0.5800	0.9015	0.4140	0.4840	0.5400	0.5000	0.9039	0.3571	0.5511
0.4800	0.8200	0.8570	0.5255	0.0288	0.5000	0.7000	0.8850	0.4809	0.3092	0.5200	0.6000	0.8972	0.4234	0.4538	0.5400	0.5200	0.9004	0.3679	0.5275
0.4800	0.8400	0.8479	0.5254	-0.0409	0.5000	0.7200	0.8789	0.4867	0.2640	0.5200	0.6200	0.8925	0.4321	0.4214	0.5400	0.5400	0.8966	0.3782	0.5023
0.4800	0.8600	0.8382	0.5239	-0.1163	0.5000	0.7400	0.8723	0.4915	0.2151	0.5200	0.6400	0.8876	0.4402	0.3865	0.5400	0.5600	0.8925	0.3880	0.4752
0.4800	0.8800	0.8275	0.5208	-0.1919	0.5000	0.7600	0.8652	0.4953	0.1628	0.5200	0.6600	0.8823	0.4476	0.3494	0.5400	0.5800	0.8882	0.3972	0.4469
0.4800	0.9000	0.8162	0.5161	-0.2773	0.5000	0.7800	0.8576	0.4980	0.1066	0.5200	0.6800	0.8766	0.4542	0.3093	0.5400	0.6000	0.8835	0.4058	0.4152
0.4800	0.9200	0.8036	0.5096	-0.3753	0.5000	0.8000	0.8493	0.4995	0.0460	0.5200	0.7000	0.8704	0.4599	0.2661	0.5400	0.6200	0.8785	0.4138	0.3818
0.4800	0.9400	0.7899	0.5011	-0.4761	0.5000	0.8200	0.8404	0.4998	-0.0191	0.5200	0.7200	0.8639	0.4648	0.2200	0.5400	0.6400	0.8732	0.4211	0.3461
0.4800	0.9600	0.7749	0.4905	-0.5843	0.5000	0.8400	0.8307	0.4987	-0.0894	0.5200	0.7400	0.8568	0.4687	0.1706	0.5400	0.6600	0.8674	0.4276	0.3079
0.4800	0.9800	0.7584	0.4777	-0.7013	0.5000	0.8600	0.8203	0.4962	-0.1600	0.5200	0.7600	0.8492	0.4716	0.1175	0.5400	0.6800	0.8613	0.4334	0.2670
0.4800	1.0000	0.7403	0.4624	-0.8261	0.5000	0.8800	0.8091	0.4922	-0.2401	0.5200	0.7800	0.8409	0.4734	0.0605	0.5400	0.7000	0.8547	0.4383	0.2232
0.4800	1.0200	0.7204	0.4446	-0.9634	0.5000	0.9000	0.7968	0.4865	-0.3310	0.5200	0.8000	0.8321	0.4740	-0.0006	0.5400	0.7200	0.8476	0.4423	0.1761
0.4800	1.0400	0.6982	0.4238	-1.1080	0.5000	0.9200	0.7834	0.4790	-0.4235	0.5200	0.8200	0.8225	0.4733	-0.0664	0.5400	0.7400	0.8400	0.4453	0.1259
0.4800	1.0600	0.6737	0.4002	-1.2650	0.5000	0.9400	0.7688	0.4695	-0.5239	0.5200	0.8400	0.8122	0.4713	-0.1374	0.5400	0.7600	0.8318	0.4473	0.0723
0.4800	1.0800	0.6462	0.3731	-1.4331	0.5000	0.9600	0.7529	0.4580	-0.6324	0.5200	0.8600	0.8010	0.4678	-0.2077	0.5400	0.7800	0.8230	0.4482	0.0147
0.4800	1.1000	0.6153	0.3428	-1.6104	0.5000	0.9800	0.7354	0.4442	-0.7468	0.5200	0.8800	0.7891	0.4629	-0.2879	0.5400	0.8000	0.8135	0.4479	-0.0472
0.4800	1.1200	0.5803	0.3086	-1.8145	0.5000	1.0000	0.7162	0.4280	-0.8724	0.5200	0.9000	0.7760	0.4562	-0.3793	0.5400	0.8200	0.8033	0.4463	-0.1139
0.4800	1.1400	0.5396	0.2702	-2.0113	0.5000	1.0200	0.6949	0.4092	-1.0075	0.5200	0.9200	0.7617	0.4478	-0.4720	0.5400	0.8400	0.7923	0.4433	-0.1797
0.4800	1.1600	0.4929	0.2280	-2.2280	0.5000	1.0400	0.6714	0.3877	-1.1509	0.5200	0.9400	0.7462	0.4373	-0.5714	0.5400	0.8600	0.7805	0.4390	-0.2547
0.4800	1.1800	0.4366	0.1809	-2.4684	0.5000	1.0600	0.6452	0.3631	-1.2989	0.5200	0.9600	0.7292	0.4248	-0.6786	0.5400	0.8800	0.7676	0.4331	-0.3401
0.4800	1.2000	0.3671	0.1292	-2.7204	0.5000	1.0800	0.6159	0.3356	-1.4703	0.5200	0.9800	0.7105	0.4101	-0.7940	0.5400	0.9000	0.7536	0.4254	-0.4264

T/T_e	v_0/v_∞	$\epsilon_0/\epsilon_\infty$	v/v_∞	dv/dv_0	T/T_e	v_0/v_∞	$\epsilon_0/\epsilon_\infty$	v/v_∞	dv/dv_0	T/T_e	v_0/v_∞	$\epsilon_0/\epsilon_\infty$	v/v_∞	dv/dv_0	T/T_e	v_0/v_∞	$\epsilon_0/\epsilon_\infty$	v/v_∞	dv/dv_0
0.5400	0.9200	0.7384	0.4160	-0.5191	0.5600	0.8400	0.7710	0.4149	-0.2261	0.5800	0.7800	0.7829	0.3960	-0.0762	0.6000	0.7400	0.7813	0.3716	-0.0071
0.5400	0.9400	0.7218	0.4046	-0.6185	0.5600	0.8600	0.7583	0.4095	-0.3058	0.5800	0.8000	0.7720	0.3939	-0.1395	0.6000	0.7600	0.7712	0.3710	-0.0627
0.5400	0.9600	0.7037	0.3912	-0.7253	0.5600	0.8800	0.7445	0.4026	-0.3865	0.5800	0.8200	0.7603	0.3904	-0.2015	0.6000	0.7800	0.7604	0.3691	-0.1221
0.5400	0.9800	0.6838	0.3755	-0.8395	0.5600	0.9000	0.7295	0.3940	-0.4734	0.5800	0.8400	0.7479	0.3858	-0.2721	0.6000	0.8000	0.7488	0.3661	-0.1806
0.5400	1.0000	0.6618	0.3575	-0.9616	0.5600	0.9200	0.7132	0.3836	-0.5657	0.5800	0.8600	0.7343	0.3795	-0.3528	0.6000	0.8200	0.7364	0.3618	-0.2476
0.5400	1.0200	0.6376	0.3370	-1.0929	0.5600	0.9400	0.6955	0.3713	-0.6656	0.5800	0.8800	0.7195	0.3716	-0.4336	0.6000	0.8400	0.7229	0.3561	-0.3225
0.5400	1.0400	0.6107	0.3138	-1.2291	0.5600	0.9600	0.6761	0.3570	-0.7717	0.5800	0.9000	0.7035	0.3621	-0.5201	0.6000	0.8600	0.7083	0.3489	-0.3982
0.5400	1.0600	0.5805	0.2878	-1.3777	0.5600	0.9800	0.6547	0.3404	-0.8844	0.5800	0.9200	0.6860	0.3508	-0.6122	0.6000	0.8800	0.6924	0.3401	-0.4799
0.5400	1.0800	0.5464	0.2586	-1.5450	0.5600	1.0000	0.6312	0.3215	-1.0055	0.5800	0.9400	0.6670	0.3376	-0.7111	0.6000	0.9000	0.6752	0.3297	-0.5659
0.5400	1.1000	0.5075	0.2259	-1.7211	0.5600	1.0200	0.6051	0.3002	-1.1347	0.5800	0.9600	0.6461	0.3223	-0.8170	0.6000	0.9200	0.6565	0.3175	-0.6583
0.5400	1.1200	0.4621	0.1897	-1.8987	0.5600	1.0400	0.5760	0.2761	-1.2733	0.5800	0.9800	0.6231	0.3048	-0.9292	0.6000	0.9400	0.6360	0.3033	-0.7570
0.5400	1.1400	0.4083	0.1499	-2.0777	0.5600	1.0600	0.5433	0.2492	-1.4159	0.5800	1.0000	0.5978	0.2851	-1.0487	0.6000	0.9600	0.6134	0.2872	-0.8614
0.5400	1.1600	0.3417	0.1064	-2.2959	0.5600	1.0800	0.5060	0.2193	-1.5811	0.5800	1.0200	0.5695	0.2628	-1.1771	0.6000	0.9800	0.5886	0.2688	-0.9726
0.5400	1.1800	0.2508	0.0580	-2.5168	0.5600	1.1000	0.4627	0.1859	-1.7459	0.5800	1.0400	0.5378	0.2380	-1.3091	0.6000	1.0000	0.5610	0.2482	-1.0920
0.5400	1.2000	0.0772	0.0057	-2.7378	0.5600	1.1200	0.4122	0.1495	-1.9150	0.5800	1.0600	0.5018	0.2104	-1.4634	0.6000	1.0200	0.5300	0.2251	-1.2174
					0.5600	1.1400	0.3500	0.1092	-2.1119	0.5800	1.0800	0.4602	0.1794	-1.6138	0.6000	1.0400	0.4951	0.1994	-1.3621
					0.5600	1.1600	0.2681	0.0649	-2.3186	0.5800	1.1000	0.4119	0.1457	-1.7789	0.6000	1.0600	0.4546	0.1706	-1.4953
0.5600	0.0000	0.9299	0.0000	0.7611	0.5600	1.1800	0.1333	0.0164	-2.5254	0.5800	1.1200	0.3525	0.1082	-1.9503	0.6000	1.0800	0.4080	0.1395	-1.6431
0.5600	0.0200	0.9299	0.0152	0.7604						0.5800	1.1400	0.2768	0.0676	-2.1346	0.6000	1.1000	0.3512	0.1048	-1.8074
0.5600	0.0400	0.9297	0.0304	0.7597						0.5800	1.1600	0.1594	0.0228	-2.3189	0.6000	1.1200	0.2790	0.0671	-1.9870
0.5600	0.0600	0.9295	0.0456	0.7582	0.5800	0.0000	0.9190	0.0000	0.7344						0.6000	1.1400	0.1699	0.0253	-2.1667
0.5600	0.0800	0.9291	0.0608	0.7559	0.5800	0.0200	0.9189	0.0147	0.7337										
0.5600	0.1000	0.9286	0.0758	0.7530	0.5800	0.0400	0.9188	0.0294	0.7330	0.6000	0.0000	0.9070	0.0000	0.7067					
0.5600	0.1200	0.9280	0.0909	0.7494	0.5800	0.0600	0.9185	0.0440	0.7314	0.6000	0.0200	0.9069	0.0141	0.7060	0.6200	0.0000	0.8939	0.0000	0.6779
0.5600	0.1400	0.9273	0.1058	0.7451	0.5800	0.0800	0.9181	0.0586	0.7290	0.6000	0.0400	0.9067	0.0282	0.7052	0.6200	0.0200	0.8938	0.0136	0.6771
0.5600	0.1600	0.9265	0.1207	0.7400	0.5800	0.1000	0.9176	0.0732	0.7259	0.6000	0.0600	0.9064	0.0423	0.7035	0.6200	0.0400	0.8936	0.0271	0.6763
0.5600	0.1800	0.9256	0.1354	0.7343	0.5800	0.1200	0.9169	0.0876	0.7221	0.6000	0.0800	0.9060	0.0564	0.7010	0.6200	0.0600	0.8933	0.0406	0.6746
0.5600	0.2000	0.9245	0.1500	0.7278	0.5800	0.1400	0.9161	0.1020	0.7176	0.6000	0.1000	0.9054	0.0704	0.6978	0.6200	0.0800	0.8928	0.0541	0.6720
0.5600	0.2200	0.9234	0.1645	0.7205	0.5800	0.1600	0.9153	0.1163	0.7124	0.6000	0.1200	0.9047	0.0843	0.6938	0.6200	0.1000	0.8922	0.0675	0.6687
0.5600	0.2400	0.9221	0.1788	0.7125	0.5800	0.1800	0.9143	0.1305	0.7064	0.6000	0.1400	0.9039	0.0981	0.6891	0.6200	0.1200	0.8914	0.0808	0.6646
0.5600	0.2600	0.9206	0.1930	0.7036	0.5800	0.2000	0.9131	0.1446	0.6996	0.6000	0.1600	0.9029	0.1119	0.6837	0.6200	0.1400	0.8905	0.0941	0.6597
0.5600	0.2800	0.9191	0.2070	0.6938	0.5800	0.2200	0.9118	0.1585	0.6920	0.6000	0.1800	0.9018	0.1255	0.6774	0.6200	0.1600	0.8895	0.1072	0.6540
0.5600	0.3000	0.9174	0.2208	0.6832	0.5800	0.2400	0.9104	0.1723	0.6836	0.6000	0.2000	0.9006	0.1389	0.6704	0.6200	0.1800	0.8883	0.1202	0.6475
0.5600	0.3200	0.9155	0.2343	0.6716	0.5800	0.2600	0.9089	0.1858	0.6744	0.6000	0.2200	0.8992	0.1523	0.6625	0.6200	0.2000	0.8869	0.1331	0.6402
0.5600	0.3400	0.9135	0.2476	0.6590	0.5800	0.2800	0.9072	0.1992	0.6642	0.6000	0.2400	0.8977	0.1654	0.6538	0.6200	0.2200	0.8854	0.1458	0.6321
0.5600	0.3600	0.9113	0.2607	0.6454	0.5800	0.3000	0.9053	0.2124	0.6531	0.6000	0.2600	0.8960	0.1784	0.6441	0.6200	0.2400	0.8838	0.1584	0.6230
0.5600	0.3800	0.9090	0.2734	0.6307	0.5800	0.3200	0.9033	0.2254	0.6410	0.6000	0.2800	0.8941	0.1912	0.6335	0.6200	0.2600	0.8819	0.1707	0.6130
0.5600	0.4000	0.9065	0.2859	0.6148	0.5800	0.3400	0.9011	0.2380	0.6280	0.6000	0.3000	0.8921	0.2038	0.6222	0.6200	0.2800	0.8799	0.1829	0.6021
0.5600	0.4200	0.9037	0.2980	0.5977	0.5800	0.3600	0.8987	0.2505	0.6138	0.6000	0.3200	0.8899	0.2161	0.6097	0.6200	0.3000	0.8777	0.1948	0.5902
0.5600	0.4400	0.9008	0.3098	0.5794	0.5800	0.3800	0.8962	0.2626	0.5985	0.6000	0.3400	0.8876	0.2281	0.5960	0.6200	0.3200	0.8754	0.2065	0.5773
0.5600	0.4600	0.8977	0.3212	0.5596	0.5800	0.4000	0.8934	0.2744	0.5821	0.6000	0.3600	0.8850	0.2399	0.5814	0.6200	0.3400	0.8728	0.2179	0.5633
0.5600	0.4800	0.8944	0.3322	0.5385	0.5800	0.4200	0.8905	0.2859	0.5644	0.6000	0.3800	0.8822	0.2514	0.5656	0.6200	0.3600	0.8700	0.2290	0.5482
0.5600	0.5000	0.8908	0.3427	0.5158	0.5800	0.4400	0.8873	0.2970	0.5454	0.6000	0.4000	0.8793	0.2625	0.5486	0.6200	0.3800	0.8671	0.2398	0.5319
0.5600	0.5200	0.8869	0.3528	0.4916	0.5800	0.4600	0.8840	0.3077	0.5250	0.6000	0.4200	0.8761	0.2733	0.5304	0.6200	0.4000	0.8639	0.2503	0.5144
0.5600	0.5400	0.8828	0.3624	0.4656	0.5800	0.4800	0.8803	0.3180	0.5034	0.6000	0.4400	0.8727	0.2837	0.5108	0.6200	0.4200	0.8604	0.2604	0.4956
0.5600	0.5600	0.8784	0.3714	0.4376	0.5800	0.5000	0.8765	0.3278	0.4800	0.6000	0.4600	0.8690	0.2937	0.4898	0.6200	0.4400	0.8567	0.2701	0.4754
0.5600	0.5800	0.8737	0.3798	0.4078	0.5800	0.5200	0.8723	0.3371	0.4548	0.6000	0.4800	0.8651	0.3033	0.4674	0.6200	0.4600	0.8528	0.2794	0.4539
0.5600	0.6000	0.8687	0.3877	0.3759	0.5800	0.5400	0.8679	0.3460	0.4282	0.6000	0.5000	0.8609	0.3124	0.4434	0.6200	0.4800	0.8486	0.2882	0.4310
0.5600	0.6200	0.8633	0.3949	0.3418	0.5800	0.5600	0.8631	0.3543	0.3996	0.6000	0.5200	0.8564	0.3210	0.4177	0.6200	0.5000	0.8441	0.2966	0.4063
0.5600	0.6400	0.8575	0.4013	0.3054	0.5800	0.5800	0.8580	0.3620	0.3690	0.6000	0.5400	0.8517	0.3291	0.3903	0.6200	0.5200	0.8392	0.3045	0.3800
0.5600	0.6600	0.8514	0.4071	0.2664	0.5800	0.6000	0.8526	0.3690	0.3364	0.6000	0.5600	0.8465	0.3366	0.3611	0.6200	0.5400	0.8341	0.3118	0.3520
0.5600	0.6800	0.8447	0.4120	0.2247	0.5800	0.6200	0.8468	0.3754	0.3014	0.6000	0.5800	0.8411	0.3436	0.3297	0.6200	0.5600	0.8286	0.3186	0.3220
0.5600	0.7000	0.8377	0.4160	0.1802	0.5800	0.6400	0.8406	0.3810	0.2642	0.6000	0.6000	0.8352	0.3498	0.2964	0.6200	0.5800	0.8227	0.3247	0.2901
0.5600	0.7200	0.8301	0.4192	0.1323	0.5800	0.6600	0.8340	0.3859	0.2247	0.6000	0.6200	0.8290	0.3554	0.2610	0.6200	0.6000	0.8164	0.3301	0.2563
0.5600	0.7400	0.8219	0.4213	0.0814	0.5800	0.6800	0.8269	0.3900	0.1823	0.6000	0.6400	0.8223	0.3602	0.2231	0.6200	0.6200	0.8097	0.3349	0.2201
0.5600	0.7600	0.8131	0.4224	0.0272	0.5800	0.7000	0.8193	0.3932	0.1370	0.6000	0.6600	0.8152	0.3643	0.1827	0.6200	0.6400	0.8026	0.3389	0.1817
0.5600	0.7800	0.8037	0.4224	-0.0310	0.5800	0.7200	0.8111	0.3955	0.0887	0.6000	0.6800	0.8076	0.3675	0.1397	0.6200	0.6600	0.7949	0.3422	0.1407
0.5600	0.8000	0.7936	0.4211	-0.0938	0.5800	0.7400	0.8024	0.3967	0.0372	0.6000	0.7000	0.7994	0.3699	0.0938	0.6200	0.6800	0.7867	0.3445	0.0973
0.5600	0.8200	0.7826	0.4186	-0.1557	0.5800	0.7600	0.7930	0.3969	-0.0179	0.6000	0.7200	0.7907	0.3713	0.0449	0.6200	0.7000	0.7780	0.3460	0.0509

T/T_e	v_0/v_∞	$\epsilon_0/\epsilon_\infty$	v/v_∞	dv/dv_0	T/T_e	v_0/v_∞	$\epsilon_0/\epsilon_\infty$	v/v_∞	dv/dv_0	T/T_e	v_0/v_∞	$\epsilon_0/\epsilon_\infty$	v/v_∞	dv/dv_0	T/T_e	v_0/v_∞	$\epsilon_0/\epsilon_\infty$	v/v_∞	dv/dv_0
0.6200	0.7200	0.7686	0.3666	0.0011	0.6400	0.7200	0.7447	0.3214	-0.0426	0.6600	0.7400	0.7072	0.2935	-0.1358	0.6800	0.7800	0.6505	0.2571	-0.3004
0.6200	0.7400	0.7585	0.3661	-0.0514	0.6400	0.7400	0.7339	0.3200	-0.0962	0.6600	0.7600	0.6950	0.2903	-0.1919	0.6800	0.8000	0.6368	0.2505	-0.3645
0.6200	0.7600	0.7477	0.3645	-0.1080	0.6400	0.7600	0.7223	0.3175	-0.1479	0.6600	0.7800	0.6815	0.2858	-0.2562	0.6800	0.8200	0.6178	0.2425	-0.4324
0.6200	0.7800	0.7361	0.3617	-0.1626	0.6400	0.7800	0.7100	0.3140	-0.2072	0.6600	0.8000	0.6670	0.2800	-0.3197	0.6800	0.8400	0.5993	0.2332	-0.5043
0.6200	0.8000	0.7238	0.3579	-0.2255	0.6400	0.8000	0.6966	0.3092	-0.2750	0.6600	0.8200	0.6514	0.2730	-0.3874	0.6800	0.8600	0.5792	0.2223	-0.5806
0.6200	0.8200	0.7104	0.3527	-0.2971	0.6400	0.8200	0.6821	0.3030	-0.3420	0.6600	0.8400	0.6345	0.2645	-0.4592	0.6800	0.8800	0.5572	0.2099	-0.6619
0.6200	0.8400	0.6959	0.3460	-0.3685	0.6400	0.8400	0.6665	0.2955	-0.4140	0.6600	0.8600	0.6161	0.2546	-0.5354	0.6800	0.9000	0.5330	0.1958	-0.7478
0.6200	0.8600	0.6801	0.3379	-0.4447	0.6400	0.8600	0.6495	0.2865	-0.4902	0.6600	0.8800	0.5960	0.2431	-0.6169	0.6800	0.9200	0.5062	0.1800	-0.8373
0.6200	0.8800	0.6631	0.3282	-0.5258	0.6400	0.8800	0.6311	0.2758	-0.5716	0.6600	0.9000	0.5740	0.2299	-0.7029	0.6800	0.9400	0.4763	0.1623	-0.9340
0.6200	0.9000	0.6445	0.3968	-0.6122	0.6400	0.9000	0.6110	0.2636	-0.6578	0.6600	0.9200	0.5499	0.2149	-0.7937	0.6800	0.9600	0.4426	0.1426	-1.0327
0.6200	0.9200	0.6243	0.2837	-0.7038	0.6400	0.9200	0.5890	0.2495	-0.7489	0.6600	0.9400	0.5232	0.1981	-0.8907	0.6800	0.9800	0.4039	0.1209	-1.1446
0.6200	0.9400	0.6021	0.2686	-0.8017	0.6400	0.9400	0.5647	0.2336	-0.8464	0.6600	0.9600	0.4933	0.1793	-0.9927	0.6800	1.0000	0.3582	0.0967	-1.2646
0.6200	0.9600	0.5776	0.2516	-0.9057	0.6400	0.9600	0.5378	0.2156	-0.9496	0.6600	0.9800	0.4597	0.1583	-1.1009	0.6800	1.0200	0.3028	0.0703	-1.3766
0.6200	0.9800	0.5504	0.2324	-1.0163	0.6400	0.9800	0.5079	0.1955	-1.0596	0.6600	1.0000	0.4212	0.1351	-1.2221	0.6800	1.0400	0.2309	0.0416	-1.5066
0.6200	1.0000	0.5201	0.2109	-1.1345	0.6400	1.0000	0.4740	0.1732	-1.1750	0.6600	1.0200	0.3760	0.1094	-1.3417	0.6800	1.0600	0.1117	0.0101	-1.6366
0.6200	1.0200	0.4858	0.1870	-1.2553	0.6400	1.0200	0.4364	0.1485	-1.3039	0.6600	1.0400	0.3216	0.0815	-1.4618					
0.6200	1.0400	0.4466	0.1606	-1.3958	0.6400	1.0400	0.3901	0.1210	-1.4321	0.6600	1.0600	0.2520	0.0508	-1.6125					
0.6200	1.0600	0.4007	0.1311	-1.5433	0.6400	1.0600	0.3357	0.0911	-1.5668	0.6600	1.0800	0.1439	0.0170	-1.7631	0.7000	0.0000	0.8288	0.0000	0.5537
0.6200	1.0800	0.3456	0.0989	-1.6756	0.6400	1.0800	0.2666	0.0582	-1.7238						0.7000	0.0200	0.8287	0.0111	0.5528
0.6200	1.1000	0.2756	0.0639	-1.8423	0.6400	1.1000	0.1633	0.0222	-1.8809						0.7000	0.0400	0.8284	0.0221	0.5519
0.6200	1.1200	0.1715	0.0252	-2.0090						0.6800	0.0000	0.8471	0.0000	0.5860	0.7000	0.0600	0.8279	0.0331	0.5500
					0.6600	0.0000	0.8640	0.0000	0.6175	0.6800	0.0200	0.8470	0.0117	0.5852	0.7000	0.0800	0.8273	0.0441	0.5471
0.6400	0.0000	0.8796	0.0000	0.6482	0.6600	0.0200	0.8639	0.0123	0.6167	0.6800	0.0400	0.8468	0.0234	0.5843	0.7000	0.1000	0.8264	0.0550	0.5433
0.6400	0.0200	0.8795	0.0130	0.6474	0.6600	0.0400	0.8637	0.0247	0.6158	0.6800	0.0600	0.8463	0.0351	0.5824	0.7000	0.1200	0.8254	0.0658	0.5386
0.6400	0.0400	0.8793	0.0259	0.6465	0.6600	0.0600	0.8633	0.0370	0.6140	0.6800	0.0800	0.8457	0.0467	0.5795	0.7000	0.1400	0.8242	0.0766	0.5331
0.6400	0.0600	0.8789	0.0388	0.6447	0.6600	0.0800	0.8627	0.0492	0.6112	0.6800	0.1000	0.8449	0.0583	0.5759	0.7000	0.1600	0.8228	0.0872	0.5267
0.6400	0.0800	0.8784	0.0517	0.6421	0.6600	0.1000	0.8620	0.0614	0.6076	0.6800	0.1200	0.8440	0.0697	0.5713	0.7000	0.1800	0.8212	0.0976	0.5194
0.6400	0.1000	0.8777	0.0645	0.6386	0.6600	0.1200	0.8611	0.0735	0.6033	0.6800	0.1400	0.8429	0.0811	0.5660	0.7000	0.2000	0.8193	0.1079	0.5111
0.6400	0.1200	0.8769	0.0772	0.6344	0.6600	0.1400	0.8601	0.0856	0.5980	0.6800	0.1600	0.8415	0.0924	0.5597	0.7000	0.2200	0.8173	0.1181	0.5016
0.6400	0.1400	0.8759	0.0899	0.6293	0.6600	0.1600	0.8589	0.0975	0.5920	0.6800	0.1800	0.8400	0.1035	0.5526	0.7000	0.2400	0.8150	0.1280	0.4914
0.6400	0.1600	0.8748	0.1024	0.6234	0.6600	0.1800	0.8575	0.1092	0.5850	0.6800	0.2000	0.8383	0.1145	0.5445	0.7000	0.2600	0.8126	0.1377	0.4805
0.6400	0.1800	0.8735	0.1148	0.6167	0.6600	0.2000	0.8559	0.1208	0.5772	0.6800	0.2200	0.8365	0.1253	0.5356	0.7000	0.2800	0.8098	0.1472	0.4682
0.6400	0.2000	0.8721	0.1271	0.6091	0.6600	0.2200	0.8541	0.1323	0.5685	0.6800	0.2400	0.8344	0.1359	0.5257	0.7000	0.3000	0.8069	0.1564	0.4549
0.6400	0.2200	0.8704	0.1392	0.6007	0.6600	0.2400	0.8522	0.1436	0.5589	0.6800	0.2600	0.8321	0.1463	0.5147	0.7000	0.3200	0.8037	0.1654	0.4406
0.6400	0.2400	0.8686	0.1511	0.5913	0.6600	0.2600	0.8501	0.1547	0.5482	0.6800	0.2800	0.8295	0.1565	0.5028	0.7000	0.3400	0.8002	0.1741	0.4255
0.6400	0.2600	0.8667	0.1628	0.5810	0.6600	0.2800	0.8477	0.1655	0.5366	0.6800	0.3000	0.8268	0.1664	0.4899	0.7000	0.3600	0.7965	0.1824	0.4089
0.6400	0.2800	0.8645	0.1743	0.5698	0.6600	0.3000	0.8452	0.1761	0.5241	0.6800	0.3200	0.8238	0.1761	0.4759	0.7000	0.3800	0.7925	0.1904	0.3904
0.6400	0.3000	0.8621	0.1856	0.5575	0.6600	0.3200	0.8424	0.1865	0.5104	0.6800	0.3400	0.8206	0.1854	0.4602	0.7000	0.4000	0.7882	0.1980	0.3710
0.6400	0.3200	0.8596	0.1966	0.5442	0.6600	0.3400	0.8394	0.1965	0.4956	0.6800	0.3600	0.8172	0.1945	0.4437	0.7000	0.4200	0.7836	0.2052	0.3505
0.6400	0.3400	0.8568	0.2074	0.5298	0.6600	0.3600	0.8362	0.2063	0.4795	0.6800	0.3800	0.8134	0.2032	0.4273	0.7000	0.4400	0.7786	0.2120	0.3285
0.6400	0.3600	0.8538	0.2178	0.5143	0.6600	0.3800	0.8328	0.2157	0.4623	0.6800	0.4000	0.8094	0.2115	0.4078	0.7000	0.4600	0.7733	0.2184	0.3051
0.6400	0.3800	0.8506	0.2279	0.4974	0.6600	0.4000	0.8290	0.2248	0.4439	0.6800	0.4200	0.8051	0.2195	0.3869	0.7000	0.4800	0.7676	0.2242	0.2797
0.6400	0.4000	0.8471	0.2377	0.4794	0.6600	0.4200	0.8250	0.2334	0.4243	0.6800	0.4400	0.8005	0.2270	0.3668	0.7000	0.5000	0.7616	0.2295	0.2530
0.6400	0.4200	0.8434	0.2471	0.4602	0.6600	0.4400	0.8208	0.2417	0.4031	0.6800	0.4600	0.7956	0.2341	0.3429	0.7000	0.5200	0.7551	0.2343	0.2249
0.6400	0.4400	0.8395	0.2561	0.4395	0.6600	0.4600	0.8162	0.2496	0.3805	0.6800	0.4800	0.7903	0.2407	0.3185	0.7000	0.5400	0.7482	0.2385	0.1958
0.6400	0.4600	0.8352	0.2647	0.4175	0.6600	0.4800	0.8113	0.2569	0.3558	0.6800	0.5000	0.7847	0.2469	0.2923	0.7000	0.5600	0.7409	0.2421	0.1633
0.6400	0.4800	0.8307	0.2728	0.3940	0.6600	0.5000	0.8061	0.2638	0.3309	0.6800	0.5200	0.7787	0.2524	0.2642	0.7000	0.5800	0.7330	0.2450	0.1284
0.6400	0.5000	0.8258	0.2804	0.3689	0.6600	0.5200	0.8005	0.2702	0.3040	0.6800	0.5400	0.7723	0.2574	0.2354	0.7000	0.6000	0.7246	0.2473	0.0928
0.6400	0.5200	0.8206	0.2875	0.3420	0.6600	0.5400	0.7945	0.2759	0.2740	0.6800	0.5600	0.7655	0.2618	0.2031	0.7000	0.6200	0.7156	0.2487	0.0545
0.6400	0.5400	0.8151	0.2941	0.3131	0.6600	0.5600	0.7882	0.2811	0.2431	0.6800	0.5800	0.7582	0.2655	0.1696	0.7000	0.6400	0.7060	0.2494	0.0139
0.6400	0.5600	0.8092	0.3000	0.2827	0.6600	0.5800	0.7814	0.2856	0.2101	0.6800	0.6000	0.7504	0.2686	0.1340	0.7000	0.6600	0.6957	0.2493	-0.0293
0.6400	0.5800	0.8029	0.3054	0.2504	0.6600	0.6000	0.7742	0.2895	0.1750	0.6800	0.6200	0.7420	0.2709	0.0962	0.7000	0.6800	0.6847	0.2483	-0.0707
0.6400	0.6000	0.7961	0.3100	0.2158	0.6600	0.6200	0.7664	0.2926	0.1378	0.6800	0.6400	0.7331	0.2724	0.0564	0.7000	0.7000	0.6731	0.2464	-0.1188
0.6400	0.6200	0.7889	0.3140	0.1791	0.6600	0.6400	0.7581	0.2950	0.0981	0.6800	0.6600	0.7236	0.2731	0.0139	0.7000	0.7200	0.6605	0.2435	-0.1735
0.6400	0.6400	0.7812	0.3172	0.1399	0.6600	0.6600	0.7493	0.2965	0.0564	0.6800	0.6800	0.7134	0.2729	-0.0316	0.7000	0.7400	0.6469	0.2395	-0.2271
0.6400	0.6600	0.7730	0.3196	0.0987	0.6600	0.6800	0.7398	0.2972	0.0117	0.6800	0.7000	0.7025	0.2718	-0.0800	0.7000	0.7600	0.6323	0.2344	-0.2845
0.6400	0.6800	0.7642	0.3211	0.0546	0.6600	0.7000	0.7297	0.2970	-0.0361	0.6800	0.7200	0.6908	0.2697	-0.1261	0.7000	0.7800	0.6164	0.2281	-0.3451
0.6400	0.7000	0.7548	0.3217	0.0073	0.6600	0.7200	0.7189	0.2958	-0.0870	0.6800	0.7400	0.6785	0.2667	-0.1794	0.7000	0.8000	0.5993	0.2205	-0.4092
										0.6800	0.7600	0.6650	0.2625	-0.2407	0.7000	0.8200	0.5807	0.2117	-0.4773

T/T_c	v_0/v_{00}	ϵ_0/ϵ_{00}	v/v_{00}	dv/dv_0
0.7000	0.8400	0.5605	0.2014	-0.5493
0.7000	0.8600	0.5383	0.1897	-0.6249
0.7000	0.8800	0.5139	0.1764	-0.7058
0.7000	0.9000	0.4869	0.1614	-0.7919
0.7000	0.9200	0.4567	0.1447	-0.8820
0.7000	0.9400	0.4224	0.1261	-0.9775
0.7000	0.9600	0.3830	0.1055	-1.0819
0.7000	0.9800	0.3363	0.0828	-1.1906
0.7000	1.0000	0.2786	0.0579	-1.2940
0.7000	1.0200	0.2017	0.0309	-1.4175
0.7000	1.0400	0.0363	0.0012	-1.5410
0.7200	0.0000	0.8089	0.0000	0.5207
0.7200	0.0200	0.8088	0.0104	0.5198
0.7200	0.0400	0.8085	0.0208	0.5188
0.7200	0.0600	0.8080	0.0312	0.5168
0.7200	0.0800	0.8073	0.0415	0.5138
0.7200	0.1000	0.8064	0.0517	0.5099
0.7200	0.1200	0.8053	0.0619	0.5051
0.7200	0.1400	0.8040	0.0719	0.4995
0.7200	0.1600	0.8024	0.0818	0.4929
0.7200	0.1800	0.8007	0.0916	0.4853
0.7200	0.2000	0.7987	0.1012	0.4769
0.7200	0.2200	0.7965	0.1107	0.4675
0.7200	0.2400	0.7941	0.1199	0.4571
0.7200	0.2600	0.7914	0.1290	0.4456
0.7200	0.2800	0.7885	0.1378	0.4331
0.7200	0.3000	0.7853	0.1463	0.4195
0.7200	0.3200	0.7819	0.1545	0.4048
0.7200	0.3400	0.7781	0.1625	0.3890
0.7200	0.3600	0.7741	0.1701	0.3719
0.7200	0.3800	0.7698	0.1773	0.3535
0.7200	0.4000	0.7652	0.1842	0.3345
0.7200	0.4200	0.7602	0.1907	0.3136
0.7200	0.4400	0.7548	0.1967	0.2898
0.7200	0.4600	0.7491	0.2023	0.2662
0.7200	0.4800	0.7430	0.2074	0.2414
0.7200	0.5000	0.7365	0.2119	0.2140
0.7200	0.5200	0.7295	0.2159	0.1860
0.7200	0.5400	0.7221	0.2194	0.1546
0.7200	0.5600	0.7141	0.2221	0.1222
0.7200	0.5800	0.7056	0.2242	0.0885
0.7200	0.6000	0.6966	0.2256	0.0512
0.7200	0.6200	0.6868	0.2263	0.0126
0.7200	0.6400	0.6765	0.2261	-0.0289
0.7200	0.6600	0.6653	0.2251	-0.0678
0.7200	0.6800	0.6536	0.2234	-0.1133
0.7200	0.7000	0.6408	0.2205	-0.1659
0.7200	0.7200	0.6271	0.2167	-0.2167
0.7200	0.7400	0.6123	0.2119	-0.2712
0.7200	0.7600	0.5963	0.2059	-0.3286
0.7200	0.7800	0.5789	0.1987	-0.3895
0.7200	0.8000	0.5601	0.1903	-0.4534
0.7200	0.8200	0.5396	0.1805	-0.5213
0.7200	0.8400	0.5171	0.1694	-0.5941
0.7200	0.8600	0.4924	0.1567	-0.6703
0.7200	0.8800	0.4648	0.1425	-0.7506
0.7200	0.9000	0.4340	0.1267	-0.8349
0.7200	0.9200	0.3989	0.1091	-0.9329
0.7200	0.9400	0.3578	0.0894	-1.0226
0.7200	0.9600	0.3096	0.0682	-1.1156
0.7200	0.9800	0.2485	0.0447	-1.2230
0.7200	1.0000	0.1610	0.0192	-1.3303
0.7400	0.0000	0.7874	0.0000	0.4869
0.7400	0.0200	0.7872	0.0097	0.4860
0.7400	0.0400	0.7869	0.0195	0.4850
0.7400	0.0600	0.7864	0.0291	0.4829
0.7400	0.0800	0.7856	0.0388	0.4798
0.7400	0.1000	0.7846	0.0483	0.4759
0.7400	0.1200	0.7834	0.0578	0.4710
0.7400	0.1400	0.7820	0.0672	0.4652
0.7400	0.1600	0.7804	0.0764	0.4585
0.7400	0.1800	0.7785	0.0855	0.4508
0.7400	0.2000	0.7764	0.0944	0.4421
0.7400	0.2200	0.7740	0.1032	0.4325
0.7400	0.2400	0.7714	0.1117	0.4219
0.7400	0.2600	0.7685	0.1200	0.4102
0.7400	0.2800	0.7654	0.1281	0.3974
0.7400	0.3000	0.7619	0.1359	0.3835
0.7400	0.3200	0.7582	0.1434	0.3685
0.7400	0.3400	0.7542	0.1507	0.3523
0.7400	0.3600	0.7499	0.1575	0.3349
0.7400	0.3800	0.7452	0.1640	0.3163
0.7400	0.4000	0.7402	0.1702	0.2962
0.7400	0.4200	0.7348	0.1759	0.2748
0.7400	0.4400	0.7291	0.1812	0.2522
0.7400	0.4600	0.7229	0.1860	0.2279
0.7400	0.4800	0.7163	0.1903	0.2019
0.7400	0.5000	0.7093	0.1940	0.1743
0.7400	0.5200	0.7017	0.1972	0.1453
0.7400	0.5400	0.6937	0.1998	0.1141
0.7400	0.5600	0.6851	0.2018	0.0827
0.7400	0.5800	0.6759	0.2031	0.0465
0.7400	0.6000	0.6660	0.2036	0.0091
0.7400	0.6200	0.6555	0.2035	-0.0290
0.7400	0.6400	0.6442	0.2025	-0.0673
0.7400	0.6600	0.6323	0.2007	-0.1102
0.7400	0.6800	0.6193	0.1980	-0.1602
0.7400	0.7000	0.6054	0.1943	-0.2084
0.7400	0.7200	0.5903	0.1897	-0.2600
0.7400	0.7400	0.5741	0.1839	-0.3150
0.7400	0.7600	0.5564	0.1770	-0.3727
0.7400	0.7800	0.5373	0.1690	-0.4338
0.7400	0.8000	0.5163	0.1597	-0.4983
0.7400	0.8200	0.4933	0.1490	-0.5666
0.7400	0.8400	0.4679	0.1370	-0.6386
0.7400	0.8600	0.4397	0.1235	-0.7143
0.7400	0.8800	0.4078	0.1084	-0.7940
0.7400	0.9000	0.3713	0.0916	-0.8852
0.7400	0.9200	0.3282	0.0730	-0.9711
0.7400	0.9400	0.2766	0.0528	-1.0567
0.7400	0.9600	0.2086	0.0306	-1.1631
0.7400	0.9800	0.0930	0.0063	-1.2696
0.7600	0.0000	0.7640	0.0000	0.4525
0.7600	0.0200	0.7639	0.0090	0.4515
0.7600	0.0400	0.7635	0.0181	0.4505
0.7600	0.0600	0.7629	0.0271	0.4484
0.7600	0.0800	0.7621	0.0360	0.4453
0.7600	0.1000	0.7611	0.0449	0.4412
0.7600	0.1200	0.7598	0.0536	0.4362
0.7600	0.1400	0.7582	0.0623	0.4303
0.7600	0.1600	0.7565	0.0709	0.4234
0.7600	0.1800	0.7544	0.0792	0.4156
0.7600	0.2000	0.7521	0.0875	0.4068
0.7600	0.2200	0.7496	0.0955	0.3969
0.7600	0.2400	0.7468	0.1033	0.3859
0.7600	0.2600	0.7437	0.1109	0.3739
0.7600	0.2800	0.7403	0.1183	0.3611
0.7600	0.3000	0.7366	0.1254	0.3469
0.7600	0.3200	0.7325	0.1322	0.3317
0.7600	0.3400	0.7282	0.1386	0.3151
0.7600	0.3600	0.7235	0.1448	0.2976
0.7600	0.3800	0.7185	0.1505	0.2785
0.7600	0.4000	0.7131	0.1559	0.2579
0.7600	0.4200	0.7073	0.1608	0.2364
0.7600	0.4400	0.7010	0.1653	0.2134
0.7600	0.4600	0.6944	0.1694	0.1887
0.7600	0.4800	0.6872	0.1729	0.1623
0.7600	0.5000	0.6796	0.1758	0.1344
0.7600	0.5200	0.6714	0.1782	0.1048
0.7600	0.5400	0.6627	0.1800	0.0739
0.7600	0.5600	0.6533	0.1812	0.0407
0.7600	0.5800	0.6433	0.1816	0.0047
0.7600	0.6000	0.6326	0.1814	-0.0286
0.7600	0.6200	0.6213	0.1805	-0.0679
0.7600	0.6400	0.6090	0.1786	-0.1122
0.7600	0.6600	0.5958	0.1760	-0.1556
0.7600	0.6800	0.5815	0.1724	-0.2031
0.7600	0.7000	0.5661	0.1678	-0.2522
0.7600	0.7200	0.5495	0.1623	-0.3041
0.7600	0.7400	0.5314	0.1557	-0.3589
0.7600	0.7600	0.5118	0.1479	-0.4168
0.7600	0.7800	0.4902	0.1390	-0.4780
0.7600	0.8000	0.4665	0.1288	-0.5425
0.7600	0.8200	0.4403	0.1172	-0.6111
0.7600	0.8400	0.4108	0.1043	-0.6830
0.7600	0.8600	0.3774	0.0899	-0.7581
0.7600	0.8800	0.3388	0.0739	-0.8411
0.7600	0.9000	0.2925	0.0562	-0.9305
0.7600	0.9200	0.2342	0.0367	-1.0114
0.7600	0.9400	0.1517	0.0158	-1.0923
0.7800	0.0000	0.7386	0.0000	0.4174
0.7800	0.0200	0.7385	0.0083	0.4164
0.7800	0.0400	0.7381	0.0167	0.4154
0.7800	0.0600	0.7375	0.0250	0.4133
0.7800	0.0800	0.7366	0.0332	0.4101
0.7800	0.1000	0.7355	0.0414	0.4059
0.7800	0.1200	0.7341	0.0494	0.4009
0.7800	0.1400	0.7324	0.0574	0.3947
0.7800	0.1600	0.7305	0.0652	0.3877
0.7800	0.1800	0.7283	0.0729	0.3798
0.7800	0.2000	0.7258	0.0804	0.3708
0.7800	0.2200	0.7231	0.0877	0.3607
0.7800	0.2400	0.7200	0.0948	0.3497
0.7800	0.2600	0.7167	0.1017	0.3375
0.7800	0.2800	0.7130	0.1083	0.3243
0.7800	0.3000	0.7090	0.1147	0.3099
0.7800	0.3200	0.7046	0.1207	0.2943
0.7800	0.3400	0.6999	0.1264	0.2775
0.7800	0.3600	0.6949	0.1318	0.2597
0.7800	0.3800	0.6894	0.1368	0.2402
0.7800	0.4000	0.6835	0.1414	0.2194
0.7800	0.4200	0.6772	0.1456	0.1977
0.7800	0.4400	0.6705	0.1493	0.1742
0.7800	0.4600	0.6632	0.1525	0.1490
0.7800	0.4800	0.6554	0.1552	0.1224
0.7800	0.5000	0.6471	0.1574	0.0941
0.7800	0.5200	0.6382	0.1590	0.0642
0.7800	0.5400	0.6287	0.1600	0.0323
0.7800	0.5600	0.6185	0.1603	0.0023
0.7800	0.5800	0.6078	0.1600	-0.0334
0.7800	0.6000	0.5960	0.1589	-0.0737
0.7800	0.6200	0.5834	0.1571	-0.1129
0.7800	0.6400	0.5698	0.1544	-0.1555
0.7800	0.6600	0.5552	0.1508	-0.1997
0.7800	0.6800	0.5394	0.1464	-0.2448
0.7800	0.7000	0.5222	0.1410	-0.2942
0.7800	0.7200	0.5036	0.1346	-0.3480
0.7800	0.7400	0.4832	0.1271	-0.4028
0.7800	0.7600	0.4609	0.1185	-0.4608
0.7800	0.7800	0.4362	0.1086	-0.5223
0.7800	0.8000	0.4086	0.0976	-0.5852
0.7800	0.8200	0.3775	0.0852	-0.6528
0.7800	0.8400	0.3418	0.0714	-0.7301
0.7800	0.8600	0.2993	0.0560	-0.8057
0.7800	0.8800	0.2480	0.0392	-0.8811
0.7800	0.9000	0.1785	0.0207	-0.9637
0.7800	0.9200	0.0285	0.0006	-1.0464
0.8000	0.0000	0.7110	0.0000	0.3818
0.8000	0.0200	0.7109	0.0076	0.3808
0.8000	0.0400	0.7105	0.0152	0.3797
0.8000	0.0600	0.7098	0.0228	0.3776
0.8000	0.0800	0.7089	0.0303	0.3743
0.8000	0.1000	0.7076	0.0378	0.3701
0.8000	0.1200	0.7061	0.0451	0.3649
0.8000	0.1400	0.7043	0.0524	0.3587
0.8000	0.1600	0.7022	0.0595	0.3516
0.8000	0.1800	0.6999	0.0664	0.3434
0.8000	0.2000	0.6972	0.0732	0.3343
0.8000	0.2200	0.6942	0.0798	0.3241
0.8000	0.2400	0.6909	0.0862	0.3128
0.8000	0.2600	0.6872	0.0923	0.3004
0.8000	0.2800	0.6832	0.0982	0.2869
0.8000	0.3000	0.6789	0.1038	0.2723
0.8000	0.3200	0.6742	0.1091	0.2565
0.8000	0.3400	0.6691	0.1140	0.2396
0.8000	0.3600	0.6636	0.1186	0.2213
0.8000	0.3800	0.6576	0.1229	0.2015

T/T_e	v_0/v_{00}	ϵ_0/ϵ_{00}	v/v_{00}	dv/dv_0
0.8000	0.4000	0.6512	0.1267	0.1806
0.8000	0.4200	0.6443	0.1301	0.1583
0.8000	0.4400	0.6370	0.1330	0.1342
0.8000	0.4600	0.6290	0.1354	0.1091
0.8000	0.4800	0.6205	0.1374	0.0825
0.8000	0.5000	0.6114	0.1387	0.0532
0.8000	0.5200	0.6017	0.1395	0.0263
0.8000	0.5400	0.5914	0.1397	-0.0056
0.8000	0.5600	0.5802	0.1393	-0.0408
0.8000	0.5800	0.5681	0.1381	-0.0779
0.8000	0.6000	0.5551	0.1361	-0.1171
0.8000	0.6200	0.5411	0.1334	-0.1551
0.8000	0.6400	0.5260	0.1299	-0.1979
0.8000	0.6600	0.5096	0.1255	-0.2426
0.8000	0.6800	0.4918	0.1202	-0.2895
0.8000	0.7000	0.4724	0.1139	-0.3394
0.8000	0.7200	0.4511	0.1066	-0.3898
0.8000	0.7400	0.4276	0.0983	-0.4480
0.8000	0.7600	0.4014	0.0888	-0.5060
0.8000	0.7800	0.3720	0.0781	-0.5664
0.8000	0.8000	0.3383	0.0661	-0.6294
0.8000	0.8200	0.2990	0.0529	-0.6991
0.8000	0.8400	0.2511	0.0381	-0.7703
0.8000	0.8600	0.1886	0.0220	-0.8452
0.8000	0.8800	0.0813	0.0043	-0.9201
0.8200	0.0000	0.6810	0.0000	0.3456
0.8200	0.0200	0.6808	0.0069	0.3446
0.8200	0.0400	0.6804	0.0138	0.3435
0.8200	0.0600	0.6796	0.0206	0.3413
0.8200	0.0800	0.6786	0.0274	0.3380
0.8200	0.1000	0.6772	0.0342	0.3336
0.8200	0.1200	0.6756	0.0408	0.3284
0.8200	0.1400	0.6737	0.0473	0.3221
0.8200	0.1600	0.6714	0.0537	0.3148
0.8200	0.1800	0.6688	0.0599	0.3066
0.8200	0.2000	0.6659	0.0659	0.2972
0.8200	0.2200	0.6626	0.0718	0.2869
0.8200	0.2400	0.6590	0.0774	0.2754
0.8200	0.2600	0.6550	0.0828	0.2628
0.8200	0.2800	0.6507	0.0879	0.2492
0.8200	0.3000	0.6460	0.0927	0.2343
0.8200	0.3200	0.6408	0.0973	0.2182
0.8200	0.3400	0.6352	0.1014	0.2009
0.8200	0.3600	0.6292	0.1053	0.1826
0.8200	0.3800	0.6227	0.1087	0.1627
0.8200	0.4000	0.6157	0.1118	0.1413
0.8200	0.4200	0.6081	0.1144	0.1187
0.8200	0.4400	0.6000	0.1165	0.0946
0.8200	0.4600	0.5913	0.1182	0.0683
0.8200	0.4800	0.5820	0.1193	0.0443
0.8200	0.5000	0.5722	0.1199	0.0161
0.8200	0.5200	0.5614	0.1199	-0.0173
0.8200	0.5400	0.5498	0.1193	-0.0497
0.8200	0.5600	0.5373	0.1179	-0.0838
0.8200	0.5800	0.5238	0.1158	-0.1194
0.8200	0.6000	0.5092	0.1131	-0.1577
0.8200	0.6200	0.4934	0.1095	-0.1983
0.8200	0.6400	0.4763	0.1051	-0.2407
0.8200	0.6600	0.4576	0.0999	-0.2853
0.8200	0.6800	0.4370	0.0937	-0.3326
0.8200	0.7000	0.4144	0.0866	-0.3825
0.8200	0.7200	0.3893	0.0784	-0.4352
0.8200	0.7400	0.3610	0.0691	-0.4907
0.8200	0.7600	0.3287	0.0587	-0.5467
0.8200	0.7800	0.2910	0.0472	-0.6114
0.8200	0.8000	0.2451	0.0343	-0.6723
0.8200	0.8200	0.1860	0.0203	-0.7440
0.8200	0.8400	0.0860	0.0045	-0.8157
0.8400	0.0000	0.6480	0.0000	0.3089
0.8400	0.0200	0.6478	0.0062	0.3079
0.8400	0.0400	0.6473	0.0123	0.3068
0.8400	0.0600	0.6465	0.0184	0.3046
0.8400	0.0800	0.6454	0.0245	0.3011
0.8400	0.1000	0.6439	0.0305	0.2967
0.8400	0.1200	0.6422	0.0364	0.2914
0.8400	0.1400	0.6400	0.0421	0.2850
0.8400	0.1600	0.6375	0.0478	0.2776
0.8400	0.1800	0.6347	0.0532	0.2692
0.8400	0.2000	0.6315	0.0585	0.2597
0.8400	0.2200	0.6280	0.0636	0.2492
0.8400	0.2400	0.6240	0.0685	0.2376
0.8400	0.2600	0.6197	0.0731	0.2248
0.8400	0.2800	0.6149	0.0775	0.2109
0.8400	0.3000	0.6097	0.0815	0.1959
0.8400	0.3200	0.6040	0.0853	0.1796
0.8400	0.3400	0.5979	0.0887	0.1620
0.8400	0.3600	0.5912	0.0918	0.1434
0.8400	0.3800	0.5841	0.0944	0.1233
0.8400	0.4000	0.5763	0.0967	0.1018
0.8400	0.4200	0.5680	0.0985	0.0787
0.8400	0.4400	0.5590	0.0998	0.0540
0.8400	0.4600	0.5493	0.1007	0.0311
0.8400	0.4800	0.5392	0.1010	0.0039
0.8400	0.5000	0.5280	0.1008	-0.0279
0.8400	0.5200	0.5159	0.0999	-0.0584
0.8400	0.5400	0.5028	0.0984	-0.0910
0.8400	0.5600	0.4887	0.0963	-0.1253
0.8400	0.5800	0.4734	0.0934	-0.1615
0.8400	0.6000	0.4567	0.0898	-0.2006
0.8400	0.6200	0.4385	0.0854	-0.2410
0.8400	0.6400	0.4186	0.0801	-0.2833
0.8400	0.6600	0.3964	0.0740	-0.3287
0.8400	0.6800	0.3719	0.0670	-0.3760
0.8400	0.7000	0.3442	0.0590	-0.4259
0.8400	0.7200	0.3126	0.0499	-0.4785
0.8400	0.7400	0.2766	0.0398	-0.5369
0.8400	0.7600	0.2302	0.0285	-0.5917
0.8400	0.7800	0.1711	0.0161	-0.6520
0.8400	0.8000	0.0648	0.0024	-0.7122
0.8600	0.0000	0.6117	0.0000	0.2717
0.8600	0.0200	0.6115	0.0054	0.2707
0.8600	0.0400	0.6110	0.0108	0.2696
0.8600	0.0600	0.6101	0.0162	0.2673
0.8600	0.0800	0.6089	0.0215	0.2638
0.8600	0.1000	0.6073	0.0268	0.2594
0.8600	0.1200	0.6053	0.0319	0.2539
0.8600	0.1400	0.6029	0.0369	0.2474
0.8600	0.1600	0.6002	0.0418	0.2400
0.8600	0.1800	0.5971	0.0465	0.2314
0.8600	0.2000	0.5936	0.0510	0.2218
0.8600	0.2200	0.5897	0.0554	0.2111
0.8600	0.2400	0.5853	0.0596	0.1993
0.8600	0.2600	0.5805	0.0633	0.1864
0.8600	0.2800	0.5752	0.0669	0.1723
0.8600	0.3000	0.5694	0.0702	0.1571
0.8600	0.3200	0.5632	0.0732	0.1406
0.8600	0.3400	0.5563	0.0758	0.1229
0.8600	0.3600	0.5490	0.0781	0.1036
0.8600	0.3800	0.5410	0.0800	0.0829
0.8600	0.4000	0.5323	0.0814	0.0608
0.8600	0.4200	0.5232	0.0825	0.0409
0.8600	0.4400	0.5132	0.0830	0.0141
0.8600	0.4600	0.5023	0.0831	-0.0117
0.8600	0.4800	0.4905	0.0826	-0.0394
0.8600	0.5000	0.4778	0.0815	-0.0688
0.8600	0.5200	0.4640	0.0798	-0.0999
0.8600	0.5400	0.4489	0.0775	-0.1327
0.8600	0.5600	0.4326	0.0745	-0.1675
0.8600	0.5800	0.4146	0.0708	-0.2039
0.8600	0.6000	0.3949	0.0663	-0.2426
0.8600	0.6200	0.3731	0.0610	-0.2839
0.8600	0.6400	0.3487	0.0549	-0.3268
0.8600	0.6600	0.3211	0.0480	-0.3717
0.8600	0.6800	0.2894	0.0400	-0.4189
0.8600	0.7000	0.2519	0.0312	-0.4708
0.8600	0.7200	0.2050	0.0212	-0.5226
0.8600	0.7400	0.1408	0.0103	-0.5743
0.8800	0.0000	0.5715	0.0000	0.2340
0.8800	0.0200	0.5713	0.0047	0.2330
0.8800	0.0400	0.5707	0.0093	0.2319
0.8800	0.0600	0.5697	0.0140	0.2295
0.8800	0.0800	0.5683	0.0185	0.2260
0.8800	0.1000	0.5665	0.0230	0.2215
0.8800	0.1200	0.5643	0.0274	0.2160
0.8800	0.1400	0.5617	0.0316	0.2094
0.8800	0.1600	0.5587	0.0357	0.2018
0.8800	0.1800	0.5552	0.0397	0.1932
0.8800	0.2000	0.5513	0.0435	0.1835
0.8800	0.2200	0.5469	0.0470	0.1726
0.8800	0.2400	0.5421	0.0504	0.1607
0.8800	0.2600	0.5367	0.0534	0.1476
0.8800	0.2800	0.5308	0.0562	0.1333
0.8800	0.3000	0.5243	0.0588	0.1179
0.8800	0.3200	0.5173	0.0610	0.1012
0.8800	0.3400	0.5096	0.0628	0.0830
0.8800	0.3600	0.5012	0.0643	0.0657
0.8800	0.3800	0.4925	0.0654	0.0454
0.8800	0.4000	0.4827	0.0661	0.0216
0.8800	0.4200	0.4720	0.0663	-0.0015
0.8800	0.4400	0.4605	0.0660	-0.0263
0.8800	0.4600	0.4479	0.0652	-0.0527
0.8800	0.4800	0.4343	0.0639	-0.0807
0.8800	0.5000	0.4194	0.0620	-0.1103
0.8800	0.5200	0.4031	0.0595	-0.1414
0.8800	0.5400	0.3852	0.0563	-0.1746
0.8800	0.5600	0.3654	0.0525	-0.2096
0.8800	0.5800	0.3433	0.0479	-0.2469
0.8800	0.6000	0.3186	0.0426	-0.2870
0.8800	0.6200	0.2902	0.0366	-0.3295
0.8800	0.6400	0.2573	0.0296	-0.3690
0.8800	0.6600	0.2173	0.0218	-0.4156
0.8800	0.6800	0.1652	0.0130	-0.4634
0.8800	0.7000	0.0805	0.0033	-0.5111
0.9000	0.0000	0.5263	0.0000	0.1959
0.9000	0.0200	0.5261	0.0039	0.1949
0.9000	0.0400	0.5254	0.0078	0.1938
0.9000	0.0600	0.5243	0.0117	0.1914
0.9000	0.0800	0.5228	0.0155	0.1878
0.9000	0.1000	0.5208	0.0192	0.1833
0.9000	0.1200	0.5183	0.0228	0.1777
0.9000	0.1400	0.5154	0.0263	0.1710
0.9000	0.1600	0.5119	0.0296	0.1633
0.9000	0.1800	0.5080	0.0328	0.1545
0.9000	0.2000	0.5036	0.0358	0.1447
0.9000	0.2200	0.4986	0.0386	0.1337
0.9000	0.2400	0.4931	0.0411	0.1216
0.9000	0.2600	0.4870	0.0434	0.1084
0.9000	0.2800	0.4803	0.0455	0.0939
0.9000	0.3000	0.4729	0.0472	0.0780
0.9000	0.3200	0.4648	0.0486	0.0633
0.9000	0.3400	0.4563	0.0497	0.0452
0.9000	0.3600	0.4466	0.0504	0.0290
0.9000	0.3800	0.4362	0.0507	0.0035
0.9000	0.4000	0.4247	0.0505	-0.0187
0.9000	0.4200	0.4122	0.0499	-0.0422
0.9000	0.4400	0.3985	0.0488	-0.0673
0.9000	0.4600	0.3835	0.0472	-0.0937
0.9000	0.4800	0.3670	0.0450	-0.1221
0.9000	0.5000	0.3487	0.0423	-0.1520
0.9000	0.5200	0.3283	0.0390	-0.1833
0.9000	0.5400	0.3054	0.0350	-0.2164
0.9000	0.5600	0.2793	0.0303	-0.2517
0.9000	0.5800	0.2490	0.0249	-0.2891
0.9000	0.6000	0.2125	0.0187	-0.3269
0.9000	0.6200	0.1654	0.0118	-0.3675
0.9000	0.6400	0.0943	0.0040	-0.4081
0.9200	0.0000	0.4749	0.0000	0.1575
0.9200	0.0200	0.4746	0.0031	0.1564
0.9200	0.0400	0.4739	0.0063	0.1552
0.9200	0.0600	0.4726	0.0094	0.1528
0.9200	0.0800	0.4708	0.0124	0.1492
0.9200	0.1000	0.4685	0.0153	0.1446
0.9200	0.1200	0.4657	0.0182	0.1389
0.9200	0.1400	0.4623	0.0209	0.1322

T/T_e	v_0/v_∞	$\epsilon_0/\epsilon_\infty$	v/v_∞	dv/dv_0
0.9200	0.1600	0.4583	0.0234	0.1344
0.9200	0.1800	0.4538	0.0258	0.1155
0.9200	0.2000	0.4487	0.0280	0.1055
0.9200	0.2200	0.4429	0.0301	0.0944
0.9200	0.2400	0.4365	0.0318	0.0822
0.9200	0.2600	0.4294	0.0333	0.0684
0.9200	0.2800	0.4215	0.0346	0.0557
0.9200	0.3000	0.4131	0.0355	0.0403
0.9200	0.3200	0.4035	0.0362	0.0216
0.9200	0.3400	0.3931	0.0364	0.0035
0.9200	0.3600	0.3815	0.0363	-0.0161
0.9200	0.3800	0.3688	0.0358	-0.0370
0.9200	0.4000	0.3548	0.0348	-0.0594
0.9200	0.4200	0.3393	0.0334	-0.0832
0.9200	0.4400	0.3220	0.0315	-0.1085
0.9200	0.4600	0.3027	0.0290	-0.1351
0.9200	0.4800	0.2808	0.0260	-0.1633
0.9200	0.5000	0.2558	0.0225	-0.1936
0.9200	0.5200	0.2264	0.0183	-0.2252
0.9200	0.5400	0.1906	0.0134	-0.2600
0.9200	0.5600	0.1434	0.0079	-0.2952
0.9200	0.5800	0.0642	0.0016	-0.3304
0.9400	0.0000	0.4148	0.0000	0.1186
0.9400	0.0200	0.4145	0.0024	0.1175
0.9400	0.0400	0.4136	0.0047	0.1163
0.9400	0.0600	0.4121	0.0070	0.1139
0.9400	0.0800	0.4100	0.0093	0.1103
0.9400	0.1000	0.4072	0.0114	0.1056
0.9400	0.1200	0.4039	0.0135	0.0998
0.9400	0.1400	0.3998	0.0154	0.0930
0.9400	0.1600	0.3951	0.0172	0.0851
0.9400	0.1800	0.3897	0.0188	0.0761
0.9400	0.2000	0.3835	0.0202	0.0660
0.9400	0.2200	0.3765	0.0214	0.0546
0.9400	0.2400	0.3687	0.0224	0.0440
0.9400	0.2600	0.3604	0.0232	0.0305
0.9400	0.2800	0.3507	0.0236	0.0143
0.9400	0.3000	0.3399	0.0238	-0.0013
0.9400	0.3200	0.3279	0.0236	-0.0185
0.9400	0.3400	0.3145	0.0230	-0.0370
0.9400	0.3600	0.2995	0.0221	-0.0566
0.9400	0.3800	0.2826	0.0207	-0.0777
0.9400	0.4000	0.2635	0.0190	-0.1004
0.9400	0.4200	0.2416	0.0167	-0.1244
0.9400	0.4400	0.2159	0.0140	-0.1499
0.9400	0.4600	0.1850	0.0107	-0.1770
0.9400	0.4800	0.1453	0.0069	-0.2055
0.9400	0.5000	0.0865	0.0025	-0.2340
0.9600	0.0000	0.3416	0.0000	0.0794
0.9600	0.0200	0.3412	0.0016	0.0783
0.9600	0.0400	0.3400	0.0031	0.0771
0.9600	0.0600	0.3381	0.0047	0.0746
0.9600	0.0800	0.3354	0.0061	0.0709
0.9600	0.1000	0.3320	0.0075	0.0662
0.9600	0.1200	0.3277	0.0088	0.0603
0.9600	0.1400	0.3226	0.0099	0.0534
0.9600	0.1600	0.3165	0.0109	0.0453
0.9600	0.1800	0.3095	0.0117	0.0376
0.9600	0.2000	0.3020	0.0124	0.0276
0.9600	0.2200	0.2929	0.0128	0.0152
0.9600	0.2400	0.2825	0.0130	0.0027
0.9600	0.2600	0.2707	0.0129	-0.0109
0.9600	0.2800	0.2572	0.0125	-0.0256
0.9600	0.3000	0.2418	0.0119	-0.0417
0.9600	0.3200	0.2241	0.0109	-0.0591
0.9600	0.3400	0.2034	0.0095	-0.0777
0.9600	0.3600	0.1786	0.0078	-0.0977
0.9600	0.3800	0.1475	0.0056	-0.1215
0.9600	0.4000	0.1040	0.0029	-0.1393
0.9600	0.4200	0.0040	0.0000	-0.1571
0.9800	0.0000	0.2436	0.0000	0.0399
0.9800	0.0200	0.2429	0.0008	0.0387
0.9800	0.0400	0.2413	0.0016	0.0375
0.9800	0.0600	0.2385	0.0023	0.0350
0.9800	0.0800	0.2345	0.0030	0.0312
0.9800	0.1000	0.2294	0.0035	0.0263
0.9800	0.1200	0.2229	0.0040	0.0213
0.9800	0.1400	0.2158	0.0044	0.0146
0.9800	0.1600	0.2064	0.0046	0.0058
0.9800	0.1800	0.1952	0.0046	-0.0032
0.9800	0.2000	0.1819	0.0044	-0.0136
0.9800	0.2200	0.1657	0.0041	-0.0250
0.9800	0.2400	0.1460	0.0034	-0.0377
0.9800	0.2600	0.1207	0.0025	-0.0517
0.9800	0.2800	0.0852	0.0014	-0.0656

RCA TECHNICAL PAPERS†

Second Quarter, 1964

Any request for copies of papers listed herein should be addressed to the publication to which credited.

"Designing Dynamic Test Sets for Use Optimization," F. W. Stirner, *Trans. IEEE PTGPEP* (April) 1964
"Engineering Standardization Study of Wire Terminals," B. R. Schwartz, H. R. Sutton, and Coauthor, *Trans. IEEE PTGAS* (April) 1964
"Evaluating Reliability without Specific Test Data," R. H. Fondeur, *Trans. IEEE PTGAS* (April) 1964
"Hybrid-Coupled VHF Transistor Power Amplifier," R. M. Kurzrok, S. J. Mehlman, and A. Newton, *Trans. IEEE PTGAS* (April) 1964
"Intensity-Ratio Technique for X-Ray Spectrometric Analysis of Binary Samples: Particular Application to Determination of Niobium and Tin on Nb_3Sn-Coated Metal Ribbon," E. P. Bertin, *Anal. Chem.* (April) 1964
"Magnetostatic Measurement of Spacecraft Magnetic Dipole Moment," R. Moskowitz and R. Lynch, *Trans. IEEE PTGAS* (April) 1964
"Method of Measuring the Velocity of a Continuously Flowing Plasma," J. A. Cooney, *Rev. Sci. Instr.* (April) 1964
"Minuteman Digital-Data Transmission System Tests," A. Cortizas and J. H. Wolff, *Trans. IEEE PTGAS* (April) 1964
"Multilayer Printed Circuit Interconnection Techniques," A. Levy, *Trans. IEEE PTGPEP* (April) 1964
"A Note on Tributary Switching Networks," S. Y. Levy, R. O. Winder, and Coauthor, *Trans. IEEE PTGEC* (Correspondence) (April) 1964
"Periodic Checkout and Associated Errors," W. D. Moon, *Trans. IEEE PTGAS* (April) 1964
"Pinch Off in Insulated-Gate Field-Effect Transistors," S. R. Hofstein F. P. Heiman, *Proc. IEEE* (Correspondence, Author's Reply) (April) 1964
"Power Spectra Measurements on Ultralow-Noise Beams," J. M. Hammer, *Jour. Appl. Phys.* (April) 1964
"On the Origin of Unpaired Electrons in Metal-Free Phthalocyanine," J. M. Assour and S. E. Harrison, *Jour. Phys. Chem.* (April) 1964
"Scope Adapter for Tunnel-Diode Measurements," F. M. Carlson, *Electronic Industries* (April) 1964
"Sensing Characteristics of an Electrostatic Recording Camera," T. H. Moore and I. M. Krittman, *Trans. IEEE PTGED* (April) ... 1964
"Simple Electron Diffraction Camera for the Examination of Alkali Antimonide Photoelectric Films," W. H. McCarroll and R. E. Simon, *Rev. Sci. Instr.* (April) 1964
"Traveling-Wave Masers Employing Iron-Doped Rutile," L. C. Morris and D. J. Miller, *Proc. IEEE* (Correspondence) (April) 1964
"Depositing Active and Passive Thin-Film Elements on One Chip," H. Borkan, *Electronics* (April 20) 1964
"Optical Double-Photon Absorption in CdS," R. Braunstein and N. Ockman, *Phys. Rev.* (April 20) 1964

† Report all corrections to *RCA Review*, RCA Laboratories, Princeton, New Jersey.

"Using MOS Transistors in Integrated Circuits," J. A. Olmstead, *Electronic Design* (April 27) 1964

"Adaptation, Learning, Self-Repair, and Feedback," J. Sklansky, *IEEE Spectrum* (Correspondence) (May) 1964

"Comment on 'Cerenkov Radiation in Anisotropic Ferrites'," L. W. Zelby, *Trans. IEEE PTGMTT* (Correspondence) (May) 1964

"Controlled Etching of Tunnel Diodes," A. M. Goodman, *Rev. Sci. Instr.* (Notes) (May) 1964

"The Impact of Microminiaturization," W. W. Watts, *Signal* (May) 1964

"A p-Type Tellurium Thin-Film Transistor," P. K. Weimer, *Proc. IEEE* (Correspondence) (May) 1964

"Some Applications of Metal-Oxide Semiconductors to Switching Circuits," R. D. Lohman, *Semiconductor Products* (May) 1964

"Suggestions Concerning Measurement of Stereophonic FM Receivers," A. L. R. Limberg, *Trans. IEEE PTGBTR* (May) .. 1964

"Ultra-Low-Noise Traveling-Wave-Tube Gun with Two Beam-Forming Electrodes," A. L. Eichenbaum, *Proc. IEEE* (Correspondence) (May) 1964

"Reed Switches for Breadboarding," M. B. Knight, *Electronics* (May 18) 1964

"Silicon-Germanium Thermoelectric Power Modules," H. P. Van Heyst and T. M. Cunningham, *18th Ann. Power-Sources Conf.*, Atlantic City, N. J. (May 21) 1964

"Analysis of Gate-Controlled Space-Charge-Limited Emission Processes in Semiconductors," R. C. Williams, *RCA Review* (June) 1964

"Approach to Developing Electrical Connection Comparison Data Through Variables Testing," R. A. Geshner and B. Tiger, *Trans. IEEE PTGCP* (June) 1964

"Carrier Transport Across Electroluminescent p-n Junctions in GaAs," J. I. Pankove, *Jour. Appl. Phys.* (June) 1964

"Cesium Vapor Dispenser," A. L. Eichenbaum and M. E. Moi, *Rev. Sci. Instr.* (June) 1964

"Free-Space Microwave Techniques for Plasma Measurements," M. P. Bachynski and G. G. Cloutier, *RCA Review* (June) 1964

"Injection-Luminescence Pumping of a $CaF_2:Dy^{2+}$ Laser," S. A. Ochs and J. I. Pankove, *Proc. IEEE* (Correspondence) (June) 1964

"Minimizing Electron Tube Hum," W. Austin, *Electronic Industries* (June) 1964

"The NASA Relay I Experimental Communication Satellite," J. D. Kiesling, *RCA Review* (June) 1964

"A New Surface Phenomenon in Thermoplastic Layers and Its Use in Recording Information," F. H. Nicoll, *RCA Review* (June) 1964

"A Photoconductive Thermoplastic Recording System," N. E. Wolff, *RCA Review* (June) 1964

"Preparation, Optical Properties, and Band Structure of Boron Monophosphide," C. C. Wang, M. Cardona, and A. G. Fischer, *RCA Review* (June) 1964

"Pulse Propagation in a Laser Amplifier," J. P. Wittke and Coauthor, *Jour. Appl. Phys.* (June) 1964

"Pulse Shaping and Droop Compensation with Nonuniform Transmission Lines," T. Douma, *Trans. IEEE PTGCT* (June) 1964

"Recent Photomultiplier Developments at RCA," R. M. Matheson, *Trans. IEEE PTGNS* (June) 1964

"Stabilization of Lithium-Drifted Radiation Detectors," G. Norgate and R. J. McIntyre, *Trans. IEEE PTGNS* (June) 1964

"Stable Divalent Rare Earths in Alkaline Earth Halides by Solid-State Electrolysis," F. K. Fong, *RCA Review* (June) 1964

"Storage of Electronic Components & Equipment," R. F. Ficcki and M. Raphelson, *Trans. IEEE PTGCP* (June) 1964
"Wide-Temperature-Range Ferrite Cores for Computer Memories," H. P. Lemaire, H. Lessoff, and E. Fortin, *RCA Review* (June) 1964
"Evidence for Normal Regions at Low Temperatures in the Superconducting Mixed State," B. Rosenblum and M. Cardona, *Phys. Rev. Letters* (15 June) 1964
"Preventing Second Breakdown in Transistor Circuits," P. Schiff, *Electronics* (June 15) 1964

AUTHORS

E. P. BERTIN received the degree of Ph.D. in chemistry in 1952 from the University of Illinois. He specialized in inorganic and instrumental analytical chemistry. After serving a year as an Instructor in Chemistry at Illinois, in 1953 he joined the Electron Tube Division of RCA at Harrison, New Jersey. There he has worked on problems in x-ray radiography, microradiography, diffraction, and spectrometry, and in electron microscopy arising in the design, development, manufacture, and testing of receiving-type electron tubes. More recently he has applied the same techniques in RCA's thermoelectric and superconductive development programs. Dr. Bertin is a member of the American Chemical Society, American Physical Society, Institute of Electrical and Electronics Engineers, Society for Applied Spectroscopy, American Crystallographic Association, Electron Microscopy Society of America, Society for Nondestructive Testing, American Association for the Advancement of Science, and Sigma Xi.

L. J. BERTON received the B.S.E. in 1961 from Princeton University in Electrical Engineering. He entered the Research Services Laboratory of RCA Laboratories, Princeton, N. J., where he has been working on numerical solutions of ordinary differential equations. He was accepted on the RCA Graduate Study Program in September 1962 to study at the University of Pennsylvania. He is currently completing requirements for the M.S. degree in Computer and Information Sciences, and has begun taking courses toward the Ph.D. degree in the same department. Mr. Berton is a member of the Association for Computing Machinery.

MANUEL CARDONA (see *RCA Review*, Vol. XXV, No. 2, June 1964, p. 323.)

K. LU CHENG received the B.S. degree in chemistry from the Northwestern College, China, in 1941, and the M.S. and Ph.D. degrees from the University of Illinois in 1949 and 1951, respectively. He was a postdoctoral fellow at the University of Illinois after graduation. From 1952 to 1953 he was a microchemist at the Commercial Solvents Corporation, Terre Haute, Indiana. From 1953 to 1955 he taught analytical chemistry at the University of Connecticut as an Instructor and Assistant Professor. From 1955 to 1957 he worked as an engineer with the Westinghouse Electric Corporation. From 1957 to 1959 he was an associate director of research with the Metals Division, Kelsey-Hayes Co., New Hartford, N. Y. In October 1959, he joined RCA Laboratories where he is engaged in analytical chemistry research and development. Dr. Cheng is a member of Sigma Xi, Phi Lambda Upsilon, Sigma Pi Sigma, the Electrochemical Society, the American Chemical Society, the American Physical Society, the American Microchemical Society, and a Fellow of the American Association for the Advancement of Science.

WILLIAM H. CHERRY received the B.S. degree in Physics from Massachusetts Institute of Technology in 1941, and the Ph.D. degree from Princeton University in 1958. He joined the research staff of the RCA Manufacturing Company at Harrison, N. J., in August 1941, and transferred to RCA Laboratories in Princeton in the following year. Since that time, he has studied dielectric properties of gas discharge plasma at microwave frequencies, inverted (external cathode) cavity magnetrons, the theory of the injection process and the nature of the electron orbits, the application of colorimetry and multiplex to color television, and the process of emission of slow positrons from solid surfaces. For the past two years he has been working on superconductivity.

Dr. Cherry is a member of Sigma Xi and of the American Physical Society, and is co-recipient of the Levy Medal of the Franklin Institute for a paper on the induction accelerator.

GEORGE D. CODY graduated from Harvard University in 1952, and in 1957 was awarded a Ph.D. degree. He joined the Physical and Chemical Research Laboratory of RCA Laboratories in 1957, where his initial efforts were directed toward high-temperature measurements of the thermoconductivity of semiconductors. Recently, he has done extensive research on the superconductivity properties of niobium stannide. In October 1957, Dr. Cody was awarded a John Parker Fellowship from Harvard for the study of low-temperature physics at Oxford University in England.

Dr. Cody is a member of Sigma Xi and Phi Beta Kappa.

ROGER W. COHEN received the B.S. degree in physics from M.I.T. in 1960, and the M.S. from Rutgers University in 1962. He is currently on a leave of absence under the RCA Graduate Study Program working toward the Ph.D. Work he did at RCA during the summer of 1959 on the photoelectric-magnetic effect formed the foundation of his bachelor's thesis. He joined RCA Laboratories as a full-time staff member in June 1960, and has worked on theoretical and experimental aspects of degenerate semiconductors, plasmas in solids, and the thermoelectric properties of germanium–silicon alloys. Mr. Cohen is a member of Sigma Xi.

JOHN L. COOPER was employed as an Assayer for the American Smelting and Refining Co., Perth Amboy, N. J., from 1950 to 1953. He entered the United States Army in 1953 and received training in Optical Instrument repair at Aberdeen Proving Ground, Maryland, and from 1954 to 1955 was head of the instrument repair shop at Ladd Air Force Base, Fairbanks, Alaska. He returned to the American Smelting and Refining Co. after discharge from the Army and attended Rutgers Evening College. Since 1960 he has been employed at the RCA Laboratories in Princeton, N. J., where he has been engaged in research on thermoelectric materials and the synthesis and measurement of physical properties of type II superconductors and in the development of RCA's first superconducting solenoid. Mr. Cooper received a diploma from RCA Institutes in 1963.

GLENN CULLEN received the B.S. degree in chemistry from the University of Cincinnati in 1953, and the Ph.D. degree in inorganic chemistry from the University of Illinois in 1956. During the following two years he served on the teaching staff of the U.S. Army Air Defense School at Ft. Bliss, Texas. On release from the Army in 1958 he joined the staff of RCA Laboratories, Princeton, N. J., and initially worked on the chemical stabilization of semiconductor surfaces. For the past few years he has been active in the area of preparing and studying the properties of Nb_3Sn. Dr. Cullen is a member of the American Chemical Society and the Society of Sigma Xi.

GASTON FISCHER received a diploma in physics from the Swiss Fèderal Institute of Technology, Zurich, in 1953, and the degree of Dr. ès Sc. from the University of Neuchâtel, Switzerland, in 1959. From 1953 to 1956 he was employed by the Laboratoire Suisse de Recherches Horlogères in Neuchâtel, and from 1956 to 1962 by the National Research Council, Ottawa, Canada, where he worked in the Low Temperature Group of the late D.K.C. McDonald. In 1962 he joined Laboratories RCA, Zurich, Switzerland.

Y. GOLDSTEIN received the M.S. degree in physics in 1959 from the Hebrew University in Jerusalem, and the Ph.D. degree in semiconductor physics in 1962 from the same institution. He was employed by the Hebrew University as a Laboratory Instructor in 1957. Dr. Goldstein joined RCA Laboratories in October 1962. He is a member of the American Physical Society.

JOSEPH J. HANAK received the B.S. degree in Chemistry at Manhattan College in 1953, the M.S. degree in Physical Chemistry at the University of Detroit in 1956 and the Ph.D. degree in Physical Chemistry at the Iowa State University in 1959. He was a Teaching Fellow in Chemistry at the University of Detroit in 1953 and 1954, worked for the Ethyl Corporation as a Chemist in 1955, and was a Research Assistant at the AEC Institute for Atomic Research (Ames, Iowa) from 1955 to 1959. Dr. Hanak has been active in the field of chemistry, metallurgy, and crystallography of the rare-earth elements. He is currently active in research on superconducting materials and high temperature chemistry and metallurgy. He is the inventor of the RCA vapor-deposition process of Nb_3Sn, and of stable, permanent, high-field superconducting magnets. He is a member of the American Chemical Society, Phi Lambda Upsilon, and Sigma Xi.

RICHARD HECHT received the B.S. degree in Physics at the City College of New York in 1954. He graduated magna cum laude and was awarded a National Science Foundation Fellowship. He received the Ph.D. degree from Columbia University; his thesis was on an experimental investigation of the electron spin susceptibility of the alkali metals at low temperature. Since joining RCA Laboratories at Princeton, N. J., in 1962, he has been investigating the magnetic properties of superconductors. Dr. Hecht is a member of Phi Beta Kappa, Sigma Xi, and the American Physical Society.

FRANK KOLONDRA received the B.S. degree in Electrical Engineering from Newark College of Engineering. He joined RCA Electron Tube Division in Harrison, N. J. in 1953, where he worked on electron tubes and transistors until 1959, when he joined the Physics and Chemistry Laboratory to work on Nuvistors and thermoelectric modules. Since 1962 he has been attached to the Superconductor Materials and Devices Laboratory of the RCA Special Electronic Components Division at Princeton, N.J.

J. P. McEvoy, Jr. received the B.S. degree in Physics from St. Joseph's College in 1959, and then joined RCA Defense Electronic Products, continuing his studies under the RCA Graduate Study Program. He received the MS degree in Physics from the University of Pennsylvania in 1962. For the past three years, he has been studying high-field superconductors and their application to new electronic devices. He was responsible for the development of a new class of superconducting magnets for the solid-state traveling-wave maser, and was instrumental in the integration of masers and superconducting magnets into a closed-cycle helium refrigerator. He has been awarded a David Sarnoff Fellowship for the academic year 1964-1965, and is now studying for his doctorate at the Imperial College of the University of London, specializing in low-temperature physics and physical metallurgy. Mr. McEvoy is a member of Sigma Pi Sigma and the American Physical Society.

Robert L. Novak received the B.S. degree in metallurgical engineering from the University of Pennsylvania in 1957 and completed his residence requirements for a Ph.D. in 1960. For two summers he worked at the Franklin Institute in the Solid State Division, where he was concerned with substructure in single crystals, zone refining of metals, and material preparation for thermoelectric studies. Mr. Novak joined RCA Laboratories in June 1957, where he has worked on alloy compounds for thermoelectric and power-generation applications. Since 1960, Mr. Novak has been working on irradiation effects in silicon and solar cells.

Mr. Novak is a member of Tau Beta Pi, American Institute of Metallurgical Engineers, and the American Society for Metals.

F. R. Nyman received the B.S. degree in chemistry from Wagner College in 1954. From 1954 to 1956 he performed research on high-temperature selective chlorination of titanium- and zirconium-bearing ores as a research chemist at the research laboratories of the National Lead Company. During 1956 and 1957, he was attached to the U.S. Army Ballistic Missile Agency, Huntsville, Alabama, where he performed research on physical properties of materials for use in missile and satellite programs. He joined the RCA Semiconductor and Materials Division in Somerville, N. J. in March 1959, and worked on the successful development of a miniature tantalum solid-electrolytic capacitor. Since November 1962 he has been a member of the Superconductor Materials and Devices Laboratory of the RCA Special Electronic Components Division at Princeton, N. J., and has been engaged in the development of processes for the vapor deposition of Nb_3Sn films on ceramic and metal substrates of various geometries.

R. H. PARMENTER received the B.S. degree in Engineering Physics from the University of Maine in 1947 and the Ph.D. degree in Physics from MIT in 1952. He was a staff member in the Solid State and Molecular Theory Group at MIT from 1951 to 1954, a Guest Scientist at Brookhaven National Laboratory in 1951 and 1952, and a staff member of Lincoln Laboratory from 1952 to 1954. He joined RCA Laboratories in Princeton in 1954, and spent six months in 1958 at Laboratories RCA Ltd. in Zürich, Switzerland. He was a Visiting Lecturer at Princeton University in 1960 and 1961. At present, he is acting head of the General Solid State Research Group at RCA Laboratories. Dr. Parmenter is a Fellow of the American Physical Society and a member of Sigma Xi and Tau Beta Pi.

K. G. PETZINGER received the AB degree from Princeton University in 1963 with an honor program in physics. He joined RCA Laboratories in 1963 and entered the Research Training Program and Graduate Study Program. During his training assignments he worked on superconducting disc magnets, solid-state lasers, and microwave propagation in solid-state plasmas. He is now assigned to the Microwave Research Laboratory, where he is working on plasmas in solids. Mr. Petzinger is taking graduate physics courses at Columbia University.

BRUCE ROSENBLUM received the B.S. degree from New York University in 1949 and the Ph.D. from Columbia Universtiy in 1957. He joined RCA Laboratories in 1958 after a year at the University of California in Berkeley. He has worked in the fields of microwave spectroscopy of gasses, cyclotron resonance in metals, paramagnetic resonance, plasmas, in semiconductors, and microwave studies of superconductors.

FRED D. ROSI, Associate Laboratory Director, Semiconductors, Superconductors, and Metals Research, Materials Research Laboratory, has been associated with RCA Laboratories since March, 1954. He is a graduate of Yale University, receiving the B.E. in Metallurgy in 1942, the M.E. degree in 1947, and the Ph.D. degree in 1949. He was awarded the graduate laboratory assistantship in the Department of Metallurgy at Yale, 1946-49. From 1943 to 1946 he served in the United States Navy. Dr. Rosi was an Engineering Specialist in the theoretical metallurgy group at Sylvania Electric Products, Inc., from 1949 to 1954, where he was engaged in fundamental research on mechanical properties and recrystallization phenomena in various metals and alloys. Since March 1954, he has been with RCA Laboratories, where he is now head of a group engaged in the preparation of elemental and compound semiconductor crystals for transistor and thermoelectric applications, and in research on superconductivity and electronically active organic materials. Dr. Rosi held the rank of Adjunct Professor at New York University from 1955 to 1960, where he lectured in graduate courses on crystal mechanics and advanced physical metallurgy.

Dr. Rosi is a member of the Yale Engineering Society, Sigma Xi, the American Institute of Metallurgical Engineers, and the American Physical Society. He is currently a member of the NASA Research Advisory Committee on Materials, the Semiconductor Committee of the AIME, the Thermoelectric Committee of the I.E.E.E., and past chairman of the New York–New Jersey Physical Metallurgy Group of the AIME. He has also served on the Program, Physics of Metals, and Mathewson Gold Medal Committees of the AIME.

HENRY C. SCHINDLER received the B.Ch.E. degree from Cooper Union in 1955, and an M.S. degree in Physics from the Stevens Institute of Technology in 1959, and is currently working toward a Doctorate in Physics. He was employed for four years at Picatinny Arsenal, where he was concerned with formulating and testing rockets and jatos. Subsequently he was associated with General Instrument Corporation as a senior engineer in developing semi-conductor devices. These included tunnel diodes, fast-switching diodes, and high-frequency transistors. He joined RCA in June 1962 and has been associated with the Superconductor Materials and Devices Laboratory of the Special Electronic Components Division since that date. He has been involved with the development of the niobium–tin vapor-deposition process, and is currently studying the physical, chemical, and electrical properties of Nb_3Sn films with particular reference to superconductor device applications. Mr. Schindler is a member of the American Physical Society.

EDWARD R. SCHRADER received the B.A. degree in Physics from Columbia University in 1950, the M.S. degree in Physics from the Polytechnic Institute of Brooklyn in 1953, and is currently working on a Doctorate. He was associated with the American Museum of Natural History in oceanographic exploration in 1950 and was subsequently employed as a project engineer on aircraft instrument research by the Sperry Gyroscope Co. In 1954 he joined the RCA Electron Tube Division in Harrison, N. J., where he studied the effects of tube materials upon tube performance. In 1962 he joined the Superconductor Materials and Devices Laboratory of the RCA Special Electronic Components Division, at Princeton, N. J., where he has worked on the development of manufacturing technology for the production of niobium–tin superconducting material. Mr. Schrader is a member of Sigma Xi and the American Physical Society.

KURT STRATER received the B.A. degree in Chemistry from New York University in 1953, and the M.S. degree from Newark College of Engineering in 1961. He was employed by the Wright Aeronautical Division of Curtiss Wright from 1952 to 1958. He joined the RCA Electron Tube Division at Harrison, N. J. in 1958. In 1962 he transferred to the Superconductor Materials and Devices Group of the RCA Special Electronic Component Division at Princeton, N. J. His work has included the development of a method for solution metallizing high alumina ceramics and a hypothesis of a metal-ceramic bonding, improvement of high-temperature properties of tungsten, eutectic bonding to ferrite, and superconducting material production. For the past year, he has worked on the development of a laboratory technique for coating wire and ribbon with niobium stannide. In 1964 he was made head of the Process Development Group.

Mr. Strater is a member of the American Chemical Society and the American Ceramic Society.

L. J. VIELAND received a doctorate in physical chemistry from Pennsylvania State University in 1954. He joined the RCA Semiconductor and Materials Division in 1958, where he engaged principally in materials research on gallium arsenide. Since 1962 he has been at RCA Laboratories, working on various aspects of superconductivity in intermetallic compounds. Dr. Vieland is a member of Phi Beta Kappa and the American Physical Society.

D. W. WOODARD received the B.S. degree from Princeton University in 1962 with a major in Electrical Engineering, Physics Option, an honor program in Electrical Engineering. He joined RCA Laboratories in 1962 and entered the Research Training Program and the Graduate Study Program, under which he received the M.S. degree in physics from Rutgers University in June 1964. Mr. Woodard has worked on ferrite memories, microwave measurements of the properties of InSb, the transport properties of superconducting alloys, and plasmas in solids.